University of Granada

Doctoral Programme in Biomedicine (B11.56.1) (RD 99/2011)

Spanish National Research Council (CSIC)

Institute of Parasitology and Biomedicine "López-Neyra" (IPBLN)

Molecular mechanisms underlying LRRK2-mediated centrosomal cohesion deficits as biomarker for Parkinson's disease

Antonio Jesús Lara Ordóñez

Doctoral Thesis

Granada, September 2021

Universidad de Granada

Programa de Doctorado en Biomedicina (B11.56.1) (RD 99/2011)

Consejo Superior de Investigaciones Científicas (CSIC)

Instituto de Parasitología y Biomedicina "López-Neyra" (IPBLN)

Molecular mechanisms underlying LRRK2-mediated centrosomal cohesion deficits as biomarker for Parkinson's disease

Memoria presentada por el doctorando Antonio Jesús Lara Ordóñez, graduado en Bioquímica, para optar al título de Doctor en Biomedicina por la Universidad de Granada

Directoras de la Tesis:

Dra. Sabine Hilfiker
Investigadora Principal del CSIC

Dra. María Belén Fernández López
Investigadora Postdoctoral del CSIC

Antonio Jesús Lara Ordóñez

Tesis Doctoral

Granada, Septiembre 2021

Editor: Universidad de Granada. Tesis Doctorales
Autor: Antonio Jesús Lara Ordóñez
ISBN: 978-84-1117-332-2
URI: http://hdl.handle.net/10481/74781

Declaración de autoría /
Declaration of authorship

El doctorando / *The doctoral candidate* **Antonio Jesús Lara Ordóñez** y las directoras de la Tesis / *and the Thesis supervisors*: **Dr. Sabine Hilfiker** y / *and* **Dr. María Belén Fernández López**

garantizamos, al firmar esta Tesis Doctoral, que el trabajo ha sido realizado por el doctorando bajo la dirección de las directoras de la Tesis y hasta donde nuestro conocimiento alcanza, en la realización del trabajo, se han respetado los derechos de otros autores a ser citados, cuando se han utilizado sus resultados o publicaciones.

/

guarantee, by signing this Doctoral Thesis, that the work has been done by the doctoral candidate under the direction of the Thesis supervisors and, as far as our knowledge reaches, in the performance of the work, the rights of other authors to be cited (when their results or publications have been used) have been respected.

Granada, 23 de Junio de 2021 / *Granada, June 23, 2021*

Directoras de la Tesis / *Thesis supervisors*:

Dr. Sabine Hilfiker **Dr. María Belén Fernández López**

Doctorando / *Doctoral candidate*:

Antonio Jesús Lara Ordóñez

Financiación y publicaciones / Funding and publications

La presente Tesis Doctoral ha sido realizada en el Laboratorio 114 del Departamento de Biología Molecular del Instituto de Parasitología y Biomedicina "López-Neyra" (IPBLN) de la Agencia Estatal Consejo Superior de Investigaciones Científicas (CSIC) en Granada, Andalucía (España), en el grupo de investigación Mecanismos Moleculares y Celulares en la Enfermedad de Parkinson dirigido por la Dra. Sabine Hilfiker y bajo la dirección de la Dra. Sabine Hilfiker y la Dra. María Belén Fernández López.

Parte de los resultados presentados en esta Tesis Doctoral han sido obtenidos durante una estancia de investigación predoctoral concedida al doctorando y financiada por el Ministerio de Ciencia, Innovación y Universidades del Gobierno de España, por el programa de "Ayuda a la movilidad para estancias breves y traslados temporales (EEBB 2018)" (referencia EST18/00412). La estancia de investigación predoctoral se realizó en el Centro Nacional de Microscopía e Investigación de Imagen (NCMIR) de la Universidad de California San Diego (UCSD) en San Diego, California (Estados Unidos de América) bajo la supervisión de la Dra. Daniela Boassa.

/

This Doctoral Thesis has been carried out in the Laboratory 114 of the Department of Molecular Biology at the Institute of Parasitology and Biomedicine "López-Neyra" (IBPLN) from the State Agency Spanish National Research Council (CSIC) in Granada, Andalucía (Spain), within the research group Cellular and Molecular Mechanisms of Parkinson's Disease led by Dr. Sabine Hilfiker and under supervision of Dr. Sabine Hilfiker and Dr. María Belén Fernández López.

Part of the results presented in this Doctoral Thesis have been obtained during a predoctoral research stay awarded to the doctoral candidate and funded by the Ministry of Science, Innovation and Universities from the Spanish Government, within the program "Mobility fellowship for short stays and transfers (EEBB 2018)" (reference EST18/00412). The predoctoral research stay was carried out at the National Center for Microscopy and Imaging Research (NCMIR) of the University of California San Diego (UCSD) in San Diego, California (United States of America) under supervision of Dr. Daniela Boassa.

La financiación para el trabajo realizado en esta Tesis Doctoral procede de las siguientes organizaciones y/o instituciones:

/

This Doctoral Thesis has been funded by the following organizations and/or institutions:

- Ministerio de Educación, Cultura y Deporte del Gobierno de España
  "Ayuda para la formación de profesorado universitario (FPU 2015)" al doctorando (referencia FPU15/05233).

- Ministerio de Ciencia, Innovación y Universidades del Gobierno de España
  "Ayuda a la movilidad para estancias breves y traslados temporales (EEBB 2018)" al doctorando (referencia EST18/00412).

- Ministerio de Economía, Industria y Competitividad del Gobierno de España
  Proyectos de investigación: "Estudios de la enfermedad de Parkinson asociada a LRRK2 para el desarrollo de tratamientos" (referencia SAF2014-58653-R), y "Relación entre LRRK2 y el déficit de trafico vesicular mediado por RABs en la enfermedad de Parkinson" (referencia SAF2017-89402-R) a la directora de la tesis Dra. Sabine Hilfiker.

- *The Michael J. Fox Foundation for Parkinson's Research*
  Proyectos de investigación: "*LRRK2-mediated endolysosomal alterations: mechanistic insights and validation as pharmacodynamic readout for kinase inhibitor studies*" (MJFF_2016), "*Kinase activity-mediated centrosomal alterations in LRRK2-PD and sporadic PD patient-derived cells and link to altered RAB protein localization/phosphorylation*" (referencia 10255.01), y "*LRRK2-mediated centrosomal cohesion alterations*" (referencia 10255.02) a la directora de la tesis Dra. Sabine Hilfiker.

Los resultados presentados en esta Tesis Doctoral han sido publicados en las siguientes revistas internacionales o están en vías de publicación:

/

The results presented in this Doctoral Thesis have been published in the following international journals or are in the process of being published:

Lara Ordóñez AJ, Fernández B, Fdez E, Romo-Lozano M, Madero-Pérez J, Lobbestael E, Baekelandt V, Aiastui A, López de Munaín A, Melrose HL, Civiero L and Hilfiker S. (2019) **RAB8, RAB10 and RILPL1 contribute to both LRRK2 kinase-mediated centrosomal cohesion and ciliogenesis deficits.** *Hum. Mol. Genet.* Nov 1; 28(21): 3552-3568. DOI: 10.1093/hmg/ddz201

Fernández B, **Lara Ordóñez AJ**, Fdez E, Mutez E, Comptdaer T, Leghay C, Kreisler A, Simonin C, Vandewynckel L, Defebvre L, Destée A, Bleuse S, Taymans JM, Chartier-Harlin MC and Hilfiker S. (2019) **Centrosomal cohesion deficits as cellular biomarker in lymphoblastoid cell lines from LRRK2 Parkinson's disease patients.** *Biochem. J.* Oct 15; 476(19): 2797-2813. DOI: 10.1042/BCJ20190315

Lara Ordóñez AJ, Fernández B, Fasiczka R, Naaldijk Y, Fdez E, Blanca Ramírez M, Phan S, Boassa D and Hilfiker S. **The LRRK2 signaling pathway causes centrosomal deficits via phosphorylated RAB10 and RILPL1 at centriolar subdistal appendages.** (under review)

Asimismo, los resultados obtenidos en la presente Tesis Doctoral han sido presentados en los siguientes congresos o reuniones científicas nacionales e internacionales:

/

In addition, the results obtained during this Doctoral Thesis have been presented in the following national and international congresses or scientific meetings:

Lara Ordóñez AJ, Fernández B, Madero-Pérez J, Fdez E, Lobbestael E, Baekelandt V and Hilfiker S. **RAB8 and RAB10 phosphorylation contribute to LRRK2-mediated centrosomal cohesion and ciliogenesis defects.** Biennial International LRRK2 meeting. The Botanical Garden, Padua, Italy. September 2nd – 4th, 2018. (Poster)

Lara Ordóñez AJ, Fernández B, Madero-Pérez J, Fdez E, Lobbestael E, Baekelandt V and Hilfiker S. **RAB8 and RAB10 phosphorylation contribute to LRRK2-mediated centrosomal cohesion and ciliogenesis defects.** EMBO Workshop: Cilia 2018. Copenhagen, Denmark. October 2nd – 5th, 2018. (Poster)

Lara Ordóñez AJ, Fernández B, Madero-Pérez J, Fdez E, Romo-Lozano M, Lobbestael E, Baekelandt V and Hilfiker S. **RAB8 and RAB10 phosphorylation contribute to LRRK2-mediated centrosomal cohesion and ciliogenesis defects.** I Congreso de Investigadores del PTS. Granada, Spain. February 13th – 15th, 2019 (Short talk)

A mis padres,

A mi familia

Index

Abbreviations

AD	Alzheimer's disease
ALS	Amyotrophic lateral sclerosis
ANK	Ankyrin repeats
ARM	Armadillo repeats
ASK1	Apoptosis signal-regulating kinase 1
AurA	Aurora A
BBB	Blood-brain barrier
BME	Basal medium Eagle
BSA	Bovine serum albumin
CIN	Chromosomal instability
CLEM	Correlative light and electron microscopy
CMA	Chaperone-mediated autophagy
COR	C-terminal of ROC
CRISPR-Cas9	Clusters of regularly interspaced short palindromic repeats
CSC	Cargo-selective complex
DA	Dopaminergic
DAB	3-3'-diaminobenzidine
DBS	Deep brain stimulation
DJ-1	Daisuke-Junko-1
DMEM	Dulbecco's modified Eagle medium
DMSO	Dimethyl sulfoxide
EARP	Endosome-associated retrograde protein
EGFR	Epidermal growth factor receptor
EHD	EH domain-containing protein
ERC	Endocytic recycling compartment
ERK	Extracellular signal-regulated kinase
GAP	GTPase activating protein
GARP	Golgi-associated retrograde protein
GBA	β-glucocerebrosidase
GDI	GDP dissociation inhibitor
GDP	Guanosine diphosphate
GSK	GSK2578215A

GTP	Guanosine triphosphate
GWAS	Genome-wide association studies
HBSS	Hank's balanced salt solution
IMDM	Iscove's modified Dulbecco's media
IN-1	LRRK2-IN-1
JIP	JNK-interacting protein
JNK	c-Jun NH2-terminal kinase
KO	Knockout
LB	Lewy body
LCLs	Lymphoblastoid cell lines
L-DOPA	Levodopa
LED	L-DOPA-equivalent dose
LN	Lewy neurite
LRR	Leucine-rich repeats
LRRK1	Leucine-Rich Repeat Kinase 1
LRRK2	Leucine-Rich Repeat Kinase 2
M6PR	Mannose-6-phosphate receptor
MAP	Microtubule-associated protein
MAPK	Mitogen-activated protein kinase
MAPT	Microtubule-associated protein tau
MDS-UPDRS	Movement Disorders Society Unified Parkinson's Disease Rating Scale
MEF	Mouse/murine embryonic fibroblast
MeOH	Methanol
MICAL-L1	Molecule interacting with CasL-like-1
MIP	Maximum intensity projection
MPP+	1-methyl-4-phenylpyridinium
MPTP	1-methyl-4-phenyl-1,2,3,6-tetrahydropyridine
MTOC	Microtubule-organising centre
mTOR	Mammalian target of rapamycin
PBMCs	Peripheral blood mononuclear cells
PBS	Phosphate-buffered saline
PCM	Pericentriolar material

PCP	Planar cell polarity
PD	Parkinson's disease
PET	Positron emission tomography
PFA	Paraformaldehyde
PFE-360	PF-06685360
PHA-M	Phytohemagglutinin-M
PINK1	PTEN-induced putative kinase 1
PLA	Proximity ligation assay
PLK	Polo-like kinase
PPM1H	Protein phosphatase, Mg^{+2}/Mn^{+2} dependent 1H
PRKN	Parkin
PyT	Pythagorean theorem
RAB	RAS-related protein family in brain
REM	Rapid eye movement
RGS2	Regulator of G-protein signalling 2
RILPL1	Rab interacting lysosomal protein like 1
RL1d-GFP	RILPL1 [E280-end]-eGFP
ROC	Ras of Complex
SNCA	α-synuclein (α-syn)
SNpc	Substantia nigra pars compacta
SNX	Sorting nexin complex
TBK	TANK-binding kinase
TfR	Transferrin receptor
TGN	Trans-Golgi network
TTBK2	Tau tubulin kinase 2
VPS35	Vacuolar protein sorting-associated protein 35
WD40	WD40 repeats
Wnt	Wingless/Int
WT	Wildtype

List of figures

I. Introduction

IV. Results

List of tables

Abstract / Resumen

Mutations in *Leucine-Rich Repeat Kinase 2* (*LRRK2*) are the most common cause of autosomal dominant familial Parkinson's disease (PD), and variants in this gene increase risk for the sporadic form of the disease. LRRK2 has been reported to regulate various intracellular membrane trafficking events, including endocytic and endolysosomal trafficking, autophagy and retrograde trafficking, as well as participate in cell signalling cascades. However, the precise mechanism(s) underlying these events remain largely unknown. Recently, LRRK2 has been reported to phosphorylate a subset of RAB GTPases including RAB8A and RAB10, which bind preferentially to RILPL1 and RILPL2 only when phosphorylated. Pathogenic LRRK2 has been reported to cause centrosomal cohesion deficits in dividing cells, including in peripheral patient-derived cells, in a kinase-dependent manner by phosphorylating RAB8A, which causes its accumulation in a pericentrosomal area. Additionally, LRRK2-phosphorylated RAB10 is recruited to centrosome-localised RILPL1, and this has been reported to interfere with primary cilia biogenesis.

In the present doctoral thesis, we demonstrate that the LRRK2-mediated centrosomal cohesion deficits are not only caused by accumulation of phospho-RAB8A but also of phospho-RAB10. Using CRISPR-Cas9 approaches, we identify that the LRRK2-mediated centrosomal cohesion deficits are crucially dependent on the presence of RAB8A, RAB10 and RILPL1. Previous studies have indicated that RILPL1 may be localised to the centrosome. Here we show for the first time that RILPL1 is localised to subdistal appendages of the mother centriole, which allows for the recruitment of the LRRK2-phosphorylated RAB proteins to cause the centrosomal defects. The pathogenic LRRK2-mediated ciliogenesis defects also correlate with the pericentrosomal accumulation of both phospho-RAB8A and phospho-RAB10. In addition, we show here that various LRRK2 variants that modify risk for PD, as well as currently described regulators of the LRRK2 signalling pathway (vps35 and PPM1H) impact upon centrosomal cohesion deficits.

Our data suggest that the LRRK2-mediated centrosomal cohesion and ciliogenesis defects are two distinct cellular readouts of the same underlying phospho-RAB8/RAB10/RILPL1 nexus and highlight the possibility that either centrosomal cohesion and/or ciliogenesis alterations may serve as cellular biomarkers for LRRK2-related PD. Indeed, we demonstrate that LRRK2-mediated centrosomal cohesion and ciliogenesis defects are observable under endogenous

conditions in primary astrocytes from mutant LRRK2 knockin mice as compared to control, and reverted upon LRRK2 kinase inhibition. In addition, we describe centrosomal cohesion deficits in peripheral blood mononuclear cell-derived lymphoblastoid cell lines from a larger sampling of G2019S LRRK2 mutant PD patients as compared to healthy controls, which can also be observed in a subset of sporadic PD patient samples, and which are reverted upon pharmacological LRRK2 kinase inhibition in all cases. Altogether, we describe a robust cell biological assay based on centrosomal cohesion defects which may allow for the stratification of PD patients who may benefit from LRRK2-related therapeutics in clinical settings.

Las mutaciones en *Leucine-Rich Repeat Kinase 2* (*LRRK2*) son la causa más común de la enfermedad de Parkinson familiar con herencia autosómica dominante, y otras variantes en este gen aumentan el riesgo de sufrir la forma esporádica de la enfermedad. Se ha observado que LRRK2 participa en la regulación de varios eventos del tráfico intracelular de membranas, incluyendo el tráfico endocítico y endolisosomal, autofagia y tráfico retrógrado, así como participa en cascadas de señalización celular. Sin embargo, los mecanismos celulares y moleculares que subyacen a estos eventos aún no se conocen con exactitud. Recientemente, se ha revelado que LRRK2 fosforila un subconjunto de proteínas RAB incluyendo RAB8A y RAB10, que se unen preferentemente a RILPL1 y RILPL2 cuando están fosforiladas. Se ha descrito que LRRK2 patogénico causa un déficit de cohesión centrosomal en células en división, incluyendo células periféricas de pacientes, en una manera dependiente de su actividad kinasa mediante la fosforilación de RAB8A, que causa su acumulación en un área pericentrosomal. Además, la fosforilación de RAB10 por LRRK2 causa su reclutamiento hacia el centrosoma donde se une a RILPL1, y esta unión se ha demostrado que interfiere con la biogénesis del cilio primario.

En la presente tesis doctoral, demostramos que el déficit de cohesión centrosomal mediado por LRRK2 no es sólo causado por la acumulación de RAB8A fosforilado, sino que también interviene RAB10 fosforilado. Utilizando la técnica de CRISPR-Cas9, hemos identificado que el déficit de cohesión centrosomal mediado por LRRK2 depende principal y únicamente de la presencia de las proteínas RAB8A, RAB10 y RILPL1. Estudios anteriores han indicado que RILPL1 estaría localizado en el centrosoma. Aquí, hemos identificado por primera vez que RILPL1 está localizado en los apéndices subdistales del centriolo madre, que reclutaría las proteínas RAB fosforiladas por LRRK2 para causar alteraciones centrosomales. Los defectos en ciliogenesis causados por LRRK2 patogénico se correlacionan con la acumulación de fosfo-RAB8A y fosfo-RAB10. Además, mostramos que los diferentes variantes de LRRK2 que modifican el riesgo de padecer la enfermedad de Parkinson, así como los diferentes reguladores de las rutas de señalización de LRRK2 (vps35 y PPM1H) tienen un efecto en el déficit de cohesión centrosomal.

Conjuntamente, nuestros datos sugieren que las alteraciones mediadas por LRRK2 en ciliogénesis y cohesión centrosomal son dos efectos celulares diferentes de un mismo nexo subyacente (fosfo-RAB8A/RAB10/RILPL1) y destacan la posibilidad de que las alteraciones de cohesión centrosomal y/o las alteraciones

en ciliogénesis puedan servir como biomarcadores para la enfermedad de Parkinson relacionada con LRRK2. De hecho, demostramos que los defectos de cohesión centrosomal y ciliogénesis se pueden observar en condiciones endógenas en astrocitos primarios de ratones portadores de mutaciones en LRRK2 en comparación con ratones control, y son revertidos mediante inhibición de la actividad kinasa de LRRK2. Además, describimos la presencia de déficits de cohesión centrosomal en líneas celulares linfoblastoides derivadas de células mononucleares de sangre periférica en una muestra mayor de pacientes de Parkinson que portan la mutación G2019S de LRRK2 en comparación con individuos sanos, que son observables también en algunos pacientes de Parkinson esporádico, y son revertidos mediante inhibición de la actividad kinasa de LRRK2 en todos los casos. En conjunto, describimos un ensayo biológico celular robusto basado en defectos de cohesión centrosomal que puede permitir la estratificación de pacientes de Parkinson que pueden beneficiarse de terapias relacionadas con LRRK2 en entornos clínicos.

I. Introduction

1. Parkinson's disease

In 1817, Dr. James Parkinson, a British medical practitioner, described the symptoms and clinical features (resting tremor, flexed posture and festination) observed in six individuals manifesting a distressing disease that had not been characterised. Parkinson published his observations in a monograph entitled "An Essay on the Shaking Palsy", where the name for this disorder was *paralysis agitans* (shaking palsy) (Parkinson, 1817). Later that century, French neurologist Dr. Jean-Martin Charcot identified bradykinesia and rigidity as key features of the disease and renamed it as "Maladie de Parkinson" (Parkinson's disease (PD)) in honour to its discoverer. Comprehension of the disease has been growing over the past 200 years; nevertheless, advances seemed to be insufficient and more aspects of the disease remain to be better understood (Obeso et al., 2017).

Parkinson's disease is the second most common age-related neurodegenerative disease after Alzheimer's disease (AD) affecting up to 0.3 % of the population worldwide, with approximately 8.5 million people suffering from the disease (Abbafati et al., 2020). PD is usually considered a late-onset disease, although age of onset ranges from early forties to late eighties, considering the cases diagnosed before 40 years old as early-onset PD. Prevalence of PD increases with age, affecting 2-3 % of people older than 65 years, and up to ~5 % of the population older than 85 years (Poewe et al., 2017). Despite such age-dependent prevalence, around 4 % of cases are diagnosed at around 50 years of age (Van Den Eeden et al., 2003). Due to the aging of the global population, prevalence has increased by 31 % in the past ten years, and the population affected by PD is expected to double by 2040. Thus, neurodegenerative diseases are becoming a major problem for society posing medical, social and economic challenges (Kowal et al., 2013; Abbafati et al., 2020).

1.1. Clinical manifestations

Parkinson's disease is clinically defined by the presence of motor symptoms which are the most characteristic features of the disease and include bradykinesia (slowness of movement), resting tremor (involuntary shaking), rigidity and postural instability (Fig. 1). In addition, other secondary motor symptoms have been described, including hypomimia, dysarthria, dysphagia, flexed posture, festination, freezing and

dystonia (Jankovic, 2008). PD-associated motor symptoms are correlated with the loss of dopaminergic (DA) neurons in the *substantia nigra pars compacta* (SNpc), and usually start to appear when 50-60 % of DA neurons have degenerated and there exists a 80-85 % deficiency of dopamine in the striatum (Cheng et al., 2010).

Apart from these motor symptoms, PD patients also suffer from a wide range of non-motor symptoms including cognitive impairment and neurobehavioral disorders (e.g. depression, anxiety, apathy, dementia, hallucinations), sleep disturbances (e.g. sleep-wake cycle regulation, excessive sleepiness or insomnia, rapid eye movement sleep behaviour disorder), autonomic dysfunctions (e.g. urogenital dysfunction, orthostatic hypotension, constipation, hyperhidrosis, impotence) and sensory symptoms (e.g. hyposmia or anosmia, paraesthesia, pain) (Fig. 1) (Jankovic, 2008). PD-associated non-motor symptoms have been correlated with the loss of dopaminergic, serotoninergic, noradrenergic and cholinergic neurons in specific regions of the brain, causing a dysfunction in various neurotransmitter systems (Giguère et al., 2018). Interestingly, these non-motor symptoms are present years or even decades before the onset of motor symptoms and are usually under-recognised and under-treated (Zesiewicz et al., 2006). The elapsed time window between onset of non-motors symptoms onset and PD diagnosis based on the characteristic and visible motor symptoms constitutes a significant missed opportunity for potential PD treatments (Fig. 1) (Kang and Marto, 2017).

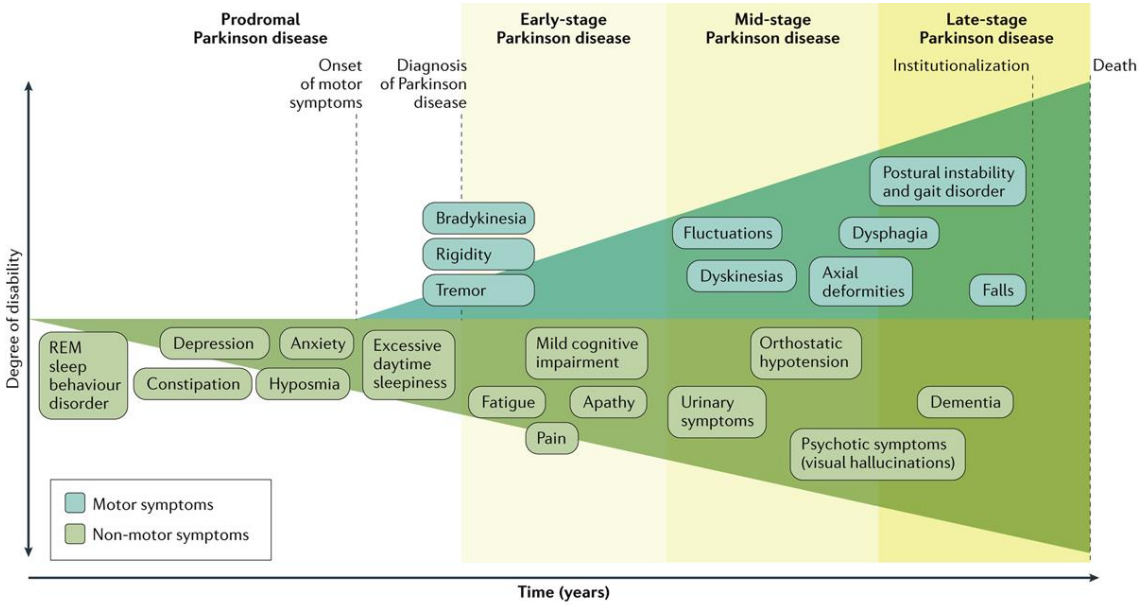

Fig. 1. Associated clinical features during Parkinson's disease progression. Non-motor symptoms occur early during a prodromal phase of PD that may last decades. Diagnosis of PD usually occurs upon onset of motor symptoms. Progression of PD is accompanied by worsening of non-motor and motor symptoms that increase patient disability. REM, rapid eye movement. From (Poewe et al., 2017).

Progression of PD is irreversible and it is presently an incurable disease. Current treatments for PD are based on symptomatic therapies (focused on dopamine replenishment with levodopa (L-DOPA), a dopamine precursor), or suppression of motor fluctuations through deep brain stimulation (DBS). However, long-term administration of L-DOPA has been associated with motor fluctuations and dyskinesia, and DBS is a complex therapy that requires surgery which can lead to some complications (Poewe et al., 2017). Therefore, a better understanding of the molecular mechanisms underlying PD may allow for the discovery of therapeutics which can improve the quality of life of many patients.

1.2. Pathology

Parkinson's disease is characterised by the progressive loss of DA neurons in the SNpc and the presence of Lewy bodies (LBs) in surviving neurons (Fig. 2) (Poewe et al., 2017). Loss of DA neurons in SNpc results in dopamine depletion in the striatum (caudate and putamen nuclei), causing an inhibitory output from the globus pallidus to the thalamus and the cortex, which in the end results in the repression of initiation of movement. Therefore, and as previously described, loss of DA neurons leads to the classical motor symptoms of PD (Shulman et al., 2011).

Lewy bodies (LBs) are intracytoplasmic proteinaceous inclusions that were first described by the German neurologist Dr. Friedrich Lewy in 1912 (Lewy, 1912). LBs are mainly composed of protein aggregates of the non-soluble form of α-synuclein (α-syn), although more than 90 proteins have been found within LBs, including different α-syn binding partners and ubiquitin. In addition, some proteins of the genetic forms of PD have also been reported in LBs, such as LRRK2, Parkin, DJ-1 and PINK1 (Kalia and Kalia, 2015). When these aggregates of α-syn are observed in neuronal processes in the form of filamentous-like structures, they receive the name of Lewy neurites (LNs) (Fig. 2F) (Wakabayashi et al., 2013). LB and LN formation during neurodegeneration have been consistently reported, although their function remains unknown. Oligomers and protofibrils of α-syn may have a neurotoxic effect, while fibrillary aggregates may be neuroprotective (Wakabayashi et al., 2013). In either case, protein aggregation in the brain has been suggested to propagate in a prion-like manner (Desplats et al., 2009). Braak and colleagues described a model for α-syn propagation in the brain that may correlate with progression of PD (Fig. 2H).

In this model, aggregation of α-syn starts in the caudal brain stem and olfactory bulb, from where it may spread to limbic and neocortical brain regions (Braak et al., 2003).

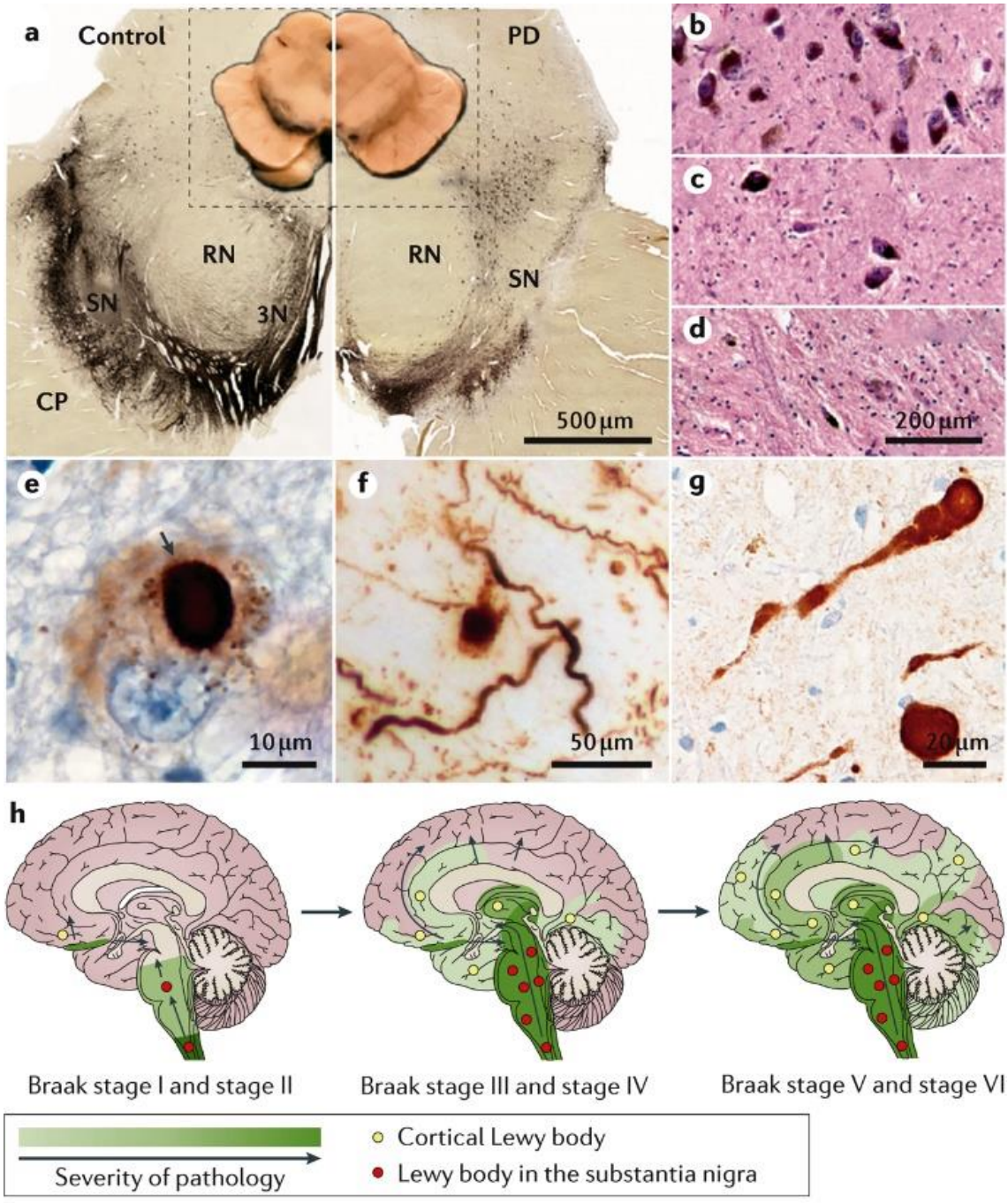

Fig. 2. Neuropathological hallmarks and stages of PD. (A) Histological sections of control and PD midbrain, depigmentation of *substantia nigra* (SN) due to loss of DA neurons is evident in PD (right panel) compared to control (left panel). 3N, 3rd nerve fibres; CP, cerebral peduncle; RN, red nucleus. **(B-D)** Haematoxylin and eosin staining of SN displaying normal distribution of pigmented neurons in healthy patients (B) and altered distribution in moderate (C) and severe (D) PD patients. **(E-G)** Immunohistochemical staining of α-syn in Lewy bodies (E), Lewy neurites (F) and α-syn spheroids in axons (G). **(H)** Schematic representation of Braak theorized α-syn aggregation and propagation stages in PD. From (Poewe et al., 2017).

1.3. Etiology

The exact mechanisms underlying PD remain unknown. Current knowledge indicates that PD is a complex multifactorial disease, with age as the main risk factor for the development of the disease (Fig. 3). The majority of PD cases are diagnosed as idiopathic or sporadic because the underlying cause is unknown. However, approximately 15 % of PD patients have family history, and 5-10 % present a monogenic form of the disease (hereditary or familial PD) (Deng et al., 2018). Importantly, the identification of the monogenic forms of PD has revolutionised our understanding of the molecular mechanisms underlying PD, allowing for the generation of different cellular and animal models to study disease pathogenesis.

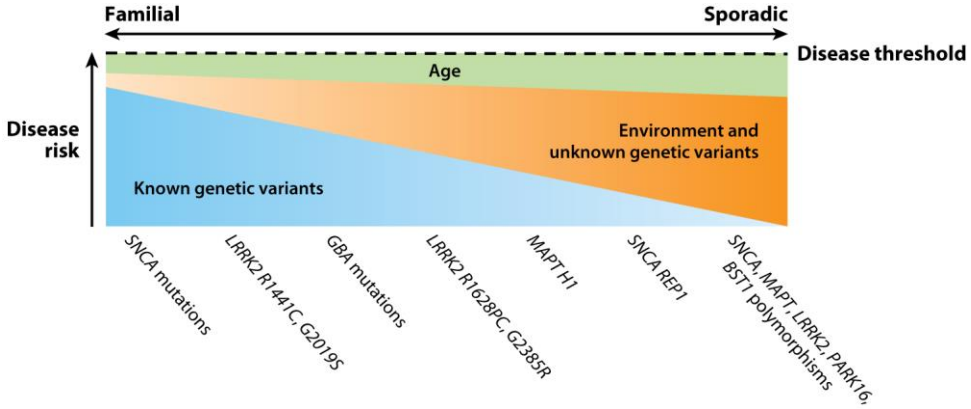

Fig. 3. Etiology of PD. Schematic representation of factors that modify risk for sporadic and familial PD. On the left (familial PD), monogenic forms of the disease represent the mayor risk factor, while age and environment have small contributions; on the right (sporadic PD), age, genetic susceptibility and environmental factors are the main determinants for the disease. SNCA, α-synuclein; GBA, β-glucocerebrosidase; MAPT H1, microtubule-associated protein tau H1 variant; BST1, bone marrow stromal cell antigen 1. From (Shulman et al., 2011).

1.3.1. Sporadic Parkinson's disease

Sporadic PD is the most common form of the disease accounting for 85-90 % of cases. The precise causes of sporadic PD are unknown, but they are likely due to a combination of age, biological sex, ethnicity, genetic susceptibility, life style and environmental risk factors (Kalia and Lang, 2015). As previously described, age constitutes the principal risk factor for sporadic PD, and there is increased disease prevalence over time. Additionally, differences in prevalence based on biological sex have been reported, which therefore is also considered a risk factor. In this context, PD is two times more common in men than in women across different populations, and several studies have suggested that female hormones (estrogen) may have a protective effect towards neurotoxic insults (Hirsch et al., 2016; Thadathil et al., 2020).

Ethnicity is also a risk factor for sporadic PD; several studies have demonstrated an increased prevalence in European, North American and South American populations compared to Asians and Africans (Sauerbier et al., 2018).

Environment and life style also play a role in modifying PD risk. Exposure to pesticides, herbicides and heavy metals increase risk for sporadic PD. The first association with pesticides dates to 1983, when the pesticide 1-methyl-4-phenyl-1,2,3,6-tetrahydropyridine (MPTP or cyperquat) was found as a contaminant in a drug used by several individuals who developed typical PD symptoms as a result. MPTP is metabolised into the neurotoxin 1-methyl-4-phenylpyridinium (MPP+), a mitochondrial complex I inhibitor that causes degeneration of DA neurons (Langston et al., 1983). Rotenone (a pesticide) and paraquat (a herbicide chemically similar to MPP+) were also associated with an increase in the development of PD in rural farmers. Rotenone and paraquat are also mitochondrial complex I inhibitors and cause the degeneration of DA neurons upon drug administration in mice (Betarbet et al., 2000). Many epidemiological studies have demonstrated the association between exposure to heavy metals and increased PD risk. The principal sources of exposure result from occupational exposure, contaminated food and water (in rural areas), and environmental pollution (Bjorklund et al., 2018). On the other hand, different life style habits have been proposed to impact upon risk of PD. Several meta-analysis studies demonstrated that smoking and coffee intake decrease PD risk (up to 50 % and 25 %, respectively), whilst alcohol intake and physical activity had only a minor impact on decreasing risk (Wirdefeldt et al., 2011). In addition, nicotine and caffeine have been shown to play neuroprotective roles in rodent models of PD triggered by neurotoxic insults (Chen et al., 2001; Bordia et al., 2015; Srinivasan et al., 2016). Therefore, there is a relationship between sporadic PD risk and exposure to pesticides and heavy metals, smoking, coffee and well-water consumption, and living in rural areas (Breckenridge et al., 2016).

Importantly, genome-wide association studies (GWAS) identified several common genetic variations that modify risk for sporadic PD. Interestingly, two monogenic forms of familial PD (discussed below) present risk modifying variants for sporadic disease, including Rep1 variant in the *SNCA* gene and G2385R, R1628P and S1647T variants in the *LRRK2* gene, respectively. GWAS also identified two other disease-causing genes as major risk factors for PD, namely *GBA* and *MAPT* (Satake et al., 2009; Simón-Sánchez et al., 2009; Deng et al., 2018). Mutations in *GBA* (*β-glucocerebrosidase*) cause an autosomal recessive lysosomal storage disorder

(Gaucher's disease), and heterozygous GBA mutations modify risk for sporadic PD ranging from a 2-fold increase for mild GBA mutations to a 21-fold increase for severe GBA mutations (Gan-Or et al., 2015). Similarly, genetic variations in *MAPT* (*microtubule-associated protein tau*) have been strongly associated with increased PD risk, and tau aggregates, also called neurofibrillary tangles, have been associated with several neurodegenerative disorders including dementia and AD (Pascale et al., 2016). In addition, Simón-Sánchez et al. reported increased PD risk by association between *PARK8* and *PARK16* locus, encoding for LRRK2 and RAB29 respectively (Simón-Sánchez et al., 2009). Finally, a recent GWAS meta-analysis has identified 90 risk loci for PD, implicating several pathways associated with disease risk (Nalls et al., 2019).

1.3.2. Familial Parkinson's disease

The past 25 years have marked an important milestone for PD research, as several genes which cause monogenic PD with Mendelian inheritance have been identified. Although familial PD only represents around 5-10 % of all cases, the study of monogenic forms of PD has provided critical information towards our understanding of sporadic PD cases, as informing on the type(s) of cellular deficits commonly observed in both familial and sporadic PD cases. To date, at least 23 loci and 19 genes have been identified and mutations in these genes are associated with PD (Table 1). Amongst those, mutations in six genes have been intensely studied as unequivocally segregating with PD in either an autosomal dominant or autosomal recessive manner. Other genes have been described to cause atypical parkinsonism in at least one family, but their firm involvement in the disease requires further studies (Poewe et al., 2017; Deng et al., 2018; Kouli et al., 2018).

Autosomal dominant Parkinson's disease

α-synuclein (SNCA)

The *SNCA* gene was the first causative monogenic form of PD identified (Polymeropoulos et al., 1996). Mutations in *SNCA* or multiplications of the gene locus have been associated with early-onset autosomal dominant familial PD (Polymeropoulos et al., 1997; Chartier-Harlin et al., 2004). The normal function of α-syn remains unknown, but some studies suggested that α-syn plays a role in DA neurotransmission

(Cherian and Divya, 2020). Mutations in α-syn inhibit its degradation (Cuervo et al., 2004), which results in the accumulation, aggregation and misfolding of α-syn into LBs (Plotegher et al., 2014; Burré et al., 2015).

Leucine-Rich Repeat Kinase 2 (LRRK2)

Mutations in *LRRK2* gene are the most common genetic cause of late-onset autosomal dominant familial PD (Paisán-Ruíz et al., 2004; Zimprich et al., 2004). Mutations in *LRRK2* represents 2-5 % of sporadic PD and 10-13 % of familial PD cases (Berg et al., 2005). The clinical manifestations of LRRK2-mediated familial PD closely resemble those observed in sporadic PD patients. Moreover, distinct variants identified in LRRK2 modify risk to develop sporadic PD (Satake et al., 2009; Simón-Sánchez et al., 2009). These evidences support the notion that LRRK2 may play a central role in PD (Kang and Marto, 2017).

Vacuolar protein sorting-associated 35 (VPS35)

Mutations in the *VPS35* gene have been associated with late-onset autosomal dominant familial PD (Vilariño-Güell et al., 2011; Zimprich et al., 2011). Although rare, mutations in *VPS35* are the second most common genetic cause of late-onset familial PD after *LRRK2* mutations. The frequency of the D620N mutation in *VPS35* remains to be determined, but it is estimated to be around 0.3 % in sporadic PD and 1.3 % in familial PD cases (Mohan and Mellick, 2017; Williams et al., 2017). An additional 13 mutations have been described in *VPS35*, but their pathogenicity remains uncertain (Sassone et al., 2020). The clinical characteristics observed in patients with mutated VPS35 are indistinguishable from the sporadic PD phenotype (Struhal et al., 2014).

VPS35 is the main component of the retromer complex, which is in charge of recycling receptors from late endosomes back to *trans*-Golgi network (TGN). Expression of D620N-VPS35 impacts upon the survival of DA neurons, altering lysosome function, autophagy and neurotransmission, and inducing mitochondrial fragmentation. Moreover, several studies demonstrated that VPS35 interacts with other PD-causing genes, such as α-syn, parkin and LRRK2. Hence, VPS35 plays an important role in PD pathogenesis (Sassone et al., 2020).

Autosomal recessive Parkinson's disease

Parkin RBR E3 ubiquitin protein ligase (PRKN or *Parkin)*

The *PRKN* gene was the second causative monogenic form of PD identified (Matsumine et al., 1997). Mutations in *PRKN* are the most common cause of early-onset autosomal recessive familial PD (Kitada et al., 1998). Mutations in *PRKN* represent 10-20 % of early-onset sporadic PD, and 77 % of early-onset familial PD (onset < 30 years) (Cherian and Divya, 2020). Parkin is an E3 ubiquitin ligase that plays an important role in the degradation of selectively targeted proteins during mitophagy through the ubiquitin-proteasome system. Parkin is also phosphorylated and recruited by PINK1 to induce mitophagy of damaged or dysfunctional mitochondria (van der Merwe et al., 2015).

PTEN-induced putative kinase 1 (PINK1)

Mutations in *PINK1* have been associated with early-onset autosomal recessive familial PD (Valente et al., 2001; Valente et al., 2004). The prevalence of *PINK1* mutations is around 4-7 % of early-onset sporadic PD and it is estimated to be up to 15 % of early-onset familial PD (Bonifati et al., 2005; Kim and Alcalay, 2017). Under certain conditions, PINK1 phosphorylates and activates Parkin, recruiting it to the outer mitochondrial membrane to induce mitophagy of depolarised mitochondria (van der Merwe et al., 2015). The majority of mutations and deletions observed in *PINK1* cause a loss-of-function phenotype by impacting upon proper mitochondria homeostasis (Cherian and Divya, 2020).

Parkinsonism-associated deglycase (PARK7 or *DJ-1)*

Mutations in *DJ-1* (*Daisuke-Junko-1*) have been associated with early-onset autosomal recessive familial PD (Van Duijn et al., 2001). Mutations in *DJ-1* are a very rare cause of PD, accounting for 1-2 % of early-onset PD cases (0.4 % of sporadic PD and 0.8 % of familial PD) (Pankratz et al., 2006; Kim and Alcalay, 2017). DJ-1 plays protective role under oxidative stress, and maintains normal DA neuron function and neurotransmission (Hernandez et al., 2016). In addition, it has been reported that DJ-1 participates in the Parkin/PINK1 pathway (van der Merwe et al., 2015).

Locus	Location	Full Gene Name	Gene	Disease onset
Autosomal dominant Parkinson's disease				
PARK1/4	4q22.1	α-synuclein	*SNCA*	Early-onset, late-onset*
PARK8	12q12	Leucine-rich repeat kinase 2	*LRRK2*	Late-onset
PARK17	16q11.2	Vacuolar protein sorting-associated 35	*VPS35*	Late-onset
Autosomal recessive Parkinson's disease				
PARK2	6q26	Parkin RBR E3 ubiquitin protein ligase	*PRKN*	Early-onset
PARK6	1p36	PTEN-induced putative kinase 1	*PINK1*	Early-onset
PARK7	1p36.23	Parkinsonism-associated deglycase	*DJ-1*	Early-onset
Unconfirmed autosomal dominant Parkinson's disease				
PARK3	2p13	Parkinson disease 3	*PARK3*	Late-onset
PARK5	4p13	Ubiquitin C-terminal hydrolase L1	*UCHL1*	Early-onset, late-onset
PARK11	2q37.1	GRB10 interacting GYF protein 2	*GIGYF2*	Late-onset
PARK13	2p13.1	HtrA serine peptidase 2	*HTRA2*	Late-onset, early-onset*
PARK18	3q27.1	Eukaryotic translation initiation factor 4 gamma 1	*EIF4G1*	Late-onset
PARK21	20p13	Transmembrane protein 230	*TMEM230*	Late-onset, early-onset*
PARK22	7p11.2	Coiled-coil-helix-coiled-coil-helix domain containing 2	*CHCHD2*	Late-onset, early-onset*
	11p15.4	RIC3 acetylcholine receptor chaperone	*RIC3*	Late-onset, early-onset*
Complex genetics forms of autosomal recessive Parkinson's disease (unconfirmed)				
PARK9	1p36.13	ATPase 13A2	*ATP13A2*	Early-onset
PARK14	22q13.1	Phospholipase A2 group VI	*PLA2G6*	Early-onset
PARK15	22q12.3	F-box protein 7	*FBXO7*	Early-onset
PARK19	1p31.3	DnaJ heat shock protein family (Hsp40) member C6	*DNAJC6*	Early-onset
PARK20	21q22.1	Synaptojanin 1	*SYNJ1*	Early-onset
PARK23	15q22.2	Vacuolar protein sorting-associated 13 homolog C	*VPS13C*	Early-onset
Risk factors for Parkinson's disease				
PARK10	1p32	Parkinson disease 10	*PARK10*	Late-onset
PARK12	Xq21-q25	Parkinson disease 12	*PARK12*	Late-onset
PARK16	1q32	Parkinson disease 16	*PARK16*	Late-onset

Table 1. PARK genes associated with Parkinson's disease. Several PD-related genes have been described, including the common familial PD genes *α-syn*, *LRRK2*, *VPS35*, *PRKN*, *PINK1* and *DJ-1*. Variants of SNCA and LRRK2 are also risk factors for PD. *PARK16* and *PARK12* genes have been suggested to be RAB29 and RAB39B, respectively. *, few cases reported. Adapted from (Poewe et al., 2017; Deng et al., 2018).

1.4. Molecular mechanisms

Several mechanisms have been proposed in PD pathogenesis, with abnormal α-syn aggregation being one of the proposed mechanisms for the development of the disease. Proposed cellular processes which contribute to neurodegeneration in PD include abnormal protein clearance, autophagosome-endolysosomal system alterations, mitochondrial dysfunction and oxidative stress, and neuroinflammation. These alterations, highly interconnected and not mutually exclusive, could explain the pathological mechanisms underlying PD (Kouli et al., 2018).

One of the major pathological hallmarks of PD is the presence of LBs. α-syn is one of the main components of LBs. Native α-syn is unfolded in neurons, but monomers of α-syn can aggregate due to different post-translational modifications to form oligomers or fibrils that can be degraded through the autophagic system. PD-associated mutations in *SNCA* promote an exacerbated oligomerization which, combined with disturbed protein clearance, may cause further generation of toxic α-syn oligomers, and their eventual aggregation into LBs. During PD, α-syn aggregates can spread through the brain in a prion-like manner, possibly affecting different populations of neurons and causing their degeneration (Kouli et al., 2018).

Mitochondrial dysfunction is tightly associated with the pathogenesis of both sporadic and familial PD. Exposure to environmental toxins (MPTP, paraquat and rotenone) causes inhibition of mitochondrial complex I which can lead to the subsequent degeneration of DA neurons. In addition, monogenic forms of PD have also been reported to impact upon mitochondrial homeostasis. Most prominently, mutations in Parkin/PINK1/DJ-1 impair the proper degradation of damaged mitochondria by mitophagy (Hu and Wang, 2016).

Neuroinflammation has been associated as an underlying mechanism for the development of disease. Microenvironment surrounding DA neurons is of vital importance for the surveillance of the cells. Post-mortem analysis of PD brains revealed the presence of numerous pro-inflammatory cytokines and chemokines in the SNpc confirming an exacerbated activation of microglia and astrocytes that impact upon DA neuron survival. Additionally, infiltration of lymphocytes and macrophages from the peripheral immune system has been observed which may contribute to neuroinflammation in the SNpc. The specific initiation of neuroinflammation remains unknown, but it may be triggered by environmental neurotoxins (6-hydroxydopamine (6-OHDA) and MPTP) or mutations in α-syn and LRRK2, which have been demonstrated to regulate microglia and T-cell function (Gelders et al., 2018).

2. Leucine-Rich Repeat Kinase 2

In 2002, Funayama and colleagues reported for the first time the association of a new locus, termed *PARK8*, located in the centromeric region of chromosome 12, with autosomal dominant Parkinson's disease in a Japanese family (Funayama et al., 2002). Studies in different families with PD from Canada, Germany, England and Spain carried out by two independent groups achieved the identification and sequencing of the *DKFZp434H2111* gene. The gene was later renamed as *LRRK2*, and the protein was called LRRK2 or dardarin (from the Basque word *dardara*, tremor) (Paisán-Ruíz et al., 2004; Zimprich et al., 2004). Those studies identified several point mutations across the *LRRK2* gene that segregated with the disease in the families studied. Interestingly, one of these mutations, I2020T, was then confirmed in the Japanese family where the locus was discovered (Funayama et al., 2005).

Mutations in LRRK2 have been associated with late-onset autosomal dominant PD, with the G2019S mutation being the most frequent mutation encountered worldwide, accounting for 1-3 % of sporadic and 4-8 % of familial PD cases (Di Fonzo et al., 2005; Kachergus et al., 2005; Healy et al., 2008). Such worldwide distribution is attributed to migration and the early occurrence of the mutation event approximately 2250 years ago (Zabetian et al., 2006). Despite such worldwide distribution, the prevalence of the G2019S mutation varies amongst populations, and can be as high as 37 % and 23 % in North African Arab and Ashkenazi Jew families, respectively (Fig. 4) (Lesage et al., 2006; Ozelius et al., 2006). Genetic studies show an incomplete penetrance for the G2019S mutation, ranging from 29 % at 59 years, 51 % at 69 years and 74 % at 79 years, respectively (Kay et al., 2005; Carmine Belin et al., 2006; Clark et al., 2006; Goldwurm et al., 2007; Healy et al., 2008). Hence, these studies suggest that there exist additional genetic and/or environmental susceptibility factors that modify disease onset/penetrance in LRRK2 mutation carriers (Latourelle et al., 2008).

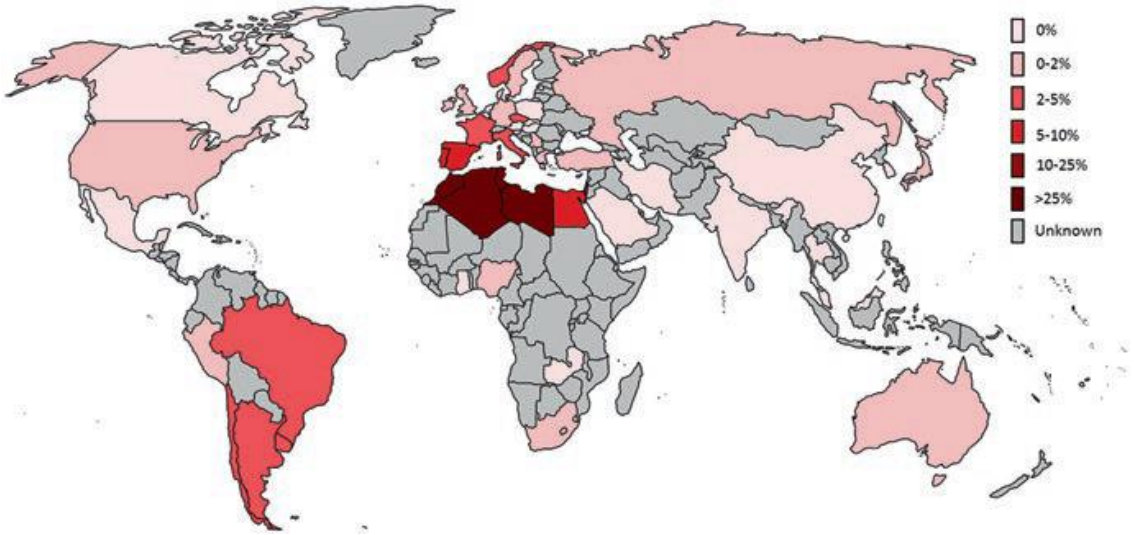

Fig. 4. Worldwide distribution and frequency of G2019S LRRK2 mutation in PD patients. Frequency shows the percentage of total PD cases (sporadic and familial) caused by G2019S LRRK2 mutation. From (Monfrini and Di Fonzo, 2017).

Mutations in LRRK2 comprise the most frequent genetic cause of PD known to date, accounting for approximately 2-5 % of sporadic and 10-13 % of familial PD cases (Berg et al., 2005). While age of onset ranges from 40 to 80 years, clinical and neuropathological features observed within different families with mutations in LRRK2 are largely indistinguishable from those observed in sporadic PD cases (Zimprich et al., 2004; Aasly et al., 2005). Moreover, pathogenic LRRK2 may share some molecular and cellular alterations also observed in sporadic PD. Therefore, understanding the role and function of LRRK2 may shed light on our understanding of the entire PD disease spectrum.

2.1. Structure and mutations

The *LRRK2* gene encodes a multi-domain protein consisting in 2527 amino acids (approximately 286 kDa) that belongs to ROCO protein family, a member of the RAS GTPase superfamily (Bosgraaf and Van Haastert, 2003). In mammals, the closest LRRK2 paralog belonging to the same protein family is Leucine-Rich Repeat Kinase 1 (LRRK1). However, despite its evolutionary conserved domain structure and sequence similarity, mutations in LRRK1 have not been associated with the development of PD. Moreover, mimicking pathogenic LRRK2 mutations in LRRK1 resulted in lower toxic effects *in vitro* compared to LRRK2 (Greggio et al., 2007; Taylor et al., 2007).

LRRK2 protein domains are comprised of a catalytic core with a Ras of Complex (ROC) GTPase domain, followed by a C-terminal of ROC (COR) domain, and a kinase domain. The catalytic core is flanked by several protein-protein interaction domains, including armadillo repeats (ARM), ankyrin repeats (ANK), leucine-rich repeats (LRR), and WD40 repeats (WD40) domains, respectively (Fig. 5).

Since its discovery, several mutations have been identified, but only eight have been conclusively confirmed to cause and segregate with the disease. Interestingly, all of them are clustered within the catalytic core: R1441C/G/H/S and N1437H in the ROC domain, Y1699C in the COR domain, and G2019S and I2020T in the kinase domain (Fig. 5) (Paisán-Ruíz et al., 2004; Zimprich et al., 2004; Di Fonzo et al., 2005; Zabetian et al., 2005; Aasly et al., 2010; Mata et al., 2016). G2019S, the most frequent LRRK2 mutation, displays a 3-4 fold enhanced kinase activity *in vitro*, and at least upon overexpression has been shown to cause neuronal degeneration *in vivo*. These findings support the idea that kinase activity is required for LRRK2-mediated neuronal toxicity (Smith et al., 2005; West et al., 2005; Gloeckner et al., 2006; Greggio et al., 2006).

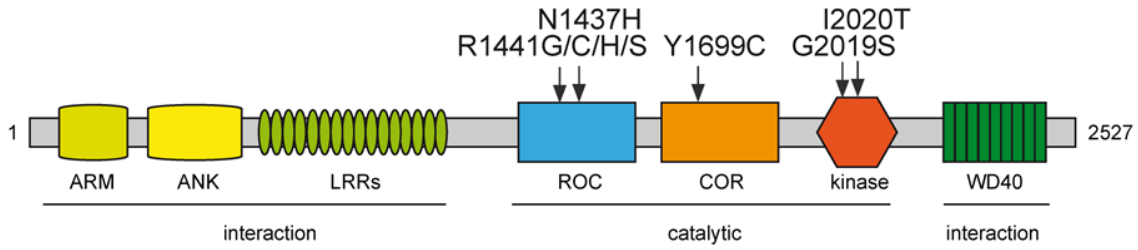

Fig. 5. LRRK2 domain structure and PD-associated mutations. Schematic representation of LRRK2 structure indicating several protein-protein interaction domains (armadillo repeats, ARM; ankyrin repeats, ANK; leucine-rich repeats, LRR; and WD40 repeats) and a central catalytic core (Ras of Complex GTPase, ROC; C-terminal of ROC, COR; and kinase domain). Pathogenic mutations are indicated above their corresponding domain.

The LRRK2 kinase activity is not the only player in neuronal pathogenicity of LRRK2. As described above, LRRK2 contains a GTPase domain and as occurs with other ROCO proteins, there is a crosstalk between the GTPase and the kinase domain (Weiss, 2008). Under normal conditions, the kinase activity is regulated by the GTP binding capacity of LRRK2, rather than GTP hydrolysis (West et al., 2007; Taymans et al., 2011). Hence, mutations in the GTPase domain may impact drastically on the kinase domain, either by inactivating the kinase activity as observed with point mutations K1347A and T1348N, or by augmenting kinase activity as observed with pathogenic mutants in ROC-COR domain. K1347A and T1348N mutants impede GTP binding resulting in an inactivation of the GTPase domain, which abolishes kinase activity downstream (Ito et al., 2007; Jaleel et al., 2007; West et al., 2007). *In vitro* studies have shown that pathogenic mutants R1441C/G/H and Y1699C display increased GTP binding and lower GTP

hydrolysis compared to WT LRRK2, resulting in increased kinase activity (Guo et al., 2007; Li et al., 2007). The N1437H mutant shows increased GTP binding but unaltered GTP hydrolysis activity (Aasly et al., 2010), although a recent study suggests that alterations of the kinase activity with this mutation might be due to conformational changes rather than GTP binding (Huang et al., 2019).

LRRK2 is a threonine/serine kinase that undergoes autophosphorylation modifying its kinase activity, although generally autophosphorylation events occur at a very low stoichiometry. Pathogenic LRRK2 mutants display increased autophosphorylation of residue S1292 which is reverted upon kinase inhibition; therefore, autophosphorylation of this residue is an indicator of LRRK2 kinase activity (Luzón-Toro et al., 2007; Sheng et al., 2012; Reynolds et al., 2014). Importantly, to date, S1292 is the only autophosphorylation site identified *in vivo* and has been detected in brain, lung and kidney lysates from transgenic G2019S knockin mice (Sheng et al., 2012; Kluss et al., 2018). In addition, *in vitro* kinase assays have identified two autophosphorylation clusters: one in the ROC-COR and the other in the kinase domain; although whether they exist under endogenous conditions remains unclear (Greggio et al., 2008; Kamikawaji et al., 2009; Marchand et al., 2020). Autophosphorylation sites identified in the ROC-COR domain range from residues 1335 to 1510, which form the GTP binding pocket (Gloeckner et al., 2010). Thus, LRRK2 might regulate its own GTPase activity throughout these autophosphorylation sites as several studies have demonstrated that mimicking phosphorylation at residues T1491 or T1503 drastically decreases GTP binding, whereas phosphorylation at T1410 regulates GTP hydrolysis. Other residues have been described as accessory; for example, phosphorylation of S1403, T1404 and T1410 may be necessary for subsequent phosphorylation of T1491 (Greggio et al., 2009; Kamikawaji et al., 2009; Pungaliya et al., 2010; Webber et al., 2011). Altogether, GTPase domain phosphorylation affects GTPase activity (GTP binding and GTP hydrolysis) that eventually may regulate kinase activity. The other autophosphorylation cluster is found in the kinase domain where residues T1967, T1969, T2031, S2032 and T2035 have been identified; although, only T1967, S2032 and T2035 have been found to be relevant for the kinase activity (Greggio et al., 2008; Kamikawaji et al., 2009; Li et al., 2010). Finally, another autophosphorylation residue has been identified in the WD40 domain, T2483, which shows increased autophosphorylation with the different pathogenic mutants *in vitro* (Reynolds et al., 2014). Fig. 6 shows several autophosphorylation sites in red that have been identified consensually by different groups.

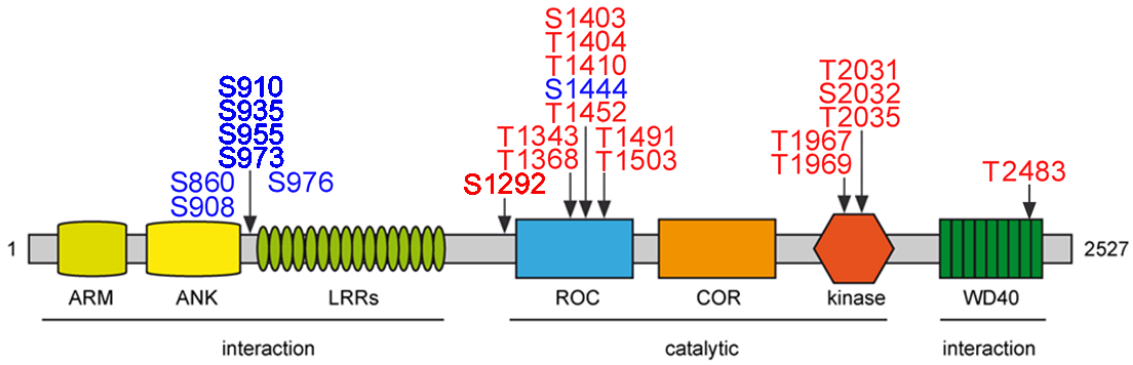

Fig. 6. LRRK2 phosphorylation sites. Schematic representation of some well characterized phosphorylation sites of LRRK2. Cellular sites phosphorylated by external kinases are depicted in blue, and autophosphorylation sites are depicted in red. Phosphorylation sites highlighted in bold are the best characterised and have been confirmed *in vivo*.

Apart from these autophosphorylation sites, there is another cluster of phosphorylation sites (cellular sites) at the N-terminal region of LRRK2 and one in the ROC domain (Fig. 6). Residues S860, S908, S910, S935, S955, S973, S976 and S1444 are phosphorylated by other kinases (PKA, IκB kinase, CK1α) (Dzamko et al., 2012; Chia et al., 2014; Muda et al., 2014) and regulated by cellular phosphatases (PP1, PP2A) (Lobbestael et al., 2013; Athanasopoulos et al., 2016). The phosphorylation status of residues S910/935/955/973 is important for the binding of 14-3-3 proteins and they have been found to regulate cytoplasmic localisation of LRRK2. Indeed, pathogenic mutants or kinase-inhibited LRRK2 show lower phosphorylation of S910 and S935, disrupting 14-3-3 binding and causing a relocalisation of LRRK2 from the cytoplasm and templating onto microtubules (Dzamko et al., 2010; Nichols et al., 2010; Blanca Ramírez et al., 2017). As these cellular sites are rapidly dephosphorylated upon kinase inhibition, S935 has been used as a readout of LRRK2 activity (Vancraenenbroeck et al., 2014).

Since LRRK2 pathogenicity has been linked to increased kinase activity of pathogenic mutants, kinase inhibition has emerged as a potential treatment for LRRK2-related PD. Several research groups and pharmaceutical companies have developed different kinase inhibitors with high potency, selectivity and blood-brain barrier (BBB) permeability. First- and second-generation inhibitors include CZC-25146 by Cellzome (Ramsden et al., 2011), TAE684 (Zhang et al., 2012), LRRK2-IN-1 (IN-1) (Deng et al., 2011) and GSK2578215A (GSK) by GlaxoSmithKline (Reith et al., 2012); these inhibitors were potent and selective against LRRK2, although they failed in their ability to cross the BBB. Third-generation kinase inhibitors brought a set of new compounds with further improved potency, selectivity and importantly with brain permeability, including GNE-7915 and GNE-0877 by Genentech (Estrada et al., 2012;

Estrada et al., 2014), PF-06447475 and PF-06685360 (PFE-360) by Pfizer (Henderson et al., 2015; Baptista et al., 2020), and MLi-2 by Merck (Fell et al., 2015). MLi-2 has been identified as the most potent and selective LRRK2 kinase inhibitor to date. However, long-term drug administration or high doses of GNE-7915, PFE-360 or MLi-2 in nonhuman primates showed histological changes of type II lung pneumocytes (Fuji et al., 2015; Baptista et al., 2020), similar to the phenotype observed in LRRK2 knockout rodent models (Herzig et al., 2011; Baptista et al., 2013; Fuji et al., 2015). Whilst the lung phenotype was reversible after drug removal and was not associated with apparent impairment of lung function, these studies raised potential safety issues. Recently, Denali Therapeutics has developed two new inhibitors, DNL201 and DNL151, which have successfully completed clinical trial phase 1a in healthy volunteers and phase 1b in PD patients without serious side effects encountered (Denali Therapeutics Inc, 2020), and they are currently progressing to phase 2 trials with PD patients.

Apart from pathogenic mutations, genetic studies have also identified polymorphisms which modify risk for PD, and which have been catalogued as risk or protective variants. Two polymorphisms have been identified in the COR domain (R1628P and S1647T) and one in the WD40 domain (G2385R) which have been associated with increased PD risk (Fig. 7) (Mata et al., 2005). G2385R is the most common risk variant and was first identified by Mata and colleagues in 2005 in a family from Taiwan. Different genetic association studies linked it to a 2-fold increased PD risk in Asian populations (Di Fonzo et al., 2006; Funayama et al., 2007; An et al., 2008). The frequency of the G2385R risk variant is around 4-5 % in healthy patients, and up to 15 % in sporadic PD or 23 % familial PD patients. This high frequency and wide distribution across Asian population might be due to its projected early mutation event dated approximately 4800 years ago (Farrer et al., 2007). The second most common risk variant is R1628P, which has also been associated with increased PD risk in Asian populations (Ross et al., 2008; Zhang et al., 2009), with a frequency of around 3 % in healthy patients versus 8 % in sporadic PD patients (Lu et al., 2008; Tan et al., 2008). Clinical features of G2385R and R1628P risk variants are very similar to those observed in sporadic PD (Liang et al., 2018). Finally, an association of the S1647T LRRK2 mutation with PD was confirmed (Zheng et al., 2011), although little is known about this less frequent risk variant that seems not to alter kinase activity (Tan et al., 2010). The effect of the G2385R mutation on the LRRK2 kinase activity has been controversial; some studies have shown that it has decreased kinase and increased GTPase activity as compared to wildtype LRRK2 (Rudenko et al., 2012; Ho et al., 2016), although a recent study suggests that it displays increased kinase activity, even though also

decreased stability (Leandrou et al., 2019). The R1628P variant may increase the LRRK2 kinase activity by causing its phosphorylation by another unknown kinase (Shu et al., 2016). Recent studies have shown that risk variants induce subtle kinase activity changes that may have an impact in cells *in* vivo (Christensen et al., 2018; Leandrou et al., 2019).

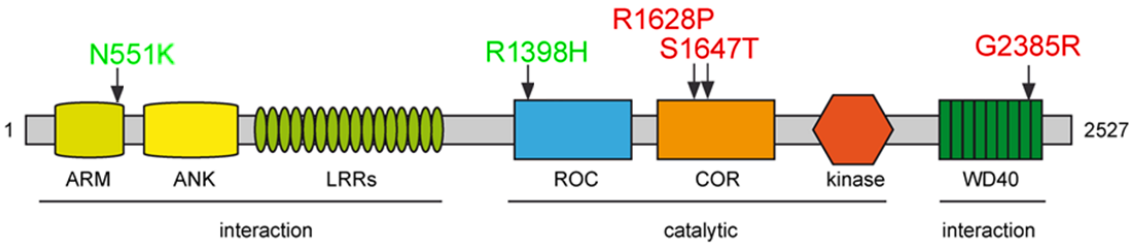

Fig. 7. LRRK2 polymorphisms that modify PD risk. Schematic representation of identified polymorphisms that modify risk for PD, protective variants are depicted in green and risk variants in red.

Conversely, two polymorphisms, one located in the ARM domain (N551K) and another one in the ROC domain (R1398H), decrease risk for PD indicating that they play a protective role (Fig. 7) (Mata et al., 2005; Tan et al., 2010; Chen et al., 2011). Genetic studies have also identified a protective haplotype in some families with N551K/R1398H/K1423K substitutions (Ross et al., 2011). The residue R1398 is located in the Switch II motif of the ROC domain; in small GTPases, the equivalent Switch II motif is highly conserved and functionally important. The R1398H LRRK2 mutation has been shown to cause a decrease in GTP binding and enhance GTP hydrolysis, which thereby downregulates the LRRK2 kinase activity (Nixon-Abell et al., 2016; Blanca Ramírez et al., 2017). T1343 is a residue located in the P-loop of LRRK2, and the equivalent P-loop in small GTPases is also crucial for GTP binding/hydrolysis. Synthetic mutations in those two residues in LRRK2 (R1398L and T1343V) have also been employed to show that R1398L and R1398L/T1343V attenuate kinase activity when combined with pathogenic mutants (Xiong et al., 2010; Biosa et al., 2013). Thus, these studies indicate that the R1398H variant may be playing a protective role by decreasing the LRRK2 kinase activity.

2.2. Functions

Understanding the cell biological functions of LRRK2 has been the focus of many studies in the field. LRRK2 is widely expressed in many cell types and tissues, and can be found in the cytosol or associated with various subcellular compartments including endosomes, lysosomes, mitochondria, Golgi apparatus, centrosomes and microtubules (Fig. 8) (Biskup et al., 2006; Hatano et al., 2007; Alegre-Abarrategui et al., 2009; Berger et al., 2010). In addition, membrane-bound LRRK2 seems to be more catalytically active than cytosolic LRRK2. Such wide subcellular distribution and membrane association indicates that LRRK2 may play a role in membrane trafficking events.

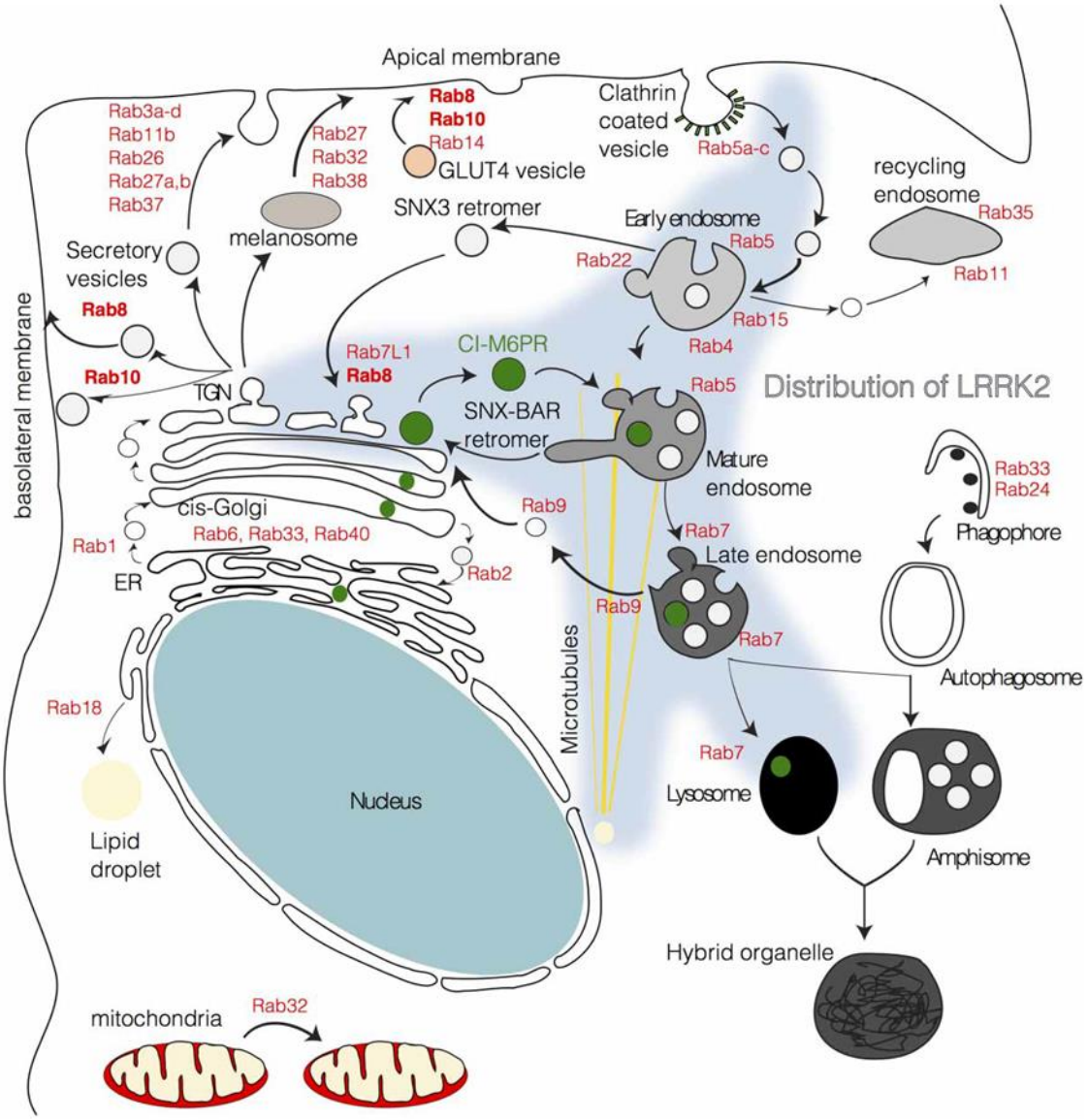

Fig. 8. Cellular distribution of LRRK2. Generic representation of different membrane trafficking events indicating some of the RAB proteins implicated in the processes. Localisation of LRRK2 is represented by a light blue shadow. From (Cookson, 2016).

2.2.1. Membrane trafficking

Membrane trafficking is a highly regulated and interdependent process that englobes exo- and endocytosis, retrograde trafficking between the Golgi and the endosome, autophagy and endolysosomal trafficking as well as other membrane transport events. Importantly, it is well established that alterations in autophagy and lysosome biology are associated with different forms of PD (Beilina and Cookson, 2016).

Endocytosis and endolysosomal trafficking

Endocytosis regulates plasma membrane composition by establishing a recycling turnover of transmembrane proteins, and allows for the internalisation of extracellular molecules. The endocytic pathway comprises a series of vesicular compartments and trafficking steps (Hu et al., 2015). Endosomes are dynamic structures that undergo morphological changes during their maturation process, including increment of vesicular structures, decrease in pH, and subcellular relocalisation from plasma membrane toward the centrosome (Huotari and Helenius, 2011). These membrane trafficking and sorting steps are coordinated by distinct RAB proteins, a family of small GTPases, and the different RAB proteins can be used as markers for the distinct endosomal compartments (Stenmark, 2009).

Endocytosis commences with the engulfment of the extracellular material or transmembrane receptors via clathrin-mediated endocytosis, clathrin-independent endocytosis, pinocytosis or phagocytosis. The vesicles which bud off from the plasma membrane instantly fuse with each other or with already existing early endosomes, a process which is controlled by the RAB5 GTPase (Li, 2012). Early endosomes act as intermediate station from where receptors can follow two paths: either recycling or degradation. Vesicles containing receptors can be generated from the early endosome and recycled directly back to the plasma membrane (process known as fast recycling pathway), or they can traffic to the endocytic recycling compartment (ERC) (RAB8 and RAB10-positive) from where cargoes will return back to the plasma membrane (process known as slow recycling pathway). These recycling pathways are controlled by RAB4 and RAB11 GTPases respectively (Sönnichsen et al., 2000). The ERC is a compartment of tubular shape that is in close contact with the centrosome, specifically with subdistal appendages of the mother centriole, and which regulates the recycling of several proteins and receptors such as TfR and EGFR

(Hehnly et al., 2012; O'sullivan and Lindsay, 2020). The recycling through the ERC is mastered by RAB GTPases, concretely RAB8, RAB11 and RAB35 (Rozés-Salvador et al., 2020).

The degradative pathway occurs when early endosomes mature into late endosomes, a process which involves the generation of intraluminal vesicles inside the late endosome (also called multivesicular body (MVB)), acidification of the lumen and RAB5 replacement by RAB7, a transition known as RAB conversion (Rink et al., 2005; Hu et al., 2015). Finally, late endosomes relocate to a perinuclear area by moving along microtubules where they can fuse with other late endosomes to form larger compartments and/or fuse with a lysosome for final proteolytic degradation (Huotari and Helenius, 2011). Subsequently, degraded products are liberated into the cytoplasm and lysosomes reform by extrusion of tubular structures (proto-lysosomes) that eventually mature into new functional lysosomes (Chen and Yu, 2017).

Various studies demonstrate that LRRK2 interacts directly or functionally with different proteins throughout the endocytic pathway, and that altered expression or pathogenic mutants disrupt early steps of vesicle trafficking and/or late steps of protein degradation (Erb and Moore, 2020; Rivero-Ríos et al., 2020a). Alteration of LRRK2 kinase activity causes an impairment of synaptic vesicle endocytosis in primary neurons. Shin et al. showed a direct interaction between LRRK2 and RAB5B, and that the synaptic vesicle endocytosis defect was rescued upon RAB5B overexpression (Shin et al., 2008; Arranz et al., 2015). LRRK2 also affects late endosome trafficking in a RAB7-dependent manner. Pathogenic LRRK2 causes a slight delay in early-to-late endosome conversion and a drastic delay in late endosome trafficking, increased lysosomal pH, elongated tubular late endosomes and a disruption of proper lysosomal protein degradation (Higashi et al., 2009; Gómez-Suaga et al., 2014; Schapansky et al., 2018; Rivero-Ríos et al., 2019; Wallings et al., 2019).

Retrograde trafficking

Some proteins including endolysosomal hydrolases are synthesized in the Golgi and trafficked to the late endosome via binding to the mannose-6-phosphate receptor (M6PR). This receptor needs to be recycled back to the Golgi, and such recycling is mediated by different multiprotein complexes including retromer complex and Golgi-associated retrograde protein (GARP) complex (Seaman et al., 1998; Conibear and Stevens, 2000).

The retromer complex consists of two protein structures: the cargo-selective complex (CSC), comprising a heterotrimer of the vacuolar protein sorting-associated proteins VPS35-VPS29-VPS26, and the sorting nexin complex (SNX), a heterodimer of the sorting nexins SNX1/SNX2 and SNX5/SNX6 (Seaman, 2012). Retromer location is mainly endosomal and its recruitment is at least in part regulated by RAB7, which binds to VPS35 and promotes the recruitment of the other components of the retromer complex (Rojas et al., 2008; Seaman et al., 2009; Priya et al., 2015). Retromer also interacts with a wide variety of cargo proteins at the endosomal membrane and the CSC has been implicated in many cellular processes. Interestingly, alterations in CSC function have being associated with some diseases (diabetes, AD and PD) (Burd and Cullen, 2014).

VPS35 is essential for CSC function and mutations in VPS35 cause late-onset autosomal dominant PD, although the precise mechanism for pathogenicity remains largely unclear (Vilariño-Güell et al., 2011; Zimprich et al., 2011). The disease-causing D620N-VPS35 mutation does not seem to affect CSC function, but overexpression of D620N-VPS35 in rodent models induces neuronal cell death (Tsika et al., 2014). Recent studies indicate that it may cause PD by activating LRRK2. Studies in MEFs carrying D620N-VPS35 mutation display a hyperactivation of LRRK2 which is even greater than that observed with pathogenic LRRK2 mutations, causing an increase in phosphorylated RAB10 and LRRK2 autophosphorylation that is reverted upon kinase inhibition with MLi-2 (Mir et al., 2018; Chen et al., 2019).

The GARP complex consists of a heterotetramer of VPS51-VPS52-VPS53-VPS54 and shares high similarity with the endosome-associated retrograde protein (EARP) complex. Indeed, EARP complex shares VPS51, VPS52 and VPS53 subunits, together with VPS50. Both complexes regulate the tethering of retrograde vesicles, the GARP complex at the TGN, and the EARP complex at recycling endosomes (Liewen et al., 2005; Schindler et al., 2015). To a lesser extent, the GARP complex has been found at recycling endosomes where together with EARP complex it may participate in the recycling of transferrin receptor (TfR) to the plasma membrane (Schindler et al., 2015). At the TGN, the GARP complex regulates the retrograde trafficking of the M6PR, TGN46 and Niemann-Pick C2 protein from endosomes to the TGN (Pérez-Victoria et al., 2008; Wei et al., 2017). Mutations and alterations of the GARP complex result in lysosomal and autophagy dysfunction, and have been associated with a series of neurodevelopmental disorders including progressive cerebello-cerebral atrophy type 2 (PCCA2), microcephaly and amyotrophic lateral sclerosis (ALS) (Khakurel et al., 2020).

Recently, the GARP complex has been reported to interact with LRRK2 and RAB29. LRRK2 and RAB29 would act as scaffold proteins interacting with GARP component VPS52 and stabilizing GARP-SNARE association at the TGN to promote vesicle trafficking and fusion (Beilina et al., 2020). Knockdown of RAB29 decreases retrograde transport and causes an abnormal accumulation of M6PR at endosomes (Wang et al., 2014b; Beilina et al., 2020). In addition, pathogenic R1441C LRRK2 deregulates retrograde and anterograde transport as observed in primary astrocytes from R1441C knockin mice (Beilina et al., 2020). Similarly, pathogenic G2019S LRRK2 expression in rat primary neurons provokes lysosomal swelling and disrupts M6PR recycling, which is reverted upon overexpression of RAB29 or VPS35 (MacLeod et al., 2013). Therefore, these data support the role of LRRK2 in retrograde trafficking in a manner mediated by VPS35 and RAB29.

LRRK2 may also regulate retrograde trafficking through direct interactions with other members of the RAB32-subfamily (RAB29, RAB32 and RAB38) via its ARM domain. RAB32 and RAB38 complex with SNX6 and regulate retrograde transport of M6PR; and LRRK2 interacts with RAB32 and RAB38, although whether they exist together as a complex remains unknown (Waschbüsch et al., 2014; Waschbüsch et al., 2019; McGrath et al., 2021).

Autophagy

Autophagy is a highly regulated event that maintains cellular homeostasis through degradation of dysfunctional/damaged organelles and misfolded, aggregated proteins. There are three types of autophagy: microautophagy, chaperone-mediated autophagy (CMA) and macroautophagy (Hou et al., 2020). Microautophagy is the less-known mechanism of autophagy and it involves the invagination of the lysosome membrane to engulf small portions of cytoplasm and cytosolic macromolecules. CMA degrades proteins and cellular components that are selectively transported to lysosomes by chaperones, such Hsc-70, and lysosomal membrane receptor, LAMP2A (Roosen and Cookson, 2016). Pathogenic mutations of LRRK2 inhibit the CMA pathway and induce accumulation of membrane-bound LAMP2A lysosomes in brains and iPSC-derived DA neuron cultures from LRRK2 transgenic mice and PD patients, respectively (Orenstein et al., 2013; Ho et al., 2020).

Macroautophagy, henceforward called autophagy, is a tightly coordinated event that starts with the formation of the phagophore, followed by enlargement and surrounding of for example a defunct organelle to form an autophagosome. Finally, this autophagosome fuses directly with a lysosome to degrade the cargo, or with a late endosome to form an amphisome which then ends up fusing with a lysosome (Roosen and Cookson, 2016). Several studies have associated autophagy alterations with PD, and numerous alterations have been described for the different PD genes. Pathogenic LRRK2 also causes alterations in the autophagy-lysosomal system. However, autophagy is a complex cellular process, and the effects of LRRK2 on either enhancing or inhibiting autophagy, and the underlying mechanisms remain controversial and largely unknown, possibly due to the variety of LRRK2 models and approaches employed in these studies (Madureira et al., 2020).

2.2.2. Signalling pathways

Signal transduction in cells is relevant for proper cell maintenance and for many cell biological processes. Signalling pathways are often controlled by a series of kinases and GTPases, and mutations in those proteins can alter signalling cascades and have been associated with several diseases (Berwick and Harvey, 2011). The domain structure of LRRK2 implies that it could function as a regulator for signalling pathways either mediated by its kinase or GTPase activities, or mediated by regulating protein-protein interactions as a scaffolding protein. Indeed, LRRK2 has been suggested to play a role in different signalling pathways including MAPK and Wnt signalling cascades.

LRRK2, MAPK signalling pathway and Parkinson's disease

The mitogen-activated protein kinase (MAPK) signalling pathway is an intracellular pathway that receives extracellular signals and regulates the response through different cascades. The MAPK pathway can regulate cell differentiation and proliferation, migration or inflammation amongst other functions (Pearson et al., 2001). In mammals, four distinct groups of MAPKs have been identified: extracellular signal-regulated kinase 1 and 2 (ERK), p38 MAPK, c-Jun NH_2-terminal kinases 1, 2 and 3 (JNK) and ERK5 (Berwick and Harvey, 2011). Dysregulation of MAPK cascades has been associated with the pathogenesis of various neurodegenerative disorders

(AD, PD and ALS) (Kim and Choi, 2010). For example, α-syn accumulation has been reported to activate ERK, p38 and JNK pathways in microglia and astrocytes, causing a chronic inflammation which may eventually induce apoptosis of neighbouring DA neurons (Zhang et al., 2005; Klegeris et al., 2006; Klegeris et al., 2008). Additionally, distinct neurotoxins and pesticides (MPTP, 6-OHDA, rotenone, paraquat) may induce cell death of DA neurons in animal models of PD and DA SH-SY5Y cells through activation of the JNK and p38 pathways (Saporito et al., 2000; Newhouse et al., 2004; Peng et al., 2004; Ouyang and Shen, 2006).

The link between LRRK2 and MAPK signalling pathways remains controversial. On the one hand, overexpression of WT or pathogenic LRRK2 mutants did not cause a significant increase in p-ERK, suggesting that the LRRK2 kinase activity does not modulate the ERK pathway, but that regulation may occur in its role as a scaffolding protein (Berwick and Harvey, 2011). On the other hand, it has been demonstrated that LRRK2 acts as a MAPKKK by phosphorylating apoptosis signal-regulating kinase 1 (ASK1), MKK3/6 and MKK4/7 *in vitro*, which then presumably will phosphorylate and activate p38 and JNK pathways respectively (Gloeckner et al., 2009; Yoon et al., 2017). Further studies *in vivo* showed that G2019S LRRK2 phosphorylates MKK4 and activates the JNK pathway, causing a degeneration of DA neurons of SNpc in transgenic mice (Chen et al., 2012). Additionally, biochemical assays demonstrated that LRRK2 binds to MKK3, MKK6 and MKK7, and JNK-interacting proteins 1-4 (JIPs) (Hsu et al., 2010b; Hsu et al., 2010a). Indeed, overexpression of MKK6 recruits LRRK2 to membrane compartments, and LRRK2 acts as a scaffolding protein by binding to the different components of the ASK1-MKK3/6-p38 MAPK cascade (Hsu et al., 2010a; Yoon et al., 2017). Altogether, whilst further work is required, the current data suggest that LRRK2 may regulate different MAPK pathways, and that pathogenic LRRK2 may contribute to MAPK-mediated neuroinflammation and subsequent DA neurodegeneration.

LRRK2, Wnt signalling and Parkinson's disease

The Wingless/Int (Wnt) signalling pathway is a well-conserved intracellular pathway that regulates animal embryogenesis and adult neurogenesis, cancer biology and neuronal function by affecting transcriptional activity and cytoskeleton stability (Freese et al., 2010; Zhang et al., 2011). There are three signalling cascades: the canonical Wnt/β-catenin, planar cell polarity (Wnt/PCP) and calcium-dependent (Wnt/Ca^{+2}) pathways. Alterations in Wnt signalling have been associated with a wide

variety of human diseases ranging from cardiovascular, renal, hepatic and pulmonary diseases to cancer and neurological disorders (AD, PD, schizophrenia and depression) (Cheng et al., 2007; Königshoff et al., 2008; Maiese et al., 2008; Berwick and Harvey, 2012a; Inestrosa et al., 2012; Voleti and Duman, 2012; Kawakami et al., 2013). Importantly, neurodegenerative disorders have been associated with the loss of DA neurons due to disturbed Wnt signalling. For instance, disruption of parkin expression activates Wnt/β-catenin pathway inducing ventral midbrain DA neuronal cell death (Rawal et al., 2009).

Under basal conditions of the canonical pathway, β-catenin is constitutively phosphorylated by glycogen synthase kinase 3β (GSK3β), then ubiquitinated by parkin and targeted for proteosomal degradation. Activation of Wnt/β-catenin pathway represses phosphorylation, ubiquitination and degradation of β-catenin, allowing its translocation to the nucleus and inducing expression of different transcription factors. LRRK2 acts as a scaffolding protein in both basal and activated conditions (Berwick and Harvey, 2014). However, alterations in LRRK2 expression or activity may regulate the Wnt signalling pathway. Pathogenic mutants or LRRK2 risk variants further enhance β-catenin degradation, while knockdown or protective variant LRRK2 induce activation of Wnt signalling (Berwick and Harvey, 2012b; Nixon-Abell et al., 2016; Berwick et al., 2017). Moreover, LRRK2 also interacts with different components of the Wnt/PCP cascade and has been suggested to act as a modulator between Wnt/β-catenin and Wnt/PCP pathways (Salašová et al., 2017). Taken together, these data suggest a role for LRRK2 in the different Wnt signalling pathways.

2.3. LRRK2 interactors and regulators

Due to the presence of four protein-protein interaction domains, its expression in many distinct cell types, and its ubiquitously intracellular localisation, it is unsurprising that LRRK2 may interact with a wide variety of proteins. Several studies along the years have been cataloguing an enormous number of interactors for LRRK2 in public interaction databases. At the time of writing this dissertation, there are 4930 annotations in IntAct database, reporting interactions with 2350 proteins. However, most of these interactors have been described in only one publication, using a single detection method, using truncated forms of LRRK2, or based solely on *in vitro* observations (Gloeckner and Porras, 2020). In 2015, Manzoni and colleagues performed an extensive curation of all the existing interactions that were annotated

by that date and came up with a reduced list of 62 proteins. These proteins belonged to different families: heat-shock protein 90 family, tubulin and actin families, Rho family, STE Ser/Thr protein kinase family, dynamin-like GTPase family, Dishevelled family, 14-3-3 family and RAB GTPase family, amongst others (Manzoni et al., 2015).

Many studies have established an interaction between LRRK2 and different members of the cytoskeleton, including microtubules and filamentous actin. Microtubules are heterodimers of α/β-tubulin, that undergo post-translational modifications such as acetylation or detyrosination (both associated with stable microtubules) (Civiero et al., 2018). LRRK2 interacts with α/β-tubulin heterodimers through the ROC domain in a guanine nucleotide state-independent manner (Gandhi et al., 2008). Moreover, LRRK2 can phosphorylate β-tubulin *in vitro*, and this phosphorylation is enhanced by G2019S mutation, which may cause an alteration in microtubule dynamics (Gillardon, 2009). Interestingly, the LRRK2 association with microtubules is enhanced by pathogenic LRRK2 ROC/COR mutants and by pharmacologically kinase-inhibited LRRK2 (Dzamko et al., 2010; Kett et al., 2012). Mechanistically, Blanca Ramírez and colleagues demonstrated that LRRK2 binds preferentially to stable microtubules and that this interaction is modulated by GTP binding (Blanca Ramírez et al., 2017). In addition, cryo-electron tomography ultrastructural studies showed that LRRK2 forms a double helix around microtubules (Deniston et al., 2020; Watanabe et al., 2020). This LRRK2 conformation around microtubules has been reported to interfere with proper retrograde and anterograde transport along microtubules (Deniston et al., 2020).

Interaction of LRRK2 with different members of the RAB GTPase family had been described above. Briefly, LRRK2 had been reported to interact with RAB5 and RAB7 which regulate endocytic trafficking events (Shin et al., 2008; Higashi et al., 2009; Gómez-Suaga et al., 2014) and with members of the RAB32 subfamily (RAB29, RAB32 and RAB38) which control different aspects of retrograde transport. In addition, RAB29 recruits LRRK2 to the TGN which can hyperactivate the LRRK2 kinase activity (MacLeod et al., 2013; Waschbüsch et al., 2014; Liu et al., 2018). Finally, LRRK2 interacts with a subset of RAB proteins which also serve as kinase substrates and will be described further below.

2.4. LRRK2 kinase substrates

The emerging role of LRRK2 in PD pathogenesis has directed the LRRK2 research field towards the identification of physiological LRRK2 kinase substrates during the past years. Identification of LRRK2 substrates is of great importance to allow for the measurement of pathogenic kinase activity in PD patients, and to determine on-target effects of kinase inhibitors in clinical trials. Many proteins have been identified as LRRK2 substrates in relation to the functions described above, such as microtubule-associated proteins (MAPs) (moesin, β-tubulin, tau, microtubule affinity-regulated kinase 1 (MARK1) and Futsch) (Jaleel et al., 2007; Gillardon, 2009; Lee et al., 2010; Kawakami et al., 2012; Krumova et al., 2015), transcription and translation machinery proteins (FoxO1, 4E-BP1 and ribosomal protein s15 (RSP15)) (Imai et al., 2008; Kanao et al., 2010; Martin et al., 2014), LRRK2 GTPase activating proteins (GAPs) (ArfGAP1 and RGS2) (Xiong et al., 2012; Dusonchet et al., 2014), and synaptic transmission proteins (endophilin A1, snapin, N-ethylmaleimide sensitive fusion (NSF) and synaptojanin-1) (Matta et al., 2012; Yun et al., 2013; Belluzzi et al., 2016; Islam et al., 2016). However, most of these proteins have been described to be phosphorylated only in *in vitro* experiments or in LRRK2 overexpressing cell models, and there currently exists a lack of *in vivo* confirmation for many of these putative substrates.

A breakthrough phosphoproteomic analysis combined with genetic and pharmacological approaches identified unambiguously that LRRK2 phosphorylates a subset of RAB GTPase proteins. Assays were performed in murine embryonic fibroblast (MEFs) from G2019S LRRK2 knockin mice compared to wildtype, LRRK2 knockout or inhibitor-resistant A2016T LRRK2 knockin MEFs in the presence or absence of three structurally distinct LRRK2 kinase inhibitors. Four RAB proteins were identified (RAB3A, RAB8A, RAB10 and RAB12) as key substrates of LRRK2 (Steger et al., 2016). Interestingly, all pathogenic mutants displayed enhanced phosphorylation of RAB proteins *in vivo*. A further systematic proteomic analysis of the RAB GTPase family revealed that 14 RAB proteins (RAB3A/B/C/D, RAB5A/B/C, RAB8A/B, RAB10, RAB12, RAB29, RAB35 and RAB43) are phosphorylated by LRRK2 in HEK293 cells under co-overexpression conditions. Ten were phosphorylated under pathogenic LRRK2 overexpression and endogenous levels of RAB proteins (RAB3A/B/C/D, RAB8A/B, RAB10, RAB12, RAB35 and RAB43), and only four under endogenous levels of LRRK2 and RAB proteins (RAB8A, RAB10, RAB35 and RAB43) (Steger et al., 2017). These RAB proteins were phosphorylated at an evolutionarily

conserved residue within the Switch II motif (Fig. 9), which is implicated in guanine nucleotide exchange and binding to regulator and effector proteins. Phosphorylation of this region in LRRK2 suggests that it will affect the physiological functions of these RABs (Madero-Pérez et al., 2017).

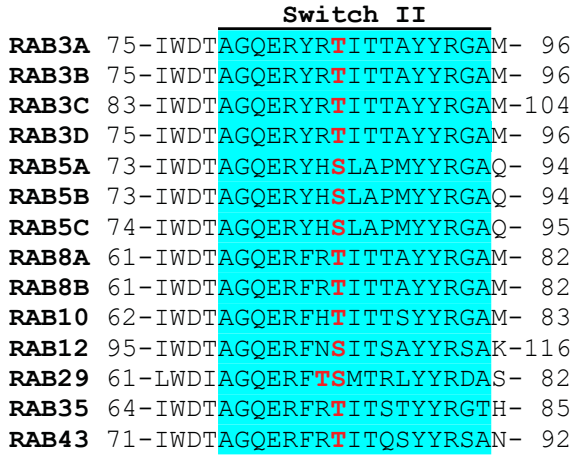

Fig. 9. Sequence alignment of the 14 RAB proteins phosphorylated by LRRK2. Sequences are aligned with respect to Switch II motif. Phosphorylation site of LRRK2 is marked in red and Switch II motif is highlighted in light blue. Adapted from (Lis et al., 2018).

Importantly, other groups have independently validated *in vitro* or *in vivo* the phosphorylation of some of these RAB proteins by LRRK2. For instance, RAB3C, RAB8A/B, RAB10 and RAB35 were confirmed as LRRK2 substrates using *in vitro* kinase assays and *in vivo* when co-expressed with LRRK2 in HEK293 cells (Jeong et al., 2018). In addition, the development of new phospho-state-specific antibodies against the different RAB proteins (Lis et al., 2018) allowed the observation of phosphorylated RAB10 and RAB12 in cultured and immunologically stimulated human peripheral mononuclear blood cells and human peripheral blood neutrophils treated with or without MLi-2 (Thirstrup et al., 2017; Fan et al., 2018).

3. RAB GTPases

The first mammalian RAB proteins were identified around 30 years ago (Touchot et al., 1987). The RAB GTPase family (also known as RAS-related protein family in brain) belongs to the RAS superfamily of small GTPases, and in humans is comprised of more than 70 evolutionary highly conserved members (Szatmári, 2018). RAB proteins are small GTPases consisting of around 200-250 amino acids (approximately 20-25 kDa) which comprise a highly conserved GTPase domain. Although RAB proteins share 55-75 % amino acid identity and common structural features, they present a hypervariable C-terminal region which helps to determine their subcellular location (Szatmári, 2018; Homma et al., 2021). RAB proteins are localised at the cytoplasmic face of vesicles and peripheral membranes, where they function as the master regulators of membrane trafficking events, such as vesicle budding, tethering, transport and membrane fusion. By regulating membrane trafficking, RAB GTPases are also crucial for various specialised cellular functions (Guadagno and Progida, 2019; Homma et al., 2021).

In order to regulate membrane trafficking events, RAB GTPases are inserted into membranes in a tightly regulated process which first involves their prenylation. RAB proteins contain one or two cysteine residues at the very C-terminal end of the protein. When RAB proteins are synthesised, they bind to RAB escort proteins (REP1/2). The RAB-REP complex is then recognised by geranylgeranyl transferase type II (GGTII) which transfers prenyl groups to the cysteine(s) of the prenylation motif. Then, RABs are delivered to a membranous compartment where they dissociate from REPs and are inserted into the membranes through their hydrophobic anchors (Fig. 10) (Madero-Pérez et al., 2017).

Similar to other small GTPases, RAB proteins function as molecular switches by cycling between active GTP-bound and inactive GDP-bound states, with the GTP-bound form interacting with distinct effector proteins to regulate multiple steps of membrane trafficking. The RAB GTPase cycle between these two states is facilitated by regulatory proteins such as guanine nucleotide exchange factors (GEFs) which activate RABs by exchanging GDP for GTP, and GTPase-activating proteins (GAPs) which inactivate RABs by stimulating its GDP dissociation and GTPase activity. The GTPase cycle also includes a membrane association and dissociation cycle which is mediated by GDP dissociation inhibitors (GDIs). GDIs extract RAB proteins from the membrane and keep them soluble in the cytosol, and later also deliver them to the membrane compartment where they are activated by a GEF (Fig. 10) (Banworth and Li, 2018; Szatmári, 2018; Guadagno and Progida, 2019).

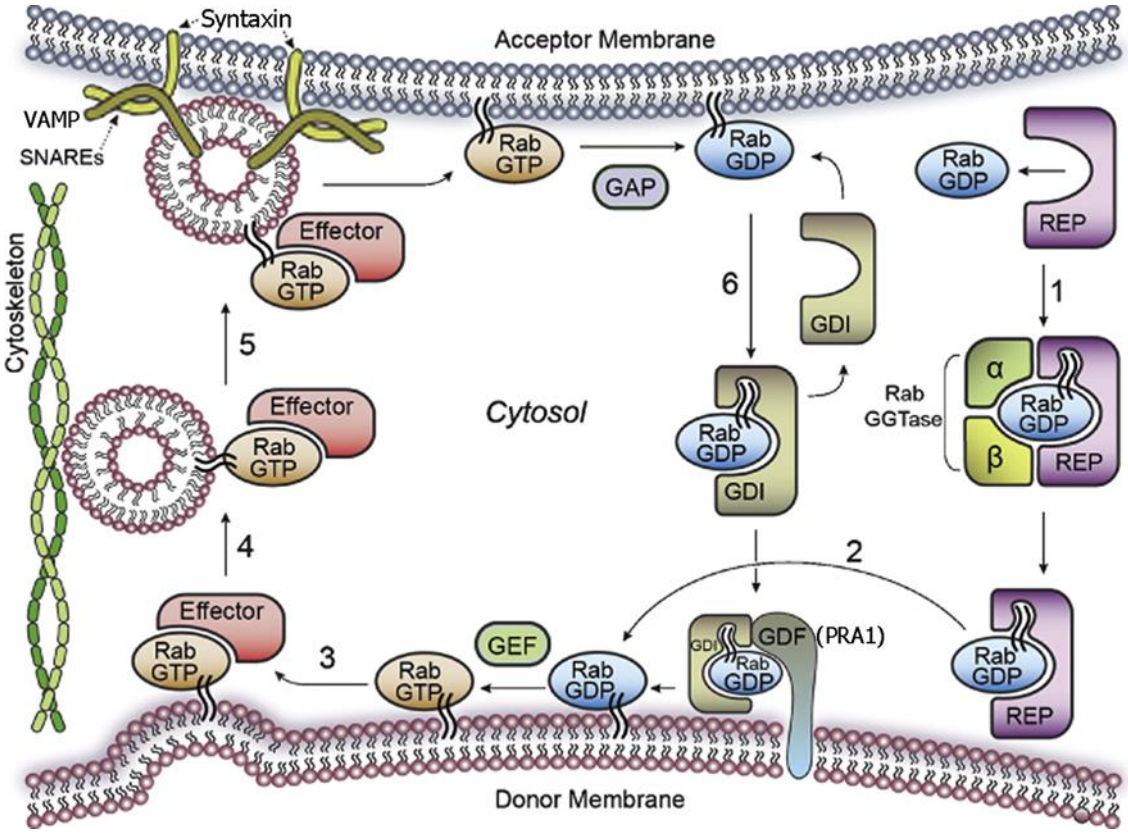

Fig. 10. RAB GTPase cycle. From (Wang and Deretic, 2014)

With such important role in membrane trafficking, it is not surprising that dyshomeostasis of RAB protein function by various means is associated with a wide variety of inherited disorders and diseases including diabetes, cancer and neurodegenerative diseases (Huntington's disease (HD), Charcot-Marie-Tooth disease (CMT), ALS, AD and PD) (Madero-Pérez et al., 2017; Banworth and Li, 2018; Guadagno and Progida, 2019). Indeed, mutations in RAB32 have been associated with late-onset autosomal dominant familial PD (Gustavsson et al., 2017), mutations in RAB39B cause early-onset X-linked recessive familial PD with intellectual disability (Wilson et al., 2014; Lesage et al., 2015), and genetic variants of RAB29 modify risk for developing PD (Simón-Sánchez et al., 2009; Chang et al., 2017). In addition, and as described above, the PD-related kinase LRRK2 has been reported to phosphorylate a subset of RAB proteins including RAB3A/B/C/D, RAB8A/B, RAB10, RAB12, RAB35 and RAB43 which is predicted to affect their proper physiological functions (Steger et al., 2016; Steger et al., 2017). The PD-related kinase PINK1 has also been reported to regulate the phosphorylation of RAB8A/B and RAB13 during mitophagy or upon mitochondria depolarisation, even though not directly mediated by PINK1 and requiring further study into potential pathobiological relevance (Lai et al., 2015).

3.1. RAB8

RAB8 was one of the first members of mammalian RAB GTPases identified. In humans, there are two isoforms which show 83 % similarity, RAB8A and RAB8B, and they display a high similarity with the yeast ortholog SEC4 (Chavrier et al., 1990; Armstrong et al., 1996). The two isoforms distribute differently across the human body; RAB8A is expressed mainly in lung and kidney, while RAB8B is more abundant in heart, spleen and brain. RAB8 belongs to RAB8 subfamily, which based on their high similarity and homology includes RAB8A/B, RAB10 and RAB13 (Ward and Wandinger-Ness, 2018).

As with other RAB proteins, RAB8 cycles through active GTP-bound and inactive GDP-bound states. Activation of membrane-bound RAB8 may occur through one of its several GEFs such as Rabin8/Rabin3, MSS4, retinitis pigmentosa GTPase regulator (RPGR), Rabin3-like GRAB, or C9ORF72 (Sellier et al., 2016; Ward and Wandinger-Ness, 2018). Upon completion of its function, RAB8 inactivation may be facilitated by generic RAB GAPs of the TBC (Tre-2/Bub2/Cdc16) protein family such as TBC1D1, TBC1D4 or TBC1D17, or the specific RAB8 GAP TBC1D30 (Yoshimura et al., 2007; Ward and Wandinger-Ness, 2018).

RAB8A functions in exocytic events, but also plays a role in endocytic pathways. RAB8A has been reported to be involved in various cellular events including regulation of cell shape, neurite outgrowth, membrane trafficking and primary cilia formation (described below) (Ward and Wandinger-Ness, 2018). RAB8 may play a role in cell morphogenesis and cell migration by reorganising the cytoskeleton; for example, overexpression of RAB8 has been reported to promote cell protrusion formation (Hattula et al., 2006; Peränen, 2011). RAB8A also participates in a number of membrane trafficking events. For example, RAB8A regulates the exocytosis of newly synthesised receptors from TGN to plasma membrane and the delivery of newly synthesised lysosomal enzymes from TGN to lysosomes (del Toro et al., 2009; Sun et al., 2010). RAB8A also regulates the recycling of several receptors and proteins from ERC to plasma membrane; for example, the recycling of TfR is regulated by RAB8A and effector proteins MICAL-L1 and EHD-1, whilst the recycling of junctional proteins (e.g. integrin and e-cadherin) is controlled by RAB8A and its effector MICAL-L2 (Sharma et al., 2009; Rahajeng, 2010).

3.2. RAB10

RAB10 is the closest homolog to RAB8, and was first cloned from Madin-Darby Canine kidney cells (MDCK) (Chavrier et al., 1990). RAB10 is ubiquitously expressed and has been found associated with numerous membranous compartments such as endoplasmic reticulum, TGN, endosomes and primary cilia (Babbey et al., 2010; Chua and Tang, 2018). Thus, and similar to RAB8, RAB10 has been implicated in various membrane trafficking events, including those related to neurite outgrowth and ciliogenesis (Chua and Tang, 2018). RAB10 is crucial for ERC formation and maintenance, and also regulates endoplasmic reticulum dynamics and morphology (English and Voeltz, 2013; Etoh and Fukuda, 2019). In epithelial cells, RAB10 regulates apical and basolateral polarised transport (Babbey et al., 2006). In adipocytes, RAB10 is particularly involved in insulin-induced glucose transport by mediating the exocytosis and recycling of the GLUT4 transporter (Jaldin-Fincati et al., 2017; Brumfield et al., 2021). By regulating membrane trafficking, RAB10 also plays a key role in neuronal polarisation and development, axonal growth and dendritic arborisation (Liu et al., 2013; Zou et al., 2015). Finally, RAB10 co-localises with different components of the exocyst complex at the base of the cilium, which suggests that RAB10 may have a role in the first steps of formation of nascent primary cilia (Babbey et al., 2010). Indeed, knockdown of RAB10 drastically reduces primary cilia biogenesis (Sato et al., 2014) and depletion of RAB10 causes early death of murine embryos (before E9.5) (Lv et al., 2015). Primary cilia are necessary for proper embryonic development (Wheway et al., 2018), and although ciliogenesis could not be investigated in that study, it was suggested that the early embryonic lethality could be due to the lack of primary cilia. Therefore, RAB10 is crucial for primary cilia biogenesis.

3.3. RAB12

RAB12 GTPase was firstly identified in rat brain together with RAB13, RAB14 and RAB15 (Elferink et al., 1992). RAB12 is highly expressed in the brain and mutations in RAB12 have been associated with movement disorders including Musician's dystonia (MD) and Writer's dystonia (WD), although no variants have been identified in PD patients (Hebert et al., 2017). RAB12 is localised to membranous compartments such as Golgi apparatus, endosomes and lysosomes, where it regulates the degradation of transmembrane proteins like TfR (Matsui et al., 2011; Hebert et al., 2017). It has been demonstrated that RAB12 also regulates autophagy, mTORC1 activity and amino acid transport through regulating the degradation of proton/amino acid transporter 4 (PAT4) (Matsui and Fukuda, 2013; Matsui et al., 2014). In all these processes, endogenous RAB12 may be activated by RAB GEF DENND3 as it has been shown to activate RAB12 *in vitro* (Yoshimura et al., 2010).

3.4. RAB35

RAB35 GTPase was cloned in 1994 from human skeletal muscle cells and was found to be ubiquitously expressed (Zhu et al., 1994). RAB35 was firstly called H-Ray and renamed as RAB1C due to its high homology to RAB1A/B. However, later studies showed that there were sequence differences not justifying it´s classification as a RAB1 protein, and it was finally renamed as RAB35, belonging to the RAB1 GTPase subfamily (Klöpper et al., 2012; Klinkert and Echard, 2016).

Several GAPs and GEFs have been described for RAB35 GTPase, with most evidence available for DENDD1A (GEF) and EPI64A-C (GAP) (Klinkert and Echard, 2016). Reported RAB35 GEFs include connecdenn1/DENND1A, connecdenn2/DENND1B and connecdenn3/DENND1C, belonging to DENND1 protein family (DENN domain-containing protein 1), and folliculin (FLCN). Similar to other RABs, the RAB35 GAPs belong to the TBC family and include TBC1D10A-C/EPI64A-C, TBC1D13 and Skywalker/TBC1D24 (Chaineau et al., 2013).

RAB35 localises to plasma membrane and endosomes (Kouranti et al., 2006). RAB35 has a key function in endocytic recycling of several cargoes from endosomes to plasma membrane in tight regulation with its effectors OCRL, MICAL-L1 and ACAP-2 (Klinkert and Echard, 2016). RAB35 GTPase is a unique RAB due to its presence at the plasma membrane. RAB35 has been reported to play roles in cell migration, cell

polarity, cell division, cytokinesis, neurite outgrowth, phagocytosis and at the immunological synapse (Klinkert and Echard, 2016).

3.5. RAB43

RAB43 GTPase belongs to the RAB19 subfamily (Homma et al., 2021), and unlike other RAB GTPases, its function remains poorly understood. RAB43 is localised to the Golgi apparatus and it has been shown to play a role maintaining its structure and integrity (Haas et al., 2007; Cox et al., 2016). Several studies have demonstrated that RAB43 is involved in retrograde and anterograde endoplasmic reticulum to Golgi trafficking (Dejgaard et al., 2008; Li et al., 2017) and retrograde endosome and plasma membrane to TGN transport (Haas et al., 2007). RAB43 has also been described in immunological processes regulating phagosome maturation and antigen presentation by dendritic cells (Seto et al., 2011; Kretzer et al., 2016). A recent study has shown a novel function for RAB43 in regulating post-synaptic trafficking and sorting of G protein-coupled receptors (GPCRs) in neurons (Wei et al., 2021).

3. 6. RAB29

RAB29 GTPase gene (also known as RAB7L1) is localised within the *PARK16* locus and variations in the gene modify risk for PD (Simón-Sánchez et al., 2009; Chang et al., 2017). RAB29 GTPase is of particular interest as it has been described as a LRRK2 interactor. Moreover, GWAS have reported an increased PD risk by association of both genes (Simón-Sánchez et al., 2009).

RAB29 is localised to the Golgi apparatus, at both cis-, medial- and trans- compartments, where it plays a role maintaining Golgi integrity and regulating retrograde transport from endosomes to TGN of certain receptors like M6PR (MacLeod et al., 2013; Wang et al., 2014b). RAB29 acts upstream of LRRK2. In overexpression studies, RAB29 recruits LRRK2 to the Golgi compartment (TGN) and activates the LRRK2 kinase activity (Fujimoto et al., 2018; Liu et al., 2018; Purlyte et al., 2018). However, a recent study in endogenous and RAB29-KO conditions showed that RAB29 does not impact upon LRRK2 kinase activity and phosphorylation of RAB10 or RAB12 (Kalogeropulou et al., 2020).

3.7. RAB kinases and phosphatases

RAB proteins undergo post-translational modifications such as prenylation to be able to be inserted into membranes, as mentioned above. RABs are also phosphorylated as a means to regulate their function, and such phosphorylation is mediated by several kinases and phosphatases (Homma et al., 2021). The first identification of a RAB phosphorylation event dates to 1991, when a study reported the phosphorylation of RAB1 and RAB4 by the mitotic kinase CDK1. Phosphorylation of RAB4 impeded its association with endosomes, thereby pausing membrane trafficking events prior to a cell entering mitosis (Bailly et al., 1991; van der Sluijs et al., 1992). RAB7A is phosphorylated upon epidermal growth factor (EGF) stimulation by an unknown kinase to induce the switch from EGF receptor (EGFR) recycling to rapid degradation of receptors in the lysosomes (Francavilla et al., 2016). The function of RAB7A during EGFR trafficking is also controlled by phosphorylation/dephosphorylation by LRRK1 or PTEN, respectively (Shinde and Maddika, 2016; Hanafusa et al., 2019). On the other hand, RAB7A phosphorylation by TANK-binding kinase 1 (TBK1) is required during PINK1-Parkin-mediated mitophagy (Heo et al., 2018). Protein kinase C (PKC) isoforms are able to phosphorylate a subset of RAB GTPases (RAB6, RAB37, RAB11 and RAB5A) to regulate their cellular function (Homma et al., 2021). Thus, phosphorylation of RAB GTPases modulates their physiological function. However, as mentioned above, phosphorylation of RABs may induce an abnormal dysregulation resulting in diseases such as PD (e.g. LRRK2 phosphorylation of RAB8A and RAB10) (Steger et al., 2017; Madero-Pérez et al., 2018a). Recently, LRRK2 phosphorylated RAB8A and RAB10 have been shown to be specifically dephosphorylated by PPM1H phosphatase (Berndsen et al., 2019).

3.8. Phosphorylated RAB interactors

As described above, RAB proteins decorate distinct organelles and membranes, and can interact with a wide variety of effectors. Such interactions are dependent on the GTP-bound and the post-translational modification state of the RAB protein. The LRRK2-mediated phosphorylation of RAB proteins alters the Switch II motif, which disrupts their interaction with their effectors and with GDI. As a consequence, the phosphorylated RAB proteins get trapped in the membrane, without being able to accomplish their functions via their effectors (Steger et al., 2016; Steger et al., 2017; Gomez et al., 2019). Interestingly, it has been shown that phosphorylated RAB8A and RAB10 lose their ability to bind to their physiological effectors; at the same time, in their phosphorylated state, they acquire the ability to bind to new binding partners. These new effectors include RAB interacting lysosomal-like protein 1 (RILPL1) and RILPL2, which interact with LRRK2 phosphorylated RAB8A and RAB10 (Steger et al., 2017). RILPL1 and RILPL2 are involved in primary cilia biogenesis, and pathogenic LRRK2 mutations have been described to interfere with ciliogenesis by a mechanism that implies the binding of RAB8A and RAB10 to RILPL1, which impedes the recruitment of Tau tubulin kinase 2 (TTBK2), necessary for the removal of CP110 before initiation of ciliogenesis (Schaub and Stearns, 2013; Dhekne et al., 2018; Sobu et al., 2021). Phosphorylated RAB10 may also interfere with primary cilia biogenesis by binding to RILPL2 and sequestering Myosin Va to a pericentrosomal area (Dhekne et al., 2021). A recent study has identified two additional effectors that bind to LRRK2 phosphorylated RAB10, JIP3 and JIP4 (Waschbüsch et al., 2020). Thus, effector proteins of RAB GTPases are important in both normal and pathological conditions and identification of pathogenic effectors may contribute to understand the molecular mechanisms underlying different diseases such as PD (Taylor and Alessi, 2020).

4. Detection of LRRK2 kinase activity as biomarker for LRRK2-related PD

Diagnosis of PD is based on the identification of motor symptoms and, as mentioned above, these motor features only manifest when there exists a 80-85 % deficiency of dopamine in the striatum due to DA neuron degeneration (Cheng et al., 2010). Unfortunately, by the time of diagnosis, the disease progression is unstoppable and therapies are aimed at restoring dopamine levels in the brain. Hence, strategies to develop biomarkers for early diagnosis of the disease are of vital importance. At present, potential clinical biomarkers during the prodromal phase include measurements of olfactory dysfunction, REM sleep behaviour disorder, detectable DA neuron loss as measured by positron emission tomography (PET) and measurements of α-syn from colon biopsies. However, these techniques are not reliable nor specific; for example, PET imaging cannot distinguish from other pathologies associated with DA neuron loss, and α-syn deposits in colon have been also observed in healthy patients (Postuma et al., 2012; Kalia and Lang, 2015).

Since familial PD shares certain molecular pathomechanisms with sporadic PD, monogenic forms of PD may help in the development of biomarkers useful for the whole spectrum of the disease. In this context, pharmaceutical efforts have led to the development of a series of compounds and inhibitors towards the different PD-related kinases and altered pathways. However, and at least in part due to genetic background differences across population, drug therapies are not fully effective and some patients do not respond as expected to validated drugs. Thus, there exists a need to develop biomarkers which help stratify patients who may benefit from specific treatments options (Schlossmacher and Mollenhauer, 2010; Taymans et al., 2017; Trifonova et al., 2020).

Preclinical studies have demonstrated that depletion of LRRK2 or pharmacological LRRK2 kinase inhibition prevent DA neuron loss in mice (Daher et al., 2014; Daher et al., 2015), supporting the idea that under certain circumstances, in the absence of known pathogenic mutations, LRRK2 may be driving disease pathophysiology. In addition, several studies have shown that LRRK2 shares some molecular mechanisms with sporadic PD cases. Given these evidences, it is possible that LRRK2 kinase inhibitors may be suitable therapeutics also for sporadic PD and

other familial PD cohorts (Rideout et al., 2020). Therefore, the research community is focused on the development of LRRK2 biomarkers.

A series of measurements for the LRRK2 kinase activity have been identified that may be useful biomarkers in clinical trials including LRRK2 protein levels, LRRK2 phosphorylation status (S935) or autophosphorylation status (S1292), and detection of phosphorylated LRRK2 substrates (RAB10, RAB12). The methodologies employed to detect these measures include immunoblotting, ELISA-based approaches and quantitative proteomics and phosphoproteomics approaches, depending on the origin of the sample examined. Ideally, samples should be obtained by the least invasive procedure, such that urine or blood are the perfect candidates, since LRRK2 is highly expressed in the kidney, lung and in peripheral immune cells (Rideout et al., 2020).

LRRK2 expression levels vary amongst the different cell types within peripheral blood mononuclear cells (PBMCs), with the higher expression in neutrophils, monocytes and dendritic cells (Dzamko, 2017; Fan et al., 2018). Since LRRK2 levels are heterogeneous across PBMCs, there exists some controversy about significant differences in the levels of LRRK2 in PD patients compared to healthy controls, with some studies showing either an increase or no differences (Dzamko et al., 2013; Cook et al., 2017). In addition, several studies have detected endogenous pS935 LRRK2 in PBMCs, although there was no significant differences in PD samples compared to healthy controls (Delbroek et al., 2013; Dzamko et al., 2013). Moreover, LRRK2 kinase activity does not correlate with levels of pS935 LRRK2 phosphorylation, and some pathogenic LRRK2 mutants can display a decreased S935 phosphorylation status, yet increased kinase activity. However, since pS935 LRRK2 is quickly dephosphorylated upon pharmacological LRRK2 kinase inhibition, it is being used as a pharmacodynamic readout for on-target effects of LRRK2 kinase inhibitors (Dzamko et al., 2010; Ito et al., 2014; Perera et al., 2016).

Currently the best approaches to detect the LRRK2 kinase activity include measurements of S1292 LRRK2 autophosphorylation and substrate phosphorylation. Initially, pS1292 could only be detected in transgenic mouse models overexpressing LRRK2, or in exosomes enriched from urine or cerebrospinal fluid (Sheng et al., 2012; Fraser et al., 2016; Wang et al., 2017). More recent approaches using a fraction-based enrichment method or proximity ligation assays have allowed for the identification of endogenous pS1292 LRRK2 in mouse tissues and in post-mortem brains from sporadic PD patients (Kluss et al., 2018; Di Maio et al., 2018), indicating that

measurement of autophosphorylation of LRRK2 may allow for the identification of LRRK2-driven sporadic PD cases.

LRRK2 substrate phosphorylation represents another potential biomarker to monitor LRRK2 kinase activity. As described above, several RAB GTPases were identified as LRRK2 substrates and a series of phospho-state-specific antibodies for certain RAB proteins have been developed (Steger et al., 2016; Lis et al., 2018). One of the first studies trying to validate RAB proteins phosphorylation as biomarker for clinical trials was in 2017, when researchers could detect endogenous phosphorylated RAB10 and RAB12 upon activation of LRRK2, which was reverted after kinase inhibition (Thirstrup et al., 2017). Later studies tried to correlate an increase in LRRK2 substrate phosphorylation in different PD cohorts. Indeed, initial analysis of a small set of sporadic PD and LRRK2-related PD showed an increase in phosphorylated RAB10 in neutrophils isolated from those patients as compared to healthy controls. However, a larger study involving more patients showed no differences in phosphorylated RAB10 (Fan et al., 2018). Similarly, another study reported no differences in the levels of phosphorylated RAB10 in neutrophils and PBMCs from sporadic PD patients compared to healthy controls (Atashrazm et al., 2019). In either case, both studies reported a decrease in LRRK2 phosphorylated RAB10 upon treatment with LRRK2 kinase inhibitor. Taken together, pS935 LRRK2 seems to be a good biomarker to detect target engagement of LRRK2 kinase inhibitors, and pS1292 LRRK2 and phosphorylated RAB10 and RAB12 seem to be promising biomarkers to measure LRRK2 kinase activity in clinical trials. However, whether these measures can be used to stratify PD patients during clinical trials remains unclear.

5. Centrosome and primary cilium

The centrosome is a non-membranous, structurally complex organelle consisting of two orthogonally-positioned centrioles surrounded by a proteinaceous matrix called pericentriolar material (PCM). Even though its subcellular location within the cell may vary depending on the cell type and function, the centrosome is usually localised in a central position closely apposed to the nuclear membrane, the Golgi complex and the ERC. Centrioles are evolutionary conserved barrel-shaped, microtubule-based structures. In mammalian cells, centrioles are around 230 nm in diameter and 500 nm in length, and are composed of nine triplets of microtubules

(structure 9x3 + 0) organised as a cylinder with proximal-distal polarity. Recent ultrastructural studies have demonstrated that microtubule composition changes along the centriole, with triplet microtubules at the proximal and doublet microtubules at the distal end, respectively (Greenan et al., 2018). Depending on their stage of maturity, centrioles present distal and subdistal appendages, which are therefore generally present at the (mature) mother centriole (Fig. 11). Distal appendages are necessary for the docking of the mother centriole to the plasma membrane during primary cilia biogenesis, while subdistal appendages are required to anchor microtubules during interphase (Breslow and Holland, 2019; Arslanhan et al., 2020).

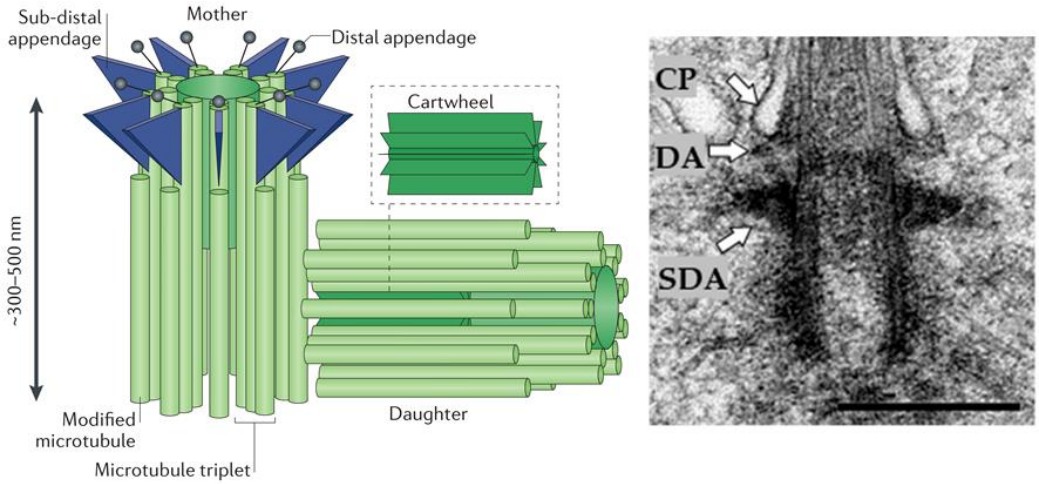

Fig. 11. Centrosome structure. (Left) Schematic representation of a mother centriole with its newly synthesised daughter centriole in engaged configuration. The mother centriole presents proteinaceous structures at its distal part known as distal appendages and subdistal appendages. The newly synthesised daughter centriole is nucleated from the cartwheel structure. During G0 phase, centrioles are disengaged. **(Right)** Electron micrograph of a mother centriole with distal appendages (DA), subdistal appendages (SDA) and a nascent primary cilium, as evidenced by the presence of the ciliary pocket (CP). Scale bar, 400 nm. Adapted from (Conduit et al., 2015; Sullenberger et al., 2020).

In dividing cells, the centrosome duplicates during each cell cycle, a process which is tightly regulated and coupled to cell cycle progression (Fig. 12). During G1 phase and G1-to-S transition, the biogenesis of centrioles is initiated by the recruitment of the master regulator of centriole duplication Polo-like kinase 4 (PLK4) to the pre-existing centriole walls (mother and daughter centrioles). PLK4 phosphorylates and recruits STIL, which at the same time recruits SAS-6 and initiates the assembly of the cartwheel, which acts as structural foundation for the pro-centrioles (Dzhindzhev et al., 2014; Ohta et al., 2014). During S phase and S-to-G2 transition, elongation of pro-centrioles occurs, a process which is regulated by the CEP120-SPICE1-CPAP complex, and ends with the "capping" of the centrioles by CP110 and CEP97 (Schmidt et al., 2009; Comartin et al., 2013). During G2 phase, duplicated centrosomes mature and accumulate more PCM (increase in size), and the original daughter centriole matures and acquires distal and subdistal appendages; maturation of centrosomes is regulated

by PLK1 and Aurora A (AurA). The duplicated mature centrosomes are bound by a centrosomal linker, maintaining centrosome cohesion. In late G2 phase, the proteinaceous linker between the two centrosomes (between original mother and daughter centrioles) is severed and both centrosomes separate (centrosome splitting) to allow for the formation of the mitotic spindle. By the end of mitosis, each new cell receives one of the fully mature centrosomes (Breslow and Holland, 2019; Arslanhan et al., 2020; Jana, 2021).

The proteinaceous linker is composed of several proteins including C-Nap1, rootletin, CEP68, CEP135, LRRC45 and CDK5RAP2 (Bahe et al., 2005; Graser et al., 2007). The centrosome separation occurs at the G2-to-M transition and involves the phosphorylation of C-Nap1, rootletin, CEP68 and LRRC45 by Nek2A kinase, resulting in their displacement from the centrosome and the subsequent centrosome splitting (Faragher and Fry, 2003; Hardy et al., 2014). The activation of Nek2A kinase is tightly regulated by a signalling cascade where PP1 counteracts its function by dephosphorylating centrosomal linker proteins. Alterations in this pathway have been demonstrated to cause a "premature centrosome splitting" (Wang et al., 2014a).

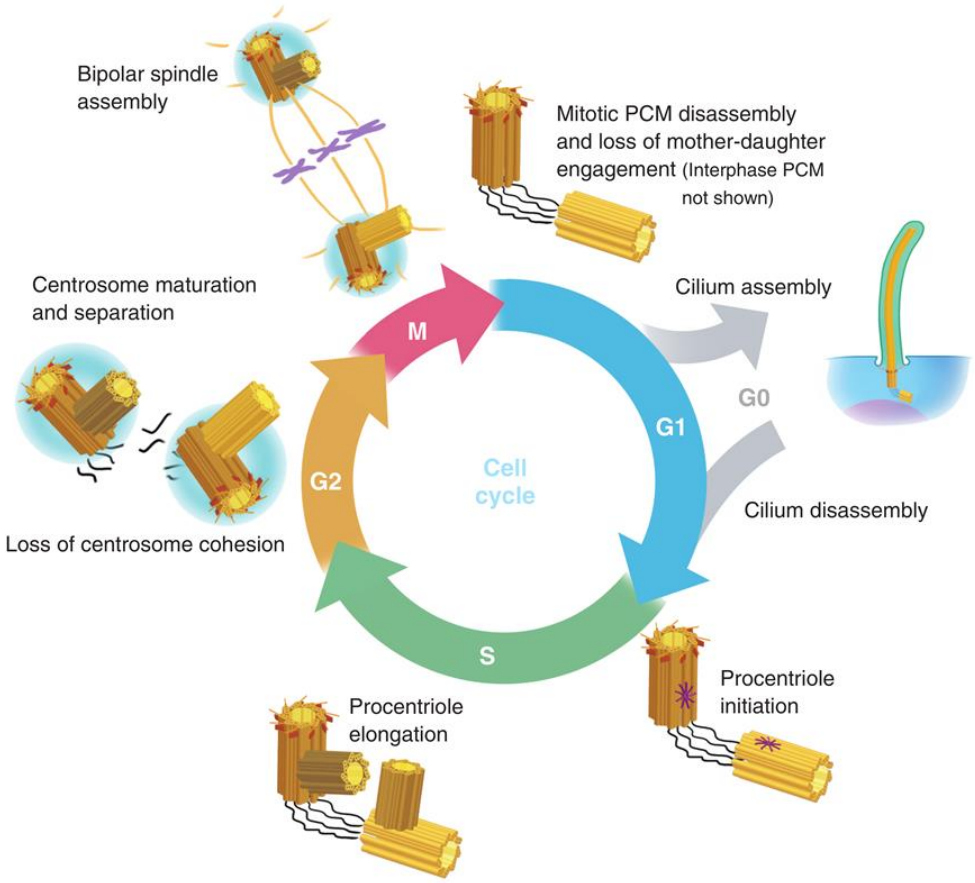

Fig. 12. Centrosome duplication cycle during cell cycle progression. Schematic representation of the duplication cycle of the centrosome. In G0 phase, the centrosome presents a primary cilium. Adapted from (Buchwalter et al., 2016).

In most mammalian cells, the mother centriole constitutes the basal body which is anchored to the plasma membrane through its distal appendages for primary cilium formation. The primary cilium is a non-motile, microtubule-based, sensory organelle surrounded by the ciliary membrane which is in continuum with the plasma membrane. The primary cilium is typically around 350 nm in diameter and 1-10 μm in length (depending on the cell type), and is compartmentalised into distinct regions: the ciliary axoneme, the transition zone and the ciliary pocket. The ciliary axoneme is formed by doublet microtubules at the proximal and singlet microtubule at the distal end, respectively; between the distal end and the ciliary membrane there exists a series of proteins that regulate length and signalling, and it is known as ciliary tip. The transition zone is localised at the base of the primary cilium and is of particular importance for compartmentalisation as it acts as a "diffusion barrier" which regulates the proteins that enter or exit the primary cilium. At the base of the primary cilium there occur an invagination of the plasma membrane known as ciliary pocket, which is important for exo/endocytosis events (Mirvis et al., 2018; Breslow and Holland, 2019; Arslanhan et al., 2020).

Primary cilium biogenesis is a highly regulated process which involves membrane trafficking steps and is initiated at the end of mitosis or when cells exit the cell cycle and enter G0 phase. Ciliogenesis may occur through two distinctive pathways depending on the cell type (Arslanhan et al., 2020). The extracellular pathway involves the docking of the mother centriole to the plasma membrane where it initiates the protrusion of the ciliary axoneme (Fig. 13). The intracellular pathway, on the other hand, involves the recruitment of preciliary vesicles from the Golgi to distal appendages of the mother centriole. These preciliary vesicles fuse to form a ciliary vesicle which comprises the start of the nascent cilium. In this pathway, the mother centriole and the nascent primary cilium migrate to the plasma membrane where the membrane fusion exposes the primary cilium to the extracellular environment (Fig. 13) (Breslow and Holland, 2019; Arslanhan et al., 2020).

In detail, early steps of intracellular ciliogenesis require the recruitment of preciliary vesicles toward the distal appendages of the mother centriole. The preciliary vesicles derive from the TGN, and this transport is regulated and dependent on Myosin Va; in addition, preciliary vesicles may be derived also from the ERC, which is in close contact with the centrosome. Subsequently, EHD1, EDH3 and SNAP29 regulate membrane fusion of the distinct preciliary vesicles to form a larger vesicle known as a ciliary vesicle which is docked to the mother centriole. Then, activation of the ERC-associated RAB11 protein

recruits its effector Rabin8 to the mother centriole which then serves as a GEF that recruits and activates RAB8, essential for the extension of the ciliary vesicle (Westlake et al., 2011; Lu et al., 2015; Wu et al., 2018). At the same time, CP110 is removed from the distal end of the mother centriole to allow for axoneme elongation. CP110 removal is driven by TTBK2 kinase, which binds the distal appendage protein CEP164 and phosphorylates CEP164 and KIF2A (Breslow and Holland, 2019). The RAB11-Rabin8-RAB8 cascade has been demonstrated to regulate the membrane trafficking of primary cilium proteins and receptors required to maintain the mature cilium (Blacque et al., 2018).

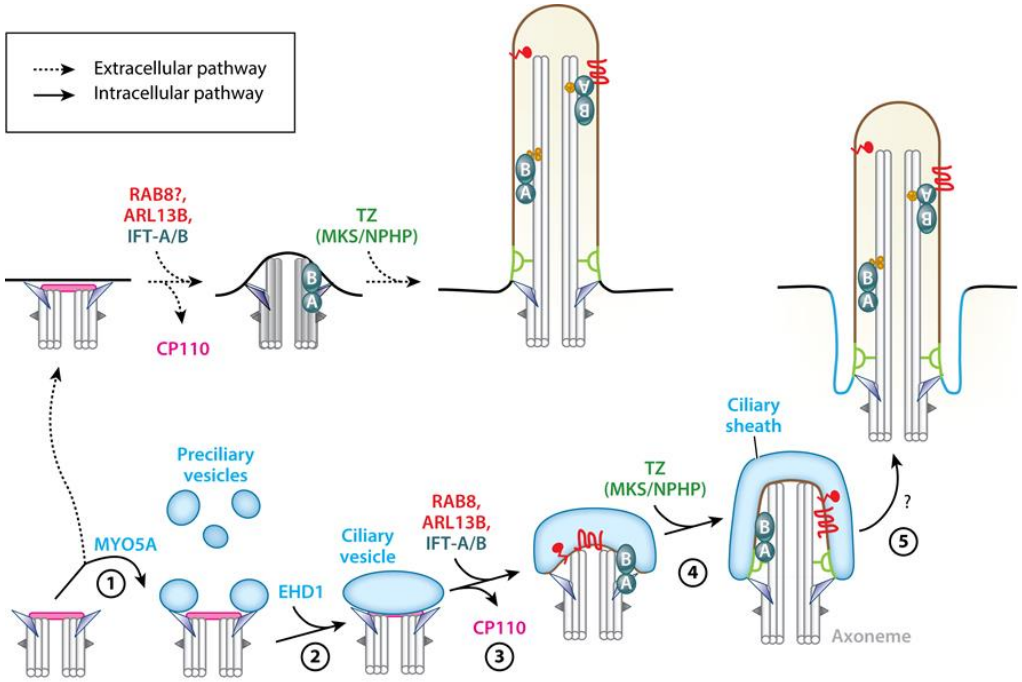

Fig. 13. Primary cilium biogenesis pathways. In the extracellular pathway, the centrosome migrates to the plasma membrane where it initiates the ciliogenesis. In the intracellular pathway, ciliogenesis starts inside the cell and then, the centrosome and the nascent primary cilium migrate to the plasma membrane. From (Breslow and Holland, 2019)

Before the next cell cycle, and prior to entering mitosis, the primary cilium is disassembled; contrary to cilium biogenesis, the mechanism(s) of primary cilium disassembly are less well understood. In mammalian cells, disassembly may occur gradually by resorption of the primary cilium which involves the depolymerisation of the axoneme and endocytosis of the ciliary membrane, or by rapid deciliation caused by "decapitation" of the whole cilium. Recently another disassembly pathway has been described, which is a combination of both gradual and rapid deciliation; this pathway involves the retraction of the axoneme by depolymerisation and "decapitation" of the ciliary membrane. The mitotic kinase AurA is considered the master regulator of primary cilium disassembly, which activates many other factors resulting in ciliary resorption or "decapitation", although the precise mechanism(s) are still unknown (Mirvis et al., 2018; Mirvis et al., 2019; Arslanhan et al., 2020).

5.1. Functions

The centrosome is the major microtubule-organising centre (MTOC) in most animal cells. PCM components serve as scaffold for nucleation and organisation of microtubules. In addition, subdistal appendages of the mother centriole anchor to microtubules during interphase. As MTOC, the centrosome may regulate organelle and vesicle trafficking, cell shape, cell polarity, cell migration and cell division (Woodruff et al., 2014; Mazo et al., 2016).

Positioning of the centrosome within the cell stablish cell polarity. The centrosome is normally located juxtaposed to nuclear membrane, although its location may vary depending on the cell type; for example, in immune cells the centrosome positions toward the immune synapse to allow for antigen presentation, and in neurons it positions toward the axon or the longest neurite to polarise membrane trafficking through it (De Anda et al., 2010; Elric and Etienne-Manneville, 2014).

Centrosomal positioning also drives cell migration, upon extracellular stimuli the centrosome faces and reorient the cytoskeleton toward the stimulus to direct cell migration toward it. Indeed, centrosome positioning and cell migration have been described to fulfil an important role during neuronal development in the brain (Meka et al., 2020; Takeda et al., 2020).

In dividing cells, centrosomes play an important role during cell division as described above, concretely in mitotic spindle formation which ensure chromosome segregation and proper cell division (Conduit et al., 2015).

Finally, the centrosome is crucial for primary cilium formation. As mechano-sensory organelle, the primary cilium participates in a wide variety of signalling processes which control embryonic development, adult tissue homeostasis and sensory signalling. Specifically, primary cilium has been demonstrated to be crucial for Sonic Hedgehog (Shh) pathway signalling, although is participation has been described in many other pathways including Wnt, TGF-β, mTor, Notch, PDGFR and GPCR-associated signalling (Bangs and Anderson, 2017; Pala et al., 2017). Indeed, neuronal primary cilia accumulate a series of DA receptors including D1, D2 and D5 (Marley and von Zastrow, 2010; Abdul-Majeed and Nauli, 2011; Domire et al., 2011). Shh signalling has been described to play a role in DA neuron survival. Loss of primary cilia and Shh signal disruption fail to trigger neuroprotective signalling toward DA circuits (Gonzalez-Reyes et al., 2012).

5.2. Alterations in human diseases

Given the above-mentioned roles of centrosomes and primary cilia in several cellular processes, it is unsurprising that alterations or dysfunctions have been associated with several human diseases (Breslow and Holland, 2019).

Centrosome abnormalities (either numerical or structural) induce chromosomal instability (CIN), which is common in many human cancers (Godinho and Pellman, 2014). CIN is caused by chromosome missegregation due to abnormal formation of the mitotic spindle or the presence of multipolar spindles due to centrosome amplification. Furthermore, centrosome amplification induces a dysregulation of the cytoskeleton, increasing cell migration and invasion (Godinho et al., 2014). Additionally, genetic centrosome abnormalities have been related to a series of congenital defects and developmental disorders including primary autosomal recessive microcephaly and primordial dwarfism syndromes (Chavali et al., 2014).

Primary cilia signalling is important for embryonic development and adult tissue homeostasis (Breslow and Holland, 2019). Primary cilia defects may alter several signalling cascades, and have been associated with a group of pediatric diseases known as ciliopathies including Joubert syndrome, Bardet-Biedl syndrome and polycystic kidney disease, amongst others (Braun and Hildebrandt, 2017). The biogenesis, maintenance and disassembly of primary cilia involve a wide variety of proteins, and, to date, many genetic alterations in those proteins have been described, constituting the principal cause of ciliopathies (e.g. mutations, protein loss, etc) (Reiter and Leroux, 2017). Apart from developmental abnormalities, primary cilia defects have been linked to cancer. Several studies have reported that alterations in primary cilia signalling, dysregulation of assembly/disassembly during cell cycle or loss of primary cilia promote cell tumorigenesis (Breslow and Holland, 2019).

Interestingly, several studies have shown that LRRK2-PD patients display an elevated predisposition to develop certain types of cancer (Saunders-Pullman et al., 2010; Inzelberg et al., 2012; Agalliu et al., 2015), although the subjacent mechanism(s) of this association is unknown.

5.3. Alterations in LRRK2-related Parkinson's disease

Although there is little or no evidence that PD is associated with centrosomal deficits in dividing cells, as neurons are not dividing, and PD is not classified as a ciliopathy, alterations in centrosome or primary cilium homeostasis may somehow modulate the survival of DA neurons.

Recent studies have demonstrated that pathogenic LRRK2 cause mispositioning of the centrosome when expressed in SH-SY5Y, which resulted in cell polarity and cell migration defects (Madero-Pérez et al., 2018a). In addition, this study showed that pathogenic LRRK2 caused neurite outgrowth defects in concordance with previous studies (Winner et al., 2011; Sepulveda et al., 2013). In dividing cells, Madero-Pérez and colleagues described for the first time that pathogenic LRRK2 caused a centrosomal cohesion deficit in a kinase-dependent manner which correlated with an abnormal accumulation of LRRK2-phosphorylated RAB8A in a pericentrosomal area. Furthermore, this centrosomal defect was observable in two distinct peripheral cell types from LRRK2 PD patients (Madero-Pérez et al., 2018a).

Pathogenic LRRK2 mutations have also been reported to interfere with ciliogenesis through a pathway which involves the phosphorylation of RAB10. Phosphorylated RAB10 disrupts primary cilium biogenesis by interaction with both RILPL1 and RILPL2, which have been previously described to regulate ciliogenesis. On the one hand, phosphorylated RAB10 binds to RILPL1 and impedes the recruitment of TTBK2, a kinase necessary for the "uncapping" of the mother centriole prior to initiation of ciliogenesis. On the other hand, phosphorylated RAB10 binds to RILPL2 and induces the sequestration of Myosin Va, a protein necessary for the recruitment of preciliary vesicles, in a pericentrosomal area (Schaub and Stearns, 2013; Steger et al., 2017; Dhekne et al., 2018; Dhekne et al., 2021; Sobu et al., 2021). In mouse brain, pathogenic LRRK2-mediated loss of primary cilia has been described to disrupt Sonic hedgehog ciliary signalling in cholinergic interneurons of the striatum, which may result in a decrease in the secretion of neurotrophic factor and an impairment of the neuroprotective signalling toward the DA neurons. Similarly, pathogenic LRRK2 has been reported to cause a ciliary deficit in striatal astrocytes which correlates with a disruption in Sonic hedgehog ciliary signalling and is proposed to result in the dysregulation of medium spiny neuron circuitry in the striatum (Dhekne et al., 2018; Khan et al., 2021).

Given the above mentioned phenotypes observed in LRRK2 models and LRRK2-PD patients related to centrosomal cohesion deficits which are mediated by LRRK2-phosphorylated RAB8A, and given the involvement of LRRK2-phosphorylated RAB10 and RILPL1 in primary cilia dysfunction, the present thesis attempts to elucidate whether the LRRK2-mediated centrosomal cohesion and ciliogenesis deficits are both mediated by the formation of a RILPL1-phospho-RAB8/10 complex, and to gain insight into the mechanism and regulation of these phenotypes. In addition, and due to the observation of centrosomal cohesion deficits in G2019S-LRRK2 PD patient-derived LCLs, this thesis also aims to determine whether the centrosomal cohesion deficits may be used as a biomarker to stratify PD patients in clinical trials.

II. Objectives

1. Determine whether membrane localisation or isoform specificity of RAB8 regulates the LRRK2-mediated centrosomal cohesion deficit.

2. Determine the role of RAB10 in the centrosomal cohesion deficit mediated by pathogenic LRRK2.

3. Analyse whether the pathogenic LRRK2-mediated cohesion deficits correlate with the centrosomal accumulation of phospho-RAB10.

4. Determine whether the pathogenic LRRK2-mediated centrosomal cohesion deficits depend on RAB8, RAB10, RILPL1 or RILPL2.

5. Analyse the impact of other RAB substrates on the pathogenic LRRK2-mediated centrosomal cohesion deficits.

6. Analyse the effect of LRRK2 risk and protective variants on the centrosomal cohesion deficits.

7. Analyse the effect of modulators of the LRRK2 kinase activity on centrosomal cohesion deficits.

8. Analyse the precise centrosomal localisation of the phospho-RAB accumulation by determining the localisation of RILPL1 at an ultrastructural level.

9. Analyse whether the pathogenic LRRK2-mediated ciliogenesis deficits correlate with the centrosomal accumulation of phospho-RABs.

10. Determine whether both centrosomal cohesion and ciliogenesis deficits can be observed in cells from LRRK2 knockin mice expressing endogenous levels of pathogenic LRRK2.

11. Analyse whether both centrosomal cohesion and ciliogenesis deficits can be observed in peripheral cells from LRRK2 Parkinson´s disease patients versus healthy controls.

12. Determine whether centrosomal cohesion deficits may serve as cellular biomarker and potential patient stratification approach in the context of LRRK2-related Parkinson´s disease.

III. Materials and methods

DNA reagents and site-directed mutagenesis

GFP-tagged human LRRK2 wildtype, LRRK2-R1441C, LRRK2-Y1699C and LRRK2-G2019S were a gift from Dr. Mark Cookson (Addgene plasmids 25044, 25046, 25048 and 25045, respectively) (Greggio et al., 2006) and 3xflag-tagged human LRRK2 wildtype, LRRK2-R1441C, LRRK2-Y1699C, LRRK2-K1906M and LRRK2-G2019S were kindly provided by Dr. Elisa Greggio (University of Padova, Italy). All mutant LRRK2 constructs were generated using QuikChange II Site-Directed Mutagenesis kit (Agilent Technologies, 200523) and identity of all constructs verified by sequencing of the entire coding region.

Human GFP-tagged RAB8A was a gift from Dr. Maxence Nachury (Addgene plasmid 24898) (Nachury et al., 2007), and myc-DDK-tagged human RAB8B and human RAB10 were obtained from OriGene (RC204651 and RC201464, respectively). N-terminally GFP-tagged, mRFP-tagged or 3xflag-tagged human RAB8A, RAB8B and RAB10 constructs were generated using Gibson Assembly® Master Mix (New England Biolabs, E26118). The RAB8A-T72A, RAB8A-C204A, RAB8B-T72A and RAB10-T73A mutations were generated by site-directed mutagenesis (QuikChange, Agilent Technologies, 200523) and the identity of all constructs verified by sequencing of the entire coding region.

Human RILPL1-DDK was purchased from GenScript, human RILPL1-eGFP and C-terminal half of human RILPL1 [E280-end] tagged at the C-terminus with eGFP (RL1d-GFP) were generous gifts from Dr. Dario Alessi (Steger et al., 2017). N-terminally eGFP-tagged or C-terminally mSOG-HA-tagged human RILPL1 constructs were generated using Gibson Assembly® Master Mix (New England Biolabs, E26118), and identity of constructs verified by sequencing of the entire coding region.

pEGFP-mSmo, encoding for the ciliary transmembrane receptor Smoothened, was a gift from Dr. Philip Beachy (Addgene plasmid 25395) (Chen et al., 2002). mKO2-mSOG, used for RILPL1-mSOG-HA cloning, was kindly provided by Dr. Daniela Boassa (University of California San Diego, United States of America).

N-terminally HA-tagged human vps35, vps35-D620N, vps35-L774M, vps35-M57I, were kindly provided by Dr. Dario Alessi (University of Dundee, United Kingdom) and are available at https://mrcppureagents.dundee.ac.uk/.

For transient transfections of mammalian cells, all DNA constructs were prepared from bacterial cultures from MAX Efficiency™ DH5α Competent cells (Invitrogen, 18258012) or XL1-Blue Supercompetent cells (Agilent Technologies, 200236) grown at 37 °C using PureYield™ Plasmid Midiprep System (Promega, A2492) according to manufacturer's instructions.

Cell culture and transfection

HEK293T/17 cells were cultured as previously described (Blanca Ramírez et al., 2017; Madero-Pérez et al., 2018a). Briefly, cells were grown in full medium (Dulbecco's modified Eagle medium (DMEM) containing low glucose (Life Technologies, 31885-023) and 10 % fetal bovine serum (Life Technologies, 10500-064), non-essential amino acids (Sigma-Aldrich, M7145-100ML), 100 U/ml penicillin and 100 µg/ml streptomycin (Life Technologies, 15140-122)) and transfected at 80 % confluence with 1 µg of LRRK2 constructs (and 100 ng of RAB constructs, 100 ng of HA-tagged vps35 constructs or 50 ng of GFP-tagged mSmo construct, where indicated) with 3 µl of LipoD293™ Transfection Reagent (SignaGen Laboratories, SL100668) per well of 12-well plate for 5 h in full medium. The next day, cells were split to 25 % confluence onto poly-L-Lysine-coated (Sigma-Aldrich, P9155-5MG) coverslips, and subjected to immunocytochemistry or Western blot analysis 48 h after transfection. For ciliogenesis experiments, cells were processed as described above, and serum starved for 12 hours in the absence or presence of MLi-2 (200 nM, 12 h).

HeLa cells were cultured as described (Gómez-Suaga et al., 2014; Rivero-Ríos et al., 2019). Briefly, cells were grown in full medium (DMEM containing high glucose (Life Technologies, 41966-029) and 10 % fetal bovine serum (Life Technologies, 10500-064), non-essential amino acids (Sigma-Aldrich, M7145-100ML), 100 U/ml penicillin and 100 µg/ml streptomycin (Life Technologies, 15140-122)) and transfected at 80 % confluence with 200 ng of RAB constructs and 1 µl of Lipofectamine® 2000 Transfection Reagent (Invitrogen, 11668-027) per well of 12-well plate following manufacturer's instructions for 5 h, followed by replacement with full medium. The following day, cells were split 1:3 onto poly-L-Lysine-coated (Sigma-Aldrich, P9155-5MG) coverslips and processed for immunocytochemistry 48 h after transfection.

SH-SY5Y cells stably expressing GFP, flag-tagged wildtype LRRK2, or flag-tagged G2019S-mutant LRRK2 were kindly provided by Dr. Evy Lobbestael and Dr. Veerle Baekelandt (KU Leuven, Belgium) and were cultured as previously described (Reyniers et al., 2014; Vancraenenbroeck et al., 2014; Madero-Pérez et al., 2018a). Briefly, SH-SY5Y cell lines were grown in DMEM containing high glucose and GlutaMAX (Life Technologies, 31966-021), supplemented with 15 % fetal bovine serum (Sigma-Aldrich, F7524-500ML), non-essential amino acids (Sigma-Aldrich, M7145-100ML), 50 µg/ml Gentamycin (Life Technologies, 15750-037) and 200 µg/ml Hygromycin B Gold™ (InvivoGen, ant-hg-1), and subcultured at a ratio of 1:6 twice a

week. Cells were transfected at 80 % confluence in DMEM containing high glucose and GlutaMAX with 400 ng of RAB constructs and 2 µL of Lipofectamine® 2000 Transfection Reagent (Invitrogen, 11668-027) per well of a 24-well plate according to manufacturer's specifications, and 5 h later, media was replaced with full medium. Cells were split 1:3 the following day onto coverslips and subjected to immunocytochemistry after 48 h of transfection.

A549 wildtype and the various CRISPR-CAS9 knockout cells (RAB8A-KO, RAB10-KO, RAB12-KO, RAB29-KO, RAB35-KO, RAB43-KO, RILPL1-KO, RILPL2-KO, vps35-KO and PPM1H-KO) were generous gifts from Dr. Dario Alessi (University of Dundee, United Kingdom) and have been previously described (Ito et al., 2016; Steger et al., 2017; Dhekne et al., 2018; Mir et al., 2018; Purlyte et al., 2018; Berndsen et al., 2019; Dhekne et al., 2021). A549 cell lines were cultured in DMEM containing high glucose and no glutamine (Life Technologies, 11960-044) supplemented with 10 % fetal bovine serum (Life Technologies, 10500-064), 2 mM L-glutamine (Life Technologies, 25030-024) and 100 U/ml penicillin and 100 µg/ml streptomycin (Life Technologies, 15140-122), and subcultured at a ratio of 1:6 - 1:10 twice a week. Cells were transfected at 90 % confluence with 1 µg of LRRK2 constructs (and 100 ng of RAB constructs or 100 ng RL1d-GFP construct, where indicated) or co-transfected with 1 µg of pCMV and 100 ng of GFP-RILPL1, RILPL1-GFP, RILPL1-DDK or RILPL1-mSOG constructs, along with 4 µl of LipoD293™ Transfection Reagent (SignaGen Laboratories, SL100668) per well of a 12-well plate according to manufacturer's instructions. Transfection media was replaced with full media after 5 h, and cells were split 1:4 the next day and processed for immunocytochemistry or Western blotting 48 h after transfection.

Primary mouse cortical astrocytes from wildtype or homozygous G2019S knockin mice were obtained from breeding homozygous G2019S knockin mice (Yue et al., 2015) and C546BL/6 wildtype control mice, respectively, and were cultured as previously described (Lobbestael et al., 2016). Briefly, 6-7 brains were obtained from P1 to P2 mouse pups, isolated cortices were mechanically dissociated in BME (Sigma-Aldrich, B1522), and dissociated cells cultured in growth medium (DMEM containing high glucose and pyruvate (Life Technologies, 41966-029) supplemented with 10 % Hyclone™ Fetal Bovine Serum (Fisher Scientific, 10309433) and 100 U/ml penicillin and 100 µg/ml streptomycin (Life Technologies, 15140-122)). Cells were seeded in two 175 cm^2 cell culture flasks, and the following day, old growth medium was removed and replaced with fresh ice-cold growth medium to purify astrocytes

from non cold-resistant cell types. Four days later, this procedure was repeated, and the cell culture was further purified by shaking exclusion procedure. Briefly, cells were placed in an incubator with an orbital shaker at 37 °C for 2 hours at 200 rpm to lift microglia, media replaced and incubated until the end of the day. Then, cells were incubated overnight at 360 rpm and media replaced to get rid of oligodendrocytes. Subsequently, 50 % of growth medium was replaced with warm growth medium every 3-4 days. Once confluent, cells were split at high density onto poly-L-Lysine-coated (Sigma-Aldrich, P9155-5MG) coverslips and processed for immunocytochemistry. For ciliogenesis, cells were serum-starved for 48 h, in the presence or absence of 200 nM MLi-2 for the last 24 h.

Primary human skin fibroblasts established from skin biopsies taken from five age- and biological sex-matched healthy control and five PD patients with the G2019S mutation were kindly provided by Dr. Adolfo López de Munain (Biodonostia Health Research Institute, Donostia University Hospital, Spain) and have been previously described (Gómez-Suaga et al., 2014; Madero-Pérez et al., 2018a). All subjects had given informed consent and ethical approval using forms accepted by the Ethical Committee on the Use of Human Subjects in Research (Donostia University Hospital, Spain). PD patients had been diagnosed with familial PD and had been sequenced for the G2019S-LRRK2 mutation. Fibroblasts were grown in Iscove's modified Dulbecco's media (IMDM) (Life Technologies, 21980-032) and 10 % fetal bovine serum (Life Technologies, 26140-079), with media exchanged every two days. Cells were subcultured at a ratio of 1:4, and seeded at equal densities onto coverslips. For ciliogenesis experiments, cells were serum-starved for 48 h in either the presence or absence of 200 nM MLi-2 for the last 24 h. Analyses were carried out on passages 5-10, with no passage-dependent differences observed.

Lymphoblastoid cell lines (LCLs), generated from healthy controls, sporadic PD patients and familial PD patients carrying G2019S-LRRK2 mutation, were kindly provided by Dr. Marie-Christine Chartier-Harlin (Jean-Pierre Aubert Research Center UMR-S 1172, Inserm, France) and have been previously described (Madero-Pérez et al., 2018a). For the generation of LCLs by Chartier-Harlin group, patients were recruited at the Movement Disorders Unit of Lille University Medical Center (Lille, France, CPP Nord-Ouest 2008/09), with the two groups matched according to age and biological sex. Blood samples were collected in BD Vacutainer® CPT™ Mononuclear Cell Preparation Tubes containing sodium heparin (BD Biosciences, 362753). Peripheral blood mononuclear cells (PBMCs) were collected and processed according to manufacturer´s

instructions, and lymphocytes were immortalized by infection with Epstein-Barr virus (EBV) as previously described (Louie and King, 1991). Briefly, cell lines were established from freshly isolated or cryopreserved lymphocytes using standard EBV transformation protocols which include cell separation by gradient centrifugation and lymphocyte growth enhancement by 1 % (v/v) with the mitogenic phytohemagglutinin-M form (PHA-M) (Thermo Fisher Scientific, 10576015). LCLs were maintained in RPMI 1640 medium (Life Technologies, 31870-025) supplemented with 20 % fetal bovine serum (Life Technologies, 10270-106), 2 % L-glutamine (Life Technologies, 25030-024), 20 U/ml penicillin and 20 µg/ml streptomycin (Life Technologies, 15140-122) in upright position with vented caps T75 flasks. Cells were maintained at a density of 10^6 cells/ml, with cell density monitored every other day using Trypan Blue staining (Sigma-Aldrich, T8154-100ML).

In all cases, cells were grown at 37 °C and 5 % CO_2 in a humidified atmosphere, and all lines were regularly tested for Mycoplasma contamination using PCR-based methods by the Cell Culture Service of the IPBLN. Where indicated, cells were treated with MLi-2 (MRC PPU, Dundee, UK), GSK2578215A (Tocris, 4629/25) or with the equivalent volume of DMSO (Sigma-Aldrich, P2650-100ML) before fixation.

Immunocytochemistry

For centrosome staining, HEK293T/17 and A549 cells were fixed with 2 % paraformaldehyde (PFA) (Electron Microscopy Sciences, 15710) in PBS (phosphate-buffered saline) for 20 minutes at room temperature, and SH-SY5Y cells were fixed with 2 % PFA in PBS containing 4 % sucrose (w/v) for 20 minutes at room temperature. For γ-tubulin staining, PFA fixation was followed by ice-cold methanol (MeOH) for 2 minutes at room temperature. For detection of primary cilia in HEK293T/17 cells, primary human skin fibroblast and primary murine astrocytes, primary cilia and centrosomes were stained; cells were fixed with pre-warmed 4 % PFA in PBS for 20 minutes at 37 °C, followed by ice-cold MeOH for 5 minutes at 4 °C.

For LCLs centrosome staining, coverslips (13 mm diameter) were placed into 24-well plates and coated with Corning® Cell-Tak™ Cell and Tissue Adhesive solution (Corning, 354240) according to manufacturer´s instructions. After 20 min incubation at room temperature, the solution was removed, and coverslips were rinsed twice with distilled water followed by air-drying. Lymphoblast cells (200,000/well) were added to dry Cell-Tak-coated coverslips, and cells attached by slight centrifugation at 690 g

for 10 min at room temperature (without brake). Cells were fixed with 2 % PFA in PBS for 20 min at room temperature, followed by 5 min of ice-cold MeOH fixation.

After fixation, in all cases, cells were permeabilized with 0.2 % TritonX-100/PBS for 12 minutes, followed by incubation with 0.5 % BSA (w/v) in 0.2 % TritonX-100/PBS (blocking solution) for 1 hour at room temperature. Primary antibodies were diluted in blocking solution and incubated overnight at 4 °C.

Primary antibodies included rabbit polyclonal anti-pericentrin (1:1000, Abcam, ab4448), mouse monoclonal anti-pericentrin (1:1000, Abcam, ab28144), mouse monoclonal anti-γ-tubulin (1:1000, Abcam, ab11316), mouse monoclonal anti-flag® (1:500, Sigma-Aldrich, clone M2, F1804-200UG), rat monoclonal anti-HA (1:500, Roche, clone 3F10, 11867423001), rabbit monoclonal KO-validated anti-RAB8A (1:1000, Abcam, ab188574), mouse monoclonal KO-validated anti-RAB10 (1:1000, Sigma-Aldrich, SAB5300028-100UL), rabbit monoclonal anti-RAB10 (1:100, Abcam, ab237703), mouse monoclonal anti-polyglutamylated tubulin (1:1000, AdipoGen, AG-20B-0020-C100), rabbit polyclonal anti-Arl13b (1:250, ProteinTech, 17711-1-AP), rabbit polyclonal anti-RILPL1 (1:300, Sigma-Aldrich, HPA041314-100UL), sheep polyclonal anti-RILPL1 (1:50, kindly provided by Dr. Dario Alessi), chicken polyclonal anti-GFAP (1:500, Abcam, ab4674) and mouse monoclonal p230/Golgin245 (1:400, BD Biosciences, 611280).

The sheep polyclonal anti-RAB8A and anti-phospho-T72-RAB8A (1:250 and 1:50, MRC PPU, S969D and S874D, respectively), and anti-RAB10 and anti-phospho-T73-RAB10 (1:250 and 1:50, MRC PPU, S945D and S873D, respectively) were kindly provided by Dr. Dario Alessi (University of Dundee, United Kingdom) and have been previously described (Steger et al., 2016; Lis et al., 2018). The sheep phospho-T72-RAB8A and phospho-T73-RAB10 antibodies were used in the presence of a 10-fold molar excess of the respective non-phospho-peptides, or of the respective phospho-peptides where indicated. Importantly, all double- and triple-immunocytochemistry involving sheep antibodies were performed sequentially, with the sheep antibody employed first, and omitting the MeOH fixation step. The rabbit polyclonal anti-phospho-T72-RAB8A and rabbit polyclonal anti-phospho-T73-RAB10 antibodies were employed at a dilution of 1:250; antibodies were kindly provided by Dr. Dario Alessi (University of Dundee, United Kingdom), and have been previously described (Lis et al., 2018). The rabbit monoclonal KO-validated anti-phospho-T72-RAB8A (Abcam, ab230260) was used at a dilution of 1:1000. For the rabbit monoclonal KO-validated anti-phospho-T73-RAB10 (1:1000, Abcam, ab241060) antibody, 0.2 % Triton-X100/PBS was replaced by 0.1 % saponin/PBS throughout.

Note that the sheep polyclonal total anti-RAB8A and total anti-RAB10 antibodies have been previously validated against extracts from RAB8A or RAB10 A549 knockout cell lines (MRC PPU, Dundee, United Kingdom). The commercial rabbit monoclonal total anti-RAB8A antibody has been previously validated against extracts from a RAB8A HAP1 knockout cell line (Abcam, ab188574), and the commercial mouse monoclonal total anti-RAB10 antibody has been previously validated against HeLa cell extracts in the presence or absence of siRNA of RAB10 (Sigma-Aldrich, SAB5300028-100UL; ThermoFisher, MA5-15670, clone 4E2). The sheep polyclonal phospho-RAB8A and phospho-RAB10 antibodies have been previously validated in HEK293 cells overexpressing the respective RABs in the presence or absence of a LRRK2 kinase inhibitor, as not sensitive enough to detect endogenous phospho-RAB levels by Western blotting techniques (Lis et al., 2018). The rabbit monoclonal phospho-RAB8A and phospho-RAB10 antibodies are able to detect endogenous phospho-RABs by Western blotting techniques, and have been previously validated by Western blotting using both LRRK2 knockout mice extracts, as well as A549 RAB8A or RAB10 knockout cell extracts (Lis et al., 2018).

The following day, coverslips were washed two times 10 min in 0.2 % Triton-X100/PBS (or 0.1 % saponin/PBS) (wash buffer), and were incubated with secondary antibodies diluted in wash buffer for 1 hour at room temperature.

Secondary antibodies included Alexa Fluor® 405 goat anti-mouse or goat anti-rabbit IgG (H+L) (1:1000, Invitrogen, A31553 and A31556, respectively), Alexa Fluor® 488 goat anti-mouse, goat anti-rabbit, goat anti-rat or donkey anti-sheep IgG (H+L) (1:1000, Invitrogen, A11001, A11008, A11006 and A11015, respectively), Alexa Fluor® 555 goat anti-mouse, goat anti-rabbit or goat anti-rat IgG (H+L) (1:1000, Invitrogen, A21422, A21428 and A21434, respectively), Alexa Fluor® 594 goat anti-mouse or goat anti-rabbit IgG (H+L) (1:1000, Invitrogen, A11005 and A11012, respectively), Alexa Fluor® 647 goat anti-mouse, goat anti-rabbit, goat anti-rat or donkey anti-sheep IgG (H+L) (1:1000, Invitrogen, A21235, A21245, A21247 and A21448, respectively). The Alexa Fluor® 405 goat anti-chicken IgY (H+L) (1:250, ab175675) and the Alexa Fluor® 594 donkey anti-sheep IgG (H+L) (1:1000, ab150180) were from Abcam.

Coverslips were washed two times in wash buffer, rinsed in PBS, air-dried and mounted with VECTASHIELD® Antifade Mounting Medium with DAPI (Vector Laboratories, H-1200-10). Where indicated, coverslips where incubated with TO-PRO™-3 Iodide (642/661) (1:1000, Invitrogen, T3605) for 3 minutes, followed by washes in PBS before mounting with ProLong™ Gold Antifade Mounting Medium (Invitrogen, P10144).

For the determination of the subcellular localisation of GFP-tagged RAB proteins in HeLa cells, cells were transfected and cultured as described above, and fixed 48 hours after transfection with 4 % PFA/PBS for 20 minutes at room temperature. Coverslips were washed once with PBS, air-dried and mounted with VECTASHIELD® Antifade Mounting Medium with DAPI (Vector Laboratories, H-1200-10).

Laser confocal imaging and analysis

Images were acquired on a Leica TCS-SP5 confocal microscope using a 63x 1.4 NA oil UV objective (HCX PLAPO CS). Images were collected using single excitation for each wavelength separately and dependent on secondary antibodies (405 nm UV diode and a 420-450 nm emission band pass; 488 nm Argon Laser line and a 510-540 nm emission band pass; 543 nm HeNe Laser line or 516 nm HeNe Laser line and a 555-575 nm emission band (for Alexa Fluor® 555) or a 590-620 nm emission band pass (for Alexa Fluor® 594); 633 nm HeNe Laser line and a 640-670 nm emission band pass). GFP-tagged proteins were excited with a 488 nm Argon Laser line and a 500-530 nm emission band pass, mRFP-tagged proteins with a 543 nm HeNe Laser line or a 516 nm HeNe Laser line and a 560-590 nm emission band pass, DAPI with a 405 nm UV diode and a 430-470 nm emission band pass, and TO-PRO with 633 nm HeNe Laser line and a 650-680 nm emission band pass, respectively.

For centrosome cohesion determination, 10-15 image sections of selected areas were acquired with a step size of 0.5 µm and z-stack images analysed and processed using Leica Applied Suite (LAS AF6000) image acquisition software (Leica Microsystems). The same laser intensity settings and exposure times were used for image acquisition of individual experiments to be quantified. For HEK293T/17 and SH-SY5Y cells, centrosomes were scored as being separated when the distance between their centers was > 1.5 µm (Madero-Pérez et al., 2018a). For A549 cells, the mean distance was 1.49 ± 0.13 µm (mean ± s.e.m., n = 82 cells), and duplicated centrosomes were scored as separated when the distance was > 2.5 µm. For mouse cortical astrocytes, the mean distance between duplicated centrosomes was 1.18 ± 0.06 µm (mean ± s.e.m., n = 96 cells), and duplicated centrosomes were scored as separated when the distance was > 1.5 µm. For LCLs, the mean distance in control cells was 1.3 ± 0.2 µm (mean ±s.e.m., n = 10 cells), and duplicated centrosomes were scored as being separated when the distance was > 1.3 µm (Madero-Pérez et al., 2018a). Only

LCLs which displayed clear centrosomal staining by both the anti-pericentrin and anti-γ-tubulin antibodies were analysed. In all cases, mitotic cells were excluded from the analysis. For each sample, minimally 100 cells were quantified by an observer blind to condition. Additionally, some experimental conditions were independently quantified by an additional two observers blind to condition, with identical results obtained in all cases.

Quantification of phospho-RAB10 signal in lymphoblast, SH-SY5Y or HEK293T/17 cells was performed over non-processed and non-saturated images acquired on the same day and with the same laser intensities with Leica Applied Suite (LAS AF6000) image acquisition software (Leica Microsystems). Circular ROIs of 3 μm of diameter were set on top of the centrosome signal as detected by anti-pericentrin staining, and the mean intensity from the phospho-RAB10 signal obtained from 50-70 cells per condition and experiment. Background signal was subtracted in all cases by placing the ROI in a different aleatory place within the same cell.

For determination of the percentage of ciliated cells, cells were visualized on an inverted microscope (Zeiss) using a 100X 1.4 NA Plan APO oil objective. For each experiment, around 200 random cells were scored for either the presence or absence of primary cilia as assessed by either polyglutamylated tubulin or Arl13b staining, with identical results obtained in both cases. Quantification of the percentage of ciliated cells was performed by two additional observers blind to condition, with identical results obtained in all cases. As an additional means of primary cilia quantification, 20-25 image sections were acquired with a step size of 0.25 μm, and images deconvolved using Huygens Essential Deconvolution software (Scientific Volume Imaging). For measuring cilia length, a method based on the Pythagorean theorem (PyT) was employed, and around 40 cells per condition were quantified (McGlashan et al., 2010; Dummer et al., 2016). Cilia length was also quantified based on maximum intensity projection (MIP), with the determined cilia length smaller than expected (Dummer et al., 2016), but with no difference between genotypes observed.

Electron microscopy, sample preparation and analysis

A549 cells were cultured in glass bottom MatTek dishes (MatTek Life Sciences, P35G-0-14-C) and transfected with RILPL1-mSOG-HA using LipoD293™ Transfection Reagent (SignaGen Laboratories, SL100668) as described above. Proteins were allowed to express for 48 hours and cells were processed as previously described (Boassa et al., 2013; Boassa et al., 2019). Briefly, cells were rinsed with pre-warmed PBS and fixed using pre-warmed 2.5 % glutaraldehyde (w/v) (Electron Microscopy Sciences, 16220), 0.1 % tannic acid (w/v) (Electron Microscopy Sciences, 21700), 3 mM calcium chloride in 0.1 M sodium cacodylate buffer pH 7.4 (Ted Pella Incorporated, 18851) for 5 minutes at 37 °C and then on ice for 1 hour. Subsequent steps were performed on ice, cells were rinsed 5 times using chilled 0.1 M sodium cacodylate buffer pH 7.4 (wash buffer) and treated for 30 minutes in a blocking solution (50 mM glycine, 10 mM KCN, 20 mM aminotriazole and 0.01 % hydrogen peroxide in 0.1 M sodium cacodylate buffer pH 7.4) to reduce non-specific background precipitation of DAB.

Cells were first imaged with minimum light exposure to identify transfected cells for Correlative Light and Electron Microscopy (CLEM) imaging using a Leica SPE II inverted confocal microscope outfitted with a stage chilled to 4 °C. For photo-oxidation, DAB (3-3'-diaminobenzidine, Sigma-Aldrich, D8001-10G) was dissolved in 0.1 N HCl at a concentration of 5.4 mg/ml and subsequently diluted ten-fold into blocking solution, mixed, and passed through a 0.22 µm syringe filter before use. DAB solution was freshly prepared prior to photo-oxidation and placed on ice protected from light. DAB solution was added to the MatTek dish and regions of interest were illuminated through a standard FITC filter set (EX470/40, DM510, BA520) with intense light from a 150 W Xenon lamp. Photo-oxidation was stopped as soon as an optically-dense brown reaction product began to appear in place of the mSOG green fluorescence signal, as monitored by transmitted light (around 4-6 minutes). Multiple areas on a single MatTek dish were photo-oxidized.

Subsequently, plates were placed on ice and washed 5 times 2 minutes with ice-cold wash buffer to remove unpolymerized DAB. After washing out DAB, cells were post-fixed with 2 % reduced osmium tetroxide (Electron Microscopy Sciences, 19190) (2 % osmium tetroxide, 1.5 % KFeCN in 0.1 M sodium cacodylate buffer pH 7.4) for 1 hour on ice, then washed with ice-cold double-distilled water 3 times for 1 minute. Some samples were additionally stained overnight with filtered 2 % uranyl acetate (Electron

Microscopy Sciences, 22400) in double-distilled water and compared to others in which this step was omitted. The following day, plates were washed 3 times for 1 minute with double-distilled water and were dehydrated with an ice-cold graded ethanol series (20 %, 50 %, 70 %, 90 %, 100 %, 100 %, 3 minutes each) and washed once at room temperature anhydrous ethanol (3 minutes). Samples were then embedded in Durcupan™ ACM resin (Sigma-Aldrich; Durcupan™ ACM component A, M epoxy resin (44611-500ML); Durcupan™ ACM component B, hardener 964 (44612-500ML); Durcupan™ ACM component C, accelerator 960 (DY 060) (44613-100ML); Durcupan™ ACM component D (44614-100ML)) using a 1:1 mixture of anhydrous ethanol:Durcupan™ ACM resin for 30 minutes on a platform with gentle rocking, followed by incubation with 100 % Durcupan™ ACM resin overnight with rocking. The following day, the resin was removed from MatTek dishes by decanting and gentle scraping without touching cells and changed with freshly prepared resin for 1 hour (three times). After third replacement, resin was polymerized in a vacuum oven at 60 °C vacuum for 48 hours under -10 mm Hg vacuum pressure atmosphere.

Photo-oxidized areas of interest were identified by transmitted light, sawed out using a jeweler's saw, and mounted on dummy acrylic blocks with cyanoacrylic adhesive. The coverslip was carefully removed, the resin was trimmed, and ultrathin sections (80 nm thick) were cut using a diamond knife (Diatome). Electron micrographs were recorded using a FEI Tecnai™ 12 Spirit TEM (transmission electron microscope) operated at 80 kV. For electron tomography, thicker sections (750 nm) were imaged on a FEI Titan Halo™ microscope operated at 300 kV in scanning mode, the scattered electrons being collected on a high angle annular dark field detector. Prior to imaging, the luxel grids carrying the specimen serial sections were coated with carbon on both sides; colloidal gold particles (10, 20 and 50 nm diameter) were deposited on each side of the sections to serve as fiducial markers. Because centrosomes cannot be clearly distinguished on electron micrographs of thick sections, a preliminary tomography run was first implemented using a low magnification setting on the cells of interest (spanning a 12 µm x 12 µm area). This allowed to pinpoint the exact sections containing centrosomal areas; higher resolution tomograms (with a ~1 nm pixel size) were then acquired on the spot. For each tomogram, four tilt series were collected using the SerialEM package. For each series, the sample was tilted from -60 to +60 degrees, every 0.5 degree. Tomograms were generated using an iterative reconstruction procedure (Phan et al., 2017).

Western blotting

HEK293T/17, A549 and HeLa cells were collected 48 hours after transfection from a well of a 6-well plate, washed in PBS, resuspended in 75 µl of PBS, lysed with 25 µl of NuPAGE™ LDS sample buffer (4x) (Novex, Life Technologies, NP0008) supplemented with β-mercaptoethanol to a final volume of 2.5 % (v/v), and sonicated and boiled at 70 °C for 10 minutes.

For LCLs extracts, one million cells were centrifuged at 1030 g for 5 min at 4 °C, cell pellet was washed once with Hank's Balanced Salt Solution (HBSS) (140 mM NaCl, 5 mM KCl, 1 mM $CaCl_2$, 0.4 mM $MgSO_4 \cdot 7H_2O$, 0.5 mM $MgCl_2 \cdot 6H_2O$, 0.3 mM $Na_2HPO_4 \cdot 2H_2O$, 0.4 mM KH_2PO_4, 6 mM glucose, 4 mM $NaHCO_3$, pH 7.2) and followed by resuspension in 100 µl of lysis buffer (20 mM Tris-EDTA pH 7.4, 1 mM EDTA, 150 mM NaCl, 1 % Triton-X100, 10 % glycerol, Phosphatase Inhibitor Cocktail 2 (Sigma-Aldrich, P5726-1ML) and cOmplete™ Protease Inhibitor Cocktail (Roche, 11697498001)). Extracts were incubated during 30 minutes at 4 °C on a rotary wheel, followed by a short three-pulse sonication. A small sample was taken for determination of protein concentration and the remainder of extract snap-frozen in liquid nitrogen and stored at -80 °C. Protein concentration was estimated using Pierce™ BCA Protein Assay Kit (Thermo Scientific, 23225) according to manufacturer´s specifications. For treatments with MLi-2, one million cells were incubated with or without 10 nM MLi-2 (or DMSO (Sigma-Aldrich, P2650-100ML) as control) for 2 h at 37 °C, followed by centrifugation and processing as described above.

Around 10-15 µl (around 20 µg of protein) were resolved by SDS-PAGE on polyacrylamide gels or 4-20 % Mini-PROTEAN® TGX™ precast protein gels (BioRad, 456-1096), and electrophoresed at 100 V for 2 h with SDS running buffer (25 mM Tris pH 8.6, 190 mM glycine, 1 % SDS). At the end of electrophoresis, proteins were electrophoretically transferred onto Amershan™ Protan® Western blotting nitrocellulose membranes (GE Healthcare Life Sciences, 10600002) at 40 mA overnight at 4 °C in transfer buffer (20 mM Tris pH 8.6, 122 mM glycine, 20 % MeOH (v/v)). Membranes were blocked in 0.2 % Tween-20 in Intercept® (PBS) Blocking Buffer (LI-COR Biosciences, 927-70001) (blocking buffer) for 1 h at room temperature, then cropped into pieces for LI-COR multiplexing. Membranes were incubated with primary antibodies diluted in blocking buffer overnight at 4 °C. Primary antibodies included rabbit polyclonal anti-GFP (1:1000, Abcam, ab6556), mouse monoclonal anti-GFP (1:1000, Roche, 11814460001), mouse monoclonal anti-flag® (1:500, Sigma-Aldrich, clone M2, F1804-200UG), rabbit monoclonal anti-RAB8A KO validated (1:1000, Abcam,

ab188574), mouse monoclonal anti-RAB8(A+B) (1:500, BD Biosciences, 610844), rabbit polyclonal anti-RAB8B (1:1000, Invitrogen, PA5-67354), mouse monoclonal anti-RAB10 (1:1000, Sigma-Aldrich, SAB5300028-100UL), rabbit monoclonal anti-phospho-T72-RAB8A (1:1000, Abcam, ab230260), rabbit monoclonal anti-phospho-T73-RAB10 (1:1000, Abcam, ab230261), rabbit anti-phospho-S935-LRRK2 (1:500, Abcam, ab133450), mouse monoclonal anti-α-tubulin (1:25000, Sigma-Aldrich, clone DM1A, T6199-200UL) and mouse monoclonal anti-GAPDH (1:2000, Santa Cruz, sc-32233). The following day, membranes were washed three times for 10 min in 0.1 % Tween-20/PBS, followed by incubation with secondary antibodies for 1 h at room temperature in blocking buffer. Secondary antibodies included goat anti-mouse or anti-rabbit IRDye® 800CW (1:14000, LI-COR Biosciences, 926-32210 and 926-32211 respectively) and goat anti-mouse or anti-rabbit IRDye® 680RD (1:14000, LI-COR Biosciences, 926-68070 and 926-68071 respectively). Membranes were washed with 0.1% Tween-20/PBS for three times 10 min each, followed by a wash with PBS. Blots were imaged via near-infrared fluorescent detection using Odyssey® CLx imaging system, and quantification was done using the instrument´s Image Studio™ Software (LI-COR Biosciences). The rat monoclonal anti-HA antibody (Roche, clone 3F10, 11867423001) was employed at 1:500 in 5 % BSA in 0.1 % Tween-20/TBS overnight at 4 °C. After three wash steps with 0.1 % Tween-20/TBS, membranes were incubated with HRP-conjugated rabbit polyclonal anti-rat secondary antibody (1:2000, Dako, P0450) diluted in 0.1 % Tween-20/TBS for 1 hour and developed using Amershan™ ECL™ Prime Western Blotting Detection Reagent (GE Healthcare Life Sciences, RPN2232).

For sheep antibodies, HEK293T/17 and A549 cells were collected 48 hours after transfection from a well of a 6-well plate,, washed in PBS, resuspended in 80 µl of PBS and lysed with 20 µl of Laemmli SDS sample buffer (5x) (250 mM Tris-HCl pH 6.8, 10 % SDS, 20 % glycerol, bromophenol blue) supplemented with β-mercaptoethanol to a final volume of 2.5 % (v/v). Extracts were sonicated and boiled at 95 °C for 5 minutes. Around 10-15 µl (around 20 µg of protein) were resolved by SDS-PAGE on polyacrylamide gels and analysed by Western blot. Membranes were blocked in 5 % milk in 0.1 % Tween-20/TBS (milk blocking buffer) for 8 hours, and primary antibodies diluted in milk blocking buffer and incubated overnight at 4 °C. Primary antibodies, including sheep polyclonal anti-RAB8A and anti-phospho-T72-RAB8A (1:500 and 1:250, MRC PPU, S969D and S874D, respectively), sheep polyclonal anti-RAB10 and anti-phospho-T73-RAB10 (1:500 and 1:250, MRC PPU, S945D and S873D, respectively), sheep polyclonal anti-RAB12 (1:100, MRC PPU, SA227),

sheep anti-RAB35 (1:100, MRC PPU, SA314), sheep polyclonal anti-RAB43 (1:100, MRC PPU, SA135) and sheep polyclonal anti-RILPL1 (1:500, MRC PPU), were generously provided by Dr. Dario Alessi (University of Dundee, United Kingdom) and have been previously described (Lis et al., 2018; Berndsen et al., 2019). After three wash steps with 0.1 % Tween-20/TBS, membranes were incubated with HRP-conjugated rabbit anti-sheep secondary antibody (1:6000, Invitrogen, 31480) diluted in 0.1 % Tween-20/TBS for 1 hour. Western blotting of sheep antibodies was performed with Amershan™ ECL™ Prime Western Blotting Detection Reagent (GE Healthcare Life Sciences, RPN2232).

Flow cytometry assays

For cell cycle analysis, one million cells were centrifuged at 1030 g for 5 min, followed by resuspension in 100 µl of PBS at 4 °C, and cells fixed by addition of 100 µl of 4 % PFA/PBS during 15 min on ice. After fixation, cells were centrifuged at 1030 g for 6 min at 4 °C, and the cell pellet resuspended in 340 µl of PBS, followed by incubation with 3 µl of RNAse A (10 mg/ml stock, Roche, 10109169001) and 12 µl of propidium iodide (1 mg/ml stock, Sigma-Aldrich, P4864-10ML) for 20 min at 37 °C in the dark. Flow cytometry analysis was performed in a FACSCalibur™ (Becton Dickinson), propidium iodide-positive signals analysed using a 670 nm fluorescence emission filter, and data represented with respect to the amount of DNA present per cell.

Analysis of apoptosis was performed using Dead Cell Apoptosis Kit with Annexin V Alexa Fluor™ 488 and Propidium Iodide (Invitrogen, V13241) according to manufacturer´s instructions. Briefly, one million cells were centrifuged at 500 g for 3 min, and the pellet washed with 1 ml of ice-cold PBS. Cells ($0.5 \cdot 10^6$) were resuspended in 100 µl of binding buffer and labelled with Annexin V Alexa Fluor™ 488 and propidium iodide for 15 min on ice. Cells were subsequently analysed by flow cytometry in a FACSCalibur™ (Becton Dickinson) using a 488 nm excitation laser and emission at 530 nm (Annexin V) and 670 nm (propidium iodide).

Proximity ligation assays

Proximity ligation assays (PLAs) were performed essentially as previously described (Di Maio et al., 2018) using DuoLink™ PLA® Technology according to manufacturer´s instructions (Sigma-Aldrich, Duolink™ *In Situ* PLA® probe anti-rabbit PLUS (DUO92002-100RXN), Duolink™ *In Situ* PLA® probe anti-mouse MINUS (DUO92004-100RXN), Duolink™ *In Situ* Detection Reagents Red (DUO92008-100RXN)). Briefly, cells on Cell-Tak-coated coverslips were fixed in 4 % PFA/PBS as described above, followed by three washes in PBS. Coverslips were blocked in blocking solution followed by incubation with primary antibodies overnight at 4 °C. Primary antibodies were rabbit polyclonal anti-phospho-S1292-LRRK2 (1:1000, Abcam, ab203181) and mouse monoclonal anti-LRRK2 antibody (1:1000, UC Davies/NIH Neuromab, clone N241A/34, 75-235). The proximity ligation signal was visible as individual dots, and analysed by confocal microscopy as described above. The number of PLA positive dots/cell was quantified from around 300 cells per condition from maximal intensity projections using Leica Applied Systems (LAS AF6000) image acquisition software (Leica Microsystems), and various control experiments included in each assay run.

Study participants

Subjects were recruited at the Movement Disorder Unit of the Lille University Hospital with written informed consent, and the study was approved by the local ethics committee. Patients were examined by neurologists specialized in movement disorders. The Movement Disorders Society Unified Parkinson's Disease Rating Scale (MDS-UPDRS) part III was used to define patient motor symptom severity, and L-DOPA-equivalent dose (LED) calculated for all patients. Subjects participating in the study donated blood samples for DNA extraction, routine LRRK2 genotyping (Hassin-Baer et al., 2009) and lymphocyte immortalization. Six patients heterozygous for the G2019S LRRK2 mutation, 13 sporadic PD patients and 13 unrelated, biological sex- and age-matched controls were included, and an additional three biological sex- and age-matched control lymphoblastoid cell lines (ND01087, ND02550, ND01757), and six biological sex- and age-matched lymphoblastoid cell lines from heterozygous G2019S LRRK2 patients (ND01618, ND00075, ND14317, ND02752, ND03000, ND00264) were obtained from the NINDS Coriell Cell Repository (Table 2). PD family history in the three groups was defined as the presence of at least one PD patient in 1-3

generations of the family. None of the control or sporadic PD patients had a family history of PD, and all were found negative for the G2019S mutation. Of the six G2019S LRRK2 PD patients recruited to the study, five had a PD family history, with three patients belonging to the same family, with affected members over three generations. Most of the study participants, and 100 % of the sporadic PD patients, were of Caucasian origin.

	Controls	G2019S Parkinson's disease	Sporadic Parkinson's disease
Participants number	16	12	13
Age (y)	60 ± 9 (46-76)	63 ± 10 (46-77)	64 ± 8 (50-77)
Biological sex (% male)	50 %	50 %	54 %
Disease duration (y)	-	9 ±5 (1-19)	9 ± 7(1-27)
Age at diagnosis (y)	-	59 ± 11 (45-74)	57 ± 9 (40-72)
Disease severity	-	15 ± 5 (5-19)	18 ± 10 (3-35)
LED	-	633 ± 547 (0-1370)	1027 ± 663 (0-2300)

Table 2. Demographic details for Parkinson's disease and control patients. Data shown are mean ± s.d., with the range indicated in parentheses. Disease severity was measured using the Movement Disorders Society Unified Parkinson's Disease Rating Scale (MDS-UPDRS) part III, as well as Hoehn & Yahr (not shown). LED is the calculated L-dopa-equivalent dose. For the six G2019S LRRK2 LCLs from Coriell Cell Repository, information regarding age at diagnosis, UPDRS part III, Hoehn & Yahr and LED was not available.

Ethics approval for animal experimentation

The experiments with animals reported in this dissertation followed the ethical guidelines for investigations of experimental animals approved by the Ethical Committee of Spanish National Research Council (CSIC) and performed in accordance with the guidelines from Directive 2010/63/EU of the European Parliament on the protection of animals used for scientific purposes.

Statistical analysis

Data were checked for normal distribution using the Shapiro-Wilk test. Normally distributed data were analysed by one-way ANOVA with Tukey´s *post-hoc* test, with significance set at $p < 0.05$. Non-normally distributed data were analysed by Kruskal-Wallis test and Dunn's multiple comparison. Spearman correlations were used to determine associations between levels of LRRK2 or LRRK2 Ser935 and RAB10 Thr73. Paired t-test analysis was performed for comparison of the cohesion phenotypes in the presence and absence of MLi-2. All statistical analysis and graphs were performed using Prism software version 7.0 (GraphPad, San Diego, CA).

List of primary antibodies

Antibody	Species	ICC	WB	Source	Reference
anti-Arl13b	pRb	1:250	-	ProteinTech	17711-1-AP
anti-Flag®	mMs	1:500	1:500	Sigma-Aldrich	F1804-200UG
anti-GAPDH	mMs	-	1:2000	Santa Cruz	sc-32233
anti-GFAP	pChk	1:500	-	Abcam	ab4674
anti-GFP	mMs	-	1:1000	Sigma-Aldrich	11814460001
anti-GFP	pRb	-	1:1000	Abcam	ab6556
anti-Golgin245 (p230)	mMs	1:400	-	BD Biosciences	611280
anti-HA	mRat	1:500	1:500	Sigma-Aldrich	11867423001
anti-LRRK2	mMs	1:1000	-	Neuromab	75-253
anti-LRRK2 (pS935)	mRb	-	1:500	Abcam	ab133450
anti-LRRK2 (pS1292)	pRb	1:1000	-	Abcam	ab203181
anti-pericentrin	mMs	1:1000	-	Abcam	ab28144
anti-pericentrin	pRb	1:1000	-	Abcam	ab4448
anti-polyglut. tubulin	mMs	1:1000	-	AdipoGen	AG-20B-0020-C100
anti-RAB10	pSh	1:250	1:500	MRC PPU	S945D
anti-RAB10	mRb	1:100	-	Abcam	ab237703
anti-RAB10 KO val	mMs	1:1000	1:1000	Sigma-Aldrich	SAB5300028-100UL
anti-RAB10 (pT73)	pSh	1:50	1:250	MRC PPU	S873D
anti-RAB10 (pT73)	pRb	1:250	-	Dr. Dario Alessi	
anti-RAB10 (pT73)	mRb	-	1:1000	Abcam	ab230261
anti-RAB10 (pT73) KO val	mRb	1:1000	-	Abcam	ab241060
anti-RAB12	pSh	-	1:100	Dr. Dario Alessi	
anti-RAB35	pSh	-	1:100	Dr. Dario Alessi	
anti-RAB43	pSh	-	1:100	Dr. Dario Alessi	
anti-RAB8A	pSh	1:250	1:500	MRC PPU	S969D
anti-RAB8A KO val	mRb	1:1000	1:1000	Abcam	ab188574
anti-RAB8B	pRb	-	1:1000	Invitrogen	PA5-67354
anti-RAB8(A+B)	mMs	-	1:500	BD Biosciences	610844
anti-RAB8A (pT72)	pSh	1:50	1:250	MRC PPU	S874D
anti-RAB8A (pT72)	pRb	1:250	-	Dr. Dario Alessi	
anti-RAB8A (pT72) KO val	mRb	1:1000	1:1000	Abcam	ab230260
anti-RILPL1	pSh	1:50	1:500	Dr. Dario Alessi	
anti-RILPL1	pRb	1:300	-	Sigma-Aldrich	HPA041314-100UL
anti-α-tubulin	mMs	-	1:25000	Sigma-Aldrich	T6199-200UL
anti-γ-tubulin	mMs	1:1000	-	Abcam	ab11316

Table 3. List of primary antibodies. ICC, immunocytochemistry; WB, Western blot; pChk, Chicken polyclonal; mMs, Mouse monoclonal; pRb, Rabbit polyclonal; mRb, Rabbit monoclonal; pSh, Sheep polyclonal.

IV. Results

Analysis of the mechanism underlying LRRK2-mediated centrosomal cohesion deficits

Both RAB8A/B and RAB10 cause centrosomal cohesion deficits when co-expressed with wildtype LRRK2

We first wondered whether the centrosomal cohesion deficits induced upon co-expression of wildtype LRRK2 with RAB8A (Madero-Pérez et al., 2018a) are dependent on the RAB8A prenylation status, since prenylation is known to increase the affinity of RAB proteins for membranes and is required for their function (Gabe Lee et al., 2009). We mutated the residue required for prenylation, and confirmed that the RAB8A-C204A mutant was diffusely distributed as compared to wildtype RAB8A when expressed in HeLa cells, consistent with the intended effect of the mutation in blocking prenylation (Fig. 14C). Whilst expression of either RAB8A or LRRK2 on their own was without effect, co-expression of both caused centrosomal cohesion deficits, which was not observed when co-expressing LRRK2 with RAB8A-C204A (Fig. 14A), even though both wildtype and prenylation-deficient RAB8A mutant were expressed to similar degrees (Fig. 14B). Interestingly, and as previously described for RAB10 (Liu et al., 2018), only wildtype but not RAB8A-C204A was phosphorylated by LRRK2 (Fig. ***14*** 14B), indicating that RAB8A needs to be prenylated to be phosphorylated, so as to then cause the resultant LRRK2-mediated effects on centrosome cohesion.

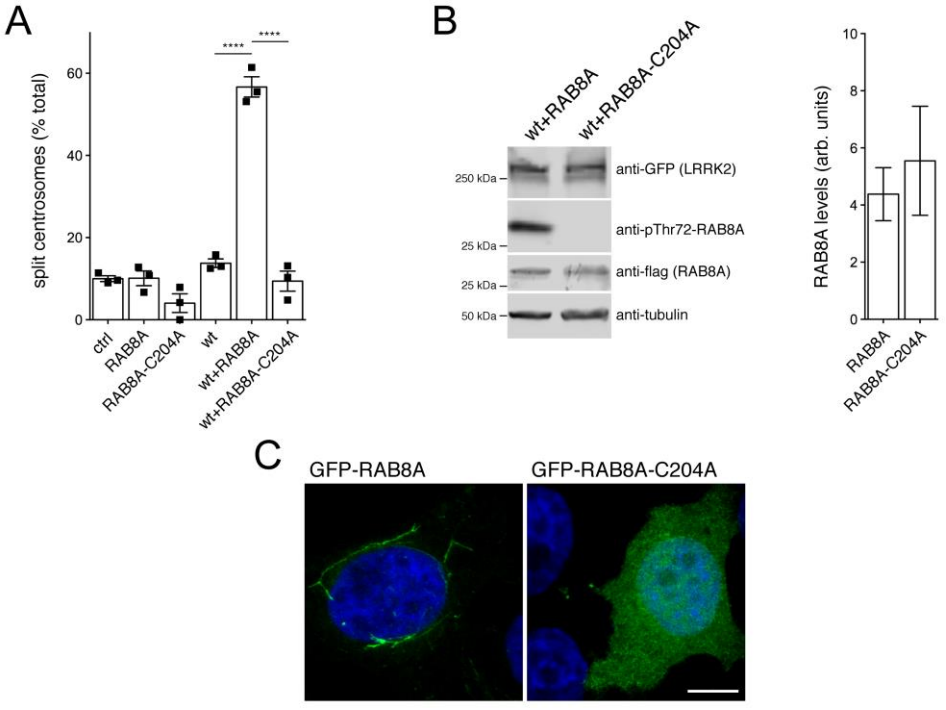

Fig. 14. Expression of prenylation-deficient RAB8A with LRRK2 does not cause centrosomal cohesion deficits. (A) Quantification of the percentage of cells with split centrosomes in HEK293T cells transfected with the different constructs as indicated. Bars represent mean ± s.e.m. (n = 3 experiments); ****, $p < 0.001$. **(B)** Left: HEK293T cells were co-transfected with either wildtype LRRK2 and RAB8A, or RAB8A-C204A as indicated, and extracts blotted for LRRK2, RAB8A and phospho-RAB8A levels, and tubulin as loading control. Right: Quantification of RAB8A or RAB8A-C204A expression levels normalized to tubulin from blots on the left. Bars represent mean ± s.e.m. (n = 6 experiments). **(C)** Example of HeLa cells transfected with GFP-RAB8A constructs, briefly fixed, washed and stained with DAPI. Scale bar, 10 µm.

LRRK2 phosphorylates both the A and B isoforms of RAB8 (Steger et al., 2016; Steger et al., 2017). These isoforms are encoded by different genes, are highly similar in sequence, but display differential tissue-specific expression patterns (Armstrong et al., 1996), and their functions are not redundant in all cases (Yoshimura et al., 2007; Sato et al., 2014). We therefore next analysed whether RAB8B may play similar roles in modulating the LRRK2-mediated centrosomal cohesion deficits. Indeed, when co-expressed with wildtype LRRK2, RAB8B caused cohesion deficits identical to those observed for RAB8A, which were not observed with a phosphorylation-deficient RAB8B-T72A mutant (Fig. 15A,B). Both wildtype and mutant RAB8B were expressed to similar degrees and localised to a perinuclear tubular-like compartment like RAB8A, but additional cytosolic localization was observed with the phosphorylation-deficient RAB8B mutant (Fig. 15C,D). As an additional means to assure that the effects were mediated by the LRRK2 kinase activity, we employed the LRRK2 kinase inhibitor GSK2578215A, which largely reverted the centrosomal cohesion deficits in the presence of LRRK2 and RAB8B (Fig. 15B). Thus, both RAB8A and RAB8B cause centrosomal cohesion deficits in a LRRK2 kinase activity-dependent manner.

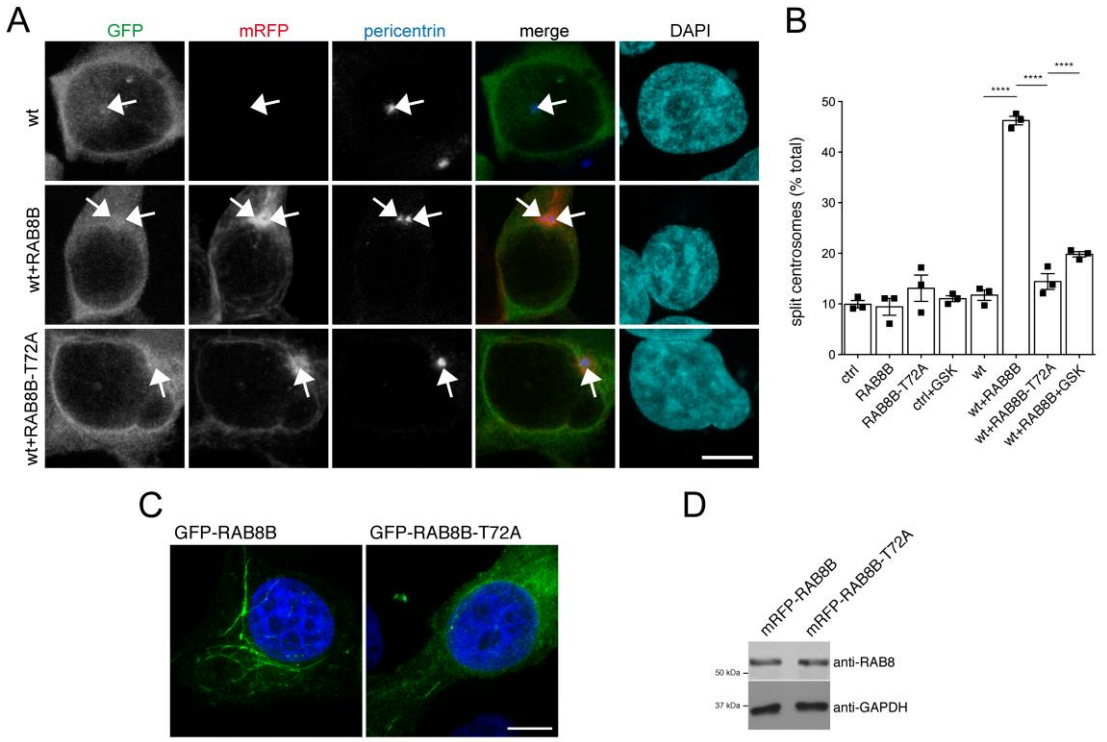

Fig. 15. Co-expression of RAB8B with LRRK2 causes centrosomal cohesion deficits in a manner dependent on LRRK2 kinase activity. (A) Example of HEK293T cells transfected with either GFP-tagged wildtype LRRK2 (wt), or wildtype LRRK2 along with either mRFP-tagged RAB8B or phosphorylation-deficient RAB8B-T72A mutant as indicated, and stained for pericentrin antibody and DAPI. Scale bar, 5 µm. **(B)** Quantification of the split centrosome phenotype in cells expressing the indicated constructs, in either the absence or presence of the LRRK2 kinase inhibitor GSK2578215A (500 nM, 2 h) before fixation. Bars represent mean ± s.e.m. (n = 3 experiments); ****, $p < 0.001$. **(C)** Example of HeLa cells transfected with the indicated GFP-tagged RAB8B constructs, briefly fixed, washed and stained with DAPI. Scale bar, 10 µm. **(D)** HEK293T cells were transfected with mRFP-tagged RAB8B constructs as indicated, and extracts blotted with antibodies against RAB8 and GAPDH as loading control as indicated.

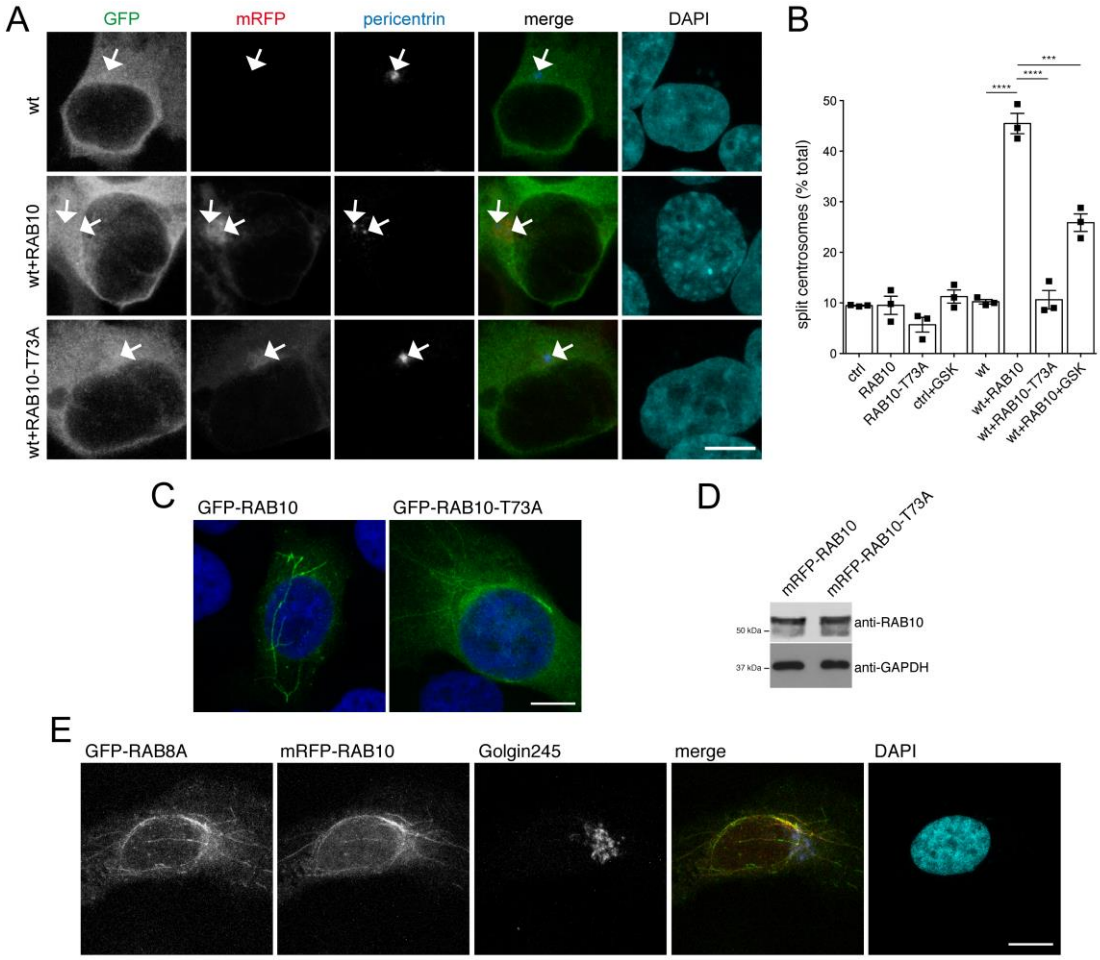

Fig. 16. Co-expression of RAB10 with LRRK2 causes centrosomal cohesion deficits mediated by the LRRK2 kinase activity. (A) Example of HEK293T cells transfected with either GFP-tagged wildtype LRRK2 (wt), or wildtype LRRK2 along with either mRFP-tagged RAB10 or phosphorylation-deficient RAB10-T73A mutant as indicated, and stained for pericentrin antibody and DAPI. Scale bar, 5 µm. **(B)** Quantification of the centrosomal cohesion phenotype in cells expressing the indicated constructs, in either the absence or presence of the LRRK2 kinase inhibitor GSK2578215A (500 nM, 2 h) before fixation. Bars represent mean ± s.e.m. (n = 3 experiments); ****, $p < 0.001$; ***, $p < 0.005$. **(C)** Example of HeLa cells transfected with the indicated GFP-tagged RAB10 constructs, briefly fixed, washed and stained with DAPI. Scale bar, 10 µm. **(D)** HEK293T cells were transfected with mRFP-tagged RAB10 constructs as indicated, and extracts blotted with antibodies against RAB10 and GAPDH as loading control as indicated. **(E)** Example of HeLa cell co-transfected with GFP-tagged RAB8A and mRFP-tagged RAB10, and stained with Golgi marker Golgin245 and DAPI. Scale bar, 10 µm.

RAB10 has been identified as another prominent LRRK2 kinase substrate (Steger et al., 2016; Steger et al., 2017), and both RAB8 and RAB10 have been reported to be involved in centrosome-related events (Sato et al., 2014). These findings prompted us to analyse for the effects of RAB10 expression on centrosomal alterations in the presence of LRRK2. Co-expression of wildtype LRRK2 with RAB10, but not a phosphorylation-deficient RAB10-T73A mutant, caused centrosomal cohesion deficits identical to those observed with RAB8A or RAB8B, respectively (Fig. 16A,B). Both wildtype and mutant RAB10 were expressed to similar degrees and localised to a perinuclear tubular-like compartment identical to RAB8A, with additional cytosolic localization observed with the phosphorylation-deficient RAB10 mutant (Fig. 16C-E).

Application of the LRRK2 kinase inhibitor GSK2578215A largely reverted the centrosomal cohesion deficits observed in the presence of LRRK2 and RAB10 (Fig. 16B). Therefore, co-expression of wildtype LRRK2 with either RAB8A/B or RAB10 causes centrosomal cohesion deficits in a manner dependent on the LRRK2 kinase activity.

Pathogenic LRRK2-induced centrosomal cohesion deficits correlate with aberrant pericentrosomal/centrosomal accumulation of phospho-RAB8/RAB10

We previously showed that the pathogenic LRRK2-induced centrosomal cohesion deficits correlate with an aberrant centrosomal/pericentrosomal accumulation of endogenous phosphorylated RAB8 (Madero-Pérez et al., 2018a). Given that increasing RAB10 levels also caused centrosomal cohesion deficits in the presence of wildtype LRRK2, we wondered whether pathogenic LRRK2 may also trigger the pericentrosomal/centrosomal accumulation of endogenous phosphorylated RAB10.

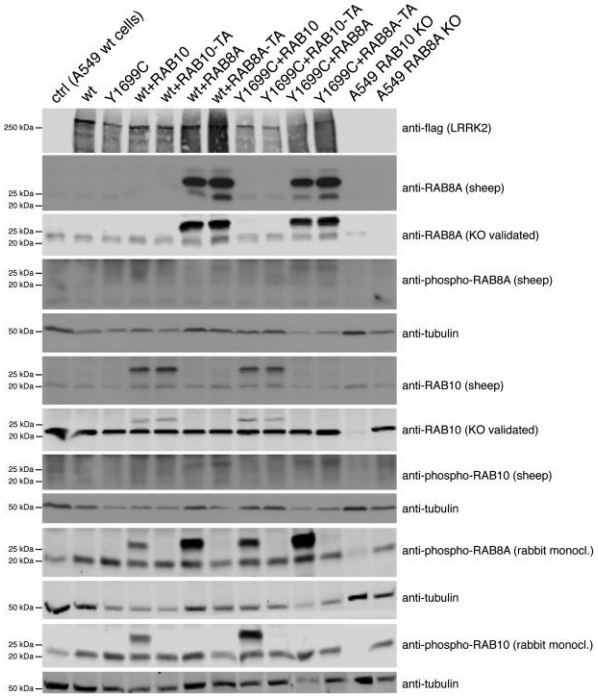

Fig. 17. Specificity of the various RAB8, RAB10 and phospho-RAB8/phospho-RAB10 antibodies as assessed by Western blotting techniques. A549 cells were either left untreated, transfected with flag-tagged wildtype or Y1699C mutant LRRK2, or co-transfected with flag-tagged RAB10, RAB10-T73A, RAB8A, or RAB8A-T72A as indicated. Extracts, along with extracts from A549 RAB10 and A549 RAB8A knockout cells, were analysed by Western blotting using various antibodies as indicated. A sheep anti-RAB8A antibody (MRC PPU, S969D) detected overexpressed RAB8A, but not RAB10. A mouse knockout-validated RAB8A antibody (Abcam, ab188574) specifically detected overexpressed RAB8A as well as endogenous RAB8A. A sheep anti-RAB10 antibody (MRC PPU, S945D) detected overexpressed RAB10, but not RAB8A. A mouse knockout-validated RAB10 antibody (Sigma-Aldrich, SAB5300028) was specific for RAB10. Whilst the sheep anti-phospho-RAB8A antibody (MRC PPU, S874D) and anti-phospho-RAB10 antibody (MRC PPU, S873D) displayed poor affinity, a rabbit monoclonal anti-phospho-RAB8A antibody (Abcam, ab230260) potently detected phospho-RAB8A, and to a lesser degree also phospho-RAB10, as previously described (Lis et al., 2018). A rabbit monoclonal phospho-RAB10 antibody (Abcam, ab230261) potently and specifically detected only phospho-RAB10.

We first analysed for the specificity of distinct RAB8, RAB10, phospho-RAB8 and phospho-RAB10 antibodies by Western blotting and immunocytochemistry techniques. As assessed by Western blotting, both KO-validated sheep and mouse total anti-RAB10 antibodies were specific for RAB10, and both KO-validated sheep and mouse total anti-RAB8 antibodies were specific for RAB8, respectively (Fig. 17) (Madero-Pérez et al., 2018a). By immunocytochemistry, the sheep KO-validated total anti-RAB10 and anti-RAB8 antibodies were also specific for the respective RAB proteins (Fig. 18A,B). In contrast, the sheep phospho-RAB10 antibody detected accumulation of phosphorylated RAB species in cells expressing wildtype LRRK2 with either RAB10 or with RAB8, indicating that it was detecting both phosphorylated RAB species, and similar results were obtained for the sheep phospho-RAB8 antibody (Fig. 18C,D). Since the high-affinity KO-validated commercial rabbit monoclonal anti-phospho-RAB10 and anti-phospho-RAB8 antibodies (Lis et al., 2018) were not suitable for immunocytochemistry purposes under the conditions employed (Fig. 19A,B), we used the sheep phospho-RAB10 antibody, which detects both phosphorylated RAB10/8 (Fig. 18D), as well as the KO-validated mouse monoclonal anti-RAB10 antibody highly specific for total RAB10 (Fig. 18E), for further cell biological analysis.

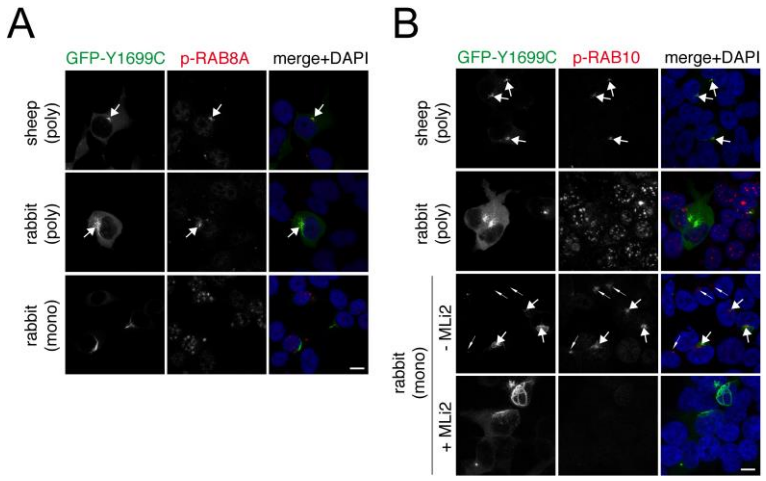

Fig. 18. Specificity of the various RAB8, RAB10 and phospho-RAB8/phospho-RAB10 antibodies as assessed by immunocytochemistry techniques in HEK293T cells. (A) HEK293T cells were transfected with GFP-tagged Y1699C mutant LRRK2, and stained with either a sheep polyclonal phospho-RAB8A antibody (MRC PPU, S874D), a rabbit polyclonal phospho-RAB8A antibody, or a rabbit monoclonal phospho-RAB8A antibody (Abcam, ab230260), and DAPI. Scale bar, 10 µm. The sheep and rabbit polyclonal antibodies specifically detect endogenous accumulation of phospho-RAB8 (Madero-Perez et al., 2018a), whilst the rabbit monoclonal antibody is unsuitable for immunocytochemistry under these conditions. **(B)** HEK293T cells were transfected with GFP-tagged Y1699C mutant LRRK2, and stained with either a sheep polyclonal phospho-RAB10 antibody (MRC PPU, S873D), a rabbit polyclonal phospho-RAB10 antibody, or a rabbit monoclonal phospho-RAB10 antibody (Abcam, ab230261), and DAPI. Scale bar, 10 µm. The sheep polyclonal antibody specifically detects endogenous accumulation of phospho-RAB10 (see also Fig. 20), whilst the rabbit polyclonal antibody is unsuitable for immunocytochemistry under our conditions. The rabbit monoclonal phospho-RAB10 antibody detects perinuclear phospho-RAB10 accumulation in transfected cells (arrows), with no detectable phospho-signal upon treatment of cells with 100 nM MLi-2 for 60 min prior to immunocytochemistry (bottom row). However, signal was also detected to a similar degree in some non-transfected cells (small arrows), and the antibody therefore was not deemed suitable for immunocytochemistry under our conditions.

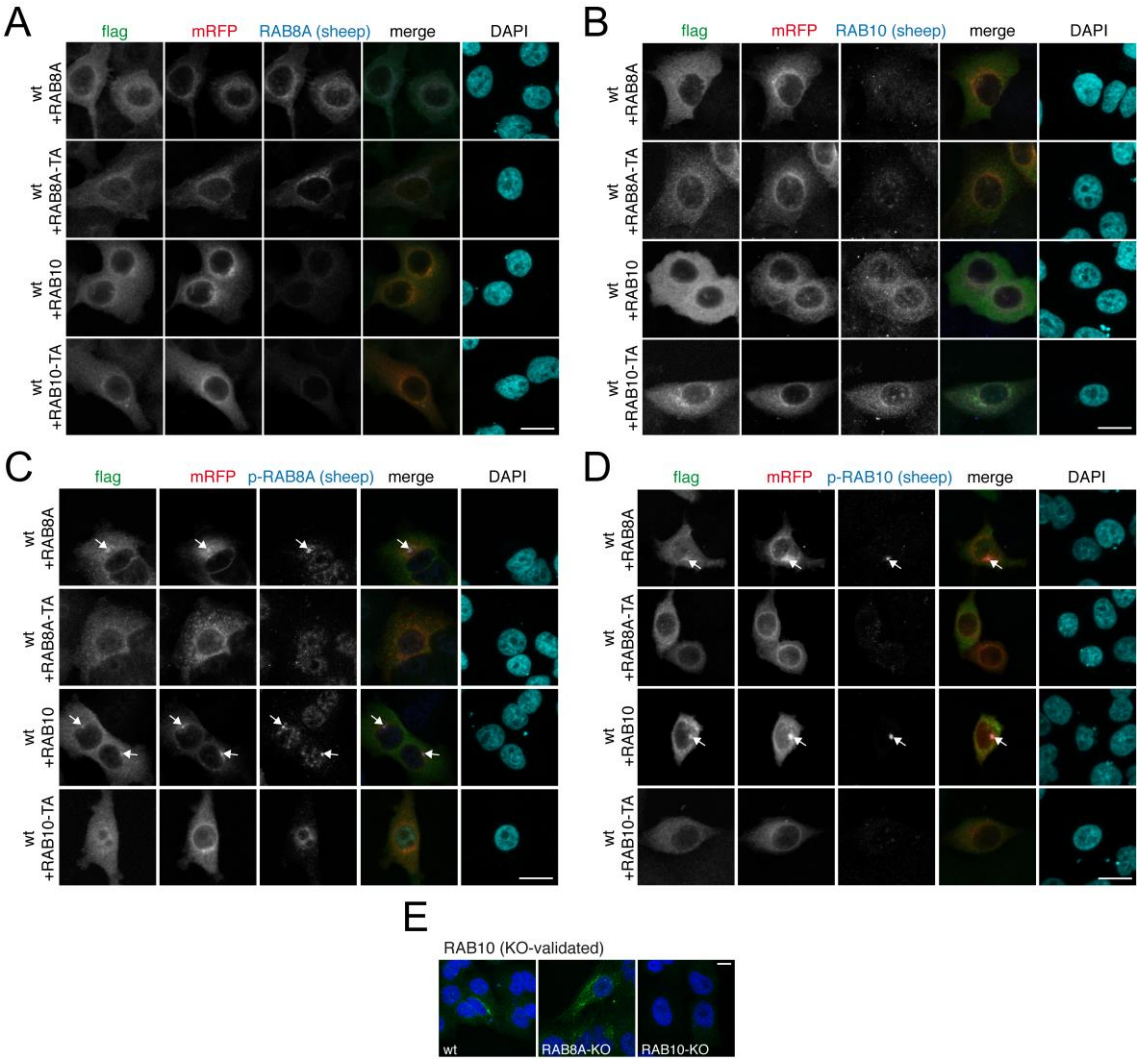

Fig. 19. Specificity of the various RAB8, RAB10 and phospho-RAB8/phospho-RAB10 antibodies as assessed by immunocytochemistry techniques in A549 cells. (A) A549 cells were co-transfected with flag-tagged wildtype LRRK2 and either mRFP-tagged RAB8A, RAB8A-T72A, RAB10 or RAB10-T73A as indicated, and cells stained with a sheep anti-RAB8A antibody and DAPI. Scale bar, 20 µm. **(B)** Same as in (A), but cells stained with a sheep anti-RAB10 antibody. Scale bar, 20 µm. **(C)** Same as in (A), but cells stained with a sheep anti-phospho-RAB8A antibody. Scale bar, 20 µm. **(D)** Same as in (A), but cells stained with a sheep anti-phospho-RAB10 antibody. Scale bar, 20 µm. The sheep anti-RAB8A antibody specifically detects RAB8A, and the sheep anti-RAB10 antibody specifically detects RAB10, whilst both sheep anti-phospho-RAB8A and sheep anti-phospho-RAB10 detect both phosphorylated RAB species. **(E)** A549 cells (wt, RAB8A-KO or RAB10-KO cells) were stained with a mouse knockout-validated RAB10 antibody (Sigma-Aldrich, SAB5300028), which stained a tubular compartment in wildtype and RAB8A-KO cells, but not in RAB10-KO cells. Scale bar, 10 µm.

Staining of HEK293T cells expressing pathogenic Y1699C LRRK2 revealed pericentrosomal/centrosomal phospho-RAB10/8 accumulation (Fig. 20A,B). The signal was specific for detecting the phosphorylated RAB species, as not observed upon preincubation of the antibody with phospho-peptide or upon treatment of cells with MLi-2, another distinct and highly specific LRRK2 kinase inhibitor (Fig. 20A,B). We further used a knockout-validated total anti-RAB10 antibody highly specific for RAB10 (Fig. 18E). Endogenous RAB10 was localized to a pericentrosomal/centrosomal area in cells expressing either pathogenic Y1699C, R1441C or G2019S mutant LRRK2

(Fig. 20C,D). Such localization was reverted upon application of MLi-2, and was not observed in non-transfected, wildtype LRRK2-transfected or kinase-inactive G2019S-K1906M LRRK2-transfected cells, respectively, indicating that it reflects a phosphorylated species of RAB10 (Fig. 20C,D).

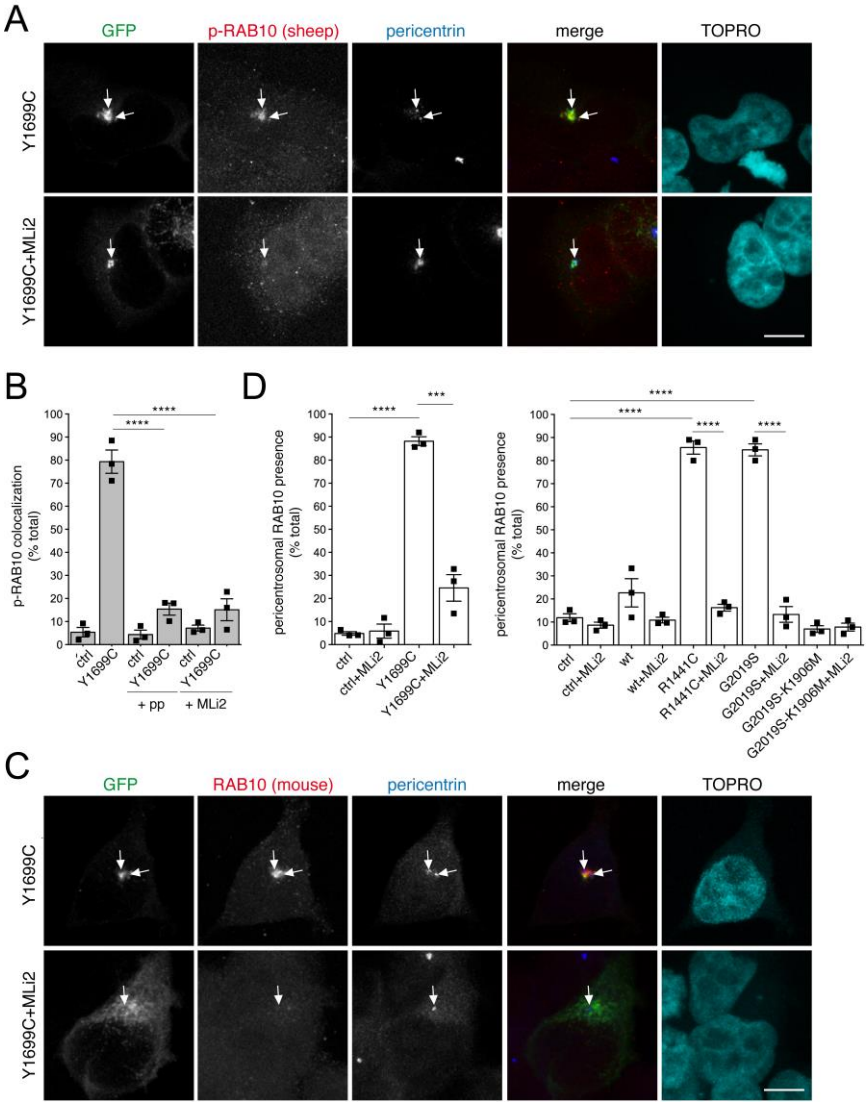

Fig. 20. Pathogenic LRRK2 causes kinase-dependent pericentrosomal/centrosomal accumulation of endogenous phospho-RAB10/8. (A) Example of HEK293T cells transfected with Y1699C mutant GFP-tagged LRRK2, in either the absence or presence of 100 nM of the LRRK2 kinase inhibitor MLi-2 for 60 min prior to immunocytochemistry as indicated. Cells were stained using a sheep anti-phospho-RAB10 antibody preabsorbed with non-phospho-peptide, an anti-pericentrin antibody and TOPRO. Scale bar, 5 µm. **(B)** Quantification of the percentage of cells displaying pericentrosomal/centrosomal phospho-RAB10/8 staining colocalising with centrosomes within a 3 µm diameter circle in either non-transfected cells (ctrl), or in pathogenic LRRK2-transfected cells as indicated, in either the absence or presence of antibody preabsorption with non-phospho-peptide or phospho-peptide (+pp), or pretreatment of cells with MLi-2 as described above. Around 100-150 cells were quantified per condition per experiment. Bars represent mean ± s.e.m. (n = 3 experiments); ****, $p < 0.001$. **(C)** Cells were transfected with pathogenic GFP-tagged LRRK2, and subjected to immunocytochemistry using a knockout-validated anti-RAB10 antibody, pericentrin and TOPRO upon incubation of cells with 100 nM MLi-2 for 60 min prior to immunocytochemistry as indicated. Scale bar, 5 µm. **(D)** Quantification of the percentage of cells displaying pericentrosomal RAB10 accumulation in either non-transfected cells (ctrl), wildtype, pathogenic LRRK2, or kinase-inactive pathogenic LRRK2 (G2019S-K1906M) transfected cells as indicated, either in the absence or presence of MLi-2 (100 nM, 1 h). Bars represent mean ± s.e.m. (n = 3 experiments); ****, $p < 0.001$; ***, $p < 0.005$.

The accumulation of phospho-RAB10 was next evaluated in another cell system. The phospho-RAB10/8 antibodies were not of sufficient affinity to detect the centrosomal accumulation of endogenous phospho-RABs in G2019S LRRK2 mutant SH-SY5Y cells, but did detect centrosomal accumulation of phospho-RAB10/8 when expressing wildtype RAB10 in either wildtype or G2019S LRRK2-mutant SH-SY5Y cells to increase the phosphorylated RAB10 species (Fig. 21A,B). The increase in the phospho-RAB10 signal disappeared when pretreating cells with MLi-2, and was not detected when expressing the non-phosphorylatable RAB10-T73A mutant (Fig. 21A,B), indicating that it was specifically detecting a LRRK2-phosphorylated version of RAB10. Expression of wildtype RAB10, but not phosphorylation-deficient RAB10 mutant, in wildtype or G2019S LRRK2-mutant SH-SY5Y cells caused a centrosomal cohesion deficit which was reversed by MLi-2 (Fig. 22A,B). Therefore, as analysed in two distinct cell systems, increasing the pericentrosomal/centrosomal amount of phosphorylated RAB10 also correlates with the observed centrosomal cohesion deficits.

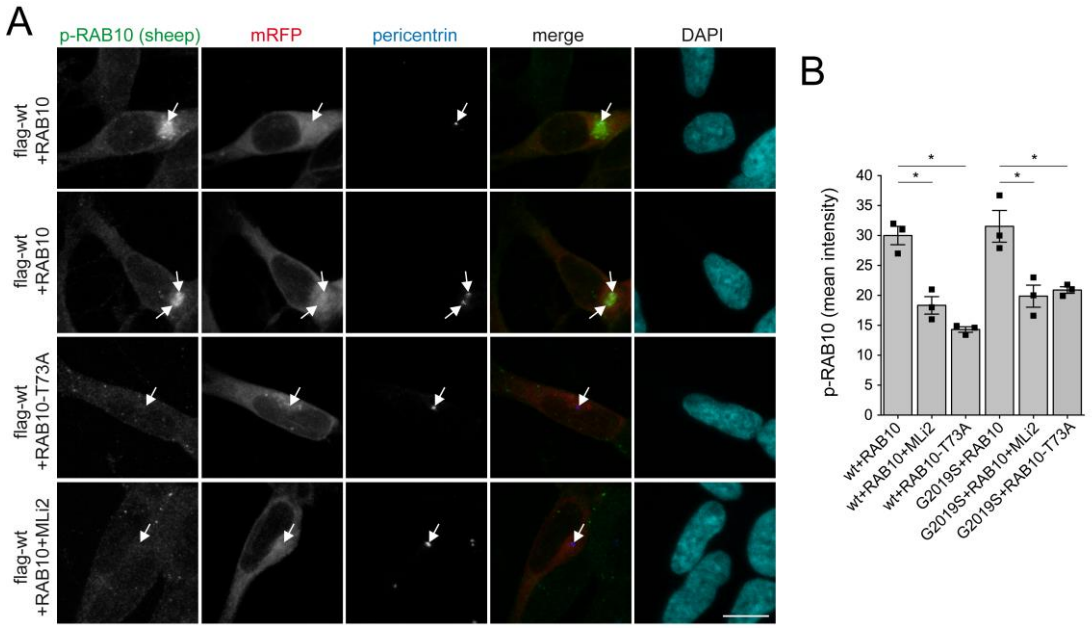

Fig. 21. Expression of wildtype but not phosphorylation-deficient RAB10 causes pericentrosomal/centrosomal accumulation of phospho-RAB10 in wildtype LRRK2-expressing SH-SY5Y cells. (A) Example of SH-SY5Y cells stably expressing flag-tagged wildtype LRRK2, and transfected with mRFP-tagged wildtype or T73A-mutant RAB10 as indicated, stained with a sheep anti-phospho-T73-RAB10 antibody preabsorbed with non-phospho-peptide, for pericentrin and DAPI. Where indicated, cells were treated with 100 nM MLi-2 for 2 h before immunocytochemistry. Scale bar, 10 µm. **(B)** Quantification of mean fluorescence intensity of phospho-RAB10 as described in Materials and Methods in cells either stably expressing wildtype (wt) or G2019S mutant LRRK2, transfected with mRFP-tagged RAB10 or T73-mutant RAB10, and treated with 100 nM MLi-2 for 2 h before immunocytochemistry as indicated. Bars represent mean ± s.e.m. (n = 3 experiments); *, $p < 0.05$.

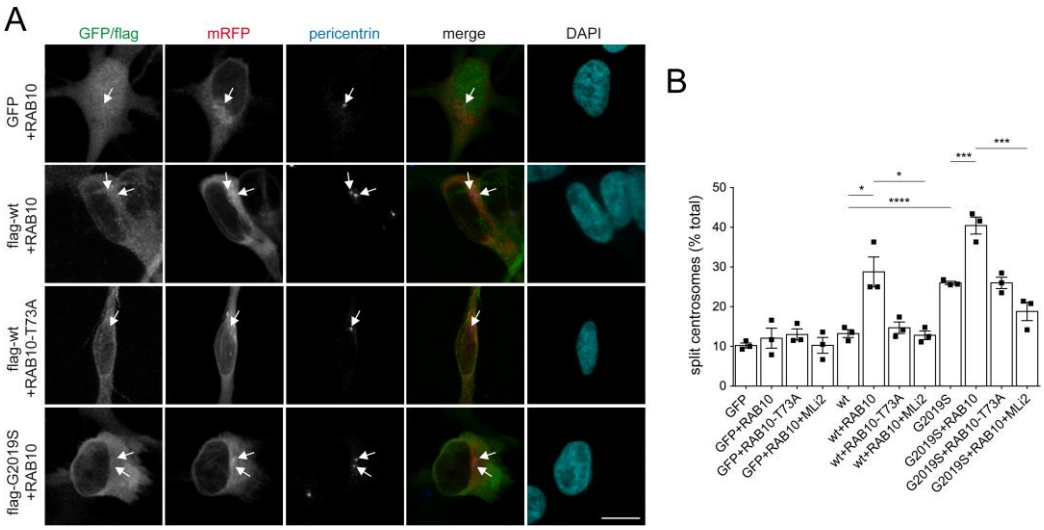

Fig. 22. Expression of wildtype but not phosphorylation-deficient RAB10 causes centrosome cohesion deficits in wildtype LRRK2-expressing SH-SY5Y cells. (A) Example of non-differentiated SH-SY5Y cells stably expressing GFP, flag-tagged wildtype or G2019S-mutant LRRK2 as indicated, and transfected with RAB10 or phosphorylation-deficient RAB10-T73A as indicated, and stained for flag, pericentrin and DAPI. Scale bar, 10 µm. **(B)** Quantification of the split centrosome phenotype in SH-SY5Y cells from the type of experiments depicted in (A). Bars represent mean ± s.e.m. (n = 3 experiments); ****, $p < 0.001$; ***, $p < 0.005$; *, $p < 0.05$.

Pathogenic LRRK2-mediated centrosomal cohesion deficits depend on RAB8A, RAB10 and RILPL1

To further analyse how pathogenic LRRK2 causes centrosomal cohesion deficits, we expressed wildtype or distinct LRRK2 mutants in either wildtype A549 cells, or in cells deficient in RAB8A, RAB10 or RILPL1. In wildtype cells, expression of pathogenic G2019S, R1441C or Y1699C LRRK2 mutant caused a centrosomal cohesion phenotype which was abolished upon treatment with the LRRK2 kinase inhibitor MLi-2, and was not observed when expressing wildtype or kinase-dead K1906M LRRK2 (Fig. 23A,B), with all constructs expressed to similar degrees (Fig. 23C,D). We next attempted to correlate the LRRK2-mediated centrosomal cohesion phenotype with alterations in the levels of phospho-RAB8/RAB10 as assessed by Western blotting techniques. In non-transfected A549 RAB8A-KO cells, the total anti-RAB8 antibody, previously reported to be specific for RAB8(A+B) as assessed by Western blotting of RAB8A/RAB8B double-KO mouse extracts (Sato et al., 2014), revealed the remaining presence of RAB8B. The rabbit monoclonal phospho-RAB8A antibody revealed the presence of a phospho-RAB band in the A549 RAB8A-KO cells, likely due to the reported crossreactivity of this antibody with other LRRK2-phosphorylated RAB substrates including RAB8B and/or RAB10 (Lis et al., 2018) (Fig. 23C). In contrast, the mouse monoclonal anti-RAB10, and the rabbit monoclonal anti-phospho-RAB10 antibodies were highly specific, as no signal was detected in the A549 RAB10-KO cells (Fig. 23D).

Importantly, the centrosomal cohesion deficits mediated by pathogenic LRRK2 correlated with increases in phospho-RAB8/RAB10 levels in a manner modulated by the LRRK2 kinase inhibitor MLi-2 (Fig. 23C,D).

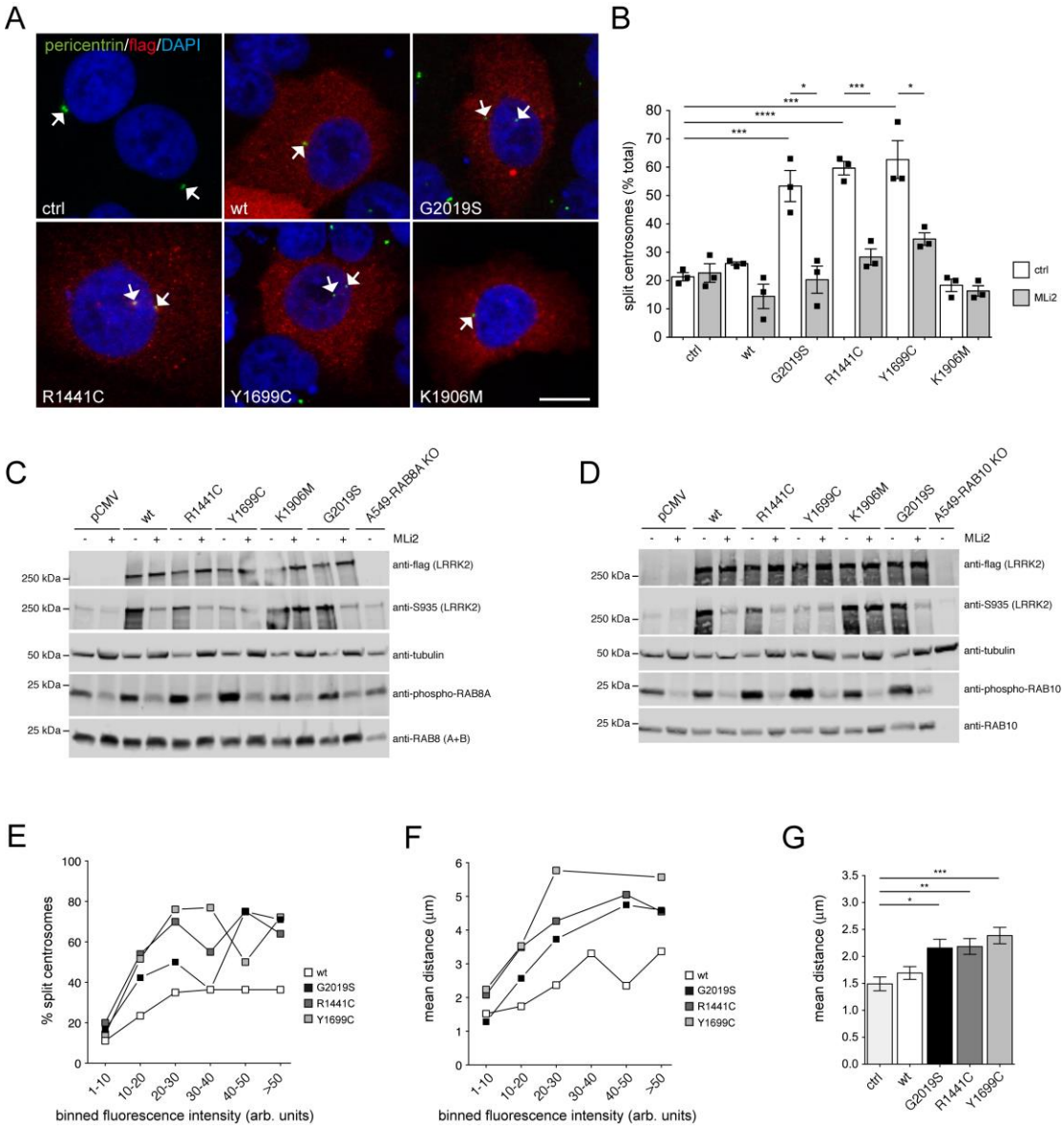

Fig. 23. Pathogenic LRRK2 causes kinase-dependent and dose-dependent centrosomal cohesion deficits. (A) Example of wildtype A549 cells transfected with either pCMV (ctrl), or with the indicated flag-tagged LRRK2 constructs, and stained with an antibody against flag, pericentrin and DAPI. Scale bar, 10 µm. **(B)** Quantification of the percentage of wildtype A549 cells with split centrosomes transfected with the different LRRK2 constructs, and either left untreated, or incubated with 500 nM MLi-2 for 2 h before immunocytochemistry as indicated. Bars represent mean ± s.e.m. (n = 3 experiments); ****, $p < 0.001$; ***, $p < 0.005$; *, $p < 0.05$. **(C)** Wildtype A549 cells were transfected with the indicated LRRK2 constructs, either left untreated or incubated with 500 nM MLi-2 for 2 h as indicated, and extracts blotted for flag-tagged LRRK2, phosphorylated LRRK2 (phospho-S935), endogenous RAB8 (A+B), phospho-T72-RAB8A (rabbit monoclonal antibody), and tubulin as loading control. **(D)** Same as in (C), but extracts blotted for flag-tagged LRRK2, phosphorylated LRRK2 (phospho-S935), endogenous RAB10, phospho-T73-RAB10 (rabbit monoclonal antibody), and tubulin as loading control. **(E)** Wildtype A549 cells were transfected with the indicated flag-tagged constructs, and the percentage of cells with split centrosomes, along with the flag staining intensity of each cell were quantified from around 100 cells with duplicated centrosomes per condition, with fluorescence intensities grouped into distinct bins as indicated. **(F)** Same as in (E), but depicting the mean distance of duplicated centrosomes against the distinct binned fluorescence intensities. **(G)** Same as in (F), but depicting the mean distance of duplicated centrosomes in cells transfected with the indicated constructs irrespective of flag staining intensity. ***, $p < 0.005$; **, $p < 0.01$; *, $p < 0.05$.

When analysing the relationship between centrosomal cohesion deficits and LRRK2 expression levels as measured by quantitative light microscopy, the percentage of split centrosomes, and the overall mean distance between duplicated centrosomes increased with increasing LRRK2 expression levels until reaching a plateau, suggesting that pathogenic LRRK2 expression causes a concentration-dependent centrosomal cohesion deficit which becomes saturated at higher expression levels (Fig. 23E,F). Measuring the distance between duplicated centrosomes in all cells irrespective of protein expression levels also revealed a significant increase in the mean distance between duplicated centrosomes in cells expressing pathogenic LRRK2 as compared to control cells, with the mean centrosomal distance in control cells similar to what has been previously described in this cell type (Dhekne et al., 2018) (Fig. 23G).

A recent report suggested that RILPL1 expression in A549 cells causes a cohesion deficit in a manner independent on expression levels (Dhekne et al., 2018). When expressing either C-terminally flag-tagged, or C-terminally or N-terminally eGFP-tagged human RILPL1, no differences in centrosomal cohesion were observed when quantifying the percentage of split centrosomes or the mean distance between duplicated centrosomes, including in cells expressing very high levels of RILPL1 (Fig. 24A-C). Thus, our data indicate that pathogenic LRRK2 causes centrosomal cohesion deficits in a concentration-dependent manner, which is not observed upon human RILPL1 expression.

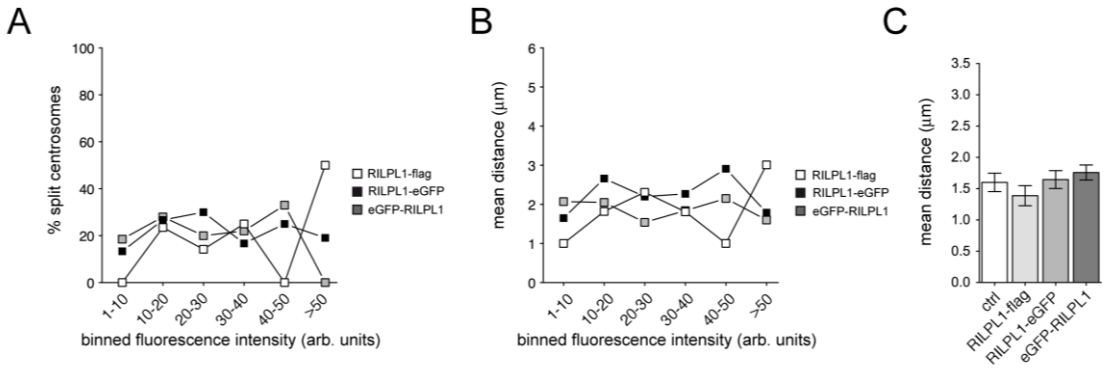

Fig. 24. Expression of human RILPL1 do not cause a centrosomal cohesion deficit. (A) Wildtype A549 cells were transfected with either C-terminally flag-tagged or eGFP-tagged human RILPL1, or N-terminally eGFP-tagged human RILPL1, and the percentage of cells with split centrosomes, along with the flag staining intensity (or eGFP fluorescence intensity) of each cell quantified from around 100 cells with duplicated centrosomes per condition, with fluorescence intensities grouped into distinct bins as indicated. **(B)** Same as in (A), but depicting the mean distance of duplicated centrosomes against the distinct binned fluorescence intensities. **(C)** Same as in (B), but depicting the mean distance of duplicated centrosomes in cells transfected with the indicated constructs irrespective of flag staining/eGFP fluorescence intensity.

To address whether the LRRK2-mediated centrosomal cohesion deficits are dependent on the presence of RAB8A, RAB10 or RILPL1, we employed A549 cells where the proteins were knocked out using CRISPR-Cas9 (Dhekne et al., 2018). Non-transfected A549 cells lacking RAB8A, RAB10 or RILPL1 did not display centrosomal cohesion deficits (Fig. 25A), with the lack of the respective proteins confirmed by Western blotting techniques (Fig. 26). In addition, no alterations were found in the levels of RAB8B in either the RAB8A or RAB10 KO cells, in the levels of RAB8A in the RAB10 or RILPL1 KO cells, or in the levels of RAB10 in the RAB8A or RILPL1 KO cells, respectively (Fig. 26). Importantly though, and as compared to A549 wildtype cells, the pathogenic LRRK2-mediated centrosomal cohesion deficits were drastically reduced in cells deficient for RAB8A (Fig. 25A,B), and abolished in cells deficient for RAB10 or RILPL1 (Fig. 25A,C,D), respectively, even though the various LRRK2 variants were expressed to similar degrees (Fig. 25E).

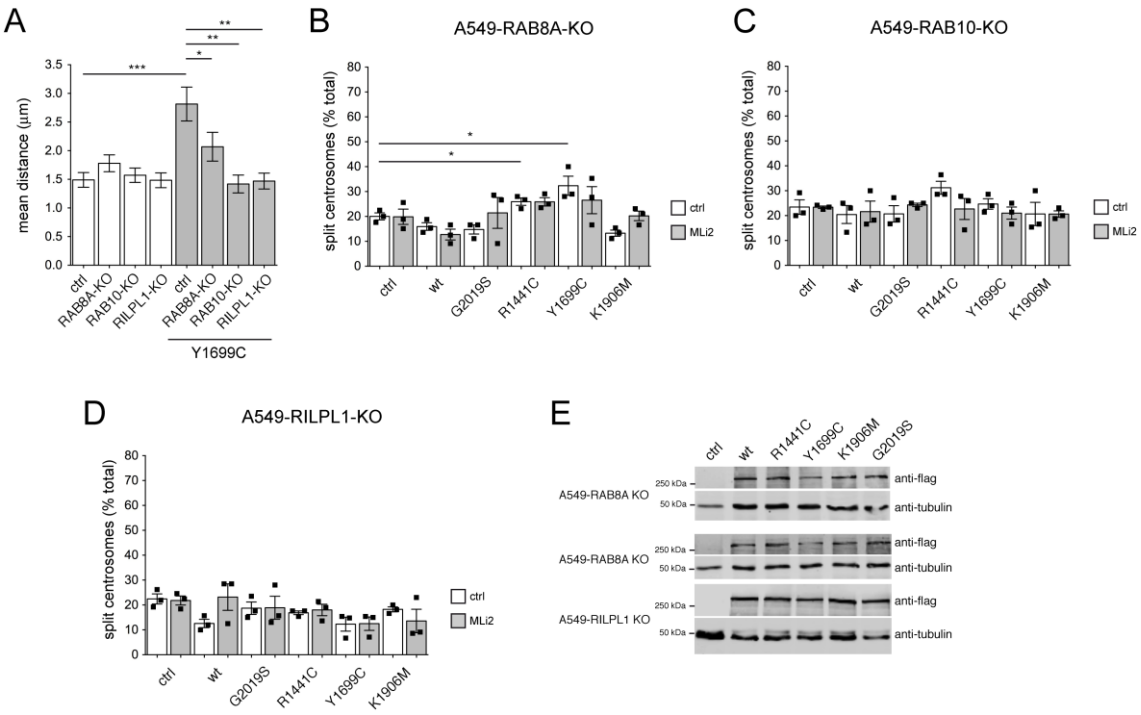

Fig. 25. Pathogenic LRRK2-mediated centrosomal cohesion deficits depend on RAB8A, RAB10 and RILPL1. (A) Quantification of the mean distance of duplicated centrosomes from either wildtype A549 cells (ctrl), or A549 knockout cells (RAB8A-KO, RAB10-KO, RILPL1-KO), in the absence or presence of Y1699C pathogenic LRRK2 expression as indicated. Between 50 and 100 cells with duplicated centrosomes per condition were analysed. ***, $p < 0.005$; *, $p < 0.05$. **(B)** Quantification of the percentage of A549 RAB8A-KO cells transfected with the different LRRK2 constructs displaying duplicated split centrosomes, in either the presence or absence of MLi-2 (500 nM, 2 h) as indicated. Bars represent mean ± s.e.m. (n = 3 experiments); *, $p < 0.05$. **(C)** Quantification of the percentage of A549 RAB10-KO cells transfected with the different LRRK2 constructs displaying duplicated split centrosomes, in either the presence or absence of MLi-2 (500 nM, 2 h) as indicated. Bars represent mean ± s.e.m. (n = 3 experiments). **(D)** Quantification of the percentage of A549 RILPL1-KO cells transfected with the different LRRK2 constructs displaying duplicated split centrosomes, in either the presence or absence of MLi-2 (500 nM, 2 h) as indicated. Bars represent mean ± s.e.m. (n = 3 experiments). **(E)** The distinct A549 knockout cells were transfected with the indicated flag-tagged LRRK2 constructs, and extracts blotted for flag, and tubulin as loading control.

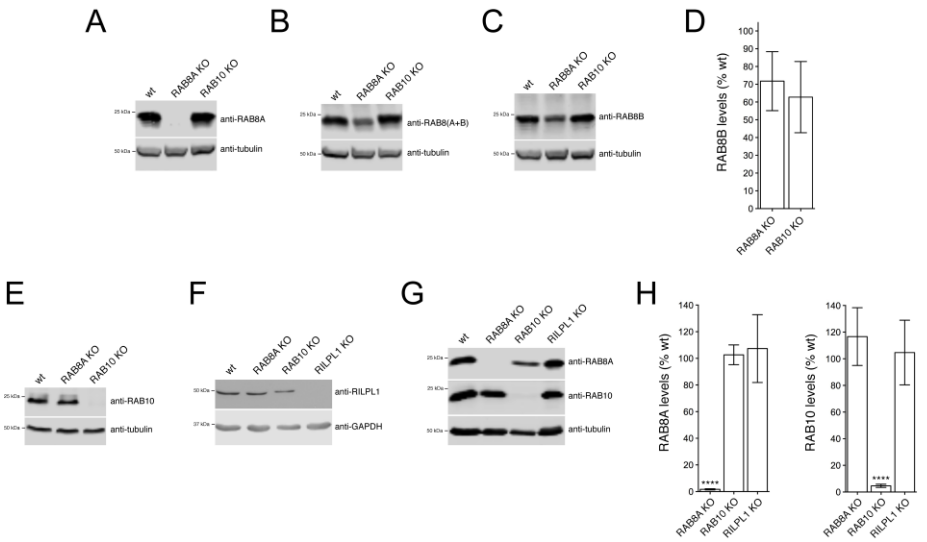

Fig. 26. Analysis of the levels of RAB8A, RAB10 and RILPL1 in A549 wildtype, RAB8A-KO, RAB10-KO and RILPL1-KO cells. (A) Extracts blotted with a KO-validated RAB8A antibody (Abcam, ab188574). **(B)** Extracts blotted with an antibody recognizing both RAB8A and RAB8B (BD Biosciences, 610844). **(C)** Extracts blotted with an antibody recognizing RAB8B (Invitrogen, PA5-67354). **(D)** Quantification of the levels of RAB8B in the RAB8A and RAB10 A549 KO cells, with values normalized to tubulin, and normalized to the levels of RAB8B in A549 wildtype cells. Bars represent mean ± s.e.m. (n = 4 experiments). **(E)** Extracts blotted with a KO-validated anti-RAB10 antibody (Sigma-Aldrich, SAB5300028). **(F)** Extracts blotted with a sheep anti-RILPL1 antibody. **(G)** Extracts blotted with a KO-validated RAB8A antibody (Abcam, ab188574), a KO-validated anti-RAB10 antibody (Sigma-Aldrich, SAB5300028), and tubulin as loading control. **(H)** Quantification of the type of experiments depicted in (G), with values normalized to tubulin, and normalized to the levels of RAB8A in A549 wildtype cells (left), or the levels of RAB10 in A549 wildtype cells (right), respectively. Bars represent mean ± s.e.m. (n = 3 experiments); ****, $p < 0.0001$.

Pathogenic LRRK2-mediated centrosomal cohesion deficits do not depend on RAB12, RAB35 or RAB43

LRRK2 also phosphorylates other endogenous RAB proteins including RAB12, RAB35 and RAB43 (Steger et al., 2017). To study the potential role of RAB12, RAB35 or RAB43, we employed A549 cells where these proteins were knocked out using CRISPR-Cas9 (Steger et al., 2017) (Fig. 27A). As described above, expression of pathogenic LRRK2 in wildtype A549 cells caused a centrosomal cohesion deficit which was reverted by MLi-2, whilst wildtype or a kinase-inactive LRRK2 mutant were without effect (Fig. 27C). Similar centrosomal cohesion deficits were observed when pathogenic LRRK2 constructs were expressed in A549 cells deficient in either RAB12 (Fig. 27B,D), RAB35 (Fig. 27E) or RAB43 (Fig. 27F). In all cases, the deficits were reverted by MLi-2, and were not observed when expressing wildtype or kinase-inactive LRRK2 mutant. The pathogenic LRRK2-mediated increase in the percentage of split centrosomes was paralleled by an increase in the overall mean distance between duplicated centrosomes (Fig. 27G). Furthermore, and as assessed by immunoblot analysis, expression of pathogenic LRRK2 caused similar increases in the levels of phospho-RAB8 and phospho-RAB10 in wildtype cells or in cells

deficient in either RAB12, RAB35 or RAB43 (Fig. 27H). Therefore, the LRRK2-mediated centrosomal cohesion deficits are crucially dependent on RAB8A, RAB10 and RILPL1, but not on the presence of RAB12, RAB35 or RAB43.

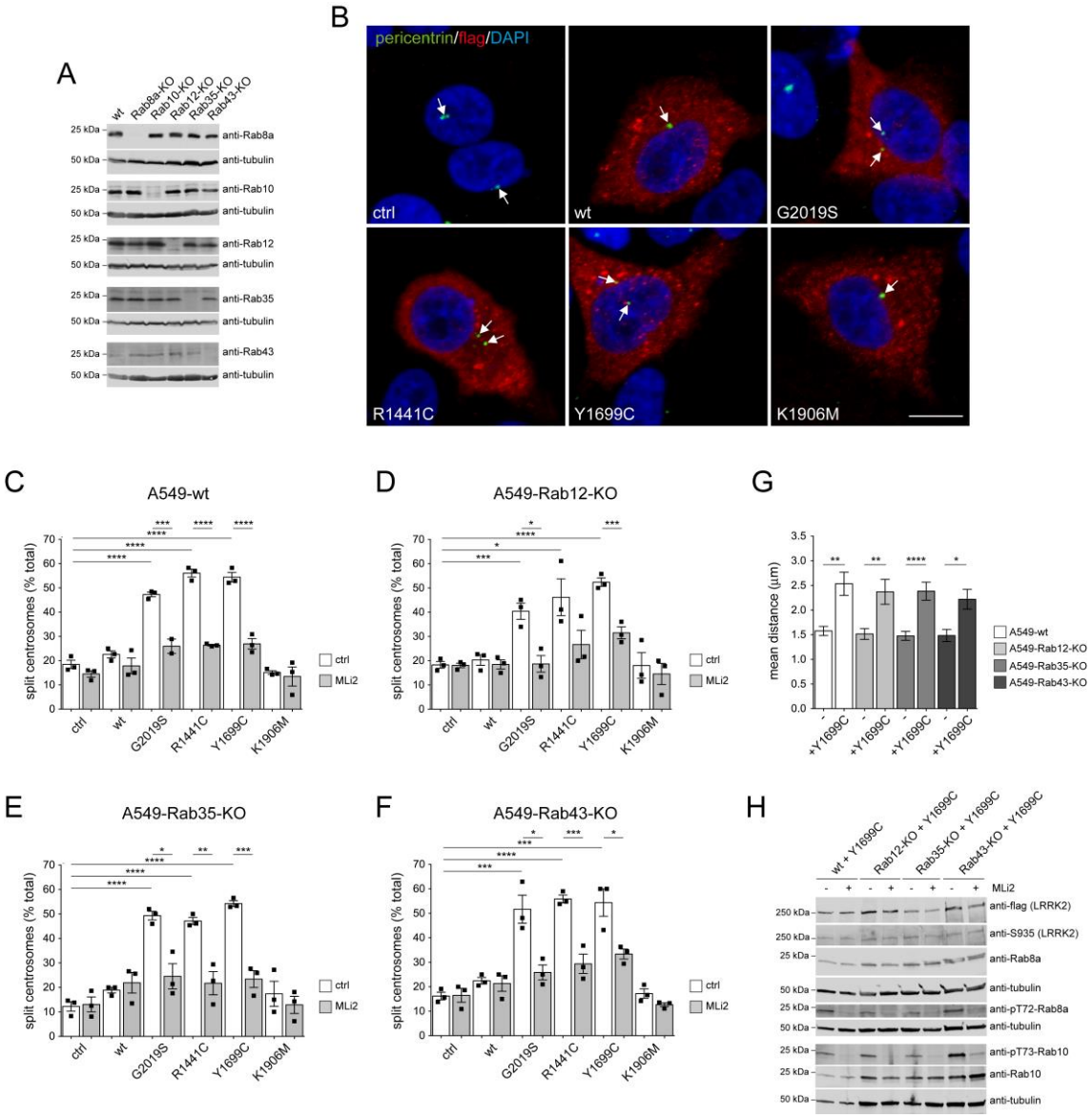

Fig. 27. Pathogenic LRRK2-mediated centrosomal cohesion deficits do not depend on the presence of RAB12, RAB35 or RAB43. (A) Wildtype A549 cells (wt), or cells where the distinct RAB proteins had been knocked out (KO) using CRISPR-Cas9 were subjected to immunoblot analysis for the presence or absence of the various RAB proteins as indicated, with tubulin as loading control. **(B)** Example of A549 RAB12-KO cells transfected with either pCMV (ctrl), or with the indicated flag-tagged LRRK2 constructs and stained with antibodies against flag, pericentrin and with DAPI. Scale bar, 10 µm. **(C)** Quantification of the percentage of wildtype A549 cells with split centrosomes transfected with the different LRRK2 constructs, and either left untreated or incubated with 500 nM MLi-2 for 2 h prior to immunocytochemistry as indicated. **(D)** Same as in (C), but employing RAB12-KO cells. **(E)** Same as in (C), but employing RAB35-KO cells. **(F)** Same as in (C), but employing RAB43-KO cells. In all cases, bars represent mean ± s.e.m. (n = 3 experiments); ****, $p < 0.001$; ***, $p < 0.005$; **, $p < 0.01$; *, $p < 0.05$. **(G)** Wildtype cells, or RAB12-KO, RAB35-KO or RAB43-KO cells were transfected with flag-tagged Y1699C LRRK2, and distances between duplicated centrosomes quantified from around 50-70 transfected or non-transfected cells each. ****, $p < 0.001$; **, $p < 0.01$; *, $p < 0.05$. **(H)** A549 wt cells, or RAB12-KO, RAB35-KO or RAB43-KO cells were transfected with Y1699C-mutant LRRK2 construct, left untreated or incubated with 500 nM MLi-2 for 2 h as indicated, and extracts were blotted for flag-tagged LRRK2, phosphorylated LRRK2 (S935), pT72-RAB8A, total RAB8A, pT73-RAB10, total RAB10, or tubulin as loading control.

RILPL1 localization is crucial for the centrosomal cohesion deficits mediated by LRRK2-phosphorylated RAB proteins

LRRK2-phosphorylated RAB8 and RAB10 bind with strong preference to RILPL1 and RILPL2 (Steger et al., 2017), and, as described above, RILPL1 is required for the centrosomal cohesion deficits mediated by pathogenic LRRK2. To evaluate the involvement of RILPL2, we transfected A549 RILPL2 knockout cells with wildtype or distinct pathogenic LRRK2 mutants. Pathogenic LRRK2 expression caused centrosomal cohesion deficits in RILPL2 knockout cells identical to those observed in wildtype cells, which were reverted by MLi-2 in all cases (Fig. 28).

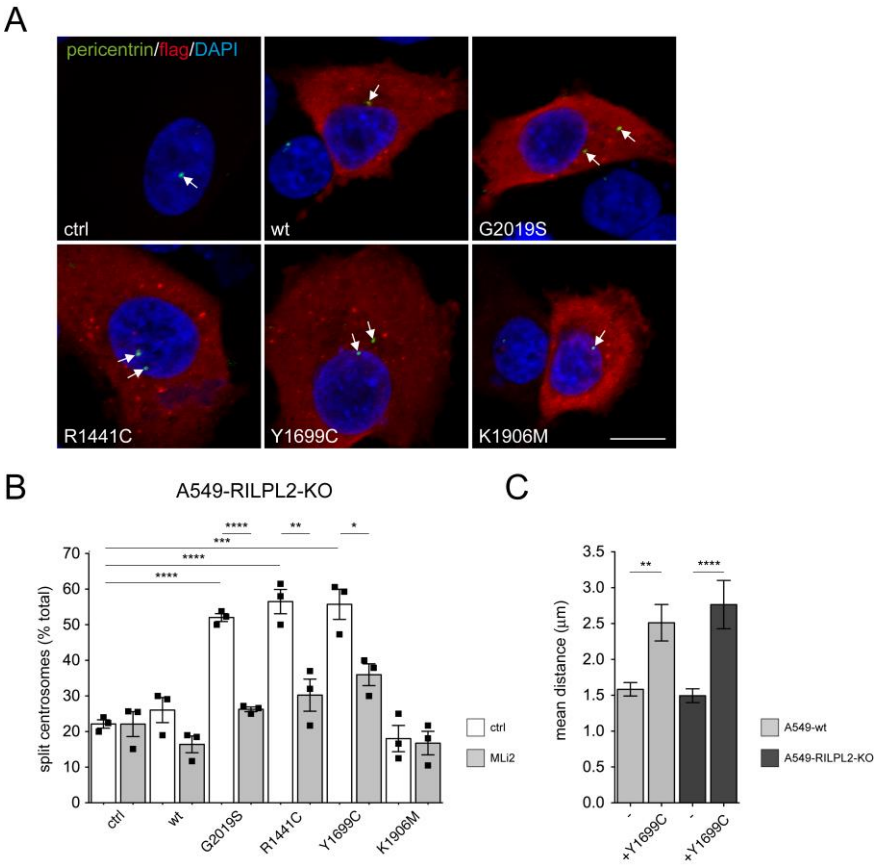

Fig. 28. RILPL2 is dispensable for the LRRK2-mediated centrosomal cohesion deficits. (A) RILPL2-KO cells were transfected with either pCMV (ctrl), or with the indicated flag-tagged LRRK2 constructs, and stained with antibodies against flag, pericentrin and with DAPI. Scale bar, 10 µm. **(B)** Quantification of the percentage of A549 RILPL2-KO cells with split centrosomes upon transfection of the indicated constructs, in either the absence or presence of MLi-2 (500 nM, 2 h) prior to immunocytochemistry. Bars represent mean ± s.e.m. (n = 3 experiments); ****, $p < 0.001$; ***, $p < 0.005$; **, $p < 0.01$; *, $p < 0.05$. **(C)** Wildtype or RILPL2-KO cells were transfected with flag-tagged Y1699C LRRK2, and distances between duplicated centrosomes quantified from around 50-70 transfected or non-transfected cells each. ****, $p < 0.001$; **, $p < 0.01$.

In addition, wildtype cells transfected with pathogenic LRRK2 displayed prominent phospho-RAB10 staining in a perinuclear area and in tubular structures, and similar staining was observed in RILPL2 knockout cells (Fig. 29). In contrast, and as previously reported (Dhekne et al., 2018), RILPL1 knockout cells transfected

with pathogenic LRRK2 showed a diminished perinuclear distribution of phospho-RAB10 accompanied by punctate staining throughout the cytosol (Fig. 29). Together, these data support the conclusion that the centrosomal cohesion phenotype mediated by pathogenic LRRK2 is largely determined by the interaction of phospho-RAB10 with RILPL1, at least in this cell system.

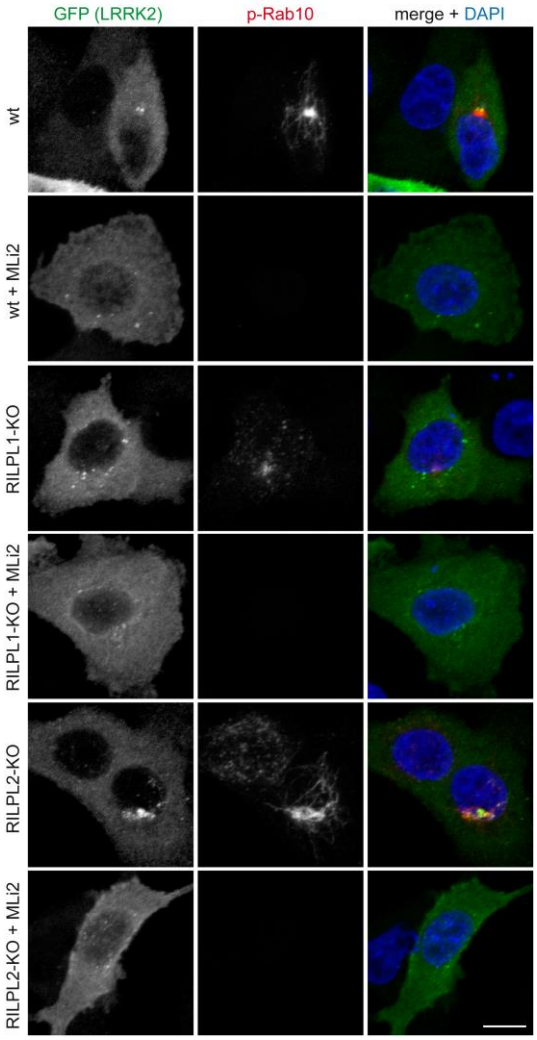

Fig. 29. Localization of phospho-RAB10 is influenced by the presence of RILPL1. Examples of wildtype, RILPL1-KO or RILPL2-KO A549 cells transfected with flag-tagged Y1699C LRRK2, and treated with or without MLi-2 (500 nM, 2 h) before immunostaining with an antibody against phospho-RAB10 (p-RAB10) and with DAPI. Perinuclear phospho-RAB10 clusters are prominent in A549 wildtype cells expressing pathogenic LRRK2. In RILPL1-KO cells, perinuclear clusters are rarely observed, but phospho-RAB10 displays an additional punctate staining throughout the cytosol. In RILPL2-KO cells, perinuclear phospho-RAB10 staining is prominent in some cells expressing pathogenic LRRK2. Scale bar, 10 µm.

To further study the involvement of RILPL1 in the LRRK2-mediated centrosomal cohesion deficits, we expressed the C-terminal half of the protein (RL1d-GFP), reported to be responsible for its interaction with the phosphorylated RAB proteins (Steger et al., 2017; Dhekne et al., 2018). When expressed in A549 cells, RL1d-GFP displayed a punctate as well as cytosolic localization (Fig. 30A). Strikingly,

RL1d-GFP expression completely reverted the centrosomal cohesion phenotype induced by pathogenic LRRK2, whilst not displaying an effect when expressed on its own (Fig. 30). Co-expression of RL1d-GFP with pathogenic LRRK2 did not decrease the total levels of phospho-RAB8 or phospho-RAB10 as assessed by immunoblot analysis (Fig. 31A). Rather, whilst pathogenic LRRK2 caused a pronounced perinuclear accumulation of phospho-RAB10, co-expression with RL1d-GFP caused the redistribution of phospho-RAB10 to cytosolic RL1d-GFP-positive punctae (Fig. 31B). These data indicate that the centrosomal phospho-RAB10 accumulation depends on the centrosomal localization of RILPL1 which is required to cause the cohesion deficits mediated by pathogenic LRRK2.

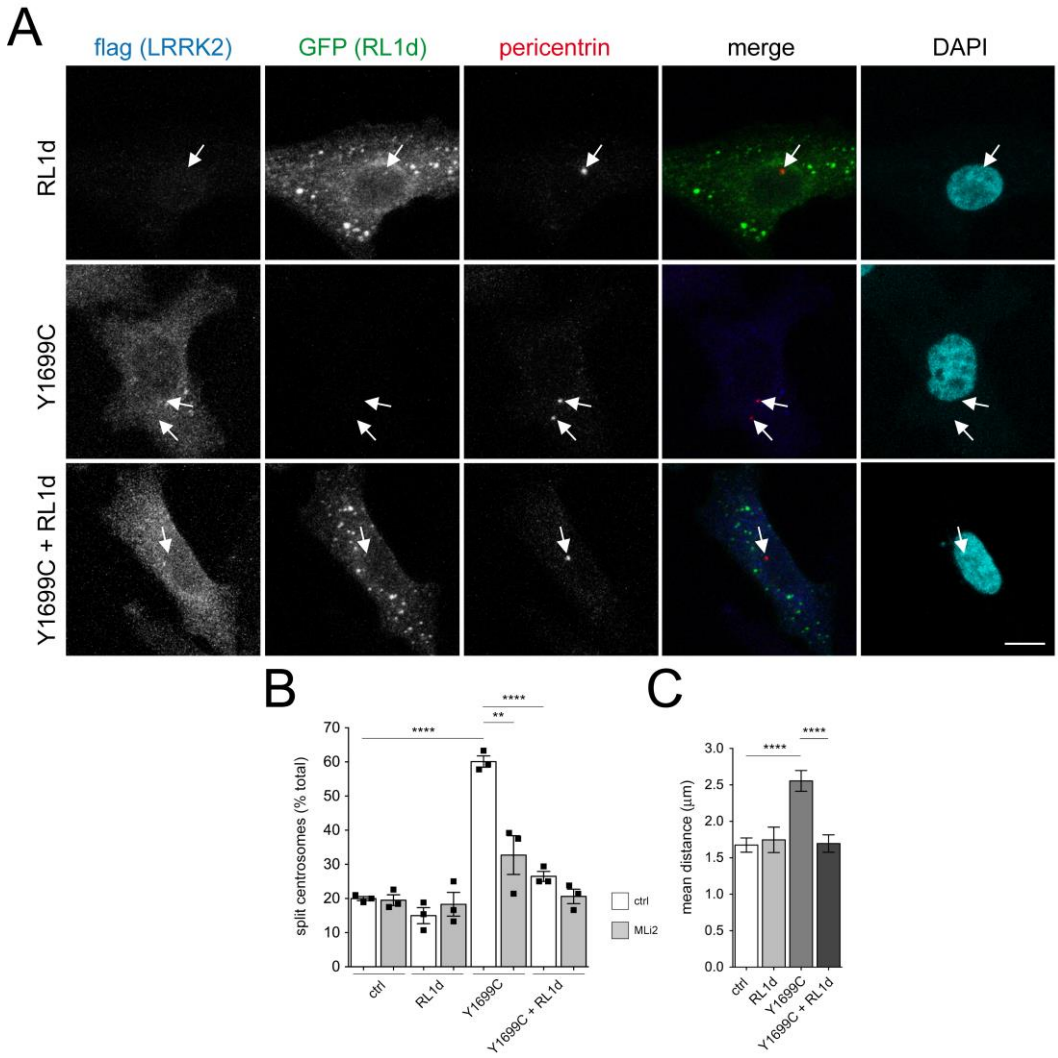

Fig. 30. Expression of C-terminal RILPL1 reverts the LRRK2-mediated centrosomal cohesion deficits. (A) Example of A549 cells transfected with the C-terminal region of RILPL1 (RL1d-GFP), flag-tagged Y1699C mutant LRRK2, or both as indicated, and stained with antibodies against flag (Alexa594 secondary antibody; pseudocolored in blue), pericentrin (Alexa647 secondary antibody; red) and with DAPI. Scale bar, 10 µm. **(B)** Quantification of the percentage of cells displaying split centrosomes transfected with either pCMV (ctrl), RL1d-GFP, flag-tagged Y1699C LRRK2, or with both, and either left untreated or incubated with MLi-2 (500 nM, 2 h) prior to immunocytochemistry. Bars represent mean ± s.e.m. (n = 3 experiments); ****, $p < 0.001$; **, $p < 0.01$. **(C)** Cells transfected with the indicated constructs were processed for immunocytochemistry, and the distances between duplicated centrosomes were quantified from around 50 cells each. ****, $p < 0.001$.

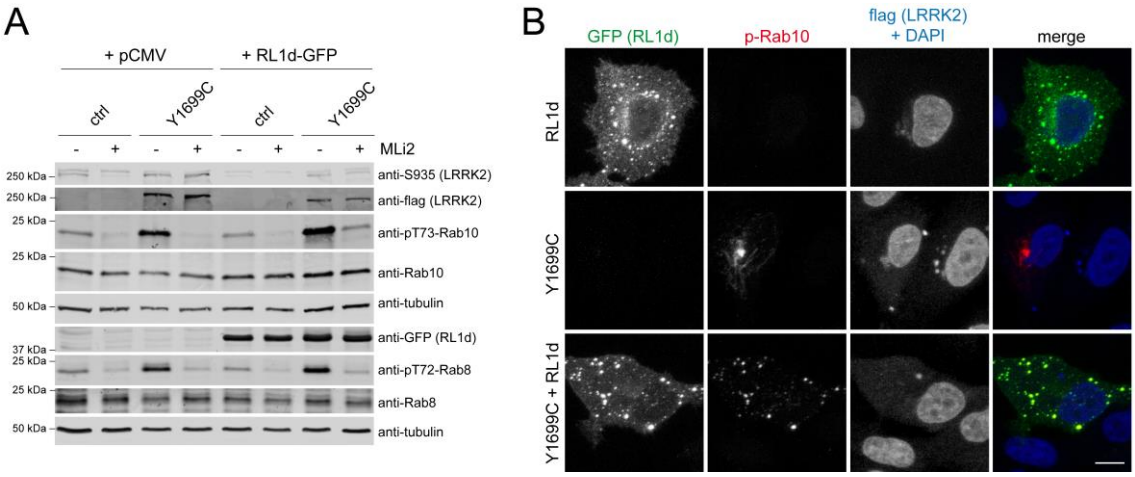

Fig. 31. Expression of C-terminal RILPL1 redistributes the LRRK2-mediated phospho-RAB10 accumulation. (A) Cells were co-transfected with the indicated constructs, left untreated or incubated with MLi-2 (500 nM, 2 h) as indicated, and extracts were blotted for flag-tagged LRRK2, phosphorylated LRRK2 (S935), pT72-RAB8a, total RAB8a, pT73-RAB10, total RAB10, or tubulin as loading control. **(B)** Cells were transfected with the indicated constructs and stained with antibodies against phospho-RAB10 (Alexa594 secondary antibody, red), flag (Alexa405 secondary antibody, blue) and DAPI. Scale bar, 10 µm.

RILPL1 localises to subdistal appendages of the mother centriole

RILPL1 associates with the mother centriole which becomes the basal body that nucleates the primary cilium (Schaub and Stearns, 2013). Employing two distinct anti-RILPL1 antibodies in HEK293T cells, we corroborated the centrosomal localisation of endogenous RILPL1, and the co-localisation of RILPL1 with endogenous phosphorylated RAB proteins in cells transfected with pathogenic LRRK2 (Fig. 32). Both N-terminally or C-terminally GFP-tagged RILPL1 proteins displayed a pericentrosomal localization when expressed in A549 cells (Dhekne et al., 2018) (Fig. 33A), and an identical pericentrosomal localization was observed when RILPL1 was fused to miniSOG (RILPL1-miniSOG), a tag suitable for correlative light and electron microscopy (CLEM) (Shu et al., 2011; Boassa et al., 2013). In addition, and as described above, transient expression of tagged RILPL1 in A549 cells had no effect on centrosomal cohesion as assessed by measuring the mean distance between duplicated centrosomes (Fig. 33B).

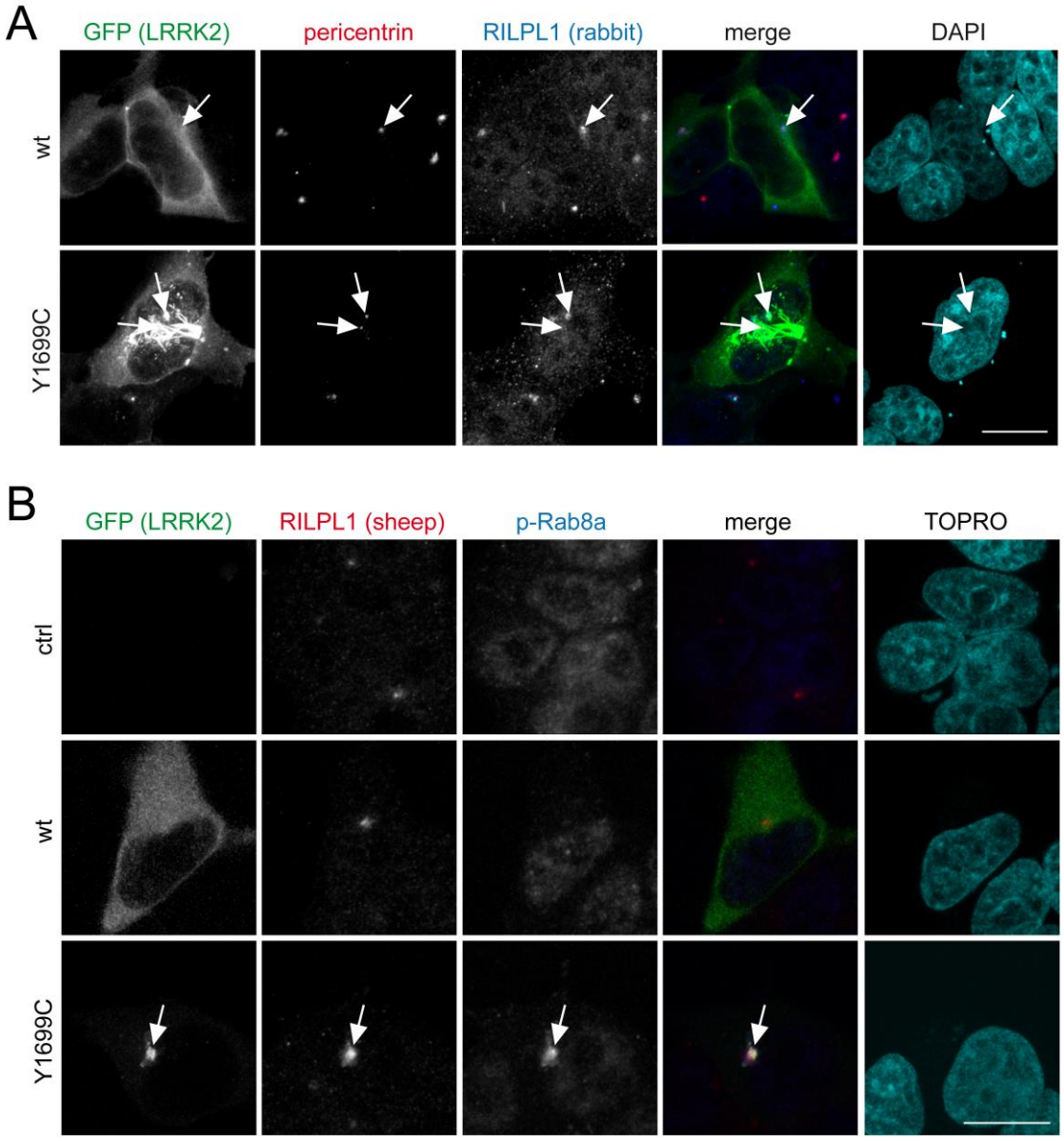

Fig. 32. Endogenous RILPL1 localizes to centrosome and recruits phospho-RABs in HEK293T cells transfected with pathogenic LRRK2. (A) Example of HEK293T cells transfected with GFP-tagged wildtype or pathogenic Y1699C LRRK2 and stained with antibodies against pericentrin (Alexa647 secondary antibody, red), RILPL1 (Alexa594 secondary antibody, pseudocolored in blue) and with DAPI (cyan). Arrows point to co-localisation of endogenous RILPL1 with the centrosomal marker pericentrin. Scale bar, 10 µm. **(B)** Example of non-transfected cells (ctrl), or cells transfected with GFP-tagged wildtype or Y1699C LRRK2 and stained with antibodies against RILPL1 (Alexa594 secondary antibody, red), phospho-RAB8 (Alexa405 secondary antibody, pseudocolored in blue) and with TOPRO (cyan). The phospho-RAB8 antibody detects both phospho-RAB8 and phospho-RAB10 by immunocytochemistry. Arrow points to pathogenic LRRK2-expressing cell, where phospho-RAB accumulation co-localises with endogenous RILPL1. Scale bar, 10 µm.

In order to image the pericentrosomal localization of RILPL1 with high spatial resolution, we performed miniSOG-induced DAB oxidation which generated a localised polymeric precipitate that could be readily identified by CLEM (Fig. 33C). Using STEM tomography (for which we combined a multiple-tilt tomography approach with the scanning mode of a TEM), we determined that RILPL1 was localized to the subdistal appendages of the mother centriole, hinting that the interaction between

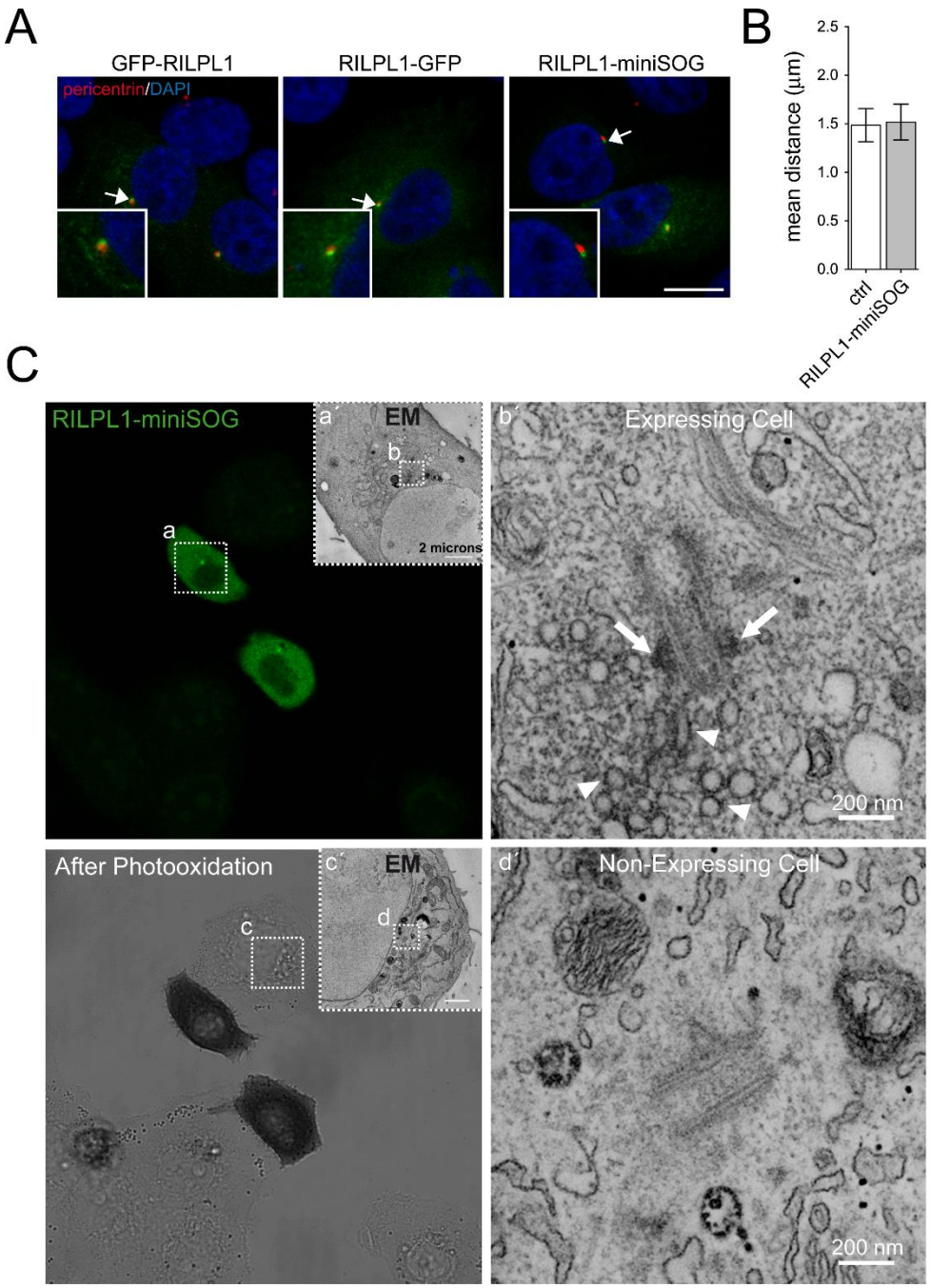

Fig. 33. RILPL1 localizes to subdistal appendages of the mother centriole. (A) Example of A549 cells transfected with GFP-RILPL1, RILPL1-GFP or RILPL1-miniSOG, and stained with antibody against pericentrin (red) and with DAPI. Scale bar, 10 µm. **(B)** A549 cells were transfected with RILPL1-miniSOG and processed for immunocytochemistry, and the distances between duplicated centrosomes quantified from around 30 non-transfected and transfected cells. Bars represent mean ± s.e.m. **(C)** Correlated light and EM imaging of RILPL1-miniSOG. Transfected A549 cells were revealed first by confocal fluorescence and then by transmitted light imaging following DAB photooxidation, where an optically dense reaction product was observed in the two expressing cells. To better discriminate the DAB precipitate, the tannic acid and uranyl acetate stainings were omitted. Low magnification TEM image of the RILPL1-miniSOG expressing cell (**a'**) corresponds to the same area indicated by the white square (**a**); similarly, the high magnification image (**b'**) corresponds to the same area indicated by the white square (**b**). White arrows point at DAB-labelled subdistal appendages of the mother centriole; arrowheads point at DAB-labelled pericentrosomal vesicles. As comparison, the low magnification TEM image of the non-expressing cell (**c'**) corresponds to the same area indicated by the white square (**c**); the high magnification image (**d'**) corresponds to the same area indicated by the white square (**d**). No labelling was observed at the subdistal appendages in the control, non-expressing cell. These observations were confirmed in cells (RILPL1-miniSOG-expressing and controls, non-expressing) from three different areas.

phospho-RAB8/phospho-RAB10 and RILPL1 may occur at this localisation. The specific DAB labelling was clearly distinguishable in RILPL1-miniSOG-expressing A549 cells as compared to adjacent non-expressing cells that were exposed to the same processing within the photooxidized area. An accumulation of DAB-labelled pericentrosomal vesicles was observed in expressing cells only, suggesting this might be induced by RILPL1 overexpression.

Pathogenic LRRK2 causes ciliogenesis deficits associated with the pericentrosomal/centrosomal accumulation of phospho-RAB10/8

We next aimed to determine whether the pericentrosomal/centrosomal accumulation of phospho-RAB10/8, shown to interfere with centrosomal cohesion in dividing cells, may also be responsible for the reported LRRK2-mediated ciliogenesis deficits (Dhekne et al., 2018). HEK293T cells were transfected with either wildtype, kinase-inactive or pathogenic mutant LRRK2 constructs, and the percentage of ciliated cells quantified in both serum-fed as well as serum-starved conditions (Fig. 34A-C). Serum starvation did not increase the amount of ciliated cells (Fig. 34B,C), likely due to the limited time of starvation possible without compromising viability in this cell type. Expression of all pathogenic LRRK2 mutants, but not of wildtype or kinase-dead LRRK2, caused a decrease in the percentage of ciliated cells in both serum-fed and serum-starved conditions (Fig. 34B,C). This was associated with a significant increase in the accumulation of phospho-RAB10/8 in transfected cells (Fig. 34D,E), with all constructs expressed to similar degrees (Fig. 34F). The phospho-RAB accumulation was reverted upon MLi-2 treatment (Fig. 34D,E), with only a slight rescue of the ciliogenesis phenotype observed (Fig. 34B,C), suggesting that the reformation of cilia upon phospho-RAB10/8 removal may take additional time.

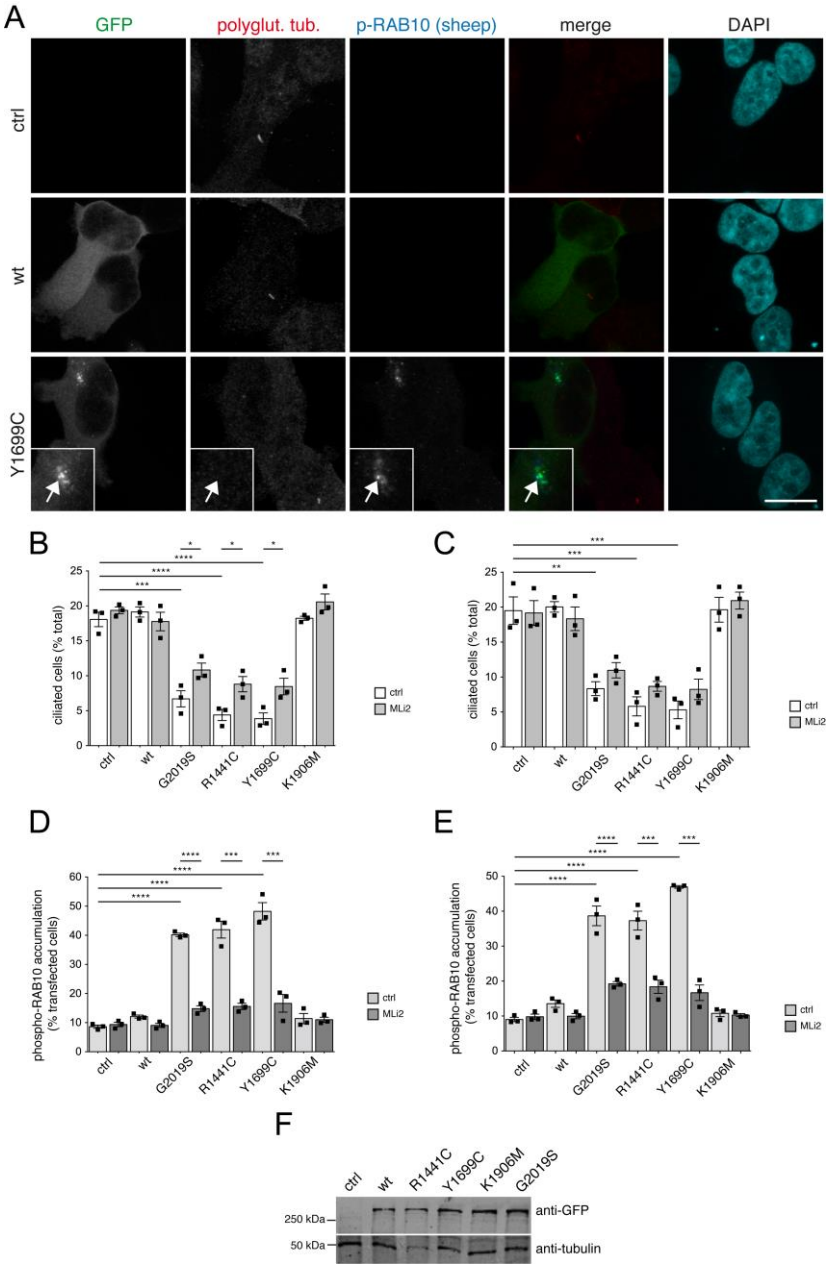

Fig. 34. Pathogenic LRRK2 causes ciliogenesis deficits in a kinase-dependent manner. (A) Example of HEK293T cells transfected with either pCMV (ctrl), or with GFP-tagged wildtype or pathogenic Y1699C constructs, and stained with an antibody against polyglutamylated tubulin, sheep anti-phospho-T73-RAB10, and DAPI. Scale bar, 10 µm. **(B)** HEK293T cells were transfected with the indicated LRRK2 constructs, and either left untreated or treated with MLi-2 (200 nM, 12 h) before immunocytochemistry using an antibody against polyglutamylated tubulin and against phospho-T73-RAB10 as described in (A). The percentage of ciliated cells expressing the distinct constructs was quantified from around 200 cells per condition per experiment. Bars represent mean ± s.e.m. (n = 3 experiments); ****, $p < 0.001$; ***, $p < 0.005$; *, $p < 0.05$. **(C)** Same as in (B), but cells were serum-starved for 12 h, either in the absence or presence of 200 nM MLi-2 as indicated, and the percentage of ciliated transfected cells quantified from around 200 cells per condition per experiment. Bars represent mean ± s.e.m. (n = 3 experiments); ***, $p < 0.005$; **, $p < 0.01$. **(D)** Same as (B), with cells either left untreated or treated with MLi-2 (200 nM, 12 h) before immunocytochemistry, and the perinuclear accumulation of phospho-T73-RAB10 quantified from around 200 transfected cells per condition and experiment. Bars represent mean ± s.e.m. (n = 3 experiments); ****, $p < 0.001$; ***, $p < 0.005$. **(E)** Same as (D), with cells serum-starved for 12 h either in the absence or presence of 200 nM MLi-2 as indicated before immunocytochemistry, and the perinuclear accumulation of phospho-T73-RAB10 quantified from around 200 transfected cells per condition and experiment. Bars represent mean ± s.e.m. (n = 3 experiments); ****, $p < 0.001$; ***, $p < 0.005$. **(F)** HEK293T cells were transfected with the indicated GFP-tagged LRRK2 constructs, and extracts analysed by Western blotting for GFP, and tubulin as loading control.

To assure that the observed phospho-RAB accumulation occurred at the ciliary base, cells were co-transfected with pathogenic LRRK2 and Smoothened-EGFP (smo-EGFP) to label cilia (Fig. 35A,B). When selectively quantifying the pathogenic LRRK2-expressing cells still displaying cilia, phospho-RAB10/8 accumulation at/around the ciliary base could be detected, but quantification of the fluorescence intensity of the phospho-RAB10/8 signal indicated that there was significantly less overall accumulation in ciliated as compared to non-ciliated cells, or as compared to only smo-EGFP-transfected ciliated or non-ciliated cells, respectively (Fig. 35B). Finally, when staining cells for both ciliary and centrosomal markers, a significant percentage of the pathogenic LRRK2-expressing cells which still contained cilia were found to display a duplicated split centrosome phenotype (Fig. 35C,D). Since cilia are usually reabsorbed in G2 phase of the cell cycle (Plotnikova et al., 2009), these data suggest that pathogenic LRRK2 may additionally interfere with proper ciliary resorption.

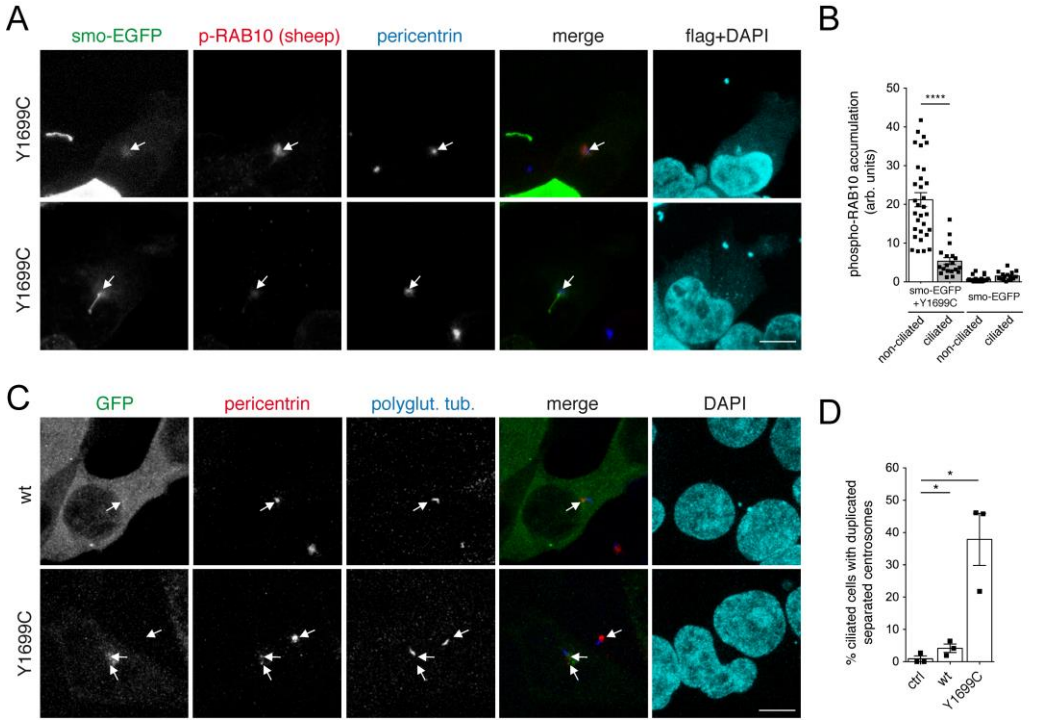

Fig. 35. Pathogenic LRRK2 causes phospho-RAB accumulation preferentially in non-ciliated cells and may cause ciliary resorption deficits. (A) HEK293T cells were co-transfected with pathogenic flag-tagged LRRK2 and smo-EGFP, and stained for phospho-T73-RAB10 (Alexa594 secondary antibody, red), pericentrin (Alexa647 secondary antibody, pseudocolored in blue), anti-flag (Alexa405 secondary antibody, pseudocolored in cyan) and DAPI (pseudocolored in cyan). Example of either non-ciliated (top) or ciliated (bottom) cell co-expressing smo-EGFP and flag-tagged Y1699C LRRK2. Scale bar, 5 µm. **(B)** Quantification of the fluorescence intensity of the phospho-T73-RAB10 accumulation at the ciliary base in cells only expressing smo-EGFP, or co-expressing pathogenic Y1699C LRRK2, according to the absence or presence of cilia from experiments of the type described in (A). Bars represent mean ± s.e.m. from around 20-30 cells analysed per condition; ****, $p < 0.001$. **(C)** Example of HEK293T cells transfected with GFP-tagged wildtype or Y1699C mutant LRRK2 as indicated, and stained for pericentrin, polyglutamylated tubulin and DAPI. Scale bar, 5 µm. **(D)** Quantification of the percentage of ciliated cells in either the absence of transfection (ctrl), or upon expression of wildtype or Y1699C mutant LRRK2 as indicated, which display a duplicated split centrosome phenotype. The centrosomal phenotype was quantified from around 50 ciliated cells per condition per experiment. Bars represent mean ± s.e.m. (n = 3 experiments); *, $p < 0.05$.

As another means to determine the effect of phospho-RAB accumulation on ciliogenesis, we co-expressed wildtype LRRK2 with either RAB8A or RAB10, respectively (Fig. 36). Whilst expression of either wildtype RAB8A or wildtype RAB10 was without effect on ciliogenesis, co-expression with LRRK2 caused a deficit in ciliogenesis (Fig. 36A-C) associated with the detection of phospho-RAB8/10 (Fig. 36D), which is analogous to what we observed regarding centrosomal cohesion deficits (Fig. 14,15,16,20). Altogether, these data indicate that pathogenic LRRK2 interferes with both ciliogenesis and centrosome cohesion events via the increased pericentrosomal/centrosomal accumulation of phospho-RAB10/8.

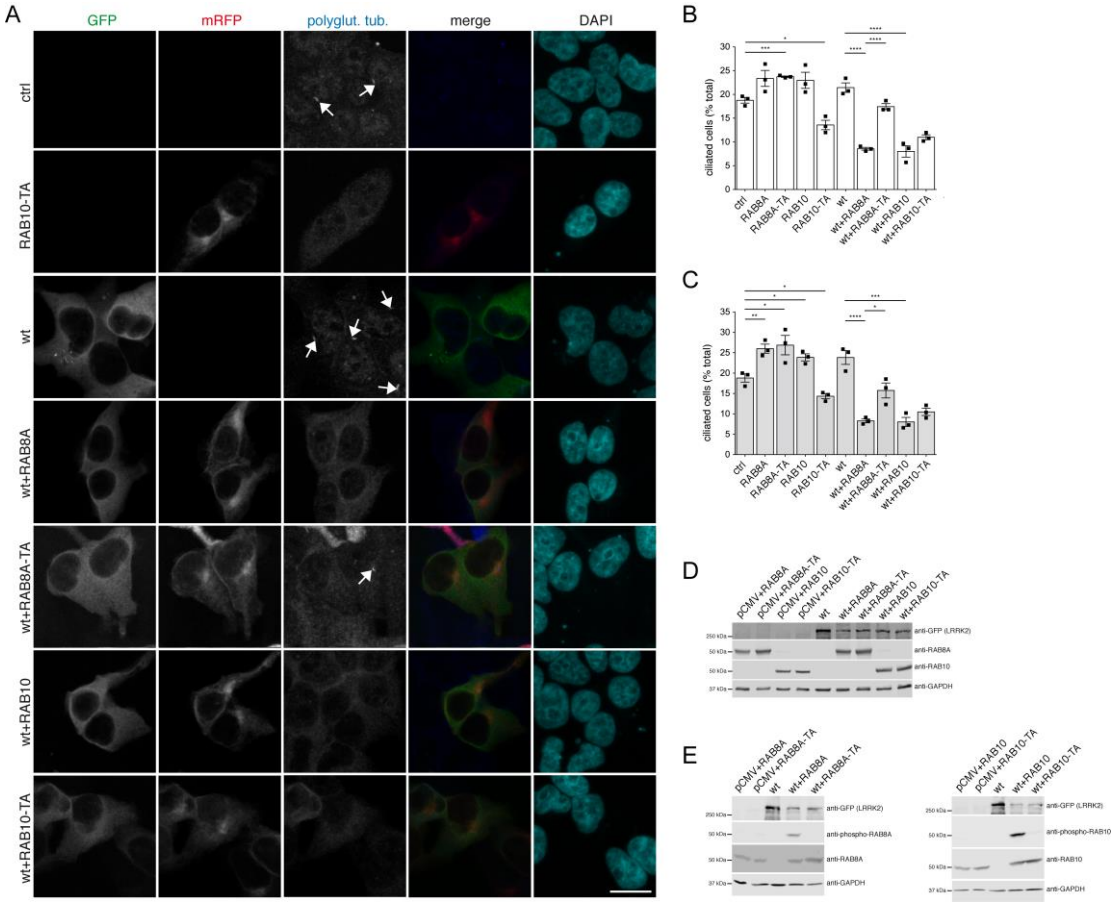

Fig. 36. Co-expression of wildtype LRRK2 with RAB8A or RAB10, but not with phospho-deficient versions thereof, causes ciliogenesis deficits. (A) HEK293T cells were either left untreated (ctrl), transfected with GFP-tagged wildtype LRRK2, or co-transfected with GFP-tagged wildtype LRRK2 and the indicated mRFP-tagged RAB constructs, and stained for polyglutamylated tubulin and DAPI. Scale bar, 10 µm. **(B)** The percentage of ciliated cells expressing the distinct constructs was quantified from around 200 cells per condition per experiment. Bars represent mean ± s.e.m. (n = 3 experiments); ****, $p < 0.001$; ***, $p < 0.005$; *, $p < 0.05$. **(C)** Same as in (B), but cells were serum-starved for 12 h before immunocytochemistry. Bars represent mean ± s.e.m. (n = 3 experiments); ****, $p < 0.001$; ***, $p < 0.005$; **, $p < 0.01$; *, $p < 0.05$. Please note that expression of the distinct RAB constructs on their own displayed slight and opposing effects on ciliogenesis. Importantly though, co-expression of wildtype LRRK2 with either wildtype RAB8A or wildtype RAB10 caused pronounced deficits in ciliogenesis. **(D)** HEK293T cells were co-transfected with the indicated constructs, and similar levels of expression of LRRK2, RAB8A and RAB10 constructs confirmed by Western blotting, with GAPDH as loading control. **(E)** HEK293T cells were transfected or co-transfected with the indicated constructs, and levels of expression of LRRK2, RAB8A, phospho-RAB8A (left), or RAB10 and phospho-RAB10 (right) determined by Western blotting with GAPDH as loading control.

LRRK2 risk variants modulate centrosomal cohesion in HEK293T cells

To explore the relationship between centrosomal cohesion phenotypes and LRRK2 variants described to positively or negatively impact PD risk, we transiently transfected HEK293T cells with wildtype LRRK2, with a point mutant described to be non-pathogenic (T1410A), distinct point mutants described to increase PD risk (R1628P, S1647T, N2081D, G2385R), or a pathogenic point mutant which served as a positive control (Y1699C) (Ross et al., 2008; Lesage et al., 2009; Abdalla-Carvalho et al., 2010; Ross et al., 2011; Zheng et al., 2011; Fu et al., 2013; Hui et al., 2018). Compared to expression of wildtype LRRK2, the pathogenic Y1699C-LRRK2 mutant caused a pronounced deficit in centrosomal cohesion, as evidenced by the percentage of cells displaying duplicated centrosomes with a distance further than 1.5 microns apart, which was significantly reduced by transient application of the LRRK2 kinase inhibitor MLi-2

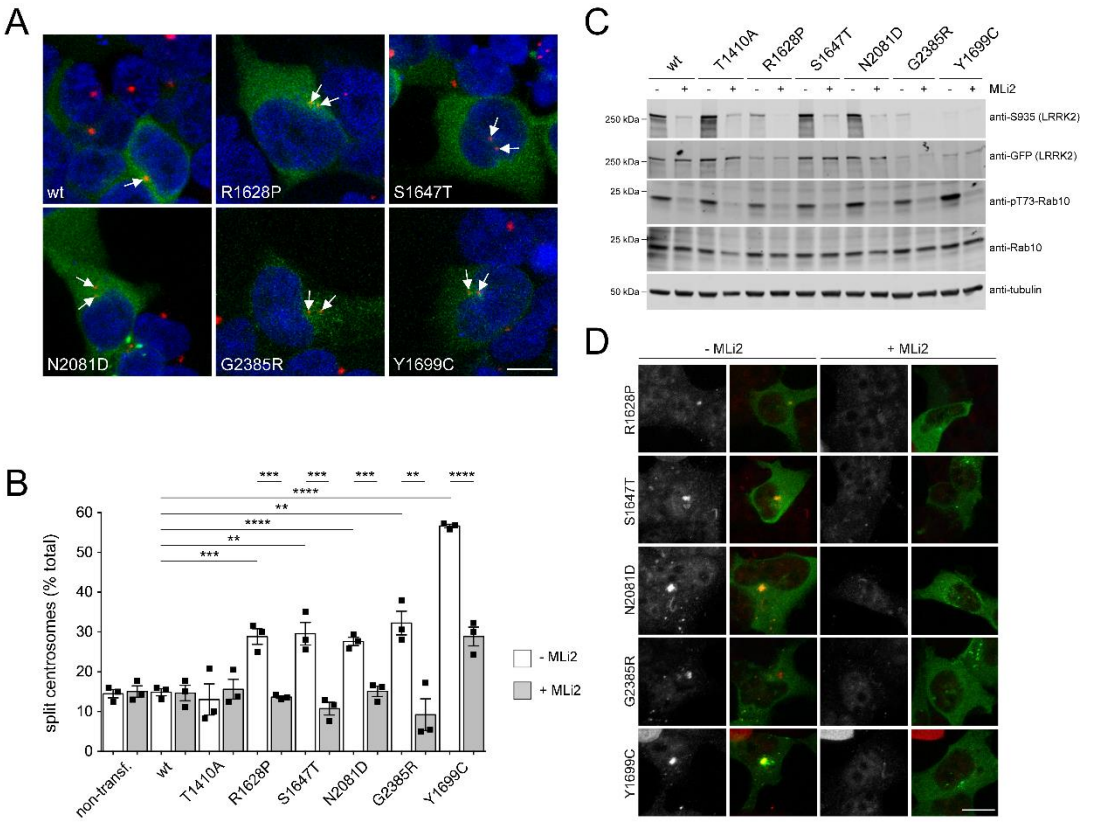

Fig. 37. LRRK2 risk variants cause centrosomal cohesion deficits. (A) HEK293T cells were transfected with GFP-tagged wildtype (wt) LRRK2, risk variants as indicated, or with pathogenic Y1699C LRRK2. Cells were stained for the centrosomal marker pericentrin (red) and DAPI (blue). Arrows point to transfected cells with duplicated centrosomes further than 1.5 microns apart (split centrosomes). Scale bar, 10 µm. **(B)** Quantification of the percentage of cells with duplicated split centrosomes from either non-transfected (ctrl) cells, or from cells transfected with the indicated constructs, in the absence or presence of MLi-2 (100 nM, 2 h) as indicated. Bars represent mean ± s.e.m. (n = 3 experiments); ****, $p < 0.001$; ***, $p < 0.005$; **, $p < 0.01$. **(C)** Cells were transfected with the indicated constructs, left untreated or treated with MLi-2 (100 nM, 2 h) as indicated, and extracts blotted for GFP-tagged LRRK2, phosphorylated LRRK2 (S935), phosphorylated RAB10 (pT73-RAB10), total Rab10, and tubulin as loading control. **(D)** Cells were transfected with the indicated GFP-tagged constructs, left untreated or treated with MLi-2 as indicated, and stained with an antibody against endogenous phosphorylated RAB10 (red). Scale bar, 10 µm.

(Fig. 37A,B). Expression of the non-pathogenic T1410A LRRK2 mutant was without effect, whilst four distinct PD risk variants caused a statistically significant centrosomal cohesion deficit which was reverted by MLi-2 (Fig. 37A,B). As assessed by immunoblotting, transient expression of the pathogenic Y1699C-LRRK2 mutant caused a detectable increase in RAB10 phosphorylation as compared to wildtype LRRK2, whilst no detectable differences were observed when expressing the various LRRK2 risk variants (Fig. 37C). However, increased accumulation of phospho-RAB10 in individually transfected cells could be detected by immunocytochemistry when expressing pathogenic LRRK2 or the various risk variants, and such accumulation was reverted in all cases by LRRK2 kinase inhibitor (Fig. 37D).

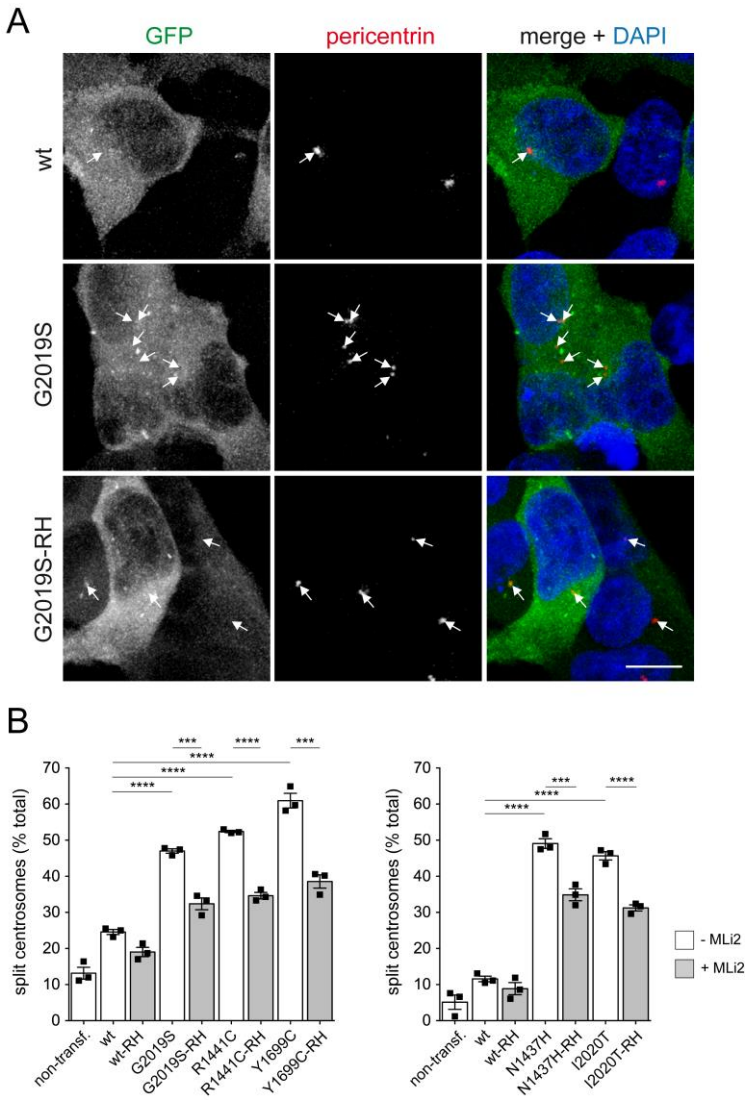

Fig. 38. The protective R1398H variant decreases centrosomal cohesion deficits mediated by pathogenic LRRK2. (A) HEK293T cells were transfected with GFP-tagged wildtype (wt) LRRK2, pathogenic G2019S mutant, or pathogenic G2019S mutant containing the protective R1398H variant (G2019S-RH). Cells were stained for the centrosomal marker pericentrin (red) and DAPI (blue). Arrows point to centrosomes in transfected cells. Scale bar, 10 µm. **(B)** Quantification of the percentage of cells with split centrosomes from either non-transfected cells, or from cells transfected with the indicated constructs in the absence or presence of MLi-2 (100 nM, 2 h) as indicated. Bars represent mean ± s.e.m. (n = 3 experiments); ****, $p < 0.001$; ***, $p < 0.005$.

To analyse the effect of the R1398H mutation in LRRK2 which is protective against PD (Tan et al., 2010; Chen et al., 2011; Ross et al., 2011), we introduced it into either wildtype or pathogenic LRRK2 constructs. Transient expression of pathogenic G2019S, R1441C, Y1699C, N1437H or I2020T LRRK2 mutants caused a significant deficit in centrosomal cohesion which was attenuated by introduction of the protective R1398H variant in all cases (Fig. 38). Similar results were obtained when introducing synthetic mutations (R1398L or R1398L/T1343V) described to alter RAB10 phosphorylation by modulating LRRK2 GTP binding/hydrolysis (Xiong et al., 2010; Biosa et al., 2013; Blanca Ramírez et al., 2017; Nguyen et al., 2020) (Fig. 39). Collectively, these data indicate that risk or protective LRRK2 variants can either negatively or positively impact upon the centrosomal cohesion deficits mediated by the LRRK2 kinase activity.

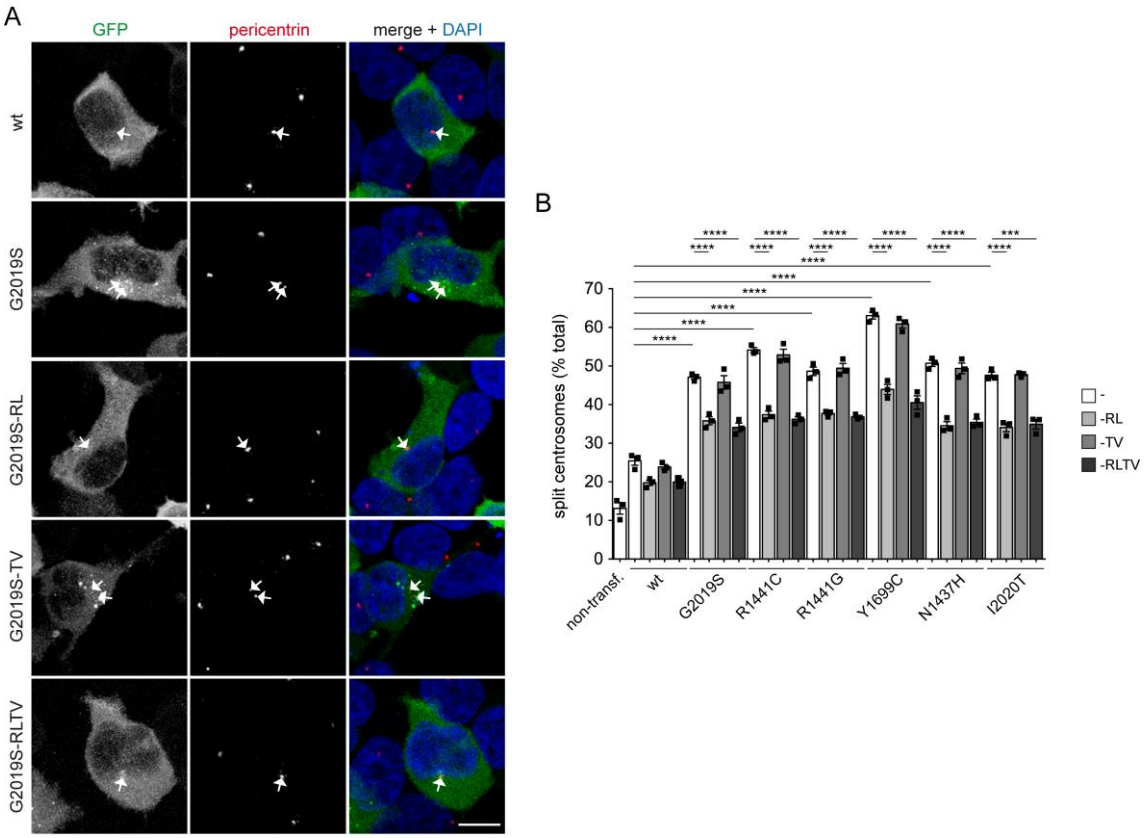

Fig. 39. Synthetic variants which modulate GTP binding/hydrolysis decrease centrosomal cohesion deficits mediated by pathogenic LRRK2. (A) HEK293T cells were transfected with GFP-tagged wildtype (wt) LRRK2, pathogenic G2019S mutant, pathogenic G2019S mutant containing the synthetic R1398L variant (G2019S-RL), the T1343V mutation (G2019S-TV), or both (G2019S-RLTV). Cells were stained for the centrosomal marker pericentrin (red) and DAPI (blue). Arrows point to centrosomes in transfected cells. Scale bar, 10 µm. **(B)** Quantification of the percentage of cells with duplicated split centrosomes from either non-transfected cells, or from cells transfected with the indicated constructs in the absence or presence of MLi-2 (100 nM, 2 h) as indicated. Bars represent mean ± s.e.m. (n = 3 experiments); ****, $p < 0.001$; ***, $p < 0.005$.

Upstream and downstream regulators of the LRRK2 signalling pathway impact upon centrosomal cohesion

Previous work has indicated that co-expression of RAB29 and LRRK2 stimulates the LRRK2 activity by recruiting it to the Golgi complex (Liu et al., 2018; Purlyte et al., 2018), and our data indicate that this is associated with centrosomal cohesion deficits (Madero-Pérez et al., 2018a). To determine whether endogenous RAB29 is required for the pathogenic LRRK2-mediated centrosomal deficits, we employed A549 cells deficient in RAB29. The centrosomal cohesion deficits mediated by pathogenic LRRK2 expression were significantly blunted in RAB29-deficient as compared to wildtype cells (Fig. 40). Since knockout of RAB29 does not seem to influence basal or pathogenic LRRK2 kinase activity (Kalogeropulou et al., 2020), these findings suggest that the presence of RAB29 may be important for the LRRK2-mediated centrosomal cohesion phenotype in a manner independent of its ability to regulate the LRRK2 kinase activity.

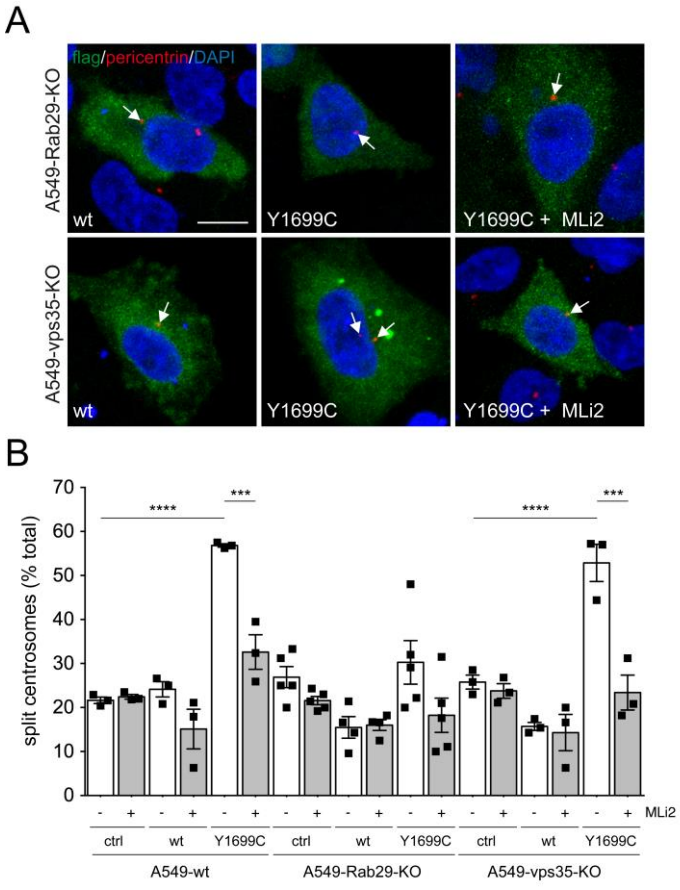

Fig. 40. Pathogenic LRRK2-mediated centrosomal cohesion deficits are blunted in RAB29-KO, but not in vps35-KO cells. (A) Example of A549 RAB29-KO cells transfected with either flag-tagged wildtype (wt) or Y1699C-mutant LRRK2, and either treated or untreated with 500 nM MLi-2 for 2 h prior to immunocytochemistry with antibodies against flag, pericentrin and with DAPI. Scale bar, 10 µm. **(B)** Quantification of the percentage of A549 wildtype cells, A549 RAB29-KO cells or A549 vps35-KO cells with split centrosomes either in the absence of transfection (ctrl), or upon transfection with either wildtype or Y1699C-mutant LRRK2. Cells were treated with or without MLi-2 (500 nM, 2 h) prior to immunocytochemistry as indicated. Bars represent mean ± s.e.m. (n = 3-5 experiments); ****, $p < 0.001$; ***, $p < 0.005$.

Vps35 is a key component of the retromer complex which regulates vesicular trafficking to and from the Golgi complex. Strikingly, a point mutation (vps35-D620N) which causes autosomal dominant late-onset PD (Vilariño-Güell et al., 2011; Zimprich et al., 2011; Sharma et al., 2012) hyperactivates LRRK2 through a currently unknown mechanism (Mir et al., 2018). We next wondered whether vps35 or mutants thereof may impact upon the LRRK2-mediated centrosomal cohesion deficits. Pathogenic LRRK2 expression in vps35-deficient A549 cells (Mir et al., 2018) caused centrosomal cohesion deficits identical to those observed in wildtype cells, indicating that the presence of endogenous vsp35 is not required for this phenotype (Fig. 40). To determine whether the pathogenic vps35-D620N mutant regulates the centrosomal cohesion deficits by activating LRRK2, we co-expressed

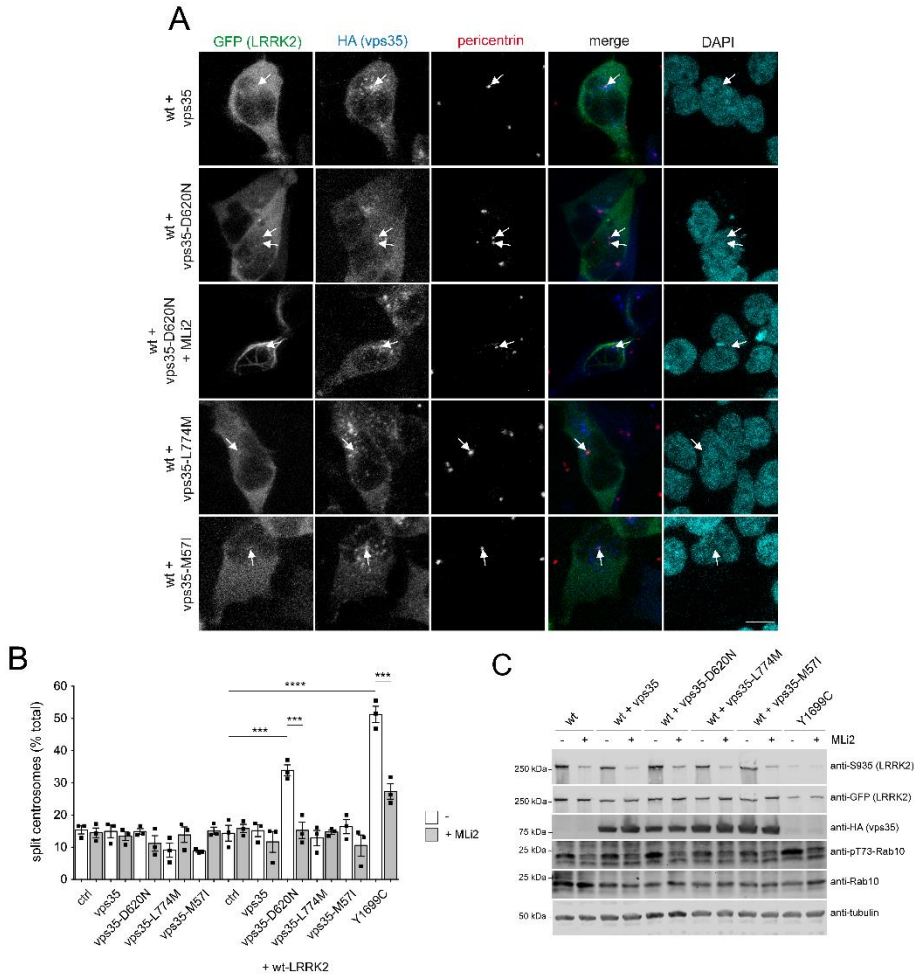

Fig. 41. Vps35-D620N expression with LRRK2 causes centrosomal cohesion deficits dependent on the LRRK2 kinase activity. (A) HEK293T cells transfected with GFP-tagged wildtype LRRK2 (wt) and HA-tagged wildtype or mutant vps35 constructs, and treated with or without MLi-2 (100 nM, 2 h) prior to immunocytochemistry as indicated. Cells were stained with an antibody against the HA-tag (Alexa647 secondary antibody; pseudocolored in blue), an antibody against pericentrin (Alexa555 secondary antibody; red) and DAPI (cyan). Scale bar, 10 µm. **(B)** Quantification of the percentage of cells with duplicated split centrosomes transfected with pCMV (ctrl) or different HA-tagged vps35 constructs, or co-transfected with GFP-tagged wildtype LRRK2, in the absence or presence of MLi-2 (100 nM, 2 h) as indicated. Bars represent mean ± s.e.m. (n = 3 experiments); ****, $p < 0.001$; ***, $p < 0.005$. **(C)** HEK293T cells were transfected with the indicated constructs, left untreated or treated with MLi-2 (100 nM, 2 h) as indicated, and extracts blotted for GFP-tagged LRRK2, phosphorylated LRRK2 (S935), HA-tagged vps35, phosphorylated RAB10 (pT73-RAB10), total RAB10, and tubulin as loading control.

wildtype LRRK2 with HA-tagged wildtype or mutant vps35 variants in HEK293T cells. Co-expression of LRRK2 with vsp35-D620N caused a centrosomal cohesion deficit which was reverted by MLi-2 treatment (Fig. 41A,B) and correlated with an increase in the levels of phospho-RAB10 as assessed by immunoblot analysis (Fig. 41C). In contrast, no effects were observed when co-expressing wildtype LRRK2 with either wildtype vps35, or with two distinct, non-pathogenic vps35 point mutants (vps35-L774M, vps35-M57I) (Zimprich et al., 2011; Sharma et al., 2012) (Fig. 41A-C). These data support the conclusion that the vps35-D620N mutant activates the LRRK2 kinase as assessed by increased RAB10 phosphorylation to cause centrosomal cohesion deficits.

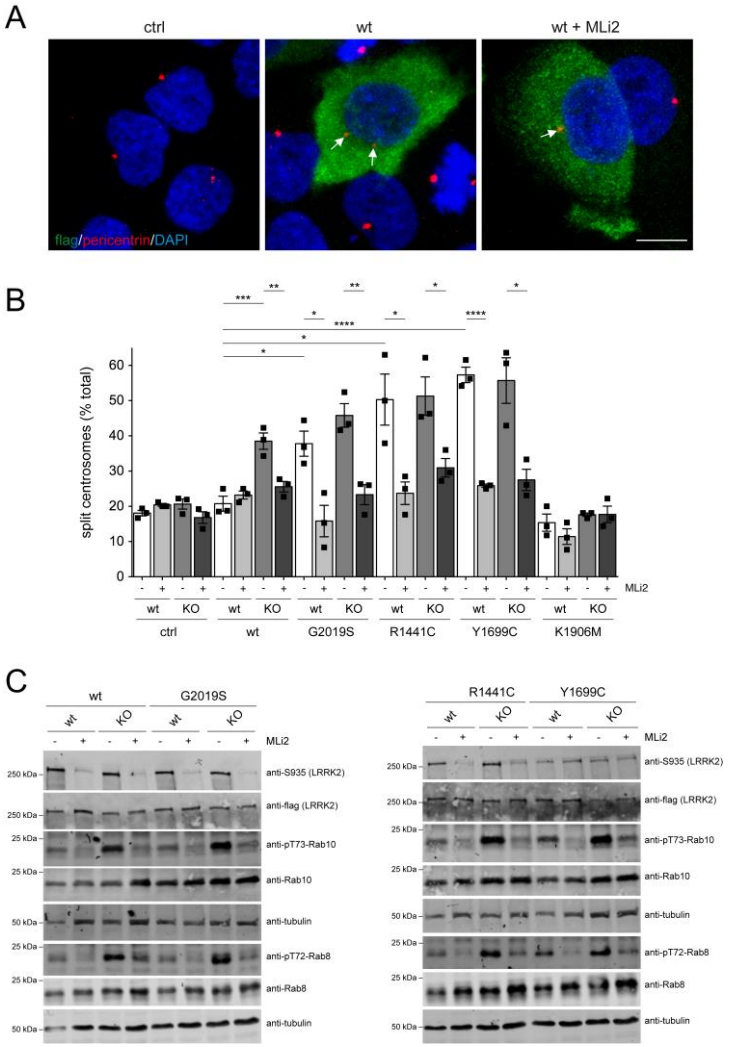

Fig. 42. Wildtype LRRK2 expression causes centrosomal cohesion deficits in PPM1H-KO A549 cells. (A) Example of PPM1H-KO cells transfected with pCMV (ctrl) or with flag-tagged wildtype LRRK2, in the presence or absence of MLi-2 (500 nM, 2 h) as indicated before immunocytochemistry with antibody against flag (green), pericentrin (red) and DAPI. Scale bar, 10 µm. **(B)** Quantification of the percentage of A549 wildtype or PPM1H-KO cells displaying split centrosomes transfected with either pCMV (ctrl) or the different LRRK2 constructs, and either left untreated or incubated with MLi-2 (500 nM, 2 h) prior to immunocytochemistry. Bars represent mean ± s.e.m. (n = 3 experiments); ****, $p < 0.001$; ***, $p < 0.005$; **. $p < 0.01$; *, $p < 0.05$. **(C)** A549 wildtype or PPM1H-KO cells were transfected with the indicated LRRK2 constructs, left untreated or incubated with MLi-2 (500 nM, 2 h) as indicated, and extracts were blotted for flag-tagged LRRK2, phosphorylated LRRK2 (S935), pT72-RAB8a, total RAB8a, pT73-RAB10, total RAB10, or tubulin as loading control.

Lastly, we evaluated the contribution of PPM1H, the protein phosphatase responsible for dephosphorylating the LRRK2-phosphorylated RAB10 and RAB8 proteins (Berndsen et al., 2019). Side-by-side comparison revealed that wildtype LRRK2 expression *per se* was able to cause a centrosomal cohesion deficit in the PPM1H-KO cells, but not in wildtype cells (Fig. 42A,B). The centrosomal deficits were reverted by MLi-2, and correlated with an increase in the levels of phospho-RAB10 and phospho-RAB8 as assessed by immunoblotting (Fig. 42C). No additional effects on centrosomal cohesion were observed when expressing distinct pathogenic LRRK2 mutants in the PPM1H-KO as compared to the control cells (Fig. 42C). Therefore, altogether these data support the conclusion that the centrosomal cohesion deficits mediated by the LRRK2 kinase activity are subject to modulation by both upstream and downstream components of the LRRK2 signalling pathway.

Ciliogenesis and centrosomal cohesion deficits in human dermal fibroblasts from G2019S LRRK2 PD patients and murine G2019S knockin astrocytes

Our previous studies reported centrosomal cohesion deficits in human dermal fibroblasts from G2019S LRRK2 patients as compared to healthy controls, which were reverted upon addition of LRRK2 kinase inhibitor (Madero-Pérez et al., 2018a). We thus wondered whether these patient-derived cells also display a ciliogenesis phenotype. Under serum-fed conditions, G2019S LRRK2-PD fibroblasts displayed a ciliogenesis deficit as compared to healthy control fibroblasts (Fig. 43A,B). In this cell type, starvation prominently induced ciliogenesis (Fig. 43B), and the deficit in ciliogenesis in the pathogenic LRRK2-expressing cells as compared to control cells was also observed under starvation conditions (Fig. 43B). Application of LRRK2 kinase inhibitor MLi-2 had a minor effect in rescuing such deficit, even though some fibroblast cells responded better than others. Further, quantification of cilia length did not show drastic differences between control and G2019S LRRK2-PD fibroblasts (Fig. 43C,D), in agreement with what has been previously described for cilia in iPSCs from LRRK2-PD patients, or in the cortex of pathogenic LRRK2-expressing mice (Dhekne et al., 2018).

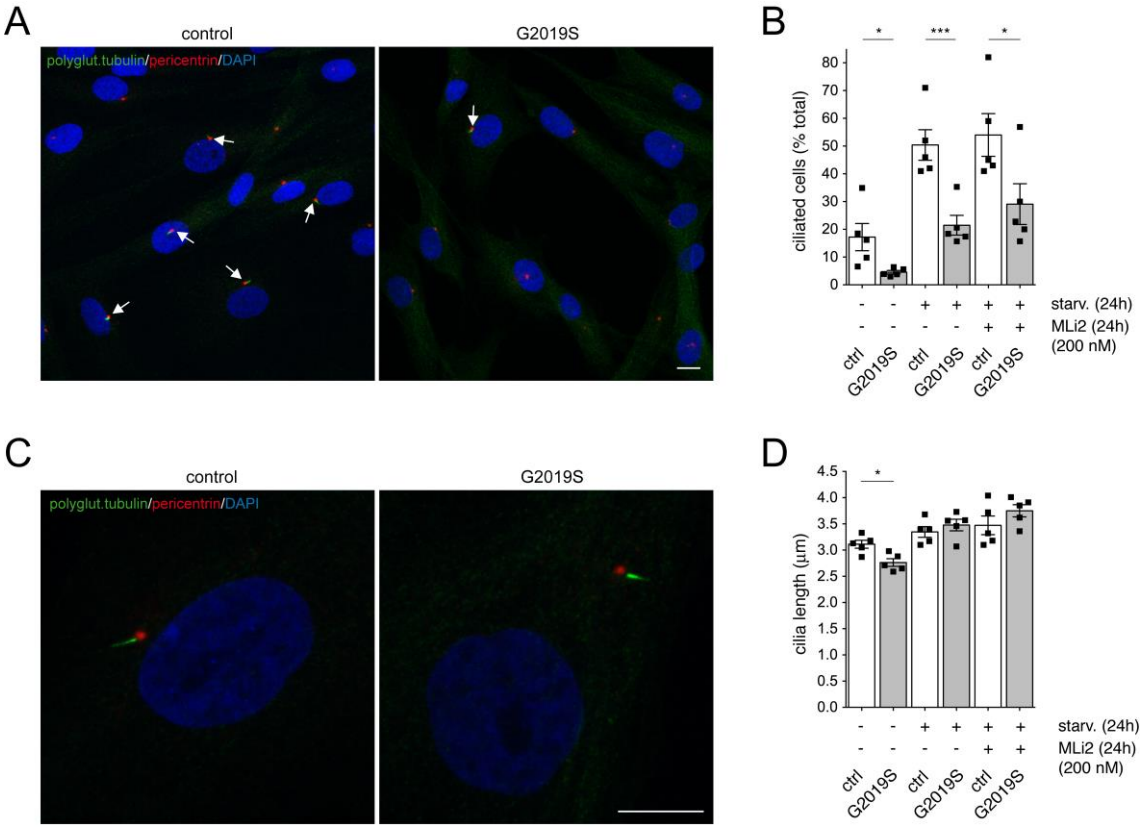

Fig. 43. Ciliogenesis deficits in human dermal fibroblasts from G2019S mutant LRRK2 PD patients compared to healthy controls. (A) Example of control and G2019S mutant LRRK2 PD patient fibroblasts stained with polyglutamylated tubulin antibody, pericentrin antibody and DAPI. Scale bar, 10 µm. **(B)** The percentage of ciliated cells was quantified from around 100 cells per line, and from five control and five G2019S mutant LRRK2 fibroblast lines. Control or G2019S mutant LRRK2 fibroblasts were treated with or without MLi-2 (200 nM, 24 h), either in the absence or presence of serum starvation (starv., 48 h) as indicated. Bars represent mean ± s.e.m. (between five independent lines); ***, $p < 0.005$; *, $p < 0.05$. **(C)** High-resolution deconvolved image of a control and G2019S mutant LRRK2 PD patient fibroblast cell stained with polyglutamylated tubulin antibody, pericentrin antibody and DAPI. Scale bar, 10 µm. **(D)** Pictures of the type acquired in (C) were analysed for cilia length as described in Materials and Methods, with 30-60 ciliated cells analysed for each cell line. Bars represent mean ± s.e.m. (between five independent lines); *, $p < 0.05$.

Finally, we analysed for both centrosomal cohesion and ciliogenesis deficits in primary mouse astrocytes cultured from either control or G2019S knockin mice (Yue et al., 2015). Cells were stained with GFAP, and centrosomal cohesion deficits quantified in both the absence and presence of starvation (Fig. 44A-C). G2019S knockin astrocytes displayed a centrosomal cohesion deficit as assessed by quantifying either the percentage of split centrosomes or the mean distance between duplicated centrosomes, and such cohesion deficit was reverted upon application of LRRK2 kinase inhibitor MLi-2 (Fig. 44B,C). Similarly, G2019S knockin astrocytes displayed a significant deficit in ciliogenesis as compared to control cells under serum-fed conditions, which was reverted by MLi-2 (Fig. 44D,E). Thus, pathogenic LRRK2 causes both centrosomal cohesion and ciliogenesis deficits in a disease-relevant cell type (Booth et al., 2017; di Domenico et al., 2019), and in a manner mediated by the LRRK2 kinase activity.

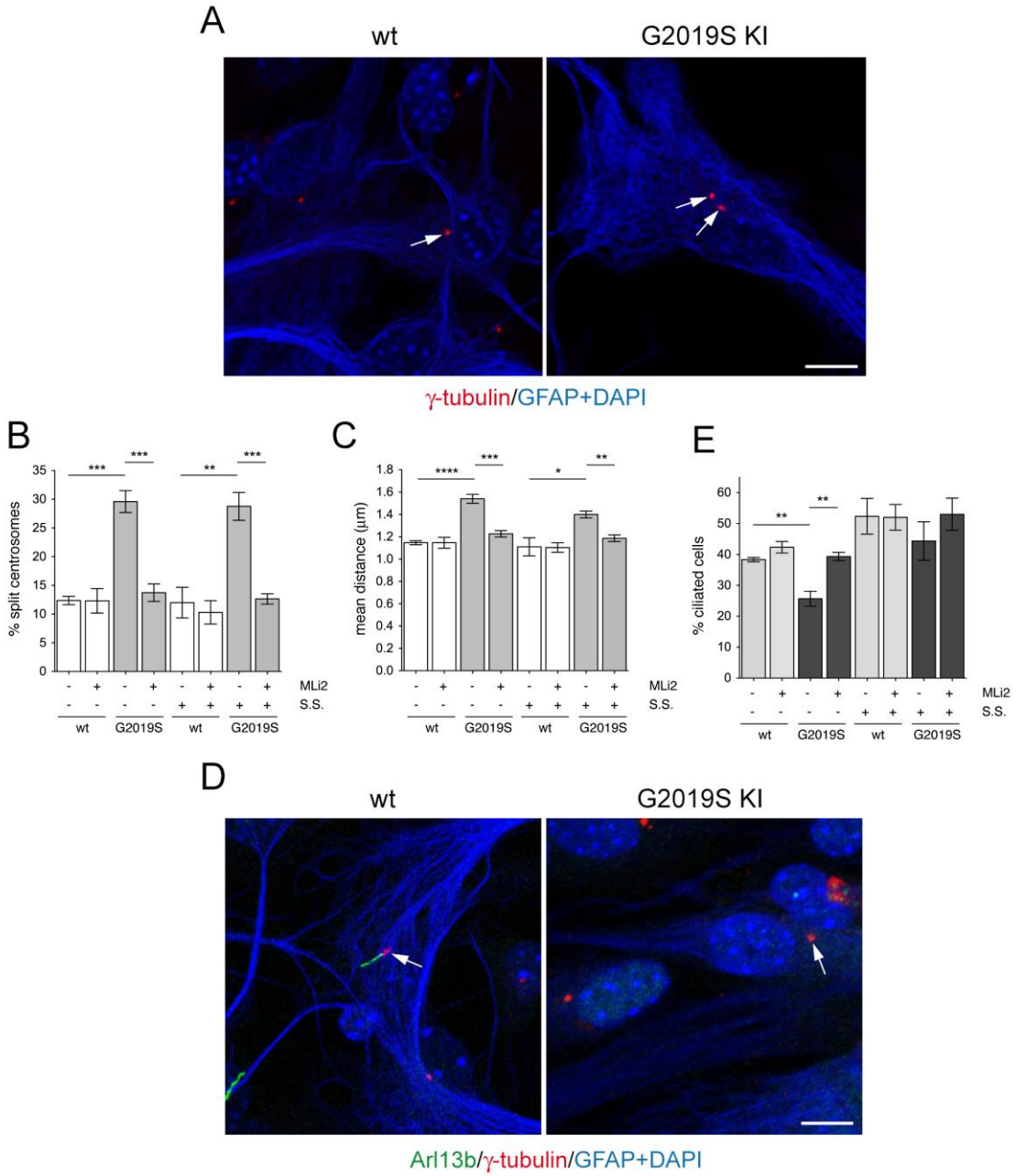

Fig. 44. Primary astrocytes from G2019S knockin mice display both centrosomal cohesion and ciliogenesis deficits as compared to control astrocytes. (A) Example of wildtype and G2019S knockin primary astrocytes stained with anti-γ-tubulin, anti-GFAP and DAPI. Scale bar, 10 µm. **(B)** Quantification of the percentage of wildtype or G2019S knockin primary astrocytes with split centrosomes, in the presence or absence of 48 h of serum starvation (S.S.), and the presence or absence of 200 nM MLi-2 for 24 h before immunocytochemistry as indicated. Around 250-350 cells were quantified per condition per experiment. Bars represent mean ± s.e.m. (n = 3 experiments); ***, $p < 0.005$; **, $p < 0.01$. **(C)** Same as in (B), but depicting the mean distance of duplicated centrosomes. Between 50 and 100 cells with duplicated centrosomes per condition per experiment were analysed. Bars represent mean ± s.e.m. (n = 3 experiments); ****, $p < 0.001$; ***, $p < 0.005$; **, $p < 0.01$; *, $p < 0.05$. **(D)** Example of wildtype and G2019S knockin primary astrocytes stained with anti-Arl13b, anti-γ-tubulin, anti-GFAP and DAPI. Scale bar, 10 µm. **(E)** The percentage of ciliated cells was quantified from around 200 cells per condition, in either the absence or presence of serum starvation (48 h, S.S.), and absence or presence of 200 nM MLi-2 (24 h) as indicated. Bars represent mean ± s.e.m. (n = 3 experiments); **, $p < 0.01$.

LRRK2-mediated centrosomal cohesion deficits as biomarker for Parkinson's disease

Centrosomal cohesion deficits in LCLs from G2019S patients do not cause cell cycle alterations

To determine whether centrosomal cohesion deficits may comprise a valid cellular biomarker in peripheral patient-derived cells, we initially used a small set of LCLs from healthy control and G2019S LRRK2 PD patients, and determined centrosomal cohesion deficits from cells stained with an improved protocol employing antibodies against two distinct centrosomal markers (pericentrin and γ-tubulin) (Fig. 45A). When quantifying the cells with duplicated centrosomes, all three G2019S LRRK2 LCLs showed a significant increase in the percentage of cells displaying a split centrosome phenotype as compared to control cells, which was reverted upon short-term incubation with the LRRK2 kinase inhibitor MLi-2 (Fig. 45B). In parallel, we analysed the effects of MLi-2 on LRRK2 phosphorylation as well as on LRRK2 substrate phosphorylation. In all cases, MLi-2 treatment significantly reduced both LRRK2 Ser935 phosphorylation as well as RAB10 Thr73 phosphorylation, confirming the on-target effect of the LRRK2 kinase inhibitor (Fig. 45C).

Around 15-20 % of all cells displayed duplicated centrosomes, a phenotype which mainly reflects cells in G2 phase of the cell cycle (Nigg and Stearns, 2011), and which was not found to be drastically different between the distinct cell lines (Fig. 45D). As an alternative means, we performed cell cycle analysis by flow cytometry, which also did not reveal significant changes between the control and G2019S LRRK2 LCLs, with a similar percentage of cells identified in G2/M phase as when scoring the percentage of cells with duplicated centrosomes by immunocytochemistry (Fig. 45E,F). Finally, G2019S LRRK2 LCLs also did not show alterations in apoptosis as compared to control LCLs (Fig. 45G,H). Therefore, the increased distance between duplicated centrosomes in G2019S LRRK2 LCLs does not impact on cell cycle progression and/or cell viability in such immortalised cell lines.

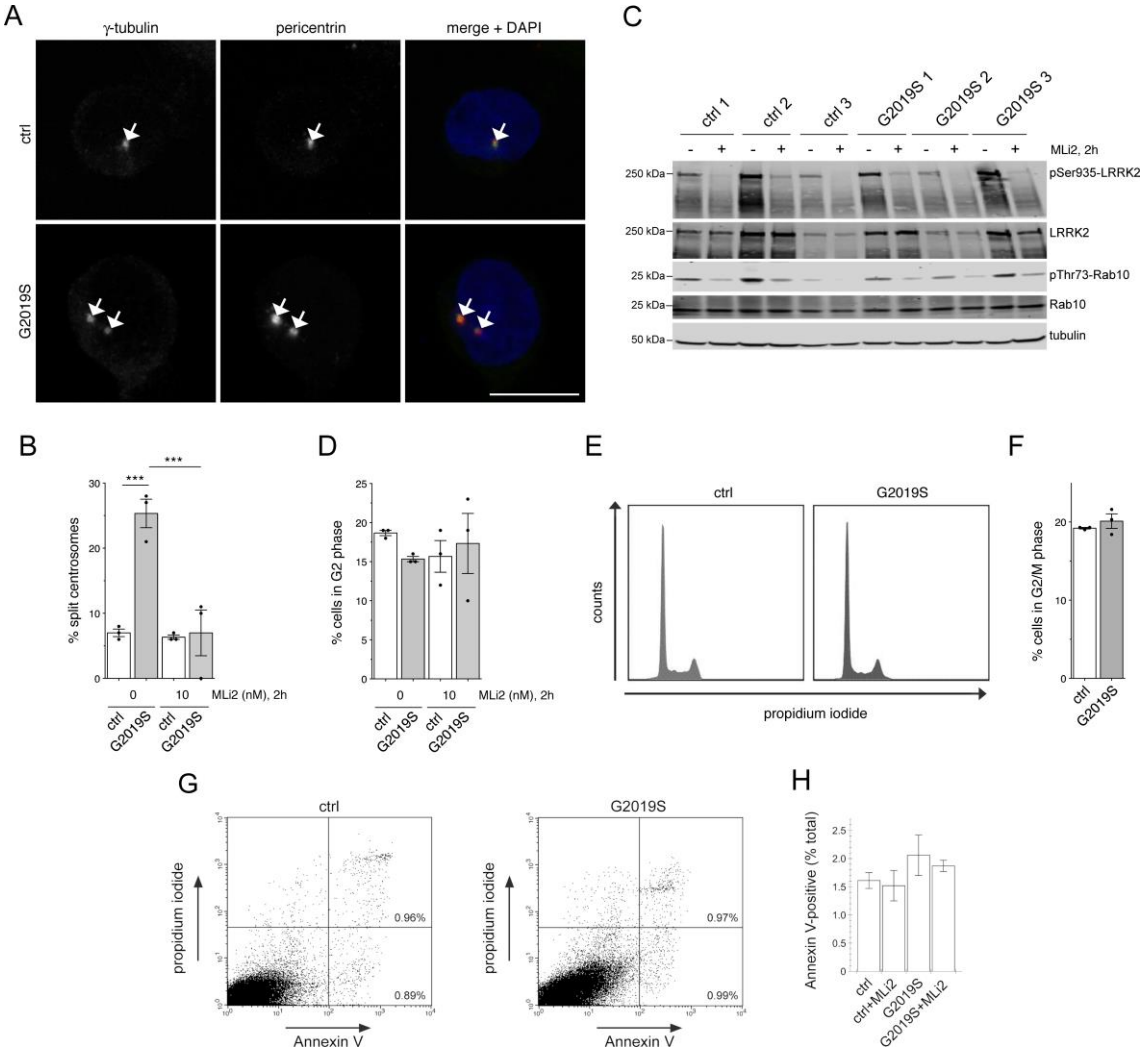

Fig. 45. Monitoring centrosomal cohesion deficits and cell cycle alterations in a subset of healthy control and G2019S LRRK2 PD LCLs. (A) Example of healthy control (ctrl) or G2019S LRRK2 PD-derived LCLs (G2019S) stained for two centrosomal markers (γ-tubulin and pericentrin) and DAPI. Scale bar, 10 μm. **(B)** The centrosome phenotype was quantified from 100 cells per line, and from three control and three G2019S LRRK2 LCL lines. Control or G2019S LRRK2 LCLs were treated with MLi-2 (10 nM) for 2 h as indicated. Bars represent mean ± s.e.m.; ***, $p < 0.005$ (one-way ANOVA with Tukey´s post-hoc test). **(C)** Cells were incubated either in the presence or absence of 10 nM MLi-2 for 2 h as indicated, and extracts analysed for LRRK2 Ser935, LRRK2, RAB10 Thr73, RAB10, or tubulin as loading control. Membranes were developed using the Odyssey CLx scan Western blot imaging system, and antibodies multiplexed as described in Materials and Methods. **(D)** Quantification of the percentage of cells displaying duplicated centrosomes, a phenotype mainly reflecting cells in G2 phase (% cells in G2 phase). A total of 100 cells per line were quantified from the three control and three G2019S LRRK2 LCL lines in the absence or presence of MLi-2 (10 nM) for 2 h as indicated. **(E)** Example of flow cytometry traces of one control and one G2019S line upon propidium iodide staining as indicated. **(F)** Quantification of the percentage of cells displaying duplicated DNA content as assessed by propidium iodide staining (% cells in G2/M phase) from three control and three G2019S LRRK2 LCL lines. **(G)** FACS-based cell viability analysis from one control and one G2019S LCL line as described in Materials and Methods. **(H)** Quantification of annexin V-positive cells from the three control and three G2019S LCLs in the absence or presence of 10 nM MLi-2 for 2 h as indicated.

Centrosomal cohesion deficits are reverted by LRRK2 kinase inhibitor in a dose-dependent and dynamic manner

To assess LRRK2 inhibitor dose response, we next treated five distinct control and G2019S LRRK2 LCLs with increasing concentrations of MLi-2 for 2 h. None of the concentrations tested altered centrosome cohesion in control cells (Fig. 46A). In contrast, the cohesion deficit observed in the G2019S LRRK2 LCLs was progressively reduced at 1 nM and 5 nM, and abolished at 10 nM and 50 nM inhibitor concentrations, respectively (Fig. 46A). When incubating cells with 50 nM MLi-2 for 2 h, followed by washout into media without inhibitor for another two hours, the centrosomal cohesion deficit in the G2019S LRRK2 LCLs was fully re-established, indicating the rapid and dynamic nature of this cellular readout (Fig. 46A). None of the treatments caused cell cycle alterations as analysed by scoring the percentage

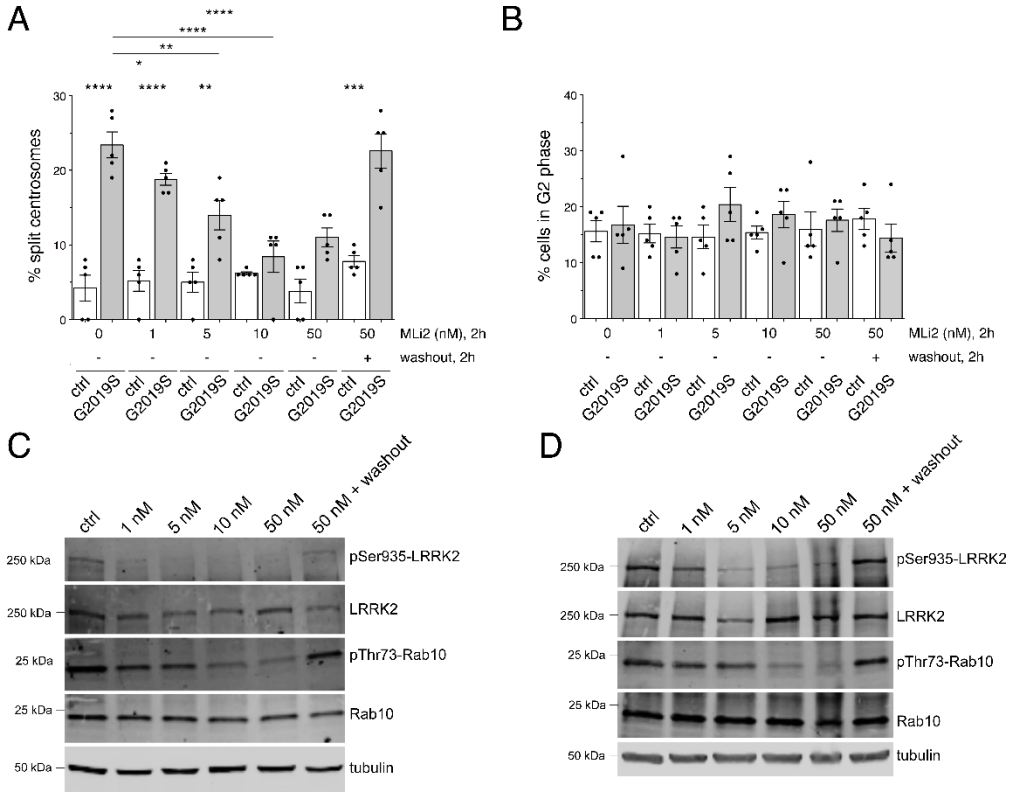

Fig. 46. Dose response and reversibility analysis of centrosomal cohesion deficits and RAB10 phosphorylation in control and G2019S LRRK2 LCLs. (A) The centrosome phenotype was quantified from five distinct control and five G2019S LRRK2 LCL lines, in either the presence or absence of the indicated concentrations of MLi-2 for 2 h. In addition, cells were treated with 50 nM MLi-2 for 2 h, followed by incubation in medium without MLi-2 for an additional 2 h (washout) before quantification. Bars represent mean ± s.e.m; *, $p < 0.05$; **, $p < 0.01$; ***, $p < 0.005$; ****, $p < 0.001$ (one-way ANOVA with Tukey´s post-hoc test). **(B)** Quantification of the percentage of cells displaying duplicated centrosomes, a phenotype mainly reflecting cells in G2 phase, from a total of 100 cells per line, for each of the five control and five G2019S LRRK2 lines. **(C)** Control LCL was incubated in either the presence or absence of the indicated concentrations of MLi-2 for 2 h as indicated, or treated with 50 nM MLi-2 for 2 h followed by incubation in medium without inhibitor for an additional 2 h (washout), and extracts analysed for LRRK2 Ser935, LRRK2, RAB10 Thr73, RAB10, or tubulin as loading control. Membranes were developed using the Odyssey CLx scan Western blot imaging system, and antibodies multiplexed as described in Materials and Methods. **(D)** Same as (C), but performed with G2019S LRRK2 LCL. Similar results were obtained in two independent experiments.

of cells with duplicated centrosomes (Fig. 46B). The dose-dependency was well matched with alterations observed in LRRK2 Ser935 phosphorylation and phospho-RAB10, with a partial decrease at 1 nM and 5 nM MLi-2, a potent decrease at 10 nM and 50 nM MLi-2, and a complete reversal upon washout (Fig. 46C,D). Such dose-dependent inhibition and reversal of LRRK2 Ser935 phosphorylation and phospho-RAB10 was observed in both control (Fig. 46C) and G2019S LRRK2 LCLs (Fig. 46D), even though MLi-2 treatment had no effect on centrosome cohesion in the control LCLs (Fig. 46A). Thus, LRRK2 kinase inhibitor causes a potent, dose-dependent and reversible inhibition of the centrosomal cohesion deficits in LRRK2 G2019S LCLs, associated with changes in LRRK2 Ser935 phosphorylation and phospho-RAB10 indicative of on-target inhibition of LRRK2 kinase activity.

Analysis of centrosomal cohesion deficits in LCLs from a larger G2019S LRRK2 PD cohort

We next sought to probe for centrosomal deficits in a larger sampling of LCLs. A total of 16 age- and biological sex-matched healthy control and 12 G2019S LRRK2 PD LCLs were analysed, which included an independent determination from the five previously employed control and G2019S LRRK2 LCLs for proper age- and biological sex-matching purposes (Fig. 47A; Table 2). Centrosomal cohesion deficits were observed in all 12 G2019S LRRK2 LCLs as compared to controls (Fig. 47A), which was not associated with a change in the percentage of cells displaying duplicated centrosomes (Fig. 47B). In all cases, these deficits were reverted upon MLi-2 treatment (Fig. 47A,C).

To analyse whether centrosomal cohesion deficits were specific to LRRK2 G2019S PD as compared to sporadic PD samples, we analysed LCLs from 13 age- and biological sex-matched sporadic PD patients negative for the G2019S LRRK2 mutation (Fig. 47; Table 2). Interestingly, three out of 13 LCLs from sporadic PD patients displayed a centrosomal cohesion deficit similar to LRRK2 G2019S LCLs, which was reverted upon MLi-2 treatment (Fig. 47A,C) and was not associated with a change in the percentage of cells displaying duplicated centrosomes (Fig. 47B). Therefore, centrosomal cohesion deficits seem to be a robust cellular readout in LCLs from LRRK2 G2019S patients, but also observable in LCLs from a subset of sporadic PD patients, and in all cases dependent on the LRRK2 kinase activity.

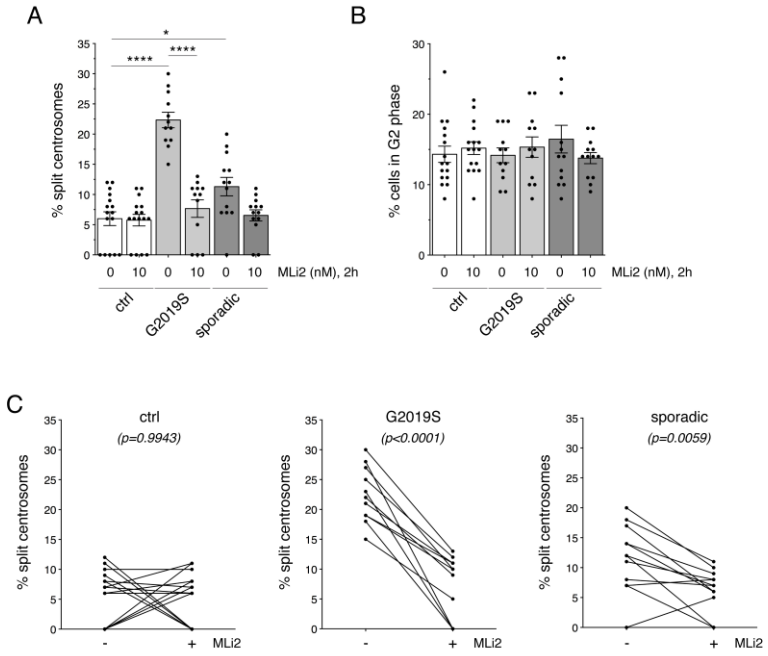

Fig. 47. Centrosomal cohesion deficits in LCLs from control, G2019S LRRK2 PD and sporadic PD patients. (A) Centrosomal cohesion deficits were quantified from a total of 16 age- and sex-matched control, 12 G2019S LRRK2 PD and 13 sporadic PD LCLs in either the absence or presence of 10 nM MLi-2 for 2 h as indicated. Bars represent mean ± s.e.m.; **, $p < 0.01$; ****, $p < 0.001$ (one-way ANOVA with Tukey´s post-hoc test). **(B)** Quantification of the percentage of cells displaying duplicated centrosomes from a total of 100 cells per LCL line. **(C)** Paired t-test analysis of centrosomal cohesion deficits from control, G2019S LRRK2 and sporadic PD LCLs for each cell line in the absence or presence of MLi-2 as indicated. Please note that differences in the values between 0-10 % are not significant given the small number of cells displaying a duplicated split centrosome phenotype.

Association between centrosomal cohesion deficits, levels of LRRK2 or RAB10 Thr73 phosphorylation, or PD clinical variables

We next wondered whether the centrosomal cohesion deficits observed in G2019S LRRK2 LCLs and sporadic LCLs were associated with increased levels of LRRK2 and/or RAB10 Thr73 phosphorylation, respectively. Levels of total LRRK2 varied drastically amongst individual LCLs, but there were no significant differences in the levels of total LRRK2 between healthy control, LRRK2 G2019S or sporadic PD LCLs (Fig. 48A,B), even though some LRRK2 G2019S lines had hardly detectable levels of total LRRK2 (Fig. 49), reminiscent of the reported decrease in LRRK2 protein levels in postmortem brain extracts from LRRK2 PD patients as compared to control or sporadic PD patients (Zhao et al., 2018). Levels of LRRK2 Ser935 phosphorylation normalized to either tubulin or to total LRRK2 were similar in LCLs from control, G2019S LRRK2 or sporadic PD patient samples, and were significantly reduced by MLi-2 in control and sporadic samples (Fig. 48C,D). The total levels of RAB10 protein were generally low, and less variable than LRRK2 protein between individual patient samples, without a difference between genotypes observed (Fig. 48E). RAB10

Thr73 phosphorylation was not different between control, G2019S or sporadic PD LCLs, but significantly decreased upon 2 h MLi-2 treatment in control and sporadic samples (Fig. 48F,G). Therefore, LCLs display a large variability in total LRRK2 protein, with more similar levels in total RAB10, but no significant differences in the amount of total proteins and/or phospho-proteins between control, G2019S LRRK2 or sporadic PD samples.

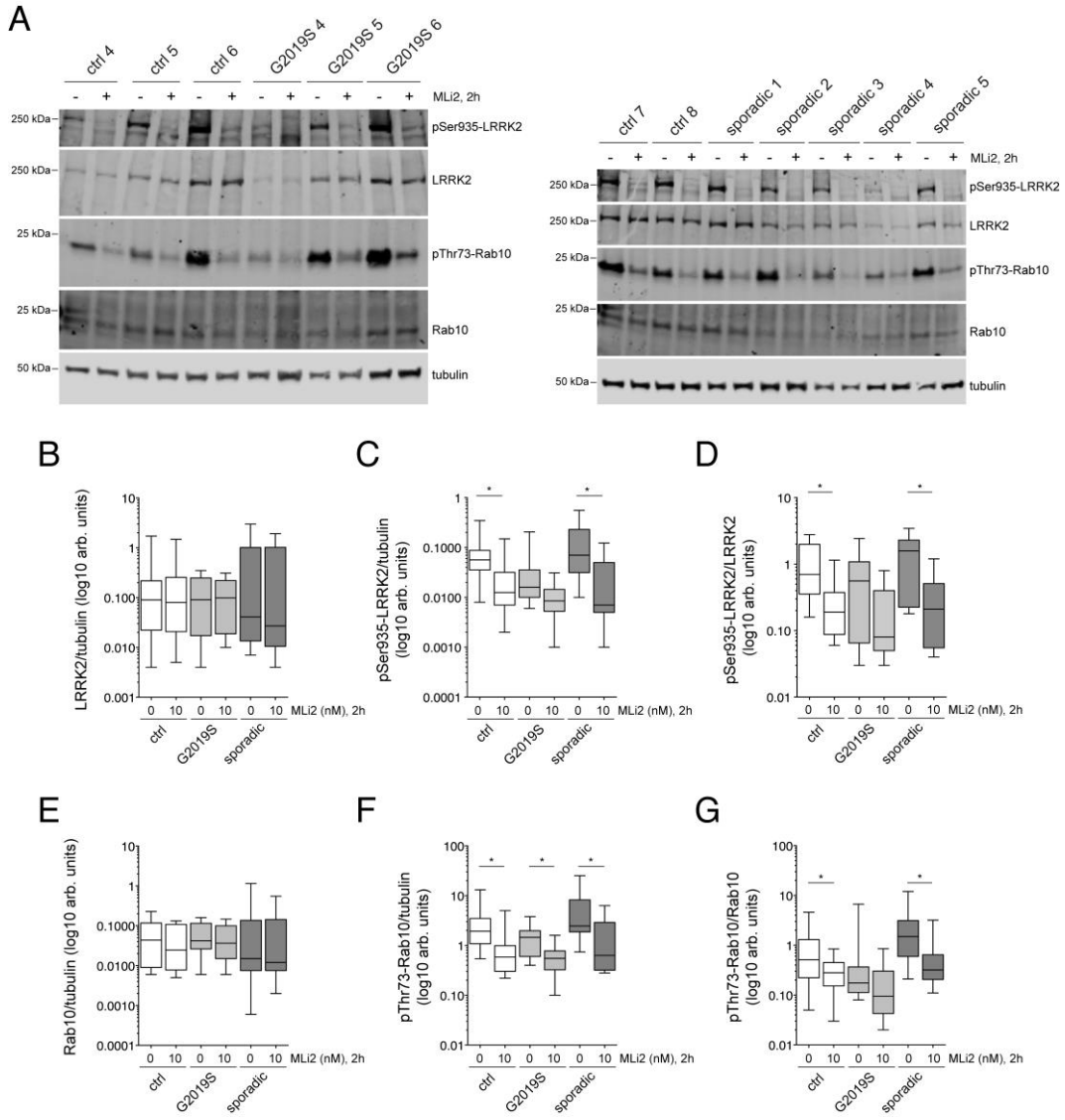

Fig. 48. Analysis of LRRK2, LRRK2 Ser935, RAB10 and RAB10 Thr73 phosphorylation in LCLs from control, G2019S LRRK2 PD and sporadic PD patients. (A) Example of three control and three G2019S LRRK2 LCL lines (left), or two distinct control and five sporadic PD LCL lines (right), treated with or without 10 nM MLi2 for 2 h. Cells were subsequently lysed and extracts subjected to quantitative immunoblot analysis with the indicated antibodies, and membranes developed using Odyssey CLx scan Western Blot imaging system. Please note that "sporadic 2" and "sporadic 4" are two out of the three sporadic PD LCLs which display a centrosomal cohesion deficit. **(B)** Control, G2019S LRRK2 and sporadic PD LCL extracts were analysed as described in (A), and immunoblots quantified for full-length LRRK2/tubulin ratio. **(C)** Immunoblots of the type depicted in (A) were quantified for LRRK2 Ser935/tubulin ratio. *, $p < 0.05$. **(D)** Immunoblots were quantified for LRRK2 Ser935/LRRK2 ratio. *, $p < 0.05$. **(E)** Immunoblots were quantified for RAB10/tubulin ratio. **(F)** Immunoblots were quantified for RAB10 Thr73/tubulin ratio. *, $p < 0.05$. **(G)** Immunoblots were quantified for RAB10 Thr73/RAB10 ratio. *, $p < 0.05$. Statistical analysis was performed with Kruskal-Wallis test with Dunn´s multiple comparison. All data are presented as whisker plots.

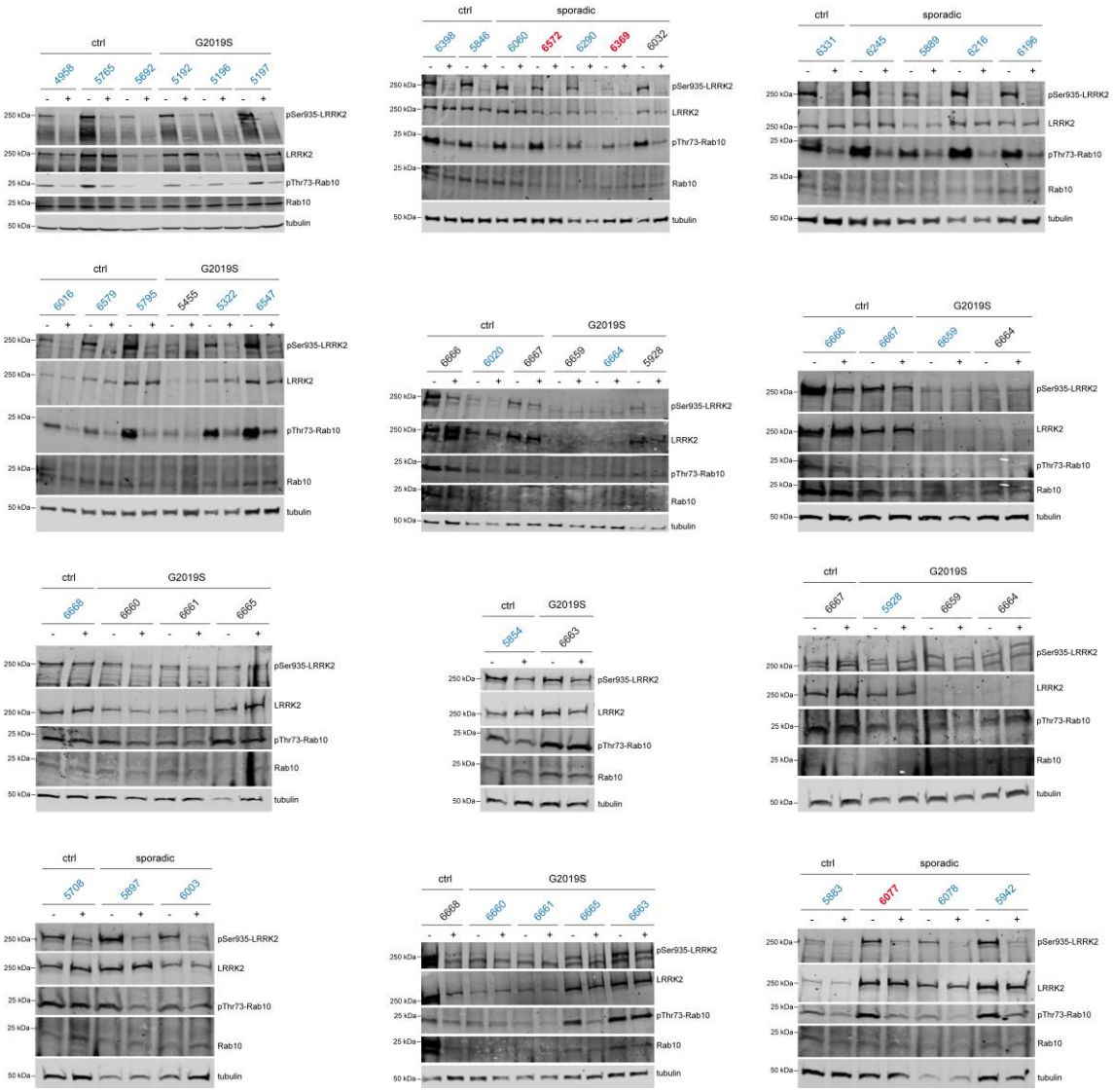

Fig. 49. Western blots detecting LRRK2, LRRK2 Ser935, RAB10 and RAB10 Thr73 phosphorylation in LCLs from control, G2019S LRRK2 PD and sporadic PD patients. All Western blots of extracts upon treating cells in presence (+) or absence (-) of 10 nM MLi-2 for 2 h from control, G2019S LRRK2 and sporadic PD LCLs analysed in the present study, and blotted with the indicated antibodies as described in Materials and Methods. Most samples were run multiple times, and sample codes in blue indicate blots where protein and phospho-protein quantifications were analysed from. Red codes indicate the three sporadic PD LCLs which display a centrosomal cohesion deficit.

Correlation analyses were performed to determine possible associations between LRRK2 and phosphorylated RAB10. In control and sporadic PD LCLs, there was a significant correlation between LRRK2 levels and RAB10 Thr73 phosphorylation (Fig. 50A). Similarly, in patients with and without the G2019S LRRK2 mutation, there was a significant correlation between LRRK2 Ser935 levels and RAB10 Thr73 phosphorylation (Fig. 50B). The lack and/or weak correlation between LRRK2 levels/LRRK2 Ser935 levels and RAB10 Thr73 phosphorylation in the G2019S LRRK2 samples correlated with a tendency of lower total LRRK2 levels in this specific patient sampling analysed (Fig. 50A,B). As correlation coefficients are sensitive to outliers, we

recalculated them after taking out the most outlying datapoint, which still yielded a significant correlation between LRRK2 levels or LRRK2 Ser935 levels and RAB10 Thr73 phosphorylation for the sporadic LCL samples, whilst significance was lost in the control samples. Thus, and at least in sporadic PD LCLs, increased LRRK2 levels seem to correlate well with an increase in RAB10 Thr73 phosphorylation levels.

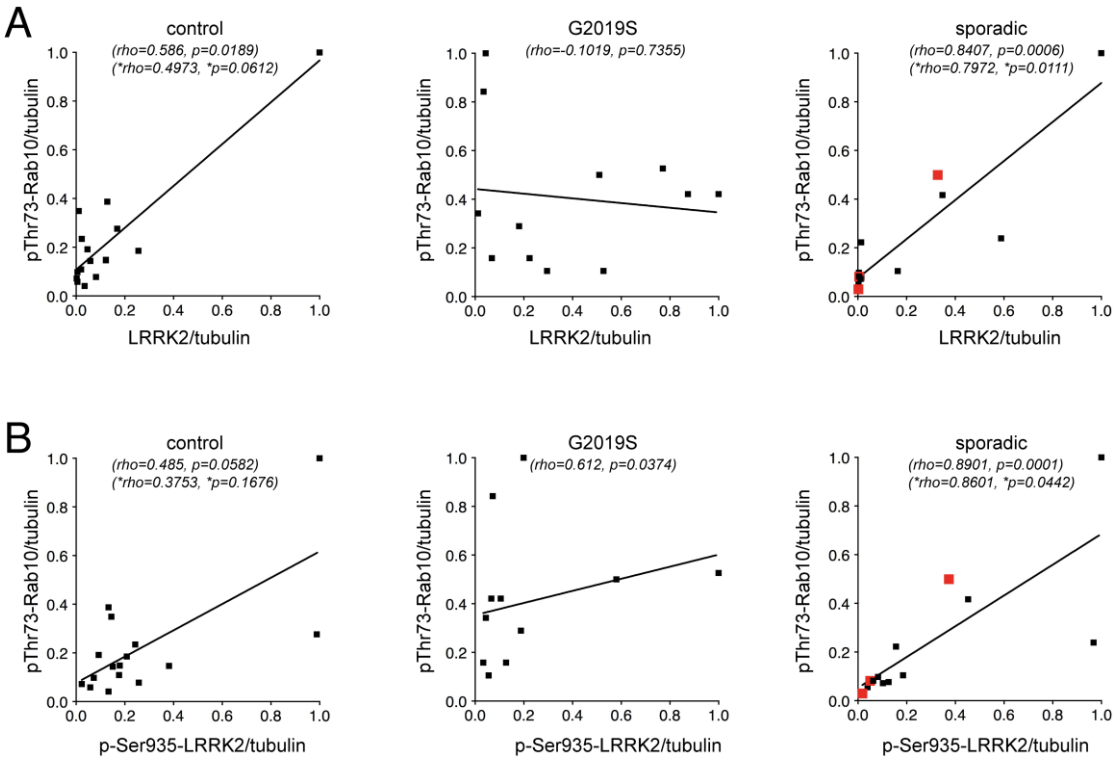

Fig. 50. Correlation analysis between levels of LRRK2 or LRRK2 Ser935 and RAB10 Thr73 in LCLs from control, G2019S LRRK2 PD and sporadic PD patients. (A) Spearman correlation analysis revealed a significant association between LRRK2 levels and RAB10 Thr73 levels in sporadic PD patients. **(B)** Spearman correlation analysis revealed a significant association between LRRK2 Ser935 levels and RAB10 Thr73 levels in sporadic PD samples. The maximal datapoint value in each genotype was normalized to 1. Rho and p values including all data sets (top), or excluding the outlying datapoint (bottom, *) are indicated for each correlation analysis. Red datapoints indicate the three sporadic PD samples which display a centrosomal cohesion deficit.

Finally, correlation analyses were performed to determine any associations between LRRK2, RAB10 or their phosphorylation with available PD clinical variables in the sporadic PD samples. No significant correlations were observed between LRRK2 levels, LRRK2 Ser935 levels or RAB10 Thr73 phosphorylation levels and UPDRS motor score, disease duration, age at onset or dopamine medication doses in the sporadic PD patient cohort samples (Fig. 51). Similarly, there were no correlations between LRRK2 levels, LRRK2 Ser935 levels or RAB10 Thr73 phosphorylation levels and clinical variables in the three sporadic PD patients which displayed a centrosomal cohesion phenotype (Fig. 51).

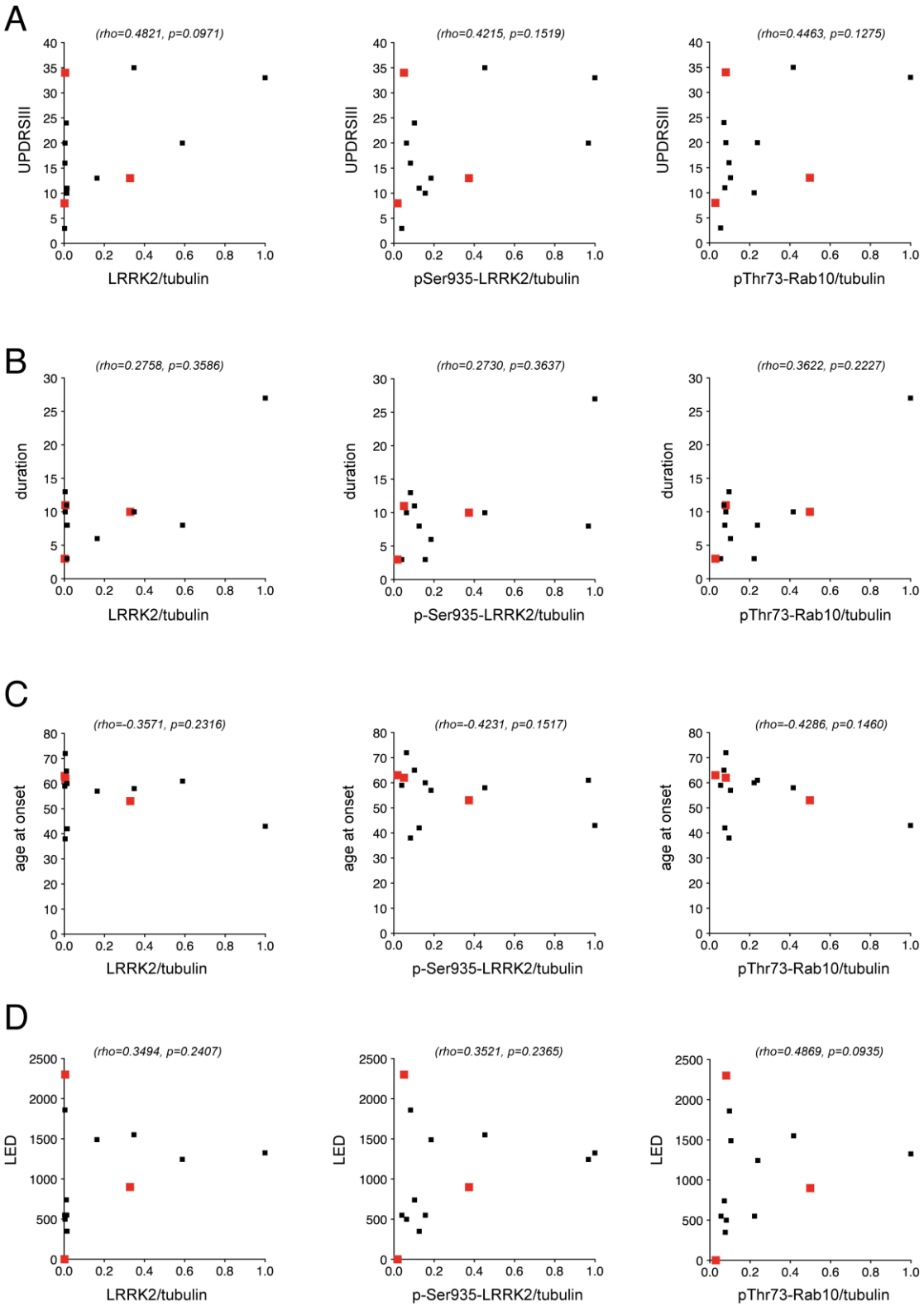

Fig. 51. Correlation analysis between the levels of LRRK2, LRRK2 Ser935 or RAB10 Thr73 and various PD clinical variables from the sporadic PD patient cohort. (A) Spearman correlation analysis between LRRK2 levels, LRRK2 Ser935 levels or RAB10 Thr73 levels and UPDRSIII score. **(B)** Spearman correlation analysis between LRRK2 levels, LRRK2 Ser935 levels or RAB10 Thr73 levels and disease duration. **(C)** Spearman correlation analysis between LRRK2 levels, LRRK2 Ser935 levels or RAB10 Thr73 levels and age at disease onset. **(D)** Spearman correlation analysis between LRRK2 levels, LRRK2 Ser935 levels or RAB10 Thr73 levels and the calculated L-dopa-equivalent dose (LED). The maximal datapoint values for the respective proteins and/or phospho-proteins were normalized to 1.

Correlation between centrosomal cohesion deficits and LRRK2 activity and/or pericentrosomal/centrosomal phospho-RAB10 accumulation

We wondered whether the centrosomal cohesion deficits observed in G2019S LRRK2 but not control LCLs may correlate with increased LRRK2 kinase activity, rather than with total LRRK2 protein levels. The autophosphorylation site Ser1292 serves as a physiological and direct marker for LRRK2 kinase activity, but current antibodies do not allow detection of this autophosphorylation site by Western blotting at endogenous levels (Sheng et al., 2012). Therefore, we employed the recently developed PLA to assess Ser1292 phosphorylation of LRRK2, whereby the signal of the anti-Ser1292 antibody is amplified and detected only when in proximity to the signal from a validated total LRRK2 antibody (Di Maio et al., 2018).

To independently validate the proximity ligation assay to detect LRRK2 kinase activity (Di Maio et al., 2018), we initially transfected HEK293 cells with GFP-tagged pathogenic Y1699C-LRRK2, which displays robust kinase activity and triggers an activity-mediated centrosomal cohesion phenotype (Steger et al., 2016; Madero-Pérez et al., 2018a). Pathogenic LRRK2 expression caused a significant increase in the phospho-Ser1292 PLA signal intensity, which was abolished upon pretreatment of cells with MLi-2 (Fig. 52A,B). In addition, and as analyzed by quantitative light microscopy, pathogenic LRRK2 expression levels correlated with the PLA signal intensity (Fig. 52C), suggesting that the signal was a dose-dependent reflection of LRRK2 kinase activity.

We next analyzed the phospho-Ser1292 PLA signal under conditions of endogenous LRRK2 expression levels by using wildtype, mutant LRRK2 knockin (KI) (G2019S/G2019S-KI or R1441G/R1441G-KI), and LRRK2-deficient (LRRK2-KO) HEK293 cells obtained by CRISPR/Cas9 gene editing (Di Maio et al., 2018). As compared to cells transiently overexpressing pathogenic LRRK2, the PLA signal in the distinct HEK293 cell lines expressing endogenous levels of LRRK2 was drastically reduced, and was quantified as the number of individual fluorescence dots per cell, rather than total PLA signal intensity per cell (Fig. 52D). Such differences in assay signal between HEK293 cells overexpressing mutant LRRK2 as compared to LRRK2-KI cells correlated with differences in LRRK2 protein levels, as well as with LRRK2 kinase activity, as assessed by Western blotting techniques (Fig. 52E). There was a significant increase in the PLA signal in the LRRK2 R1441G/R1441G-KI cells (Fig. 52D). In contrast, the assay was unable to detect endogenous LRRK2 kinase activity in the wildtype or G2019S/G2019S-KI cells, as the signal observed was identical to the one obtained

in the LRRK2-KO cells, or when omitting one of the two primary antibodies from the PLA reaction (Fig. 52D). Thus, whilst the assay can serve as a readout for LRRK2 kinase activity, it displays limited sensitivity in the context of endogenous LRRK2 levels.

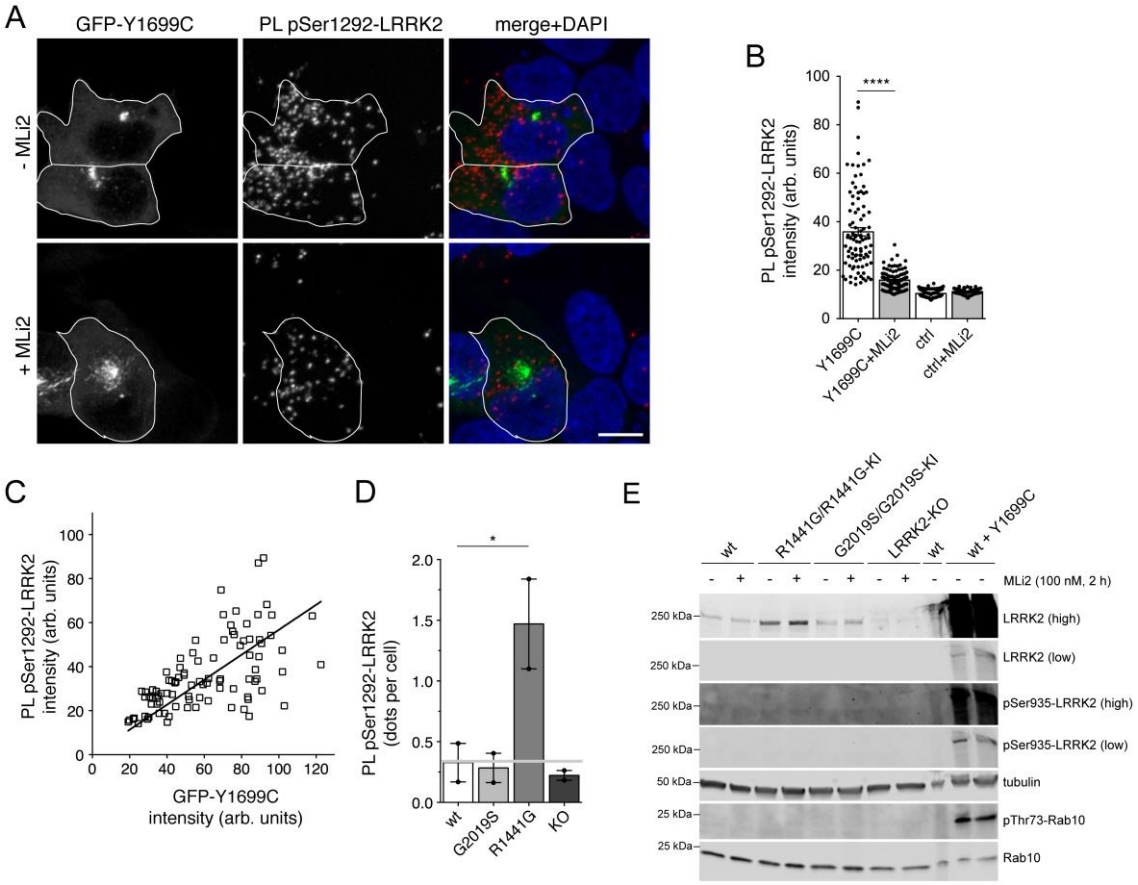

Fig. 52. Detection of active LRRK2 by proximity ligation assays in HEK293 cells. (A) Example of proximity ligation signal (PL pSer1292-LRRK2) as a readout for LRRK2 kinase activity in HEK293 cells transfected with GFP-tagged pathogenic Y1699C LRRK2, either in the absence or presence of MLi-2 (100 nM, 2 h) as indicated, and stained for DAPI. Scale bar, 10 µm. **(B)** Quantification of the proximity ligation signal intensity (PL pSer1292-LRRK2) was performed over non-processed images acquired on the same day and with the same laser intensities with Leica Applied Systems (LAS AF6000) image acquisition software, and around 100 cells quantified per condition. ****, $p < 0.001$. **(C)** Correlation between the level of GFP-tagged pathogenic Y1699C LRRK2 expression and the PLA signal intensity from around 100 transfected cells. Spearman correlation analysis indicated a significant association between LRRK2 expression levels and PLA signal intensity (rho = 0.66, $p < 0.0001$). **(D)** Quantification of the PLA signal (PL pSer1292-LRRK2) from wildtype (wt), G2019S/G2019S-KI, R1441G/R1441G-KI or LRRK2-KO HEK293 cells. PLA signal was quantified as the number of fluorescent dots per cell from around 300 individual cells per condition and experiment. The non-specific proximity ligation signal obtained when omitting the pSer1292 antibody is indicated as grey line. Bars represent mean ± s.e.m. (n = 2 experiments); *, $p < 0.05$. **(E)** Immunoblots of wildtype (wt), R1441G/R1441G-KI, G2019S/G2019S-KI, LRRK2-KO, or wildtype HEK293 cells in the absence or presence of transient transfection with GFP-tagged Y1699C mutant LRRK2 (wt + Y1699C), and in the absence or presence of MLi-2 (100 nM, 2 h) as indicated. Cells were lysed and extracts subjected to quantitative immunoblot analysis with the indicated antibodies, and membranes developed using Odyssey CLx scan Western Blot imaging system. For total LRRK2 and pSer935-LRRK2 blots, both a high exposure (to detect endogenous LRRK2) and a low exposure (to detect GFP-tagged Y1699C pathogenic LRRK2) of the same membranes are depicted. Note that phospho-Ser935-LRRK2 and pThr73-RAB10 levels were only detectable upon transient overexpression of pathogenic LRRK2 in this cell type.

When applied to the same set of LCLs from healthy controls and G2019S LRRK2 PD patients as in Figure 32, a small phospho-Ser1292 proximity ligation signal was observed in the control samples (Fig. 53A,B). G2019S LRRK2 LCLs displayed a significantly increased phospho-Ser1292 proximity ligation signal as compared to the control LCLs (Fig. 53A,B), all whilst displaying very distinct levels of total LRRK2 as assessed by Western blotting techniques (Fig. 45C). The proximity ligation signal was decreased upon MLi-2 treatment in all three G2019S LRRK2 LCLs, indicating that it was specifically reflecting intrinsic LRRK2 kinase activity (Fig. 53B,C). However, and similar to what was observed in HEK293 cells, the assay was unable to detect endogenous LRRK2 kinase activity in the control LCLs, as the signal obtained was similar to that obtained when omitting one of the two primary antibodies from the PLA reaction (Fig. 53C).

Lastly, we applied the PLA to a distinct set of age-matched LCLs including three distinct controls, two distinct G2019S LRRK2 LCLs, three sporadic LCLs without a cohesion phenotype, and the three sporadic LCLs with a centrosomal cohesion phenotype, respectively (Fig. 53D). Whilst the G2019S LRRK2 LCLs displayed an increased proximity ligation signal as compared to control LCLs which was reverted upon MLi-2 treatment, no specific signal could be detected in either control or sporadic PD LCLs (Fig. 53D). Thus, intrinsic LRRK2 kinase activity as assessed by the PLA, rather than total LRRK2 levels, seems to correlate with the observed cohesion phenotype in the G2019S LRRK2 LCLs. In contrast, the assay, at least in our hands, is unable to detect endogenous LRRK2 kinase activity in control or sporadic PD LCLs, including the sporadic PD LCLs which display a centrosomal cohesion phenotype (Fig. 53D).

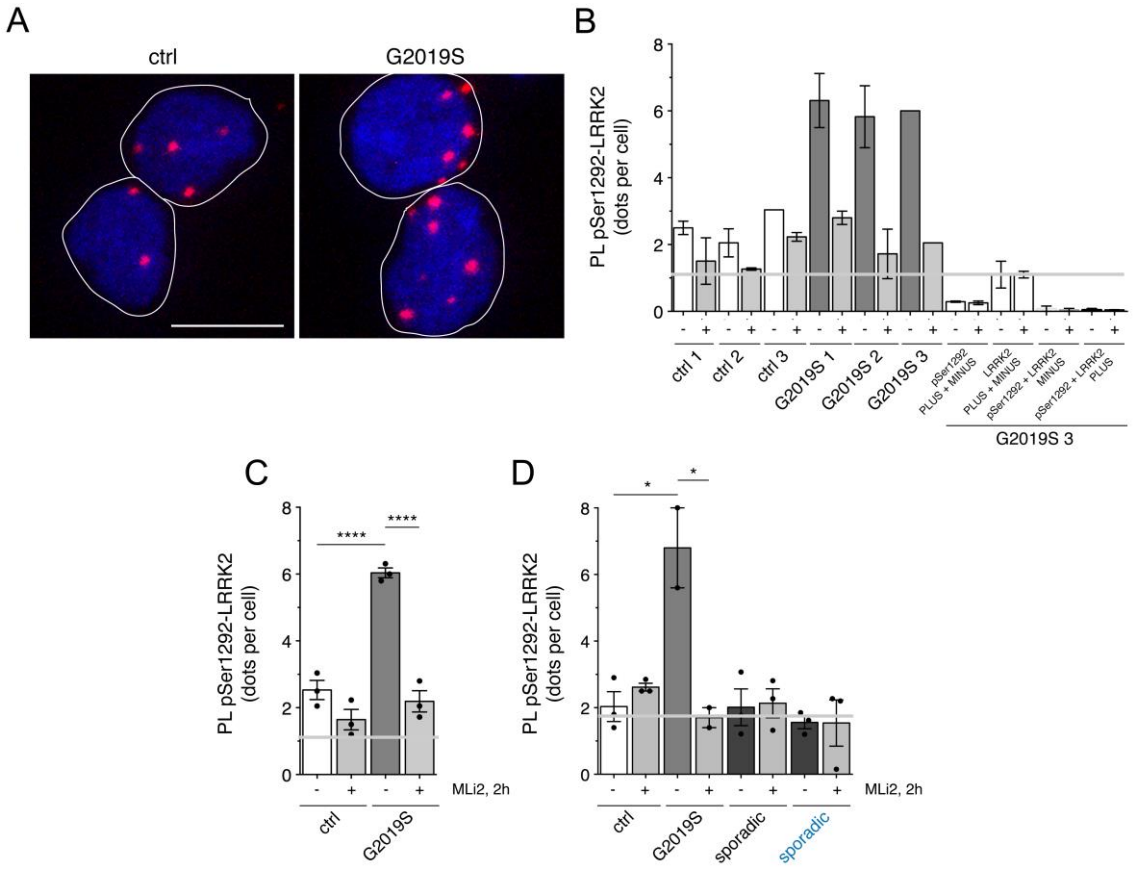

Fig. 53. Detection of active LRRK2 by proximity ligation assays in LCLs from control and G2019S PD patients. (A) Example of proximity ligation signal as a readout for LRRK2 kinase activity in control and G2019S LRRK2 PD LCL cells stained for DAPI. Scale bar, 10 µm. **(B)** Quantification of the proximity ligation signal (PL pSer1292-LRRK2) from three control and three G2019S LRRK2 PD LCLs in either the presence or absence of MLi-2 (10 nM). Four different control proximity ligation reactions were analysed on one G2019S LRRK2 LCL line (G2019S 3), which included omission of either one of the two primary antibodies (total LRRK2 antibody (LRRK2) or pSer1292 antibody (pSer1292)), or of either one of the two secondary antibodies (PLUS or MINUS), respectively. Please note that there was significant non-specific proximity ligation signal when omitting the pSer1292 antibody, and this signal was used as background against which the assay signals were evaluated (grey line). Around 300 cells were quantified per condition and experiment. Bars represent mean ± s.e.m. (n = 2 experiments). **(C)** Proximity ligation signal based on the means from each line as depicted in (B), from control and G2019S LRRK2 LCLs in either the presence or absence of MLi-2 (10 nM) as indicated. Grey line depicts background signal when omitting the pSer1292 antibody. Bars represent mean ± s.e.m (n = 3 lines); ****, $p < 0.001$. **(D)** Proximity ligation signal was determined in LCLs from three distinct age-matched control, two distinct G2019S LRRK2, three sporadic PD without a cohesion phenotype, and three sporadic PD with a cohesion phenotype (blue), respectively. The non-specific proximity ligation signal obtained when omitting the pSer1292 antibody is indicated as grey line. Bars represent mean ± s.e.m; *, $p < 0.05$.

Finally, and given previous studies reporting the pericentrosomal/centrosomal accumulation of phospho-RAB8 and phospho-RAB10 (Dhekne et al., 2018; Madero-Pérez et al., 2018a), we wondered whether the centrosomal cohesion phenotype may correlate with altered subcellular localization of these phosphorylated RAB species. The currently available phospho-RAB8A antibodies were not of sufficient affinity to detect the pericentrosomal/centrosomal accumulation of endogenous phospho-RAB8A in LCLs (Fig. 54A). A recently developed phospho-RAB10 antibody suitable for immunocytochemistry techniques detected a pericentrosomal/centrosomal signal

in some, but not all cells. When quantifying the integrated fluorescence intensity of phospho-RAB10 at/around the centrosome as defined by co-staining with a centrosomal marker, the three G2019S LRRK2 LCLs displayed a slight, but not significant increase in phospho-RAB10 accumulation as compared to control samples, which was decreased, but not abolished upon MLi-2 treatment, suggesting that the antibody was not entirely phospho-state-specific, at least under the conditions employed here (Fig. 54B,C).

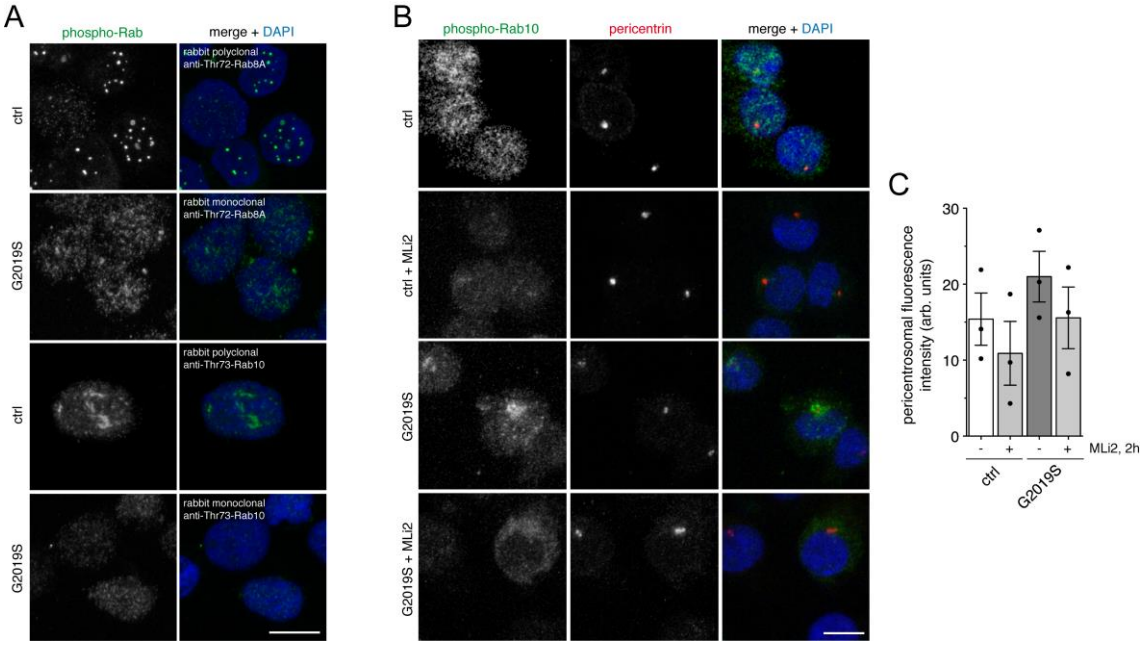

Fig. 54. Staining of control and G2019S LCLs with antibodies against phospho-RAB8A or phospho-RAB10. (A) Staining of LCLs with a rabbit polyclonal phospho-RAB8A antibody (1:250; generous gift of D. Alessi, University of Dundee, UK), a rabbit monoclonal phospho-RAB8A antibody (1:1000; Abcam, ab230260), a rabbit polyclonal phospho-RAB10 antibody (1:1000; generous gift of D. Alessi, University of Dundee, UK), or a rabbit monoclonal phospho-RAB10 antibody (1:1000; Abcam, ab230261), respectively, along with DAPI. Cells were fixed and permeabilised with Triton-X100 as described in Materials and Methods. Scale bar, 10 µm. None of these phospho-RAB antibodies were able to specifically detect the pericentrosomal/centrosomal accumulation of endogenous phospho-RABs by immunocytochemistry techniques in either control or G2019S LRRK2 LCLs, similar to what we have previously described for the currently available phospho-RAB8A antibodies in some cell types, such as SH-SY5Y cells (Madero-Pérez et al., 2018a). **(B)** Staining of LCLs with a rabbit monoclonal phospho-RAB10 antibody (1:100, Abcam, ab237703), as well as pericentrin and DAPI. Cells were treated with or without 100 nM MLi-2 for 2 h as indicated, fixed with PFA, and permeabilised with saponin as described in Materials and Methods. Scale bar, 10 µm. The phospho-RAB10 antibody detects pericentrosomal accumulation in some cells, but the signal is not gone in the presence of MLi-2. **(C)** Quantification of phospho-RAB10 fluorescence intensity in a 3 nm circle positioned over the centrosome as detected using pericentrin staining from 100 cells per condition. The experiment was repeated twice with similar results, and the mean value of fluorescence intensity from the two experiments is plotted for each control and G2019S line. Bars represent mean ± s.e.m. (from three control and three G2019S LRRK2 lines).

V. Discussion

Analysis of the mechanism underlying LRRK2-mediated centrosomal cohesion deficits

The data presented in this doctoral thesis show that pathogenic LRRK2 causes the pericentrosomal/centrosomal accumulation of phospho-RAB8 as well as of phospho-RAB10, and centrosomal cohesion deficits in a manner dependent on RAB8, RAB10 and RILPL1. RAB8 and RAB10 share various effector proteins, and the phosphorylation by pathogenic LRRK2 kinase interferes with the ability of most of these effector proteins to interact with the phosphorylated RABs (Steger et al., 2016). This is expected to lead to a loss-of-function in the membrane trafficking pathways these specific RAB-effector complexes are involved in (Rivero-Ríos et al., 2019; Rivero-Ríos et al., 2020b). However, a very small amount of effector proteins including RILPL1 behave in the opposite way by binding to only the phosphorylated forms of RAB8 and RAB10 (Steger et al., 2017). These unusual phospho-RAB-specific effectors are therefore of crucial importance to understand the downstream physiological consequences of hyperactivated LRRK2 kinase underlying PD in a possibly neomorphic gain-of-function manner.

RILPL1 localises to a pericentriolar compartment adjacent to the mother centriole, and has been reported to recruit phospho-RAB10 to this location (Schaub and Stearns, 2013; Dhekne et al., 2018). Under conditions of endogenous protein expression, pathogenic LRRK2-mediated ciliogenesis defects were rescued upon knockdown of either RAB10 or RILPL1 (Dhekne et al., 2018). Similarly, we here describe that the pathogenic LRRK2-mediated centrosomal cohesion deficits are largely and/or completely abolished in cells lacking RAB8A, RAB10 or RILPL1. These data highlight the importance of these proteins in pathogenic LRRK2 signalling with respect to both ciliogenesis and centrosomal cohesion (Figure 55). In the future, it will be important to determine how pericentrosomal/centrosomal protein complexes of phospho-RAB8/10 bound to RILPL1 block cilia formation and interfere with centrosome cohesion. In fact, a recent study has described a possible mechanism by which the phospho-RAB10/RILPL1 complex may block primary cilia biogenesis. This study shows that the recruitment and binding of phosphorylated RAB10 to RILPL1 impairs the subsequent recruitment of TTBK2, therefore not allowing for the displacement of CP110 from the mother centriole, which is a critical early step for ciliogenesis to occur (Sobu et al., 2021). By analogy, the phospho-RAB10/RILPL1 complex might be interfering with the proper localisation of a protein important for centrosomal cohesion,either by displacing it or by recruiting it to a pericentrosomal area.

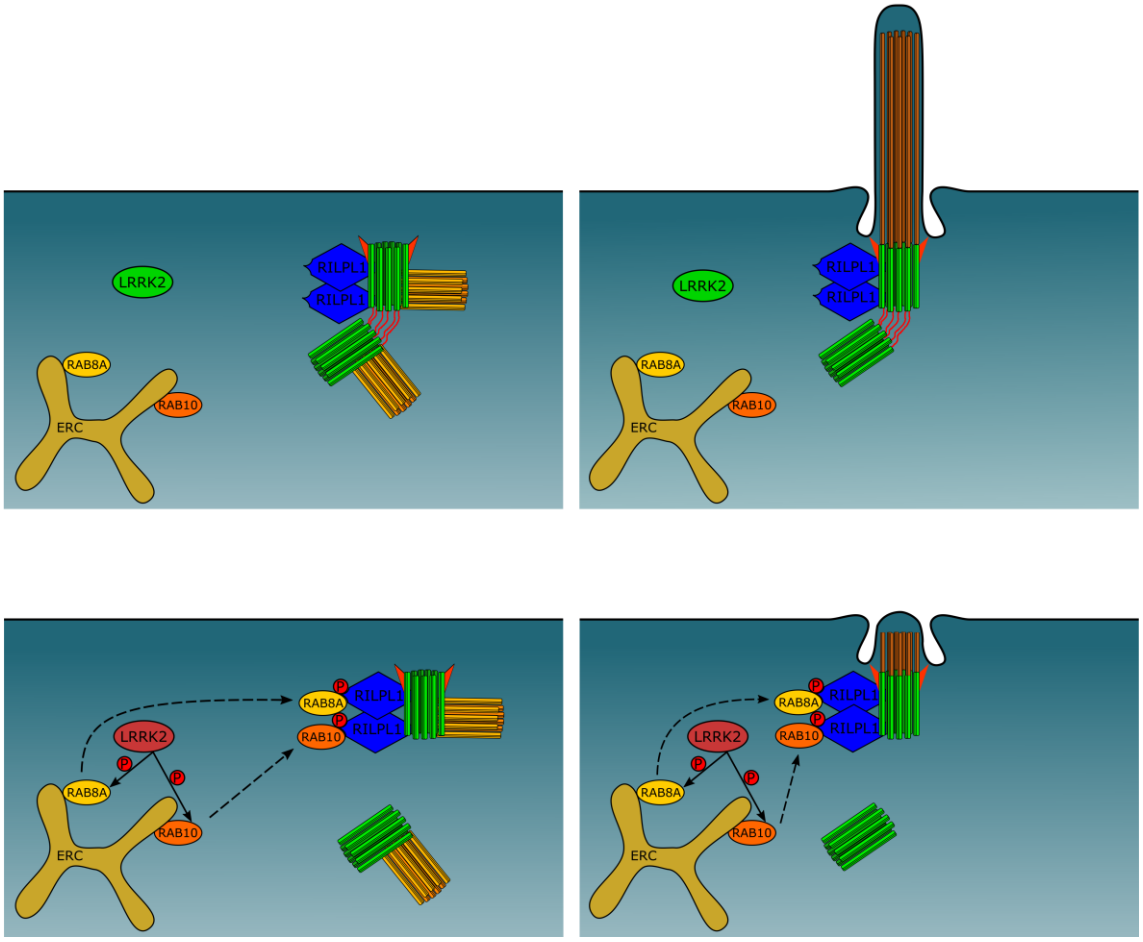

Fig. 55 Cartoon summarizing pathogenic LRRK2-mediated effects on centrosome cohesion and ciliogenesis. Top row: under normal conditions, RAB8A and RAB10 are localised to the early recycling compartment (ERC), and RILPL1 is localised to the mother centriole (green, with appendages depicted in red). In dividing cells, upon centriole duplication (daughter centrioles in yellow), the duplicated centrosomes are properly held together in G2 phase by centrosomal linker proteins (red) (left). Ciliogenesis in interphase or non-dividing cells, nucleated by the mother centriole-derived basal body, occurs normally as well (right). Bottom row: pathogenic LRRK2 phosphorylates RAB8A/RAB10, which causes their relocalisation to the centrosome via binding to RILPL1, followed by a deficit in centrosome cohesion in dividing cells (left), or a deficit in primary cilia formation in interphase or non-dividing cells (right).

Some proteins implicated in vesicular trafficking events have been reported to display additional moonlighting functions at different stages of the cell cycle, including effects on centrosome cohesion (Royle, 2011). We did not detect centrosomal cohesion deficits in A549 cells deficient for either RAB8A, RAB10 or RILPL1, indicating that these three proteins do not modulate centrosome cohesion under normal conditions. However, these three proteins are crucial for the centrosomal cohesion deficits induced by pathogenic LRRK2, since LRRK2-mediated deficits were largely abolished in either A549 RAB8A, RAB10 or RILPL1 knockout cells. Centrosomal cohesion deficits were also observed when increasing the levels of phospho-RAB8/10 by co-expressing the RABs with wildtype LRRK2, but not upon co-expression of phospho-deficient versions of these RAB proteins. Since phospho-site RAB8/10 mutants have been reported to be non-functional in various cellular contexts (Dhekne et al., 2018;

Rivero-Ríos et al., 2019), we additionally used LRRK2 kinase inhibitors to demonstrate that the effects were mediated by the LRRK2 kinase activity. Thus, the pericentrosomal/centrosomal recruitment of phospho-RAB8/10 is crucial to mediate the centrosomal cohesion deficits mediated by pathogenic LRRK2 in a kinase activity-dependent manner. LRRK2 also phosphorylates other endogenous RABs including RAB12, RAB35 and RAB43 (Steger et al., 2017). Conversely to RAB8A and RAB10, these RAB proteins were not necessary for the LRRK2-mediated centrosomal cohesion deficits, as shown in A549 deficient in RAB12, RAB35 or RAB43. We also evaluated the role of RILPL2 in the LRRK2-mediated centrosomal cohesion deficits. Expression of pathogenic LRRK2 still triggered a centrosomal cohesion phenotype in A549 cells deficient in RILPL2, indicating that RILPL2 is not necessary for the centrosomal phenotype, at least in this cell type. This is in contrast of recent data proposing a role for RILPL2 in ciliogenesis, whereby the binding of phospho-RAB10 to RILPL2 causes the sequestration of Myosin Va to a pericentrosomal area, thereby possibly interfering with primary cilia biogenesis (Dhekne et al., 2021). Altogether, the LRRK2-mediated centrosomal cohesion deficit is crucially dependent on RAB8A, RAB10 and RILPL1, but not on the presence of RAB12, RAB35, RAB43 or RILPL2.

Overexpression of RILPL1 has been suggested to cause a deficit in ciliogenesis as well as centrosomal cohesion (Dhekne et al., 2018). This is in contrast to previous studies showing no effect of RILPL1 overexpression on ciliogenesis (Schaub and Stearns, 2013), and no effect of RILPL1 overexpression on centrosomal cohesion as determined in the present study. Further work is needed to corroborate or refute the effects of increasing cellular RILPL1 levels on ciliogenesis and/or centrosomal cohesion events. In either case, loss of RILPL1 abolished the pathogenic LRRK2-mediated deficits in ciliogenesis (Dhekne et al., 2018), and our data show that loss of RILPL1 also abolishes the LRRK2-mediated deficits in centrosome cohesion. Therefore, this unique effector protein for only the phosphorylated versions of RAB8/10 plays an essential role in mediating both centrosome-related cellular readouts. In addition, we find that the centrosomal defects require accumulation of phosphorylated RAB10 in a manner dependent on RILPL1, which we show to be localised to the subdistal appendages of the mother centriole. These data strengthen the importance of RILPL1 as a key player for the LRRK2-mediated deficits by enabling recruitment of phosphorylated RAB proteins to the mother centriole, followed by downstream events which culminate in centrosomal and ciliogenesis defects.

In this thesis, we show that centrosomal cohesion is also regulated by risk and protective LRRK2 variants, and by modulators of the LRRK2 kinase signalling pathway. Expression of LRRK2 risk variants causes centrosomal cohesion deficits, whilst introduction of a protective variant into distinct pathogenic LRRK2 constructs decreases such deficits. Moreover, a point mutation in vps35 (vps35-D620N) which causes autosomal dominant PD (Vilariño-Güell et al., 2011; Zimprich et al., 2011; Sharma et al., 2012) and activates the LRRK2 kinase (Mir et al., 2018) causes a pronounced centrosomal cohesion deficit. Knockout of PPM1H, the phosphatase specific for LRRK2-phosphorylated RAB proteins (Berndsen et al., 2019) impairs centrosomal cohesion in the presence of LRRK2 expression, and a recent study shows that heterozygous loss of the PPM1H phosphatase impairs ciliogenesis in the intact mouse brain (Khan et al., 2021). These data provide strong evidence for the importance of the LRRK2 kinase activity in regulating both ciliogenesis and centrosomal cohesion deficits in non-dividing and dividing cells, respectively.

We find that all currently described modulators of the LRRK2 kinase activity impact upon centrosomal cohesion in dividing cells, which is associated with a detectable increase in the levels and centrosomal accumulation of phosphorylated RAB10. Short-term application of a LRRK2 kinase inhibitor reverts the increase in phospho-RAB10, and this in turn leads to a rapid reversal of the centrosomal cohesion deficits. Such dynamic behaviour is consistent with the direct RILPL1-mediated recruitment of phospho-RABs to a centrosomal location to cause an increase in the distance between duplicated centrosomes. It further predicts that the underlying mechanism may involve the dynamic recruitment and/or displacement of protein(s) necessary to keep duplicated centrosomes in close proximity to each other.

We have previously reported centrosomal cohesion deficits in lymphoblastoid cell lines from G2019S LRRK2-PD patients as compared to healthy controls (Madero-Pérez et al., 2018a). In future experiments, it will be interesting to determine whether centrosomal deficits can be detected in peripheral cells from PD patients harboring LRRK2 risk variants or mutations in vps35. In addition, our study shows that expression of N2081D LRRK2 mutant causes kinase activity-mediated centrosomal cohesion deficits. Since the N2081D LRRK2 mutation confers risk for PD as well as for Crohn´s disease (Hui et al., 2018), further studies are warranted to probe for centrosomal deficits in peripheral cells from Crohn´s disease patients, as this may aid in stratifying patients benefitting from LRRK2 kinase inhibitor therapeutics in clinical studies.

Recent work has shown that inducing lysosomal damage causes recruitment of LRRK2 to lysosomes, followed by the lysosomal accumulation of phospho-RAB10 (Eguchi et al., 2018; Bonet-Ponce et al., 2020; Herbst et al., 2020; Kuwahara et al., 2020). Conversely, mitochondrial depolarisation causes the mitochondrial accumulation of RAB10 to facilitate mitophagy, and such accumulation is impaired in the context of pathogenic LRRK2 (Wauters et al., 2020). Our studies were performed in the absence of treatments to induce lysosomal damage or mitochondrial depolarisation. Under such normal physiological conditions, we find that the majority of phospho-RAB10 localises to the centrosome to cause centrosomal cohesion and ciliogenesis deficits. In future experiments, it will be interesting to determine how triggers which lead to lysosomal or mitochondrial damage might impact upon the centrosomal deficits as described here. In either case, our data indicate that it is the RILPL1-mediated localisation of phospho-RAB10 to the centrosome which is responsible for the cohesion deficits mediated by pathogenic LRRK2. Interestingly, the expression of a C-terminal fragment of RILPL1 which localises to cytosolic punctate structures reverts the cohesion deficits mediated by pathogenic LRRK2 by redistributing phospho-RAB10 from its centrosomal location to those structures, without altering the total levels of phospho-RAB10 as assessed by Western blot analysis. Therefore, the subcellular location of the phospho-RAB10 accumulation, rather than total phospho-RAB10 levels, are relevant for our understanding of pathogenic LRRK2 action in a given cellular context. Furthermore, it will be interesting to determine whether interfering with the interaction of phosphorylated RAB10 with its effector RILPL1, for example by peptide approaches may turn out as a novel therapeutic approach to interfere with pathogenic LRRK2 action without inhibiting the kinase activity *per se*.

RAB8 plays an important role in ciliary vesicle trafficking required for ciliogenesis in a variety of cell types (Nachury et al., 2007; Yoshimura et al., 2007; Knödler et al., 2010; Westlake et al., 2011; Feng et al., 2012; Lu et al., 2015), whilst the role of RAB10 in primary ciliogenesis remains less clear (Chua and Tang, 2018). Ciliogenesis has been reported to be unimpaired in mouse embryonic fibroblasts from RAB8A/RAB8B double knockout mice, but is impaired when additionally silencing RAB10 (Sato et al., 2014). These data suggest that RAB10 may act synergistically with RAB8 in ciliogenesis, such that most ciliary transport processes occur normally in the absence of RAB8A/B as long as RAB10 remains available. In contrast, ciliogenesis was reported to be impaired in A549 RAB8A knockout cells, but enhanced in A549 RAB10 knockout cells, suggesting that RAB10 may act as a suppressor of cilia

formation (Dhekne et al., 2018). Further work is required to understand the relative contributions of RAB8A/B and RAB10 to ciliogenesis, which may involve cell type-specific differences in the precise vesicular trafficking steps mediated by these RABs which directly and/or indirectly impinge upon cilia formation. Importantly, our data indicate that the pericentrosomal/centrosomal accumulation of phospho-RAB8/10 upon pathogenic LRRK2 expression is observed in non-ciliated cells, but is much reduced and/or absent in ciliated cells. In addition, increasing the levels of phospho-RAB8/10 by co-expressing the RABs with wildtype LRRK2 caused a pronounced deficit in ciliogenesis, which was not observed when expressing either RAB8/10 or wildtype LRRK2 on their own. Therefore, and apart from a role for endogenous RAB8 and/or RAB10 in regulating ciliary vesicular trafficking events, our data indicate that the pericentrosomal/centrosomal accumulation of phospho-RAB8/10 interferes with ciliogenesis. Indeed, a recent study described a neomorphic role for phosphorylated RAB10 during ciliogenesis, whereby the binding of phosphorylated RAB10 to its effector RILPL1 impairs ciliogenesis by impeding the recruitment of TTBK2, which is necessary for "uncapping" (removal of CP110) of the mother centriole (Sobu et al., 2021).

The observed ciliogenesis deficits in cholinergic neurons in the striatum of pathogenic LRRK2 mutant mice (Dhekne et al., 2018) are expected to impair a described neuroprotective circuit whereby Sonic Hedgehog signalling from DA neurons is sensed by cilia in the cholinergic neurons, which in turn triggers the secretion of neuroprotective GDNF from these cholinergic neurons back towards the DA neurons, in this manner maintaining their health (Gonzalez-Reyes et al., 2012). Whilst formal proof for a deficit in this neuroprotective circuit in the context of pathogenic LRRK2 is currently lacking, LRRK2-mediated ciliogenesis deficits have also been described in distinct brain areas of pathogenic LRRK2 knockin mice, and in various cell types including iPS cells from PD patients due to LRRK2 mutations, or murine embryonic fibroblasts from pathogenic LRRK2 knockin mice (Dhekne et al., 2018). Additionally, our data indicate the presence of LRRK2-mediated centrosomal (Madero-Pérez et al., 2018a) as well as ciliogenesis deficits in primary dermal fibroblasts from LRRK2-PD patients, and centrosomal as well as ciliogenesis defects in astrocytes from pathogenic LRRK2 knockin mice. Therefore, these pathogenic LRRK2-mediated deficits seem to be a prominent cellular phenotype observed in a variety of neuronal and non-neuronal cell types, and modulated by LRRK2 kinase inhibitors. Astrocytes comprise a disease-relevant cell type which supports the health of dopaminergic neurons (Yoshimura et al., 2011; Booth et al., 2017; di Domenico et al., 2019), and aberrant

ciliary signalling can affect astrocyte survival under certain conditions (Sipos et al., 2018). Similarly, ciliogenesis deficits have recently been described in striatal astrocytes in brain, and this may dysregulate striatal neuronal circuitry (Khan et al., 2021). Further work is required to determine possible alterations in neuronal excitability in the striatum, and its effects on dopaminergic cell survival in the *substantia nigra*. In the future, it will also be important to probe for ciliary deficits in the human brain, and further evaluate the possible consequences of such deficits for dopaminergic cell survival. Finally, the potential pathophysiological relevance for the LRRK2-mediated centrosomal cohesion deficits as observed in dividing cells remains unknown. Future experiments will seek to determine whether centrosomal cohesion deficits cause alterations in cell proliferation leading to impaired adult neurogenesis as described in transgenic G2019S LRRK2 mice (Winner et al., 2011), with potential relevance for various non-motor symptoms associated with PD.

Altogether, our data demonstrate that pathogenic LRRK2 mutations, LRRK2 risk variants and modulators of the LRRK2 signalling pathway all converge upon causing centrosomal cohesion and ciliogenesis defects. These deficits are dependent on RILPL1, and directly mediated by the centrosomal accumulation of phospho-RAB8A and phospho-RAB10. The localisation of RILPL1 implicates the subdistal appendages of the mother centriole as the prime site of action for the LRRK2-mediated phospho-RAB10 accumulation, with downstream effects on centrosomal cohesion and ciliogenesis as described here.

LRRK2-mediated centrosomal cohesion deficits as biomarker for Parkinson's disease

Since our data indicate that the centrosomal cohesion readout is a reflection of the same phospho-RAB8/10-RILPL1 complex as the one underlying the LRRK2-mediated ciliogenesis deficits, it resulted important to test whether centrosomal cohesion deficits can also be observed in primary blood-derived cells from LRRK2-PD patients, and whether such readout may aid in the stratification of PD patients who may benefit from LRRK2-related treatment strategies and serve as patient enrichment biomarker for LRRK2 inhibitor clinical trials. All G2019S LRRK2 LCLs analysed displayed a centrosomal cohesion deficit without alterations in cell cycle or cell viability. Such cohesion phenotype was also observed in a subset of LCLs from sporadic PD patients, and was reverted in all cases upon kinase inhibitor treatment. Thus, whilst requiring independent validation in an increased sample size of sporadic PD patients, this cellular readout may comprise a valid patient enrichment biomarker. In future experiments, it will be important to determine whether the centrosomal cohesion readout can be observed in freshly isolated peripheral blood mononuclear cells, monocytes and/or neutrophils, or whether it is dependent on lymphocyte immortalization to generate cell-cycle active LCLs. If observed in freshly isolated cells, the assay may additionally serve as a pharmacodynamic readout of potential use in LRRK2 kinase inhibitor clinical trials.

The underlying reason(s) why a subset of sporadic PD LCL*s* displayed a cohesion phenotype similar to G2019S LRRK2 LCL*s* currently remain unknown, but were not associated with a detectable increase in the levels of LRRK2 or RAB10 Thr73 phosphorylation as compared to healthy controls as assessed by Western blotting techniques. Whilst sequenced and found negative for the G2019S mutation in LRRK2, full sequence analysis is warranted to highlight potential other genetic alterations related to LRRK2, or indeed variations in or around other genes which are known to regulate LRRK2 activity, such as *VPS35* or *RAB29* (Liu et al., 2018; Madero-Pérez et al., 2018b; Purlyte et al., 2018). In either case, these data suggest that a subset of sporadic PD patients may also benefit from LRRK2-related treatment strategies.

Previous studies in human neutrophils have reported variability between patient samples, but no consistent differences in the levels of LRRK2, LRRK2 Ser935, RAB10 or phospho-RAB10, amongst control, G2019S LRRK2 or sporadic PD samples, respectively (Fan et al., 2018). Similarly, we did not detect significant differences

in the levels of LRRK2 and RAB10 or phospho-versions thereof between control, LRRK2 G2019S and sporadic PD LCLs, with vast differences in the levels of total LRRK2 protein amongst the distinct patient-derived LCLs. This lack of difference between the different cohorts might be due to the difficulties to detect small increases in the phosphorylation of endogenous RAB10 in G2019S LRRK2-PD samples as compared to healthy controls, as other research groups have reported. Indeed, a recent study in freshly isolated neutrophils has demonstrated that the increase in phospho-RAB10 levels is a lot less pronounced in G2019S LRRK2 cells as compared to R1441G LRRK2 cells (Fan et al., 2021). Similar differences in the effect of pathogenic LRRK2 mutations on substrate phosphorylation have been described in mouse models, which show a greater increase of phospho-RAB10 R1441C-LRRK2 knockin as compared to G2019S-LRRK2 knockin mice (Iannotta et al., 2020). LRRK2 Ser935 phosphorylation and RAB10 Thr73 phosphorylation were significantly reduced upon LRRK2 inhibitor treatment in control and sporadic PD samples, with a non-significant tendency observed in LRRK2 G2019S samples. The latter is likely due to low levels of total LRRK2 observed in some LRRK2 G2019S samples, which made quantification less reliable. In either case, these data suggest that both LRRK2 Ser935 phosphorylation and RAB10 Thr73 phosphorylation are valid peripheral LRRK2 inhibition biomarkers also in LCLs, as previously described for human neutrophils and PBMCs (Fan et al., 2018; Atashrazm et al., 2019; Fan et al., 2021).

Whilst there was a correlation between total LRRK2 levels and RAB10 phosphorylation levels especially in sporadic PD samples, total LRRK2 levels were not different between control and sporadic PD samples. A previous study reported an increase in LRRK2 protein levels in B cells, T cells and CD16+ monocytes from sporadic PD patients as compared to controls as assessed by flow cytometry (Cook et al., 2017). Similarly, a recent study reported an increase in LRRK2 protein levels in neutrophils from sporadic PD patients as compared to controls as assessed by Western blotting techniques (Atashrazm et al., 2019). Both studies employed larger patient sampling sizes, such that significant increases in LRRK2 protein levels may have been missed in the present study. In addition, the LRRK2 protein levels in immortalized lymphocytes may not reflect the LRRK2 levels present in original, freshly isolated cells. Thus, the lack of increased LRRK2 protein levels in sporadic PD LCLs as reported here is not inconsistent with the possibility that a sub-population of sporadic PD patients may benefit from being targeted with LRRK2 therapeutics.

Since differences in the intrinsic LRRK2 kinase activity, rather than total protein levels, may correlate with LRRK2-related PD, we analysed LRRK2 kinase activity in a set of LCL samples using a proximity ligation-based assay (Di Maio et al., 2018). Interestingly, all G2019S LRRK2 LCLs analysed displayed an increase in LRRK2 kinase activity as compared to controls, whilst displaying very distinct total LRRK2 levels as assessed by Western blotting techniques. However, and at least in our hands and in LCLs, the assay was not able to detect endogenous LRRK2 kinase activity in either control or sporadic PD LCLs, including the ones which displayed a centrosomal cohesion phenotype. Therefore, future studies employing improved high-affinity Ser1292 antibodies, or distinct total LRRK2 antibodies for proximity ligation assays are warranted to determine whether increased intrinsic LRRK2 kinase activity may serve as patient enrichment biomarker for sporadic PD samples, and whether there exists a correlation between LRRK2 kinase activity and the centrosomal phenotype observed in a subset of sporadic PD LCLs.

Our sporadic PD patient group displayed large differences in total LRRK2 levels and in RAB10 Thr73 phosphorylation levels which did not correlate with disease severity, disease duration or age at onset, in contrast to the reported correlation between RAB10 phosphorylation and disease severity in PBMCs from a distinct sporadic PD sampling (Atashrazm et al., 2019). Such lack of correlation with PD clinical variables may be due to the smaller sample size employed here, and/or the use of immortalized cells cultured *ex vivo* as compared to freshly isolated cells. In either case, independent studies in freshly isolated PBMCs from larger patient cohorts are required to confirm or refute a correlation between phospho-RAB10 levels and clinical PD variables.

The LRRK2 G2019S LCLs, as well as a subset of LCLs from sporadic PD patients displayed a centrosomal cohesion deficit as compared to control samples, which did not correlate with RAB10 Thr73 phosphorylation levels as assessed by Western blotting techniques. Since both phospho-RAB8 and phospho-RAB10 associate with the pericentrosomal/centrosomal RILPL1 protein (Steger et al., 2017), the centrosomal cohesion phenotype may correlate with the summed increase of both of these phospho-RAB proteins. Thus, and once phospho-state-specific antibodies uniquely selective for only phospho-RAB8a have been developed, it will be interesting to analyse for alterations in the phosphorylation states of RAB8A Thr72 by Western blotting techniques. In addition, and given the lack of a significant increase in pericentrosomal/centrosomal phospho-RAB10 fluorescence intensity in the G2019S

LCLs as compared to controls, signal amplification via development of proximity ligation assays around RILPL1 and phospho-RAB8/phospho-RAB10 are warranted to determine whether the centrosomal cohesion phenotype may correlate with the pericentrosomal/centrosomal accumulation of these phosphorylated RAB species.

Control LCLs displayed phospho-RAB10 levels similar to G2019S LRRK2 LCLs, but did not show a centrosomal cohesion deficit. Application of LRRK2 kinase inhibitor to control cells caused a decrease in phospho-RAB10 levels, but no further decrease in centrosomal cohesion. Thus, the G2019S LRRK2-mediated phospho-RAB10 protein able to cause the centrosomal cohesion deficits may reflect a distinct phosphorylated protein species, driven by differences in the subcellular localisation of the phosphorylation event due to differences in the subcellular localisation of wildtype versus G2019S LRRK2 (Liu et al., 2018; Madero-Pérez et al., 2018b; Purlyte et al., 2018). This may result in the generation of a phosphorylated RAB protein species in a distinct location and/or nucleotide-bound state (Liu et al., 2018), which may be the only one selectively able to cause the centrosomal cohesion deficits. Whilst impossible to detect by Western blotting techniques, such alterations may be sensitively detected by cell biological readouts which are due to the specific phospho-RAB species generated in the context of pathogenic LRRK2. Finally, the LRRK2 kinase activity-mediated centrosomal cohesion phenotype may also be due to the phosphorylation of other RAB protein species, and/or related to other aspects of LRRK2 biology. In either case, and whilst further studies into the mechanism(s) underlying the centrosomal deficits are required, our present data indicate that centrosomal cohesion deficits are a robust cellular readout for G2019S LRRK2 kinase activity, and may be able to stratify sporadic PD patients who may also benefit from LRRK2-related therapies.

VI. Conclusions / Conclusiones

1. Membrane association is required for LRRK2-mediated RAB8 phosphorylation, and both RAB8 isoforms are implicated in the LRRK2-mediated centrosomal cohesion deficits.

2. RAB10 regulates the centrosomal cohesion deficits mediated by LRRK2.

3. The pathogenic LRRK2-mediated centrosomal cohesion defects correlate with an abnormal centrosomal accumulation of endogenous phosphorylated RAB10 which is reverted upon LRRK2 kinase inhibitor treatment.

4. The pathogenic LRRK2-mediated centrosomal cohesion deficit depends on the presence of RAB8, RAB10 and RILPL1, but not on RILPL2.

5. The pathogenic LRRK2-mediated centrosomal cohesion deficit is independent of the presence of RAB12, RAB35 or RAB43.

6. LRRK2 risk and protective variants impact upon the centrosomal cohesion deficit, at least as assessed using overexpression conditions.

7. Upstream (VPS35) or downstream (PPM1H) regulators modulate the LRRK2-mediated centrosomal cohesion deficits.

8. The phospho-RAB8A/RAB10 interactor, RILPL1, localises to subdistal appendages on the mother centriole as assessed by electron microscopy techniques, suggesting that the LRRK2-mediated phospho-RAB accumulation may occur at this subcellular location.

9. The pathogenic LRRK2-mediated ciliogenesis deficits correlate with the accumulation of phospho-RAB8/10 at the centrosome/ciliary base.

10. Both centrosomal cohesion and ciliogenesis deficits can be observed in cell types derived from knockin mice expressing endogenous levels of pathogenic LRRK2.

11. Centrosomal cohesion and primary cilia defects can be observed in primary human dermal fibroblasts from G2019S LRRK2 PD patients as compared to healthy controls, and are mediated by the LRRK2 kinase activity.

12. Centrosomal cohesion deficits in peripheral blood-derived lymphoblastoid cell lines are a robust cellular biomarker for LRRK2-related PD, and can also be observed in a subset of sporadic PD patients, suggesting that this readout may serve to stratify sporadic patients who may also benefit from LRRK2 kinase inhibitor-related treatment strategies.

1. La asociación de membrana de RAB8 es necesaria para su fosforilación por LRRK2, y ambas isoformas de RAB8 están implicadas en el déficit de cohesión centrosomal mediado por LRRK2.

2. RAB10 regula el déficit de cohesión centrosomal mediado por LRRK2.

3. El defecto de cohesión centrosomal mediado por LRRK2 patogénico se correlaciona con una acumulación centrosomal anormal de RAB10 fosforilado endógeno que es revertido mediante tratamiento con inhibidores de kinasa de LRRK2.

4. El déficit de cohesión centrosomal mediado por LRRK2 patogénico depende de la presencia de RAB8, RAB10 y RILPL1, pero no de RILPL2.

5. El déficit de cohesión centrosomal mediado por LRRK2 patogénico es independiente de la presencia de RAB12, RAB35 o RAB43.

6. Las variantes de riesgo y protección de LRRK2 modulan el defecto de cohesión centrosomal, al menos bajo condiciones de sobreexpresión.

7. Los moduladores aguas arriba (VPS35) o abajo (PPM1H) de la ruta de señalización de LRRK2 regulan el déficit de cohesión centrosomal mediado por LRRK2.

8. El interactor de fosfo-RAB8/RAB10 RILPL1 se localiza en los apéndices subdistales del centriolo madre como se ha determinado mediante microscopía electrónica, sugiriendo que la acumulación de fosfo-RAB mediada por LRRK2 podría ocurrir en esta localización subcelular.

9. Los déficits en ciliogénesis mediados por LRRK2 patogénico se correlacionan con una acumulación de fosfo-RAB8/RAB10 en el centrosoma/base ciliar.

10. Ambos defectos de cohesión centrosomal y ciliogénesis se pueden observar en diferentes tipos celulares derivados de ratones knockin que expresan niveles endógenos de LRRK2 patogénico.

11. Los déficits en cohesión centrosomal y ciliogénesis pueden ser observados en fibroblastos dérmicos humanos de pacientes de Parkinson con la mutación G2019S de LRRK2 comparados con personas sanas, y son mediados por la actividad kinasa de LRRK2.

12. El déficit de cohesión centrosomal en líneas celulares linfoblastoides derivadas de sangre periférica es un potente biomarcador para la enfermedad de Parkinson causada por LRRK2, y puede ser observado también en un conjunto de pacientes de Parkinson esporádico, sugiriendo que esta lectura podría servir para estratificar pacientes de Parkinson esporádico que podrían beneficiarse de los tratamientos de inhibición de kinasa de LRRK2.

VII. References

Aasly, J.O., Toft, M., Fernandez-Mata, I., Kachergus, J., Hulihan, M., et al. (2005). **Clinical features of LRRK2-associated Parkinson's disease in Central Norway**. *Ann. Neurol. 57*, 762–765. DOI: 10.1002/ana.20456.

Aasly, J.O., Vilariño-Güell, C., Dachsel, J.C., Webber, P.J., West, A.B., et al. (2010). **Novel pathogenic LRRK2 p.Asn1437His substitution in familial Parkinson's disease**. *Mov. Disord. 25*, 2156–2163. DOI: 10.1002/mds.23265.

Abbafati, C., Machado, D.B., Cislaghi, B., Salman, O.M., Karanikolos, M., et al. (2020). **Global burden of 369 diseases and injuries in 204 countries and territories, 1990–2019: a systematic analysis for the Global Burden of Disease Study 2019**. *Lancet 396*, 1204–1222. DOI: 10.1016/S0140-6736(20)30925-9.

Abdalla-Carvalho, C.B., Santos-Rebouças, C.B., Guimarães, B.C., Campos, M., Pereira, J.S., et al. (2010). **Genetic analysis of LRRK2 functional domains in Brazilian patients with Parkinson's disease**. *Eur. J. Neurol. 17*, 1479–1481. DOI: 10.1111/j.1468-1331.2010.03039.x.

Abdul-Majeed, S., and Nauli, S.M. (2011). **Dopamine receptor type 5 in the primary cilia has dual chemo-and mechano-sensory roles**. *Hypertension 58*, 325–331. DOI: 10.1161/HYPERTENSIONAHA.111.172080.

Agalliu, I., San Luciano, M., MirelmanMD, A., Giladi, N., Waro, B., et al. (2015). **Higher frequency of certain cancers in LRRK2 G2019S mutation carriers with Parkinson disease a pooled analysis**. *JAMA Neurol. 72*, 58–65. DOI: 10.1001/jamaneurol.2014.1973.

Alegre-Abarrategui, J., Christian, H., Lufino, M.M.P., Mutihac, R., Venda, L.L., et al. (2009). **LRRK2 regulates autophagic activity and localizes to specific membrane microdomains in a novel human genomic reporter cellular model**. *Hum. Mol. Genet. 18*, 4022–4034. DOI: 10.1093/hmg/ddp346.

An, X.K., Peng, R., Li, T., Burgunder, J.M., Wu, Y., et al. (2008). **LRRK2 Gly2385Arg variant is a risk factor of Parkinson's disease among Han-Chinese from mainland China**. *Eur. J. Neurol. 15*, 301–305. DOI: 10.1111/j.1468-1331.2007.02052.x.

De Anda, F.C., Meletis, K., Ge, X., Rei, D., and Tsai, L.H. (2010). **Centrosome motility is essential for initial axon formation in the neocortex**. *J. Neurosci. 30*, 10391–10406. DOI: 10.1523/JNEUROSCI.0381-10.2010.

Armstrong, J., Thompson, N., Squire, J.H., Smith, J., Hayes, B., et al. (1996). **Identification of a novel member of the Rab8 family from the rat basophilic leukaemia cell line, RBL.2H3**. *J. Cell Sci. 109*, 1265–1274.

Arranz, A.M., Delbroek, L., van Kolen, K., Guimarães, M.R., Mandemakers, W., et al. (2015). **LRRK2 functions in synaptic vesicle endocytosis through a kinasedependent mechanism**. *J. Cell Sci. 128*, 541–552. DOI: 10.1242/jcs.158196.

Arslanhan, M.D., Gulensoy, D., and Firat-Karalar, E.N. (2020). **A Proximity Mapping Journey into the Biology of the Mammalian Centrosome/Cilium Complex**. *Cells 9* DOI: 10.3390/cells9061390.

Atashrazm, F., Hammond, D., Perera, G., Bolliger, M.F., Matar, E., et al. (2019). **LRRK2-mediated Rab10 phosphorylation in immune cells from Parkinson's disease patients.** *Mov. Disord. 34*, 406–415. DOI: 10.1002/mds.27601.

Athanasopoulos, P.S., Jacob, W., Neumann, S., Kutsch, M., Wolters, D., et al. (2016). **Identification of protein phosphatase 2A as an interacting protein of leucine-rich repeat kinase 2**. *Biol. Chem. 397*, 541–554. DOI: 10.1515/hsz-2015-0189.

Babbey, C.M., Ahktar, N., Wang, E., Chen, C.C.H., Grant, B.D., et al. (2006). **Rab10 regulates membrane transport through early endosomes of polarized Madin-Darby Canine Kidney cells**. *Mol. Biol. Cell 17*, 3156–3175. DOI: 10.1091/mbc.E05-08-0799.

Babbey, C.M., Bacallao, R.L., and Dunn, K.W. (2010). **Rab10 associates with primary cilia and the exocyst complex in renal epithelial cells**. *Am. J. Physiol. - Ren. Physiol. 299*, F495. DOI: 10.1152/ajprenal.00198.2010.

Bahe, S., Stierhof, Y.D., Wilkinson, C.J., Leiss, F., and Nigg, E.A. (2005). **Rootletin forms centriole-associated filaments and functions in centrosome cohesion**. *J. Cell Biol. 171*, 27–33. DOI: 10.1083/jcb.200504107.

Bailly, E., McCaffrey, M., Touchot, N., Zahraoui, A., Goud, B., et al. (1991). **Phosphorylation of two small GTP-binding proteins of the Rab family by p34cdc2**. *Nature 350*, 715–718. DOI: 10.1038/350715a0.

Bangs, F., and Anderson, K. V. (2017). **Primary cilia and Mammalian Hedgehog signaling**. *Cold Spring Harb. Perspect. Biol. 9* DOI: 10.1101/cshperspect.a028175.

Banworth, M.J., and Li, G. (2018). **Consequences of Rab GTPase dysfunction in genetic or acquired human diseases**. *Small GTPases 9*, 158–181. DOI: 10.1080/21541248.2017.1397833.

Baptista, M.A.S., Dave, K.D., Frasier, M.A., Sherer, T.B., Greeley, M., et al. (2013). **Loss of leucine-rich repeat kinase 2 (LRRK2) in rats leads to progressive abnormal phenotypes in peripheral organs**. *PLoS One 8* DOI: 10.1371/journal.pone.0080705.

Baptista, M.A.S., Merchant, K., Barrett, T., Bhargava, S., Bryce, D.K., et al. (2020). **LRRK2 inhibitors induce reversible changes in nonhuman primate lungs without measurable pulmonary deficits**. *Sci. Transl. Med. 12* DOI: 10.1126/scitranslmed.aav0820.

Beilina, A., Bonet-Ponce, L., Kumaran, R., Kordich, J.J., Ishida, M., et al. (2020). **The Parkinson's Disease Protein LRRK2 Interacts with the GARP Complex to Promote Retrograde Transport to the trans-Golgi Network**. *Cell Rep. 31*, 107614. DOI: 10.1016/j.celrep.2020.107614.

Beilina, A., and Cookson, M.R. (2016). **Genes associated with Parkinson's disease: regulation of autophagy and beyond**. *J. Neurochem. 139*, 91–107. DOI: 10.1111/jnc.13266.

Belluzzi, E., Gonnelli, A., Cirnaru, M.D., Marte, A., Plotegher, N., et al. (2016). **LRRK2 phosphorylates pre-synaptic N-ethylmaleimide sensitive fusion (NSF) protein enhancing its ATPase activity and SNARE complex disassembling rate**. *Mol. Neurodegener. 11* DOI: 10.1186/s13024-015-0066-z.

Berg, D., Schweitzer, K.J., Leitner, P., Zimprich, A., Lichtner, P., et al. (2005). **Type and frequency of mutations in the LRRK2 gene in familial and sporadic Parkinson's disease***. *Brain 128*, 3000–3011. DOI: 10.1093/brain/awh666.

Berger, Z., Smith, K.A., and Lavoie, M.J. (2010). **Membrane localization of LRRK2 is associated with increased formation of the highly active lrrk2 dimer and changes in its phosphorylation**. *Biochemistry 49*, 5511–5523. DOI: 10.1021/bi100157u.

Berndsen, K., Lis, P., Yeshaw, W.M., Wawro, P.S., Nirujogi, R.S., et al. (2019). **PPM1H phosphatase counteracts LRRK2 signaling by selectively dephosphorylating rab proteins**. *Elife 8* DOI: 10.7554/eLife.50416.

Berwick, D.C., and Harvey, K. (2011). **LRRK2 signaling pathways: The key to unlocking neurodegeneration?**. *Trends Cell Biol. 21*, 257–265. DOI: 10.1016/j.tcb.2011.01.001.

Berwick, D.C., and Harvey, K. (2012a). **The importance of Wnt signalling for neurodegeneration in Parkinson's disease**. *Biochem. Soc. Trans. 40*, 1123–1128. DOI: 10.1042/BST20120122.

Berwick, D.C., and Harvey, K. (2012b). **LRRK2 functions as a wnt signaling scaffold, bridging cytosolic proteins and membrane-localized LRP6**. *Hum. Mol. Genet. 21*, 4966–4979. DOI: 10.1093/hmg/dds342.

Berwick, D.C., and Harvey, K. (2014). **The regulation and deregulation of Wnt signaling by PARK genes in health and disease**. *J. Mol. Cell Biol. 6*, 3–12. DOI: 10.1093/jmcb/mjt037.

Berwick, D.C., Javaheri, B., Wetzel, A., Hopkinson, M., Nixon-Abell, J., et al. (2017). **Pathogenic LRRK2 variants are gain-of-function mutations that enhance LRRK2-mediated repression of β-catenin signaling**. *Mol. Neurodegener. 12*, 9. DOI: 10.1186/s13024-017-0153-4.

Betarbet, R., Sherer, T.B., MacKenzie, G., Garcia-Osuna, M., Panov, A. V., et al. (2000). **Chronic systemic pesticide exposure reproduces features of Parkinson's disease**. *Nat. Neurosci. 3*, 1301–1306. DOI: 10.1038/81834.

Biosa, A., Trancikova, A., Civiero, L., Glauser, L., Bubacco, L., et al. (2013). **GTPase activity regulates kinase activity and cellular phenotypes of parkinson's disease-associated LRRK2**. *Hum. Mol. Genet. 22*, 1140–1156. DOI: 10.1093/hmg/dds522.

Biskup, S., Moore, D.J., Celsi, F., Higashi, S., West, A.B., et al. (2006). **Localization of LRRK2 to membranous and vesicular structures in mammalian brain**. *Ann. Neurol. 60*, 557–569. DOI: 10.1002/ana.21019.

Bjorklund, G., Stejskal, V., Urbina, M.A., Dadar, M., Chirumbolo, S., et al. (2018). **Metals and Parkinson's Disease: Mechanisms and Biochemical Processes**. *Curr. Med. Chem. 25*, 2198–2214. DOI: 10.2174/0929867325666171129124616.

Blacque, O.E., Scheidel, N., and Kuhns, S. (2018). **Rab GTPases in cilium formation and function**. *Small GTPases 9*, 76–94. DOI: 10.1080/21541248.2017.1353847.

Blanca Ramírez, M., Lara Ordóñez, A.J., Fdez, E., Madero-Pérez, J., Gonnelli, A., et al. (2017). **GTP binding regulates cellular localization of Parkinson's disease-associated LRRK2**. *Hum. Mol. Genet. 26* DOI: 10.1093/hmg/ddx161.

Boassa, D., Berlanga, M.L., Yang, M.A., Terada, M., Hu, J., et al. (2013). **Mapping the subcellular distribution of α-synuclein in neurons using genetically encoded probes for correlated light and electron microscopy: Implications for Parkinson's disease pathogenesis**. *J. Neurosci. 33*, 2605–2615. DOI: 10.1523/JNEUROSCI.2898-12.2013.

Boassa, D., Lemieux, S.P., Lev-Ram, V., Hu, J., Xiong, Q., et al. (2019). **Split-miniSOG for Spatially Detecting Intracellular Protein-Protein Interactions by Correlated Light and Electron Microscopy**. *Cell Chem. Biol. 26*, 1407-1416.e5. DOI: 10.1016/j.chembiol.2019.07.007.

Bonet-Ponce, L., Beilina, A., Williamson, C.D., Lindberg, E., Kluss, J.H., et al. (2020). **LRRK2 mediates tubulation and vesicle sorting from lysosomes**. *Sci. Adv. 6* DOI: 10.1126/sciadv.abb2454.

Bonifati, V., Rohé, C.F., Breedveld, G.J., Fabrizio, E., De Mari, M., et al. (2005). **Early-onset parkinsonism associated with PINK1 mutations: Frequency, genotypes, and phenotypes**. *Neurology 65*, 87–95. DOI: 10.1212/01.wnl.0000167546.39375.82.

Booth, H.D.E., Hirst, W.D., and Wade-Martins, R. (2017). **The Role of Astrocyte Dysfunction in Parkinson's Disease Pathogenesis**. *Trends Neurosci. 40*, 358–370. DOI: 10.1016/j.tins.2017.04.001.

Bordia, T., McGregor, M., Papke, R.L., Decker, M.W., Michael McIntosh, J., et al. (2015). **The α7 nicotinic receptor agonist ABT-107 protects against nigrostriatal damage in rats with unilateral 6-hydroxydopamine lesions**. *Exp. Neurol. 263*, 277–284. DOI: 10.1016/j.expneurol.2014.09.015.

Bosgraaf, L., and Van Haastert, P.J.M. (2003). **Roc, a Ras/GTPase domain in complex proteins**. *Biochim. Biophys. Acta - Mol. Cell Res. 1643*, 5–10. DOI: 10.1016/j.bbamcr.2003.08.008.

Braak, H., Del Tredici, K., Rüb, U., De Vos, R.A.I., Jansen Steur, E.N.H., et al. (2003). **Staging of brain pathology related to sporadic Parkinson's disease**. *Neurobiol. Aging 24*, 197–211. DOI: 10.1016/S0197-4580(02)00065-9.

Braun, D.A., and Hildebrandt, F. (2017). **Ciliopathies**. *Cold Spring Harb. Perspect. Biol. 9* DOI: 10.1101/cshperspect.a028191.

Breckenridge, C.B., Berry, C., Chang, E.T., Sielken, R.L., and Mandel, J.S. (2016). **Association between Parkinson's disease and cigarette smoking, rural living, well-water consumption, farming and pesticide use: Systematic review and meta-analysis**. *PLoS One 11* DOI: 10.1371/journal.pone.0151841.

Breslow, D.K., and Holland, A.J. (2019). **Mechanism and Regulation of Centriole and Cilium Biogenesis**. *Annu. Rev. Biochem. 88*, 691–724. DOI: 10.1146/annurev-biochem-013118-111153.

Brumfield, A., Chaudhary, N., Molle, D., Wen, J., Graumann, J., et al. (2021). **Insulin-promoted mobilization of GLUT4 from a perinuclear storage site requires RAB10**. *Mol. Biol. Cell 32*, 57–73. DOI: 10.1091/MBC.E20-06-0356.

Buchwalter, R.A., Chen, J. V, Zheng, Y., and Megraw, T.L. (2016). Centrosome in Cell Division, Development and Disease. In: ELS, John Wiley & Sons, Ltd, 1–12 DOI: 10.1002/9780470015902.a0020872.

Burd, C., and Cullen, P.J. (2014). **Retromer: A master conductor of endosome sorting**. *Cold Spring Harb. Perspect. Biol. 6* DOI: 10.1101/cshperspect.a016774.

Burré, J., Sharma, M., and Südhof, T.C. (2015). **Definition of a molecular pathway mediating α-synuclein neurotoxicity**. *J. Neurosci. 35*, 5221–5232. DOI: 10.1523/JNEUROSCI.4650-14.2015.

Carmine Belin, A., Westerlund, M., Sydow, O., Lundstromer, K., Hakansson, A., et al. (2006). **Leucine-rich repeat kinase 2 (LRRK2) mutations in a Swedish Parkinson cohort and a healthy nonagenarian**. *Mov Disord 21*, 1731–1734.

Chaineau, M., Ioannou, M.S., and Mcpherson, P.S. (2013). **Rab35: GEFs, GAPs and Effectors**. *Traffic 14*, 1109–1117. DOI: 10.1111/tra.12096.

Chang, D., Nalls, M.A., Hallgrímsdóttir, I.B., Hunkapiller, J., Brug, M. van der, et al. (2017). **A meta-analysis of genome-wide association studies identifies 17 new Parkinson's disease risk loci**. *Nat. Genet. 49*, 1511–1516. DOI: 10.1038/ng.3955.

Chartier-Harlin, M.C., Kachergus, J., Roumier, C., Mouroux, V., Douay, X., et al. (2004). **α-synuclein locus duplication as a cause of familial Parkinson's disease**. *Lancet 364*, 1167–1169. DOI: 10.1016/S0140-6736(04)17103-1.

Chavali, P.L., Pütz, M., and Gergely, F. (2014). **Small organelle, big responsibility: The role of centrosomes in development and disease**. *Philos. Trans. R. Soc. B Biol. Sci. 369* DOI: 10.1098/rstb.2013.0468.

Chavrier, P., Vingron, M., Sander, C., Simons, K., and Zerial, M. (1990). **Molecular cloning of YPT1/SEC4-related cDNAs from an epithelial cell line.** *Mol. Cell. Biol. 10*, 6578–6585. DOI: 10.1128/mcb.10.12.6578.

Chen, C.Y., Weng, Y.H., Chien, K.Y., Lin, K.J., Yeh, T.H., et al. (2012). **(G2019S) LRRK2 activates MKK4-JNK pathway and causes degeneration of SN dopaminergic neurons in a transgenic mouse model of PD**. *Cell Death Differ. 19*, 1623–1633. DOI: 10.1038/cdd.2012.42.

Chen, J.F., Xu, K., Petzer, J.P., Staal, R., Xu, Y.H., et al. (2001). **Neuroprotection by caffeine and A(2A) adenosine receptor inactivation in a model of Parkinson's disease.** *J. Neurosci. 21* DOI: 10.1523/jneurosci.21-10-j0001.2001.

Chen, J.K., Taipale, J., Cooper, M.K., and Beachy, P.A. (2002). **Inhibition of Hedgehog signaling by direct binding of cyclopamine to Smoothened**. *Genes Dev. 16*, 2743–2748. DOI: 10.1101/gad.1025302.

Chen, L., Zhang, S., Liu, Y., Hong, H., Wang, H., et al. (2011). **LRRK2 R1398H polymorphism is associated with decreased risk of Parkinson's disease in a Han Chinese population**. *Park. Relat. Disord. 17*, 291–292. DOI: 10.1016/j.parkreldis.2010.11.012.

Chen, X., Kordich, J.K., Williams, E.T., Levine, N., Cole-Strauss, A., et al. (2019). **Parkinson's disease-linked D620N VPS35 knockin mice manifest tau neuropathology and dopaminergic neurodegeneration**. *Proc. Natl. Acad. Sci. U. S. A. 116*, 5765–5774. DOI: 10.1073/pnas.1814909116.

Chen, Y., and Yu, L. (2017). **Recent progress in autophagic lysosome reformation**. *Traffic 18*, 358–361. DOI: 10.1111/tra.12484.

Cheng, H.C., Ulane, C.M., and Burke, R.E. (2010). **Clinical progression in Parkinson disease and the neurobiology of axons**. *Ann. Neurol. 67*, 715–725. DOI: 10.1002/ana.21995.

Cheng, J.H., She, H., Han, Y.P., Wang, J., Xiong, S., et al. (2007). **Wnt antagonism inhibits hepatic stellate cell activation and liver fibrosis**. *Am. J. Physiol. - Gastrointest. Liver Physiol. 294*, G39–G49. DOI: 10.1152/ajpgi.00263.2007.

Cherian, A., and Divya, K.P. (2020). **Genetics of Parkinson's disease**. *Acta Neurol. Belg. 120*, 1297–1305. DOI: 10.1007/s13760-020-01473-5.

Chia, R., Haddock, S., Beilina, A., Rudenko, I.N., Mamais, A., et al. (2014). **Phosphorylation of LRRK2 by casein kinase 1α regulates trans-Golgi clustering via differential interaction with ARHGEF7**. *Nat. Commun. 5* DOI: 10.1038/ncomms6827.

Christensen, K. V, Hentzer, M., Oppermann, F.S., Elschenbroich, S., Dossang, P., et al. (2018). **LRRK2 exonic variants associated with Parkinson's disease augment phosphorylation levels for LRRK2-Ser1292 and Rab10-Thr73**. *BioRxiv* DOI: 10.1101/447946.

Chua, C.E.L., and Tang, B.L. (2018). **Rab 10-a traffic controller in multiple cellular pathways and locations.** *J. Cell. Physiol. 233*, 6483–6494. DOI: 10.1002/jcp.26503.

Civiero, L., Cogo, S., Biosa, A., and Greggio, E. (2018). **The role of LRRK2 in cytoskeletal dynamics**. *Biochem. Soc. Trans. 46*, 1653–1663. DOI: 10.1042/BST20180469.

Clark, L.N., Wang, Y., Karlins, E., Saito, L., Mejia-Santana, H., et al. (2006). **Frequency of LRRK2 mutations in early- and late-onset Parkinson disease**. *Neurology 67*, 1786–1791. DOI: 10.1212/01.wnl.0000244345.49809.36.

Comartin, D., Gupta, G.D., Fussner, E., Coyaud, É., Hasegan, M., et al. (2013). **CEP120 and SPICE1 cooperate with CPAP in centriole elongation**. *Curr. Biol. 23*, 1360–1366. DOI: 10.1016/j.cub.2013.06.002.

Conduit, P.T., Wainman, A., and Raff, J.W. (2015). **Centrosome function and assembly in animal cells**. *Nat. Rev. Mol. Cell Biol. 16*, 611–624. DOI: 10.1038/nrm4062.

Conibear, E., and Stevens, T.H. (2000). **Vps52p, Vps53p, and Vps54p form a novel multisubunit complex required for protein sorting at the yeast late Golgi**. *Mol. Biol. Cell 11*, 305–323. DOI: 10.1091/mbc.11.1.305.

Cook, D.A., Kannarkat, G.T., Cintron, A.F., Butkovich, L.M., Fraser, K.B., et al. (2017). **LRRK2 levels in immune cells are increased in Parkinson's disease**. *Npj Park. Dis. 3* DOI: 10.1038/s41531-017-0010-8.

Cookson, M.R. (2016). **Cellular functions of LRRK2 implicate vesicular trafficking pathways in Parkinson's disease**. *Biochem. Soc. Trans. 44*, 1603–1610. DOI: 10.1042/BST20160228.

Cox, J. V., Kansal, R., and Whitt, M.A. (2016). **Rab43 regulates the sorting of a subset of membrane protein cargo through the medial Golgi**. *Mol. Biol. Cell 27*, 1834–1844. DOI: 10.1091/mbc.E15-03-0123.

Cuervo, A.M., Stafanis, L., Fredenburg, R., Lansbury, P.T., and Sulzer, D. (2004). **Impaired degradation of mutant α-synuclein by chaperone-mediated autophagy**. *Science (80-.). 305*, 1292–1295. DOI: 10.1126/science.1101738.

Daher, J.P.L., Abdelmotilib, H.A., Hu, X., Volpicelli-Daley, L.A., Moehle, M.S., et al. (2015). **Leucine-rich repeat kinase 2 (LRRK2) pharmacological inhibition abates α-synuclein gene-induced neurodegeneration**. *J. Biol. Chem. 290*, 19433–19444. DOI: 10.1074/jbc.M115.660001.

Daher, J.P.L., Volpicelli-Daley, L.A., Blackburn, J.P., Moehle, M.S., and West, A.B. (2014). **Abrogation of α-synuclein -mediated dopaminergic neurodegeneration in LRRK2-deficient rats**. *Proc. Natl. Acad. Sci. U. S. A. 111*, 9289–9294. DOI: 10.1073/pnas.1403215111.

Dejgaard, S.Y., Murshid, A., Erman, A., Kizilay, Ö., Verbich, D., et al. (2008). **Rab18 and Rab43 have key roles in ER-Golgi trafficking**. *J. Cell Sci. 121*, 2768–2781. DOI: 10.1242/jcs.021808.

Delbroek, L., Van Kolen, K., Steegmans, L., da Cunha, R., Mandemakers, W., et al. (2013). **Development of an enzyme-linked immunosorbent assay for detection of cellular and in vivo LRRK2 S935 phosphorylation**. *J. Pharm. Biomed. Anal. 76*, 49–58. DOI: 10.1016/j.jpba.2012.12.002.

Denali Therapeutics Inc (2020). Denali Therapeutics Announces Decision to Advance DNL151 into Late Stage Clinical Studies in Parkinson's Patients. Denali Therapeutics Inc. 2020. https://denalitherapeutics.gcs-web.com/node/7661/pdf.

Deng, H., Wang, P., and Jankovic, J. (2018). **The genetics of Parkinson disease**. *Ageing Res. Rev. 42*, 72–85. DOI: 10.1016/j.arr.2017.12.007.

Deng, X., Dzamko, N., Prescott, A., Davies, P., Liu, Q., et al. (2011). **Characterization of a selective inhibitor of the Parkinson's disease kinase LRRK2**. *Nat. Chem. Biol. 7*, 203–205. DOI: 10.1038/nchembio.538.

Deniston, C.K., Salogiannis, J., Mathea, S., Snead, D.M., Lahiri, I., et al. (2020). **Structure of LRRK2 in Parkinson's disease and model for microtubule interaction**. *Nature 588*, 344–349. DOI: 10.1038/s41586-020-2673-2.

Desplats, P., Lee, H.J., Bae, E.J., Patrick, C., Rockenstein, E., et al. (2009). **Inclusion formation and neuronal cell death through neuron-to-neuron transmission of α-synuclein**. *Proc. Natl. Acad. Sci. U. S. A. 106*, 13010–13015. DOI: 10.1073/pnas.0903691106.

Dhekne, H.S., Yanatori, I., Gomez, R.C., Tonelli, F., Diez, F., et al. (2018). **A pathway for Parkinson's Disease LRRK2 kinase to block primary cilia and Sonic hedgehog signaling in the brain**. *Elife 7* DOI: 10.7554/eLife.40202.

Dhekne, H.S., Yanatori, I., Vides, E.G., Sobu, Y., Diez, F., et al. (2021). **LRRK2-phosphorylated Rab10 sequesters Myosin Va with RILPL2 during ciliogenesis blockade**. *Life Sci. Alliance 4* DOI: 10.26508/LSA.202101050.

di Domenico, A., Carola, G., Calatayud, C., Pons-Espinal, M., Muñoz, J.P., et al. (2019). **Patient-Specific iPSC-Derived Astrocytes Contribute to Non-Cell-Autonomous Neurodegeneration in Parkinson's Disease.** *Stem Cell Reports 12*, 213–229. DOI: 10.1016/j.stemcr.2018.12.011.

Domire, J.S., Green, J.A., Lee, K.G., Johnson, A.D., Askwith, C.C., et al. (2011). **Dopamine receptor 1 localizes to neuronal cilia in a dynamic process that requires the Bardet-Biedl syndrome proteins**. *Cell. Mol. Life Sci. 68*, 2951–2960. DOI: 10.1007/s00018-010-0603-4.

Van Duijn, C.M., Dekker, M.C.J., Bonifati, V., Galjaard, R.J., Houwing-Duistermaat, J.J., et al. (2001). **PARK7, a novel locus for autosomal recessive early-onset parkinsonism, on chromosome 1p36**. *Am. J. Hum. Genet. 69*, 629–634. DOI: 10.1086/322996.

Dummer, A., Poelma, C., DeRuiter, M.C., Goumans, M.-J.T.H., and Hierck, B.P. (2016). **Measuring the primary cilium length: improved method for unbiased high-throughput analysis.** *Cilia 5*, 7. DOI: 10.1186/s13630-016-0028-2.

Dusonchet, J., Li, H., Guillily, M., Liu, M., Stafa, K., et al. (2014). **A Parkinson's disease gene regulatory network identifies the signaling protein RGS2 as a modulator of LRRK2 activity and neuronal toxicity**. *Hum. Mol. Genet. 23*, 4887–4905. DOI: 10.1093/hmg/ddu202.

Dzamko, N., Chua, G., Ranola, M., and Rowe, D.B. (2013). **Measurement of LRRK2 and Ser910/935 phosphorylated LRRK2 in peripheral blood mononuclear cells from idiopathic Parkinson's disease patients**. *J. Parkinsons. Dis. 3*, 145–152. DOI: 10.3233/JPD-130174.

Dzamko, N., Deak, M., Hentati, F., Reith, A.D., Prescott, A.R., et al. (2010). **Inhibition of LRRK2 kinase activity leads to dephosphorylation of Ser 910/Ser935, disruption of 14-3-3 binding and altered cytoplasmic localization**. *Biochem. J. 430*, 405–413. DOI: 10.1042/BJ20100784.

Dzamko, N., Inesta-Vaquera, F., Zhang, J., Xie, C., Cai, H., et al. (2012). **The IkappaB kinase family phosphorylates the Parkinson's disease kinase LRRK2 at Ser935 and Ser910 during Toll-Like Receptor signaling**. *PLoS One 7* DOI: 10.1371/journal.pone.0039132.

Dzamko, N.L. (2017). LRRK2 and the immune system. In: Advances in Neurobiology, Springer New York LLC, 123–143 DOI: 10.1007/978-3-319-49969-7_7.

Dzhindzhev, N.S., Tzolovsky, G., Lipinszki, Z., Schneider, S., Lattao, R., et al. (2014). **Plk4 phosphorylates ana2 to trigger SAS6 recruitment and procentriole formation**. *Curr. Biol. 24*, 2526–2532. DOI: 10.1016/j.cub.2014.08.061.

Van Den Eeden, S.K., Tanner, C.M., Bernstein, A.L., Fross, R.D., Leimpeter, A., et al. (2003). **Incidence of Parkinson's disease: Variation by age, gender, and race/ethnicity**. *Am. J. Epidemiol. 157*, 1015–1022. DOI: 10.1093/aje/kwg068.

Eguchi, T., Kuwahara, T., Sakurai, M., Komori, T., Fujimoto, T., et al. (2018). **LRRK2 and its substrate Rab GTPases are sequentially targeted onto stressed lysosomes and maintain their homeostasis**. *Proc. Natl. Acad. Sci. U. S. A. 115*, E9115–E9124. DOI: 10.1073/pnas.1812196115.

Elferink, L.A., Anzai, K., and Scheller, R.H. (1992). **rab15, a novel low molecular weight GTP-binding protein specifically expressed in rat brain.** *J. Biol. Chem. 267*, 5768–5775.

Elric, J., and Etienne-Manneville, S. (2014). **Centrosome positioning in polarized cells: Common themes and variations**. *Exp. Cell Res. 328*, 240–248. DOI: 10.1016/j.yexcr.2014.09.004.

English, A.R., and Voeltz, G.K. (2013). **Rab10 GTPase regulates ER dynamics and morphology**. *Nat. Cell Biol. 15*, 169–178. DOI: 10.1038/ncb2647.

Erb, M.L., and Moore, D.J. (2020). **LRRK2 and the Endolysosomal System in Parkinson's Disease**. *J. Parkinsons. Dis. 10*, 1271–1291. DOI: 10.3233/JPD-202138.

Estrada, A.A., Chan, B.K., Baker-Glenn, C., Beresford, A., Burdick, D.J., et al. (2014). **Discovery of highly potent, selective, and brain-penetrant aminopyrazole Leucine-rich repeat kinase 2 (LRRK2) small molecule inhibitors**. *J. Med. Chem. 57*, 921–936. DOI: 10.1021/jm401654j.

Estrada, A.A., Liu, X., Baker-Glenn, C., Beresford, A., Burdick, D.J., et al. (2012). **Discovery of highly potent, selective, and brain-penetrable leucine-rich repeat kinase 2 (LRRK2) small molecule inhibitors**. *J. Med. Chem. 55*, 9416–9433. DOI: 10.1021/jm301020q.

Etoh, K., and Fukuda, M. (2019). **Rab10 regulates tubular endosome formation through KIF13A and KIF13B motors**. *J. Cell Sci. 132* DOI: 10.1242/jcs.226977.

Fan, Y., Howden, A.J.M., Sarhan, A.R., Lis, P., Ito, G., et al. (2018). **Interrogating Parkinson's disease LRRK2 kinase pathway activity by assessing Rab10 phosphorylation in human neutrophils**. *Biochem. J. 475*, 23–44. DOI: 10.1042/BCJ20170803.

Fan, Y., Nirujogi, R.S., Garrido, A., Ruiz-Martínez, J., Bergareche-Yarza, A., et al. (2021). **R1441G but not G2019S mutation enhances LRRK2 mediated Rab10 phosphorylation in human peripheral blood neutrophils**. *Acta Neuropathol.* DOI: 10.1007/s00401-021-02325-z.

Faragher, A.J., and Fry, A.M. (2003). **Nek2A kinase stimulates centrosome disjunction and is required for formation of bipolar mitotic spindles**. *Mol. Biol. Cell 14*, 2876–2889. DOI: 10.1091/mbc.E03-02-0108.

Farrer, M.J., Stone, J.T., Lin, C.H., Dächsel, J.C., Hulihan, M.M., et al. (2007). **Lrrk2 G2385R is an ancestral risk factor for Parkinson's disease in Asia**. *Park. Relat. Disord. 13*, 89–92. DOI: 10.1016/j.parkreldis.2006.12.001.

Fell, M.J., Mirescu, C., Basu, K., Cheewatrakoolpong, B., DeMong, D.E., et al. (2015). **MLi-2, a potent, selective, and centrally active compound for exploring the therapeutic potential and safety of LRRK2 kinase inhibition**. *J. Pharmacol. Exp. Ther. 355*, 397–409. DOI: 10.1124/jpet.115.227587.

Feng, S., Knödler, A., Ren, J., Zhang, J., Zhang, X., et al. (2012). **A Rab8 guanine nucleotide exchange factor-effector interaction network regulates primary ciliogenesis.** *J. Biol. Chem. 287*, 15602–15609. DOI: 10.1074/jbc.M111.333245.

Di Fonzo, A., Rohé, C.F., Ferreira, J., Chien, H.F., Vacca, L., et al. (2005). **A frequent LRRK2 gene mutation associated with autosomal dominant Parkinson's disease**. *Lancet 365*, 412–415. DOI: 10.1016/S0140-6736(05)17829-5.

Di Fonzo, A., Wu-Chou, Y.H., Lu, C.S., Van Doeselaar, M., Simons, E.J., et al. (2006). **A common missense variant in the LRRK2 gene, Gly2385Arg, associated with Parkinson's disease risk in Taiwan**. *Neurogenetics 7*, 133–138. DOI: 10.1007/s10048-006-0041-5.

Francavilla, C., Papetti, M., Rigbolt, K.T.G., Pedersen, A.K., Sigurdsson, J.O., et al. (2016). **Multilayered proteomics reveals molecular switches dictating ligand-dependent EGFR trafficking**. *Nat. Struct. Mol. Biol. 23*, 608–618. DOI: 10.1038/nsmb.3218.

Fraser, K.B., Moehle, M.S., Alcalay, R.N., and West, A.B. (2016). **Urinary LRRK2 phosphorylation predicts parkinsonian phenotypes in G2019S LRRK2 carriers**. *Neurology 86*, 994–999. DOI: 10.1212/WNL.0000000000002436.

Freese, J.L., Pino, D., and Pleasure, S.J. (2010). **Wnt signaling in development and disease**. *Neurobiol. Dis. 38*, 148–153. DOI: 10.1016/j.nbd.2009.09.003.

Fu, X., Zheng, Y., Hong, H., He, Y., Zhou, S., et al. (2013). **LRRK2 G2385R and LRRK2 R1628P increase risk of Parkinson's disease in a Han Chinese population from Southern Mainland China**. *Park. Relat. Disord. 19*, 397–398. DOI: 10.1016/j.parkreldis.2012.08.007.

Fuji, R.N., Flagella, M., Baca, M., Baptista, M.A.S., Brodbeck, J., et al. (2015). **Effect of selective LRRK2 kinase inhibition on nonhuman primate lung**. *Sci. Transl. Med. 7*, 273ra15. DOI: 10.1126/scitranslmed.aaa3634.

Fujimoto, T., Kuwahara, T., Eguchi, T., Sakurai, M., Komori, T., et al. (2018). **Parkinson's disease-associated mutant LRRK2 phosphorylates Rab7L1 and modifies trans-Golgi morphology**. *Biochem. Biophys. Res. Commun. 495*, 1708–1715. DOI: 10.1016/j.bbrc.2017.12.024.

Funayama, M., Hasegawa, K., Kowa, H., Saito, M., Tsuji, S., et al. (2002). **A new locus for Parkinson's disease (PARK8) maps to chromosome 12p11.2-q13.1**. *Ann. Neurol 51*, 296–301.

Funayama, M., Hasegawa, K., Ohta, E., Kawashima, N., Komiyama, M., et al. (2005). **An LRRK2 mutation as a cause for the parkinsonism in the original PARK8 family**. *Ann. Neurol. 57*, 918–921. DOI: 10.1002/ana.20484.

Funayama, M., Li, Y., Tomiyama, H., Yoshino, H., Imamichi, Y., et al. (2007). **Leucine-Rich Repeat kinase 2 G2385R variant is a risk factor for Parkinson disease in Asian population**. *Neuroreport 18*, 273–275. DOI: 10.1097/WNR.0b013e32801254b6.

Gabe Lee, M.-T., Mishra, A., and Lambright, D.G. (2009). **Structural Mechanisms for Regulation of Membrane Traffic by Rab GTPases**. *Traffic 10*, 1377–1389. DOI: 10.1111/j.1600-0854.2009.00942.x.

Gan-Or, Z., Amshalom, I., Kilarski, L.L., Bar-Shira, A., Gana-Weisz, M., et al. (2015). **Differential effects of severe vs mild GBA mutations on Parkinson disease**. *Neurology 84*, 880–887. DOI: 10.1212/WNL.0000000000001315.

Gandhi, P.N., Wang, X., Zhu, X., Chen, S.G., and Wilson-Delfosse, A.L. (2008). **The Roc domain of leucine-rich repeat kinase 2 is sufficient for interaction with microtubules**. *J. Neurosci. Res. 86*, 1711–1720. DOI: 10.1002/jnr.21622.

Gelders, G., Baekelandt, V., and Van der Perren, A. (2018). **Linking neuroinflammation and neurodegeneration in parkinson's disease**. *J. Immunol. Res. 2018* DOI: 10.1155/2018/4784268.

Giguère, N., Nanni, S.B., and Trudeau, L.E. (2018). **On cell loss and selective vulnerability of neuronal populations in Parkinson's disease**. *Front. Neurol. 9* DOI: 10.3389/fneur.2018.00455.

Gillardon, F. (2009). **Leucine-rich repeat kinase 2 phosphorylates brain tubulin-beta isoforms and modulates microtubule stability - a point of convergence in Parkinsonian neurodegeneration?**. *J. Neurochem. 110*, 1514–1522. DOI: 10.1111/j.1471-4159.2009.06235.x.

Gloeckner, C.J., Boldt, K., Von Zweydorf, F., Helm, S., Wiesent, L., et al. (2010). **Phosphopeptide analysis reveals two discrete clusters of phosphorylation in the N-terminus and the Roc domain of the Parkinson-disease associated protein kinase LRRK2**. *J. Proteome Res. 9*, 1738–1745. DOI: 10.1021/pr9008578.

Gloeckner, C.J., Kinkl, N., Schumacher, A., Braun, R.J., O'Neill, E., et al. (2006). **The Parkinson disease causing LRRK2 mutation I2020T is associated with increased kinase activity**. *Hum. Mol. Genet. 15*, 223–232. DOI: 10.1093/hmg/ddi439.

Gloeckner, C.J., and Porras, P. (2020). **Guilt-by-Association – Functional Insights Gained From Studying the LRRK2 Interactome**. *Front. Neurosci. 14* DOI: 10.3389/fnins.2020.00485.

Gloeckner, C.J., Schumacher, A., Boldt, K., and Ueffing, M. (2009). **The Parkinson disease-associated protein kinase LRRK2 exhibits MAPKKK activity and phosphorylates MKK3/6 and MKK4/7, in vitro**. *J. Neurochem. 109*, 959–968. DOI: 10.1111/j.1471-4159.2009.06024.x.

Godinho, S.A., and Pellman, D. (2014). **Causes and consequences of centrosome abnormalities in cancer**. *Philos. Trans. R. Soc. B Biol. Sci. 369* DOI: 10.1098/rstb.2013.0467.

Godinho, S.A., Picone, R., Burute, M., Dagher, R., Su, Y., et al. (2014). **Oncogene-like induction of cellular invasion from centrosome amplification**. *Nature 510*, 167–171. DOI: 10.1038/nature13277.

Goldwurm, S., Zini, M., Mariani, L., Tesei, S., Miceli, R., et al. (2007). **Evaluation of LRRK2 G2019S penetrance: Relevance for genetic counseling in Parkinson disease**. *Neurology 68*, 1141–1143. DOI: 10.1212/01.wnl.0000254483.19854.ef.

Gómez-Suaga, P., Rivero-Ríos, P., Fdez, E., Blanca Ramírez, M., Ferrer, I., et al. (2014). **LRRK2 delays degradative receptor trafficking by impeding late endosomal budding through decreasing Rab7 activity.** *Hum. Mol. Genet. 23*, 6779–6796. DOI: 10.1093/hmg/ddu395.

Gomez, R.C., Wawro, P., Lis, P., Alessi, D.R., and Pfeffer, S.R. (2019). **Membrane association but not identity is required for LRRK2 activation and phosphorylation of Rab GTPases**. *J. Cell Biol. 218*, 4157–4170. DOI: 10.1083/JCB.201902184.

Gonzalez-Reyes, L.E., Verbitsky, M., Blesa, J., Jackson-Lewis, V., Paredes, D., et al. (2012). **Sonic Hedgehog Maintains Cellular and Neurochemical Homeostasis in the Adult Nigrostriatal Circuit**. *Neuron 75*, 306–319. DOI: 10.1016/j.neuron.2012.05.018.

Graser, S., Stierhof, Y.D., and Nigg, E.A. (2007). **Cep68 and Cep215 (Cdk5rap2) are required for centrosome cohesion**. *J. Cell Sci. 120*, 4321–4331. DOI: 10.1242/jcs.020248.

Greenan, G.A., Keszthelyi, B., Vale, R.D., and Agard, D.A. (2018). **Insights into centriole geometry revealed by cryotomography of doublet and triplet centrioles**. *Elife 7* DOI: 10.7554/eLife.36851.

Greggio, E., Jain, S., Kingsbury, A., Bandopadhyay, R., Lewis, P., et al. (2006). **Kinase activity is required for the toxic effects of mutant LRRK2/dardarin**. *Neurobiol. Dis. 23*, 329–341. DOI: 10.1016/j.nbd.2006.04.001.

Greggio, E., Lewis, P.A., Van Der Brug, M.P., Ahmad, R., Kaganovich, A., et al. (2007). **Mutations in LRRK2/dardarin associated with Parkinson disease are more toxic than equivalent mutations in the homologous kinase LRRK1**. *J. Neurochem. 102*, 93–102. DOI: 10.1111/j.1471-4159.2007.04523.x.

Greggio, E., Taymans, J.M., Zhen, E.Y., Ryder, J., Vancraenenbroeck, R., et al. (2009). **The Parkinson's disease kinase LRRK2 autophosphorylates its GTPase domain at multiple sites**. *Biochem. Biophys. Res. Commun. 389*, 449–454. DOI: 10.1016/j.bbrc.2009.08.163.

Greggio, E., Zambrano, I., Kaganovich, A., Beilina, A., Taymans, J.M., et al. (2008). **The Parkinson disease-associated leucine-rich repeat kinase 2 (LRRK2) is a dimer that undergoes intramolecular autophosphorylation**. *J. Biol. Chem. 283*, 16906–16914. DOI: 10.1074/jbc.M708718200.

Guadagno, N.A., and Progida, C. (2019). **Rab GTPases: Switching to Human Diseases**. *Cells 8*, 909. DOI: 10.3390/cells8080909.

Guo, L., Gandhi, P.N., Wang, W., Petersen, R.B., Wilson-Delfosse, A.L., et al. (2007). **The Parkinson's disease-associated protein, leucine-rich repeat kinase 2 (LRRK2), is an authentic GTPase thatstimulates kinase activity**. *Exp. Cell Res. 313*, 3658–3670. DOI: 10.1016/j.yexcr.2007.07.007.

Gustavsson, E., Follett, J., Ramirez, C.M., Trinh, J., Fox, J., et al. (2017). RAB32 as a cause for familial Parkinson's disease. In: International Congress of Parkinson's Disease and Movement Disorders,.

Haas, A.K., Yoshimura, S.I., Stephens, D.J., Preisinger, C., Fuchs, E., et al. (2007). **Analysis of GTPase-activating proteins: Rab1 and Rab43 are key Rabs required to maintain a functional Golgi complex in human cells**. *J. Cell Sci. 120*, 2997–3010. DOI: 10.1242/jcs.014225.

Hanafusa, H., Yagi, T., Ikeda, H., Hisamoto, N., Nishioka, T., et al. (2019). **LRRK1 phosphorylation of Rab7 at S72 links trafficking of EGFR-containing endosomes to its effector RILP**. *J. Cell Sci. 132* DOI: 10.1242/jcs.228809.

Hardy, T., Lee, M., Hames, R.S., Prosser, S.L., Cheary, D.M., et al. (2014). **Multisite phosphorylation of C-Nap1 releases it from Cep135 to trigger centrosome disjunction**. *J. Cell Sci. 127*, 2493–2506. DOI: 10.1242/jcs.142331.

Hassin-Baer, S., Laitman, Y., Azizi, E., Molchadski, I., Galore-Haskel, G., et al. (2009). **The leucine rich repeat kinase 2 (LRRK2) G2019S substitution mutation : AAssociation with Parkinson disease, malignant melanoma and prevalence in ethnic groups in Israel**. *J. Neurol. 256*, 483–487. DOI: 10.1007/s00415-009-0117-x.

Hatano, T., Kubo, S. ichiro, Imai, S., Maeda, M., Ishikawa, K., et al. (2007). **Leucine-rich repeat kinase 2 associates with lipid rafts**. *Hum. Mol. Genet. 16*, 678–690. DOI: 10.1093/hmg/ddm013.

Hattula, K., Furujelm, J., Tikkanen, J., Tanhuanpää, K., Laakkonen, P., et al. (2006). **Characterization of the Rab8-specific membrane traffic route linked to protrusion formation**. *J. Cell Sci. 119*, 4866–4877. DOI: 10.1242/jcs.03275.

Healy, D.G., Falchi, M., O'Sullivan, S.S., Bonifati, V., Durr, A., et al. (2008). **Phenotype, genotype, and worldwide genetic penetrance of LRRK2-associated Parkinson's disease: a case-control study**. *Lancet Neurol. 7*, 583–590. DOI: 10.1016/S1474-4422(08)70117-0.

Hebert, E., Borngräber, F., Schmidt, A., Rakovic, A., Brænne, I., et al. (2017). **Functional characterization of rare RAB12 variants and their role in musician's and other dystonias**. *Genes (Basel). 8* DOI: 10.3390/genes8100276.

Hehnly, H., Chen, C.T., Powers, C.M., Liu, H.L., and Doxsey, S. (2012). **The centrosome regulates the Rab11- dependent recycling endosome pathway at appendages of the mother centriole**. *Curr. Biol. 22*, 1944–1950. DOI: 10.1016/j.cub.2012.08.022.

Henderson, J.L., Kormos, B.L., Hayward, M.M., Coffman, K.J., Jasti, J., et al. (2015). **Discovery and preclinical profiling of 3-[4-(morpholin-4-yl)-7H-pyrrolo[2,3-d]pyrimidin-5-yl]benzonitrile (PF-06447475), a highly potent, selective, brain penetrant, and in vivo active LRRK2 kinase inhibitor**. *J. Med. Chem. 58*, 419–432. DOI: 10.1021/jm5014055.

Heo, J.M., Ordureau, A., Swarup, S., Paulo, J.A., Shen, K., et al. (2018). **RAB7A phosphorylation by TBK1 promotes mitophagy via the PINK-PARKIN pathway**. *Sci. Adv. 4* DOI: 10.1126/sciadv.aav0443.

Herbst, S., Campbell, P., Harvey, J., Bernard, E.M., Papayannopoulos, V., et al. (2020). **LRRK2 activation controls the repair of damaged endomembranes in macrophages**. *EMBO J. 39* DOI: 10.15252/embj.2020104494.

Hernandez, D.G., Reed, X., and Singleton, A.B. (2016). **Genetics in Parkinson disease: Mendelian versus non-Mendelian inheritance**. *J. Neurochem. 139*, 59–74. DOI: 10.1111/jnc.13593.

Herzig, M.C., Kolly, C., Persohn, E., Theil, D., Schweizer, T., et al. (2011). **LRRK2 protein levels are determined by kinase function and are crucial for kidney and lung homeostasis in mice**. *Hum. Mol. Genet. 20*, 4209–4223. DOI: 10.1093/hmg/ddr348.

Higashi, S., Moore, D.J., Yamamoto, R., Minegishi, M., Sato, K., et al. (2009). **Abnormal localization of leucine-rich repeat kinase 2 to the endosomal-lysosomal compartment in lewy body disease**. *J. Neuropathol. Exp. Neurol. 68*, 994–1005. DOI: 10.1097/NEN.0b013e3181b44ed8.

Hirsch, L., Jette, N., Frolkis, A., Steeves, T., and Pringsheim, T. (2016). **The Incidence of Parkinson's Disease: A Systematic Review and Meta-Analysis**. *Neuroepidemiology 46*, 292–300. DOI: 10.1159/000445751.

Ho, D.H., Jang, J., Joe, E.H., Son, I., Seo, H., et al. (2016). **G2385R and I2020T Mutations Increase LRRK2 GTPase Activity**. *Biomed Res. Int. 2016* DOI: 10.1155/2016/7917128.

Ho, P.W.L., Leung, C.T., Liu, H., Pang, S.Y.Y., Lam, C.S.C., et al. (2020). **Age-dependent accumulation of oligomeric SNCA/α-synuclein from impaired degradation in mutant LRRK2 knockin mouse model of Parkinson disease: role for therapeutic activation of chaperone-mediated autophagy (CMA)**. *Autophagy 16*, 347–370. DOI: 10.1080/15548627.2019.1603545.

Homma, Y., Hiragi, S., and Fukuda, M. (2021). **Rab family of small GTPases: an updated view on their regulation and functions**. *FEBS J. 288*, 36–55. DOI: 10.1111/febs.15453.

Hou, X., Watzlawik, J.O., Fiesel, F.C., and Springer, W. (2020). **Autophagy in Parkinson's Disease**. *J. Mol. Biol. 432*, 2651–2672. DOI: 10.1016/j.jmb.2020.01.037.

Hsu, C.H., Chan, D., Greggio, E., Saha, S., Guillily, M.D., et al. (2010a). **MKK6 binds and regulates expression of Parkinson's disease-related protein LRRK2**. *J. Neurochem. 112*, 1593–1604. DOI: 10.1111/j.1471-4159.2010.06568.x.

Hsu, C.H., Chan, D., and Wolozin, B. (2010b). LRRK2 and the stress response: Interaction with MKKs and JNK-interacting proteins. In: Neurodegenerative Diseases, 68–75 DOI: 10.1159/000285509.

Hu, Q., and Wang, G. (2016). **Mitochondrial dysfunction in Parkinson's disease**. *Transl. Neurodegener. 5* DOI: 10.1186/s40035-016-0060-6.

Hu, Y.B., Dammer, E.B., Ren, R.J., and Wang, G. (2015). **The endosomal-lysosomal system: From acidification and cargo sorting to neurodegeneration**. *Transl. Neurodegener. 4* DOI: 10.1186/s40035-015-0041-1.

Huang, X., Wu, C., Park, Y., Long, X., Hoang, Q.Q., et al. (2019). **The Parkinson's disease–associated mutation N1437H impairs conformational dynamics in the G domain of LRRK2**. *FASEB J. 33*, 4814–4823. DOI: 10.1096/fj.201802031R.

Hui, K.Y., Fernandez-Hernandez, H., Hu, J., Schaffner, A., Pankratz, N., et al. (2018). **Functional variants in the LRRK2 gene confer shared effects on risk for Crohn's disease and Parkinson's disease**. *Sci. Transl. Med. 10* DOI: 10.1126/scitranslmed.aai7795.

Huotari, J., and Helenius, A. (2011). **Endosome maturation**. *EMBO J. 30*, 3481–3500. DOI: 10.1038/emboj.2011.286.

Iannotta, L., Biosa, A., Kluss, J.H., Tombesi, G., Kaganovich, A., et al. (2020). **Divergent Effects of G2019S and R1441C LRRK2 Mutations on LRRK2 and Rab10 Phosphorylations in Mouse Tissues**. *Cells 9* DOI: 10.3390/cells9112344.

Imai, Y., Gehrke, S., Wang, H.Q., Takahashi, R., Hasegawa, K., et al. (2008). **Phosphorylation of 4E-BP by LRRK2 affects the maintenance of dopaminergic neurons in Drosophila**. *EMBO J. 27*, 2432–2443. DOI: 10.1038/emboj.2008.163.

Inestrosa, N.C., Montecinos-Oliva, C., and Fuenzalida, M. (2012). **Wnt signaling: Role in Alzheimer disease and schizophrenia**. *J. Neuroimmune Pharmacol. 7*, 788–807. DOI: 10.1007/s11481-012-9417-5.

Inzelberg, R., Cohen, O.S., Aharon-Peretz, J., Schlesinger, I., Gershoni-Baruch, R., et al. (2012). **The LRRK2 G2019S mutation is associated with Parkinson disease and concomitant non-skin cancers**. *Neurology 78*, 781–786. DOI: 10.1212/WNL.0b013e318249f673.

Islam, M.S., Nolte, H., Jacob, W., Ziegler, A.B., Pütz, S., et al. (2016). **Human R1441C LRRK2 regulates the synaptic vesicle proteome and phosphoproteome in a Drosophila model of Parkinson's disease**. *Hum. Mol. Genet. 25*, 5365–5382. DOI: 10.1093/hmg/ddw352.

Ito, G., Fujimoto, T., Kamikawaji, S., Kuwahara, T., and Iwatsubo, T. (2014). **Lack of correlation between the kinase activity of LRRK2 harboring kinase-modifying mutations and its phosphorylation at Ser910, 935, and Ser955**. *PLoS One 9* DOI: 10.1371/journal.pone.0097988.

Ito, G., Katsemonova, K., Tonelli, F., Lis, P., Baptista, M.A.S., et al. (2016). **Phos-tag analysis of Rab10 phosphorylation by LRRK2: a powerful assay for assessing kinase function and inhibitors**. *Biochem. J. 473*, 2671–2685. DOI: 10.1042/BCJ20160557.

Ito, G., Okai, T., Fujino, G., Takeda, K., Ichijo, H., et al. (2007). **GTP binding is essential to the protein kinase activity of LRRK2, a causative gene product for familial Parkinson's disease**. *Biochemistry 46*, 1380–1388. DOI: 10.1021/bi061960m.

Jaldin-Fincati, J.R., Pavarotti, M., Frendo-Cumbo, S., Bilan, P.J., and Klip, A. (2017). **Update on GLUT4 Vesicle Traffic: A Cornerstone of Insulin Action**. *Trends Endocrinol. Metab. 28*, 597–611. DOI: 10.1016/j.tem.2017.05.002.

Jaleel, M., Nichols, R.J., Deak, M., Campbell, D.G., Gillardon, F., et al. (2007). **LRRK2 phosphorylates moesin at threonine-558: Characterization of how Parkinson's disease mutants affect kinase activity**. *Biochem. J. 405*, 307–317. DOI: 10.1042/BJ20070209.

Jana, S.C. (2021). **Centrosome structure and biogenesis: Variations on a theme?**. *Semin. Cell Dev. Biol. 110*, 123–138. DOI: 10.1016/j.semcdb.2020.10.014.

Jankovic, J. (2008). **Parkinson's disease: Clinical features and diagnosis**. *J. Neurol. Neurosurg. Psychiatry 79*, 368–376. DOI: 10.1136/jnnp.2007.131045.

Jeong, G.R., Jang, E.-H., Bae, J.R., Jun, S., Kang, H.C., et al. (2018). **Dysregulated phosphorylation of Rab GTPases by LRRK2 induces neurodegeneration.** *Mol. Neurodegener. 13*, 8. DOI: 10.1186/s13024-018-0240-1.

Kachergus, J., Mata, I.F., Hulihan, M., Taylor, J.P., Lincoln, S., et al. (2005). **Identification of a novel LRRK2 mutation linked to autosomal dominant parkinsonism: Evidence of a common founder across European populations**. *Am. J. Hum. Genet. 76*, 672–680. DOI: 10.1086/429256.

Kalia, L. V., and Kalia, S.K. (2015). **α-Synuclein and Lewy pathology in Parkinson's disease**. *Curr. Opin. Neurol. 28*, 375–381. DOI: 10.1097/WCO.0000000000000215.

Kalia, L. V., and Lang, A.E. (2015). **Parkinson's disease**. *Lancet 386*, 896–912. DOI: 10.1016/S0140-6736(14)61393-3.

Kalogeropulou, A.F., Freemantle, J.B., Lis, P., Vides, E.G., Polinski, N.K., et al. (2020). **Endogenous Rab29 does not impact basal or stimulated LRRK2 pathway activity**. *Biochem. J. 477*, 4397–4423. DOI: 10.1042/BCJ20200458.

Kamikawaji, S., Ito, G., and Iwatsubo, T. (2009). **Identification of the autophosphorylation sites of LRRK2**. *Biochemistry 48*, 10963–10975. DOI: 10.1021/bi9011379.

Kanao, T., Venderova, K., Park, D.S., Unterman, T., Lu, B., et al. (2010). **Activation of FoxO by LRRK2 induces expression of proapoptotic proteins and alters survival of postmitotic dopaminergic neuron in Drosophila**. *Hum. Mol. Genet. 19*, 3747–3758. DOI: 10.1093/hmg/ddq289.

Kang, U.B., and Marto, J.A. (2017). **Leucine-rich repeat kinase 2 and Parkinson's disease**. *Proteomics 17* DOI: 10.1002/pmic.201600092.

Kawakami, F., Yabata, T., Ohta, E., Maekawa, T., Shimada, N., et al. (2012). **LRRK2 phosphorylates tubulin-associated tau but not the free molecule: LRRK2-mediated regulation of the tau-tubulin association and neurite outgrowth**. *PLoS One 7* DOI: 10.1371/journal.pone.0030834.

Kawakami, T., Ren, S., and Duffield, J.S. (2013). **Wnt signalling in kidney diseases: Dual roles in renal injury and repair**. *J. Pathol. 229*, 221–231. DOI: 10.1002/path.4121.

Kay, D.M., Kramer, P., Higgins, D., Zabetian, C.P., and Payami, H. (2005). **Escaping Parkinson's disease: A neurologically healthy octogenarian with the LRRK2 G2019S mutation**. *Mov. Disord. 20*, 1077–1078. DOI: 10.1002/mds.20618.

Kett, L.R., Boassa, D., Ho, C.C.Y., Rideout, H.J., Hu, J., et al. (2012). **LRRK2 Parkinson disease mutations enhance its microtubule association**. *Hum. Mol. Genet. 21*, 890–899. DOI: 10.1093/hmg/ddr526.

Khakurel, A., Kudlyk, T., Bonifacino, J.S., and Lupashin, V. V (2020). **The Golgi-associated retrograde protein (GARP) complex plays an essential role in the maintenance of the Golgi glycosylation machinery**. *BioRxiv* 2020.12.21.423858. DOI: 10.1101/2020.12.21.423858.

Khan, S.S., Sobu, Y., Dhekne, H.S., Tonelli, F., Berndsen, K., et al. (2021). **Pathogenic LRRK2 control of primary cilia and Hedgehog signaling in neurons and astrocytes of mouse brain**. *BioRxiv*.

Kim, C.Y., and Alcalay, R.N. (2017). **Genetic Forms of Parkinson's Disease**. *Semin. Neurol. 37*, 135–146. DOI: 10.1055/s-0037-1601567.

Kim, E.K., and Choi, E.J. (2010). **Pathological roles of MAPK signaling pathways in human diseases**. *Biochim. Biophys. Acta - Mol. Basis Dis. 1802*, 396–405. DOI: 10.1016/j.bbadis.2009.12.009.

Kitada, T., Asakawa, S., Hattori, N., Matsumine, H., Yamamura, Y., et al. (1998). **Mutations in the parkin gene cause autosomal recessive juvenile parkinsonism**. *Nature 392*, 605–608. DOI: 10.1038/33416.

Klegeris, A., Giasson, B.I., Zhang, H., Maguire, J., Pelech, S., et al. (2006). **Alpha-synuclein and its disease-causing mutants induce ICAM-1 and IL-6 in human astrocytes and astrocytoma cells**. *FASEB J. 20*, 2000–2008. DOI: 10.1096/fj.06-6183com.

Klegeris, A., Pelech, S., Giasson, B.I., Maguire, J., Zhang, H., et al. (2008). **α-Synuclein activates stress signaling protein kinases in THP-1 cells and microglia**. *Neurobiol. Aging 29*, 739–752. DOI: 10.1016/j.neurobiolaging.2006.11.013.

Klinkert, K., and Echard, A. (2016). **Rab35 GTPase: A Central Regulator of Phosphoinositides and F-actin in Endocytic Recycling and Beyond**. *Traffic 17*, 1063–1077. DOI: 10.1111/tra.12422.

Klöpper, T.H., Kienle, N., Fasshauer, D., and Munro, S. (2012). **Untangling the evolution of Rab G proteins: implications of a comprehensive genomic analysis**. *BMC Biol. 10*, 1–17. DOI: 10.1186/1741-7007-10-71.

Kluss, J.H., Conti, M.M., Kaganovich, A., Beilina, A., Melrose, H.L., et al. (2018). **Detection of endogenous S1292 LRRK2 autophosphorylation in mouse tissue as a readout for kinase activity**. *Npj Park. Dis. 4*, 1–5. DOI: 10.1038/s41531-018-0049-1.

Knödler, A., Feng, S., Zhang, J., Zhang, X., Das, A., et al. (2010). **Coordination of Rab8 and Rab11 in primary ciliogenesis.** *Proc. Natl. Acad. Sci. U. S. A. 107*, 6346–6351. DOI: 10.1073/pnas.1002401107.

Königshoff, M., Balsara, N., Pfaff, E.M., Kramer, M., Chrobak, I., et al. (2008). **Functional Wnt signaling is increased in idiopathic pulmonary fibrosis**. *PLoS One 3*, e2142. DOI: 10.1371/journal.pone.0002142.

Kouli, A., Torsney, K.M., and Kuan, W.-L. (2018). Parkinson's Disease: Etiology, Neuropathology, and Pathogenesis. In: Parkinson's Disease: Pathogenesis and Clinical Aspects, Codon Publications, 3–26 DOI: 10.15586/codonpublications.parkinsonsdisease.2018.ch1.

Kouranti, I., Sachse, M., Arouche, N., Goud, B., and Echard, A. (2006). **Rab35 Regulates an Endocytic Recycling Pathway Essential for the Terminal Steps of Cytokinesis**. *Curr. Biol. 16*, 1719–1725. DOI: 10.1016/j.cub.2006.07.020.

Kowal, S.L., Dall, T.M., Chakrabarti, R., Storm, M. V., and Jain, A. (2013). **The current and projected economic burden of Parkinson's disease in the United States**. *Mov. Disord. 28*, 311–318. DOI: 10.1002/mds.25292.

Kretzer, N.M., Theisen, D.J., Tussiwand, R., Briseño, C.G., Grajales-Reyes, G.E., et al. (2016). **RAB43 facilitates cross-presentation of cell-associated antigens by CD8α+ dendritic cells**. *J. Exp. Med. 213*, 2871–2883. DOI: 10.1084/jem.20160597.

Krumova, P., Reyniers, L., Meyer, M., Lobbestael, E., Stauffer, D., et al. (2015). **Chemical genetic approach identifies microtubule affinity-regulating kinase 1 as a leucine-rich repeat kinase 2 substrate**. *FASEB J. 29*, 2980–2992. DOI: 10.1096/fj.14-262329.

Kuwahara, T., Funakawa, K., Komori, T., Sakurai, M., Yoshii, G., et al. (2020). **Roles of lysosomotropic agents on LRRK2 activation and Rab10 phosphorylation**. *Neurobiol. Dis. 145* DOI: 10.1016/j.nbd.2020.105081.

Lai, Y., Kondapalli, C., Lehneck, R., Procter, J.B., Dill, B.D., et al. (2015). **Phosphoproteomic screening identifies Rab GTPases as novel downstream targets of PINK1**. *EMBO J. 34*, 2840–2861. DOI: 10.15252/embj.201591593.

Langston, J.W., Ballard, P., Tetrud, J.W., and Irwin, I. (1983). **Chronic parkinsonism in humans due to a product of meperidine-analog synthesis**. *Science (80-.). 219*, 979–980. DOI: 10.1126/science.6823561.

Latourelle, J.C., Sun, M., Lew, M.F., Suchowersky, O., Klein, C., et al. (2008). **The Gly2019Ser mutation in LRRK2 is not fully penetrant in familial Parkinson's disease: The GenePD study**. *BMC Med. 6*, 32. DOI: 10.1186/1741-7015-6-32.

Leandrou, E., Markidi, E., Memou, A., Melachroinou, K., Greggio, E., et al. (2019). **Kinase activity of mutant LRRK2 manifests differently in hetero-dimeric vs. Homo-dimeric complexes**. *Biochem. J. 476*, 559–579. DOI: 10.1042/BCJ20180589.

Lee, S., Liu, H.P., Lin, W.Y., Guo, H., and Lu, B. (2010). **LRRK2 kinase regulates synaptic morphology through distinct substrates at the presynaptic and postsynaptic compartments of the Drosophila neuromuscular junction**. *J. Neurosci. 30*, 16959–16969. DOI: 10.1523/JNEUROSCI.1807-10.2010.

Lesage, S., Bras, J., Cormier-Dequaire, F., Condroyer, C., Nicolas, A., et al. (2015). **Loss-of-function mutations in RAB39B are associated with typical early-onset Parkinson disease.** *Neurol. Genet. 1*, e9. DOI: 10.1212/NXG.0000000000000009.

Lesage, S., Condroyer, C., Lannuzel, A., Lohmann, E., Troiano, A., et al. (2009). **Molecular analyses of the LRRK2 gene in Europeanand North African autosomal dominant Parkinson's disease**. *J. Med. Genet. 46*, 458–464. DOI: 10.1136/jmg.2008.062612.

Lesage, S., Dürr, A., Tazir, M., Lohmann, E., Leutenegger, A.L., et al. (2006). **LRRK2 G2019S as a cause of Parkinson's disease in North African Arabs**. *N. Engl. J. Med. 354*, 422–423. DOI: 10.1056/NEJMc055540.

Lewy, F.H. (1912). **Paralysis agitans. Part I: Pathologische anatomie**. *Lewandowsky M Handb. Der Neurol. Vol. III, Spez. Neurol. II. Springer, Berlin, Pp 920–933*.

Li, C., Wei, Z., Fan, Y., Huang, W., Su, Y., et al. (2017). **The GTPase Rab43 Controls the Anterograde ER-Golgi Trafficking and Sorting of GPCRs**. *Cell Rep. 21*, 1089–1101. DOI: 10.1016/j.celrep.2017.10.011.

Li, G. (2012). Early endocytosis: Rab5, rab21, and rab22. In: Rab GTPases and Membrane Trafficking, Bentham Science Publishers Ltd., 93–107 DOI: 10.2174/978160805365011201010093.

Li, X., Moore, D.J., Xiong, Y., Dawson, T.M., and Dawson, V.L. (2010). **Reevaluation of phosphorylation sites in the parkinson disease-associated leucine-rich repeat kinase 2**. *J. Biol. Chem. 285*, 29569–29576. DOI: 10.1074/jbc.M110.127639.

Li, X., Tan, Y.-C., Poulose, S., Olanow, C.W., Huang, X.-Y., et al. (2007). **Leucine-rich repeat kinase 2 (LRRK2)/PARK8 possesses GTPase activity that is altered in familial Parkinson?s disease R1441C/G mutants**. *J. Neurochem. 0*, 070710052154004-??? DOI: 10.1111/j.1471-4159.2007.04743.x.

Liang, D., Shu, L., Pan, H., Xu, Q., Guo, J., et al. (2018). **Clinical characteristics of PD patients with LRRK2 G2385R and R1628P variants**. *Neurosci. Lett. 685*, 185–189. DOI: 10.1016/j.neulet.2018.08.015.

Liewen, H., Meinhold-Heerlein, I., Oliveira, V., Schwarzenbacher, R., Luo, G., et al. (2005). **Characterization of the human GARP (Golgi associated retrograde protein) complex**. *Exp. Cell Res. 306*, 24–34. DOI: 10.1016/j.yexcr.2005.01.022.

Lis, P., Burel, S., Steger, M., Mann, M., Brown, F., et al. (2018). **Development of phospho-specific Rab protein antibodies to monitor *in vivo* activity of the LRRK2 Parkinson's disease kinase**. *Biochem. J. 475*, 1–22. DOI: 10.1042/BCJ20170802.

Liu, Y., Xu, X.H., Chen, Q., Wang, T., Deng, C.Y., et al. (2013). **Myosin Vb controls biogenesis of post-Golgi Rab10 carriers during axon development**. *Nat. Commun. 4* DOI: 10.1038/ncomms3005.

Liu, Z., Bryant, N., Kumaran, R., Beilina, A., Abeliovich, A., et al. (2018). **LRRK2 phosphorylates membrane-bound Rabs and is activated by GTP-bound Rab7L1 to promote recruitment to the trans-Golgi network**. *Hum. Mol. Genet. 27*, 385–395. DOI: 10.1093/hmg/ddx410.

Lobbestael, E., Zhao, J., Rudenko, I.N., Beylina, A., Gao, F., et al. (2013). **Identification of protein phosphatase 1 as a regulator of the LRRK2 phosphorylation cycle**. *Biochem. J. 456*, 119–128. DOI: 10.1042/BJ20121772.

Louie, L.G., and King, M.C. (1991). **A novel approach to establishing permanent lymphoblastoid cell lines: Epstein-Barr virus transformation of cryopreserved lymphocytes**. *Am. J. Hum. Genet. 48*, 637–638.

Lu, C.S., Wu-Chou, Y.H., Van Doeselaar, M., Simons, E.J., Chang, H.C., et al. (2008). **The LRRK2 Arg1628Pro variant is a risk factor for Parkinson's disease in the Chinese population**. *Neurogenetics 9*, 271–276. DOI: 10.1007/s10048-008-0140-6.

Lu, Q., Insinna, C., Ott, C., Stauffer, J., Pintado, P.A., et al. (2015). **Early steps in primary cilium assembly require EHD1/EHD3-dependent ciliary vesicle formation**. *Nat. Cell Biol. 17*, 228–240. DOI: 10.1038/ncb3109.

Luzón-Toro, B., de la Torre, E.R., Delgado, A., Pérez-Tur, J., and Hilfiker, S. (2007). **Mechanistic insight into the dominant mode of the Parkinson's disease-associated G2019S LRRK2 mutation**. *Hum. Mol. Genet. 16*, 2031–2039. DOI: 10.1093/hmg/ddm151.

Lv, P., Sheng, Y., Zhao, Z., Zhao, W., Gu, L., et al. (2015). **Targeted disruption of Rab10 causes early embryonic lethality**. *Protein Cell 6*, 463–467. DOI: 10.1007/s13238-015-0150-8.

MacLeod, D.A., Rhinn, H., Kuwahara, T., Zolin, A., Di Paolo, G., et al. (2013). **RAB7L1 Interacts with LRRK2 to Modify Intraneuronal Protein Sorting and Parkinson's Disease Risk**. *Neuron 77*, 425–439. DOI: 10.1016/j.neuron.2012.11.033.

Madero-Pérez, J., Fdez, E., Fernández, B., Lara Ordóñez, A.J., Blanca Ramírez, M., et al. (2017). **Cellular effects mediated by pathogenic LRRK2: Homing in on Rab-mediated processes**. *Biochem. Soc. Trans. 45* DOI: 10.1042/BST20160392.

Madero-Pérez, J., Fdez, E., Fernández, B., Lara Ordóñez, A.J., Blanca Ramírez, M., et al. (2018a). **Parkinson disease-associated mutations in LRRK2 cause centrosomal defects via Rab8a phosphorylation**. *Mol. Neurodegener. 13* DOI: 10.1186/s13024-018-0235-y.

Madero-Pérez, J., Fernández, B., Lara Ordóñez, A.J., Fdez, E., Lobbestael, E., et al. (2018b). **RAB7L1-mediated relocalization of LRRK2 to the golgi complex causes centrosomal deficits via RAB8A**. *Front. Mol. Neurosci. 11* DOI: 10.3389/fnmol.2018.00417.

Madureira, M., Connor-Robson, N., and Wade-Martins, R. (2020). **"LRRK2: Autophagy and Lysosomal Activity."** *Front. Neurosci. 14*, 498. DOI: 10.3389/fnins.2020.00498.

Maiese, K., Li, F., Chong, Z.Z., and Shang, Y.C. (2008). **The Wnt signaling pathway: Aging gracefully as a protectionist?**. *Pharmacol. Ther. 118*, 58–81. DOI: 10.1016/j.pharmthera.2008.01.004.

Di Maio, R., Hoffman, E.K., Rocha, E.M., Keeney, M.T., Sanders, L.H., et al. (2018). **LRRK2 activation in idiopathic Parkinson's disease**. *Sci. Transl. Med. 10*, 5429. DOI: 10.1126/scitranslmed.aar5429.

Manzoni, C., Denny, P., Lovering, R.C., and Lewis, P.A. (2015). **Computational analysis of the LRRK2 interactome**. *PeerJ 2015* DOI: 10.7717/peerj.778.

Marchand, A., Drouyer, M., Sarchione, A., Chartier-Harlin, M.C., and Taymans, J.M. (2020). **LRRK2 Phosphorylation, More Than an Epiphenomenon**. *Front. Neurosci. 14*, 527. DOI: 10.3389/fnins.2020.00527.

Marley, A., and von Zastrow, M. (2010). **DISC1 regulates primary cilia that display specific dopamine receptors**. *PLoS One 5* DOI: 10.1371/journal.pone.0010902.

Martin, I., Kim, J.W., Lee, B.D., Kang, H.C., Xu, J.C., et al. (2014). **Ribosomal protein s15 phosphorylation mediates LRRK2 neurodegeneration in parkinson's disease**. *Cell 157*, 472–485. DOI: 10.1016/j.cell.2014.01.064.

Mata, I.F., Davis, M.Y., Lopez, A.N., Dorschner, M.O., Martinez, E., et al. (2016). **The discovery of LRRK2 p.R1441S, a novel mutation for Parkinson's disease, adds to the complexity of a mutational hotspot**. *Am. J. Med. Genet. Part B Neuropsychiatr. Genet. 171*, 925–930. DOI: 10.1002/ajmg.b.32452.

Mata, I.F., Kachergus, J.M., Taylor, J.P., Lincoln, S., Aasly, J., et al. (2005). **Lrrk2 pathogenic substitutions in Parkinson's disease**. *Neurogenetics 6*, 171–177. DOI: 10.1007/s10048-005-0005-1.

Matsui, T., and Fukuda, M. (2013). **Rab12 regulates mTORC1 activity and autophagy through controlling the degradation of amino-acid transporter PAT4**. *EMBO Rep. 14*, 450–457. DOI: 10.1038/embor.2013.32.

Matsui, T., Itoh, T., and Fukuda, M. (2011). **Small GTPase Rab12 regulates constitutive degradation of transferrin receptor**. *Traffic 12*, 1432–1443. DOI: 10.1111/j.1600-0854.2011.01240.x.

Matsui, T., Noguchi, K., and Fukuda, M. (2014). **Dennd3 functions as a guanine nucleotide exchange factor for small GTpase Rab12 in mouse embryonic fibroblasts**. *J. Biol. Chem. 289*, 13986–13995. DOI: 10.1074/jbc.M113.546689.

Matsumine, H., Saito, M., Shimoda-Matsubayashi, S., Tanaka, H., Ishikawa, A., et al. (1997). **Localization of a gene for an autosomal recessive form of juvenile parkinsonism to chromosome 6q25.2-27**. *Am. J. Hum. Genet. 60*, 588–596.

Matta, S., Van Kolen, K., da Cunha, R., van den Bogaart, G., Mandemakers, W., et al. (2012). **LRRK2 Controls an EndoA Phosphorylation Cycle in Synaptic Endocytosis**. *Neuron 75*, 1008–1021. DOI: 10.1016/j.neuron.2012.08.022.

Mazo, G., Soplop, N., Wang, W.J., Uryu, K., and Tsou, M.F.B. (2016). **Spatial Control of Primary Ciliogenesis by Subdistal Appendages Alters Sensation-Associated Properties of Cilia**. *Dev. Cell 39*, 424–437. DOI: 10.1016/j.devcel.2016.10.006.

McGlashan, S.R., Knight, M.M., Chowdhury, T.T., Joshi, P., Jensen, C.G., et al. (2010). **Mechanical loading modulates chondrocyte primary cilia incidence and length.** *Cell Biol. Int. 34*, 441–446. DOI: 10.1042/CBI20090094.

McGrath, E., Waschbüsch, D., Baker, B.M., and Khan, A.R. (2021). **LRRK2 binds to the Rab32 subfamily in a GTP-dependent manner via its armadillo domain**. *Small GTPases 12*, 133–146. DOI: 10.1080/21541248.2019.1666623.

Meka, D.P., Scharrenberg, R., and Calderon de Anda, F. (2020). **Emerging roles of the centrosome in neuronal development**. *Cytoskeleton 77*, 84–96. DOI: 10.1002/cm.21593.

van der Merwe, C., Jalali Sefid Dashti, Z., Christoffels, A., Loos, B., and Bardien, S. (2015). **Evidence for a common biological pathway linking three Parkinson's disease-causing genes: Parkin, PINK1 and DJ-1**. *Eur. J. Neurosci. 41*, 1113–1125. DOI: 10.1111/ejn.12872.

Mir, R., Tonelli, F., Lis, P., Macartney, T., Polinski, N.K., et al. (2018). **The Parkinson's disease VPS35[D620N] mutation enhances LRRK2-mediated Rab protein phosphorylation in mouse and human**. *Biochem. J. 475*, 1861–1883. DOI: 10.1042/BCJ20180248.

Mirvis, M., Siemers, K.A., Nelson, W.J., and Stearns, T.P. (2019). **Primary cilium loss in mammalian cells occurs predominantly by whole-cilium shedding**. *PLoS Biol. 17* DOI: 10.1371/journal.pbio.3000381.

Mirvis, M., Stearns, T., and Nelson, W.J. (2018). **Cilium structure, assembly, and disassembly regulated by the cytoskeleton**. *Biochem. J. 475*, 2329–2353. DOI: 10.1042/BCJ20170453.

Mohan, M., and Mellick, G.D. (2017). **Role of the VPS35 D620N mutation in Parkinson's disease**. *Park. Relat. Disord. 36*, 10–18. DOI: 10.1016/j.parkreldis.2016.12.001.

Monfrini, E., and Di Fonzo, A. (2017). Leucine-rich repeat kinase (LRRK2) genetics and parkinson's disease. In: Advances in Neurobiology, Springer New York LLC, 3–30 DOI: 10.1007/978-3-319-49969-7_1.

Muda, K., Bertinetti, D., Gesellchen, F., Hermann, J.S., Von Zweydorf, F., et al. (2014). **Parkinson-related LRRK2 mutation R1441C/G/H impairs PKA phosphorylation of LRRK2 and disrupts its interaction with 14-3-3**. *Proc. Natl. Acad. Sci. U. S. A. 111* DOI: 10.1073/pnas.1312701111.

Nachury, M. V, Loktev, A. V, Zhang, Q., Westlake, C.J., Peränen, J., et al. (2007). **A core complex of BBS proteins cooperates with the GTPase Rab8 to promote ciliary membrane biogenesis.** *Cell 129*, 1201–1213. DOI: 10.1016/j.cell.2007.03.053.

Nalls, M.A., Blauwendraat, C., Vallerga, C.L., Heilbron, K., Bandres-Ciga, S., et al. (2019). **Identification of novel risk loci, causal insights, and heritable risk for Parkinson's disease: a meta-analysis of genome-wide association studies**. *Lancet Neurol. 18*, 1091–1102. DOI: 10.1016/S1474-4422(19)30320-5.

Newhouse, K., Hsuan, S.L., Chang, S.H., Cai, B., Wang, Y., et al. (2004). **Rotenone-induced apoptosis is mediated by p38 and JNK MAP kinases in human dopaminergic SH-SY5Y cells**. *Toxicol. Sci. 79*, 137–146. DOI: 10.1093/toxsci/kfh089.

Nguyen, A.P.T., Tsika, E., Kelly, K., Levine, N., Chen, X., et al. (2020). **Dopaminergic neurodegeneration induced by Parkinson's disease-linked G2019S LRRK2 is dependent on kinase and GTPase activity**. *Proc. Natl. Acad. Sci. U. S. A. 117*, 17296–17307. DOI: 10.1073/pnas.1922184117.

Nichols, R.J., Dzamko, N., Morrice, N.A., Campbell, D.G., Deak, M., et al. (2010). **14-3-3 Binding to LRRK2 is disrupted by multiple Parkinson's disease-associated mutations and regulates cytoplasmic localization**. *Biochem. J. 430*, 393–404. DOI: 10.1042/BJ20100483.

Nigg, E.A., and Stearns, T. (2011). **The centrosome cycle: Centriole biogenesis, duplication and inherent asymmetries**. *Nat. Cell Biol. 13*, 1154–1160. DOI: 10.1038/ncb2345.

Nixon-Abell, J., Berwick, D.C., Grannó, S., Spain, V.A., Blackstone, C., et al. (2016). **Protective LRRK2 R1398H variant enhances GTPase and Wnt signaling activity**. *Front. Mol. Neurosci. 9* DOI: 10.3389/fnmol.2016.00018.

O'sullivan, M.J., and Lindsay, A.J. (2020). **The endosomal recycling pathway—at the crossroads of the cell**. *Int. J. Mol. Sci. 21*, 1–21. DOI: 10.3390/ijms21176074.

Obeso, J.A., Stamelou, M., Goetz, C.G., Poewe, W., Lang, A.E., et al. (2017). **Past, present, and future of Parkinson's disease: A special essay on the 200th Anniversary of the Shaking Palsy**. *Mov. Disord. 32*, 1264–1310. DOI: 10.1002/mds.27115.

Ohta, M., Ashikawa, T., Nozaki, Y., Kozuka-Hata, H., Goto, H., et al. (2014). **Direct interaction of Plk4 with STIL ensures formation of a single procentriole per parental centriole**. *Nat. Commun. 5*, 5267. DOI: 10.1038/ncomms6267.

Orenstein, S.J., Kuo, S.H., Tasset, I., Arias, E., Koga, H., et al. (2013). **Interplay of LRRK2 with chaperone-mediated autophagy**. *Nat. Neurosci. 16*, 394–406. DOI: 10.1038/nn.3350.

Ouyang, M., and Shen, X. (2006). **Critical role of ASK1 in the 6-hydroxydopamine-induced apoptosis in human neuroblastoma SH-SY5Y cells**. *J. Neurochem. 97*, 234–244. DOI: 10.1111/j.1471-4159.2006.03730.x.

Ozelius, L.J., Senthil, G., Saunders-Pullman, R., Ohmann, E., Deligtisch, A., et al. (2006). **LRRK2 G2019S as a cause of Parkinson's disease in Ashkenazi Jews**. *N. Engl. J. Med. 354*, 424–425. DOI: 10.1056/NEJMc055509.

Paisán-Ruíz, C., Jain, S., Evans, E.W., Gilks, W.P., Simón, J., et al. (2004). **Cloning of the gene containing mutations that cause PARK8-linked Parkinson's disease**. *Neuron 44*, 595–600. DOI: 10.1016/j.neuron.2004.10.023.

Pala, R., Alomari, N., and Nauli, S.M. (2017). **Primary cilium-dependent signaling mechanisms**. *Int. J. Mol. Sci. 18* DOI: 10.3390/ijms18112272.

Pankratz, N., Pauciulo, M.W., Elsaesser, V.E., Marek, D.K., Halter, C.A., et al. (2006). **Mutations in DJ-1 are rare in familial Parkinson disease**. *Neurosci. Lett. 408*, 209–213. DOI: 10.1016/j.neulet.2006.09.003.

Parkinson, J. (1817). **An Essay on the Shaking Palsy**. *London Print. by Whittingham Rowl. Sherwood, Neely Jones*.

Pascale, E., di Battista, M.E., Rubino, A., Purcaro, C., Valente, M., et al. (2016). **Genetic architecture of MAPT gene region in parkinson disease subtypes**. *Front. Cell. Neurosci. 10* DOI: 10.3389/fncel.2016.00096.

Peng, J., Mao, X.O., Stevenson, F.F., Hsu, M., and Andersen, J.K. (2004). **The herbicide paraquat induces dopaminergic nigral apoptosis through sustained activation of the JNK pathway**. *J. Biol. Chem. 279*, 32626–32632. DOI: 10.1074/jbc.M404596200.

Peränen, J. (2011). **Rab8 GTPase as a regulator of cell shape**. *Cytoskeleton 68*, 527–539. DOI: 10.1002/cm.20529.

Perera, G., Ranola, M., Rowe, D.B., Halliday, G.M., and Dzamko, N. (2016). **Inhibitor treatment of peripheral mononuclear cells from Parkinson's disease patients further validates LRRK2 dephosphorylation as a pharmacodynamic biomarker**. *Sci. Rep. 6* DOI: 10.1038/srep31391.

Pérez-Victoria, F.J., Mardones, G.A., and Bonifacino, J.S. (2008). **Requirement of the human GARP complex for mannose 6-phosphate-receptor- dependent sorting of cathepsin D to lysosomes**. *Mol. Biol. Cell 19*, 2350–2362. DOI: 10.1091/mbc.E07-11-1189.

Phan, S., Boassa, D., Nguyen, P., Wan, X., Lanman, J., et al. (2017). **3D reconstruction of biological structures: automated procedures for alignment and reconstruction of multiple tilt series in electron tomography**. *Adv. Struct. Chem. Imaging 2* DOI: 10.1186/s40679-016-0021-2.

Plotegher, N., Greggio, E., Bisaglia, M., and Bubacco, L. (2014). **Biophysical groundwork as a hinge to unravel the biology of α-synuclein aggregation and toxicity**. *Q. Rev. Biophys. 47*, 1–48. DOI: 10.1017/S0033583513000097.

Plotnikova, O. V., Pugacheva, E.N., and Golemis, E.A. (2009). Primary Cilia and the Cell Cycle. In: Methods in Cell Biology, 137–160 DOI: 10.1016/S0091-679X(08)94007-3.

Poewe, W., Seppi, K., Tanner, C.M., Halliday, G.M., Brundin, P., et al. (2017). **Parkinson disease**. *Nat. Rev. Dis. Prim. 3*, 1–21. DOI: 10.1038/nrdp.2017.13.

Polymeropoulos, M.H., Higgins, J.J., Golbe, L.I., Johnson, W.G., Ide, S.E., et al. (1996). **Mapping of a gene for Parkinson's disease to chromosome 4q21-q23**. *Science (80-.). 274*, 1197–1199. DOI: 10.1126/science.274.5290.1197.

Polymeropoulos, M.H., Lavedan, C., Leroy, E., Ide, S.E., Dehejia, A., et al. (1997). **Mutation in the α-synuclein gene identified in families with Parkinson's disease**. *Science (80-.). 276*, 2045–2047. DOI: 10.1126/science.276.5321.2045.

Postuma, R.B., Aarsland, D., Barone, P., Burn, D.J., Hawkes, C.H., et al. (2012). **Identifying prodromal Parkinson's disease: Pre-Motor disorders in Parkinson's disease**. *Mov. Disord. 27*, 617–626. DOI: 10.1002/mds.24996.

Priya, A., Kalaidzidis, I. V., Kalaidzidis, Y., Lambright, D., and Datta, S. (2015). **Molecular Insights into Rab7-Mediated Endosomal Recruitment of Core Retromer: Deciphering the Role of Vps26 and Vps35**. *Traffic 16*, 68–84. DOI: 10.1111/tra.12237.

Pungaliya, P.P., Bai, Y., Lipinski, K., Anand, V.S., Sen, S., et al. (2010). **Identification and Characterization of a Leucine-Rich Repeat Kinase 2 (LRRK2) Consensus Phosphorylation Motif**. *PLoS One 5*, e13672. DOI: 10.1371/journal.pone.0013672.

Purlyte, E., Dhekne, H.S., Sarhan, A.R., Gomez, R., Lis, P., et al. (2018). **Rab29 activation of the Parkinson's disease-associated LRRK2 kinase**. *EMBO J. 37*, 1–18. DOI: 10.15252/embj.201798099.

Rahajeng, J. (2010). **Important relationships between Rab and MICAL proteins in endocytic trafficking**. *World J. Biol. Chem. 1*, 254. DOI: 10.4331/wjbc.v1.i8.254.

Ramsden, N., Perrin, J., Ren, Z., Lee, B.D., Zinn, N., et al. (2011). **Chemoproteomics-based design of potent LRRK2-selective lead compounds that attenuate Parkinson's disease-related toxicity in human neurons**. *ACS Chem. Biol. 6*, 1021–1028. DOI: 10.1021/cb2002413.

Rawal, N., Corti, O., Sacchetti, P., Ardilla-Osorio, H., Sehat, B., et al. (2009). **Parkin protects dopaminergic neurons from excessive Wnt/β-catenin signaling**. *Biochem. Biophys. Res. Commun. 388*, 473–478. DOI: 10.1016/j.bbrc.2009.07.014.

Reiter, J.F., and Leroux, M.R. (2017). **Genes and molecular pathways underpinning ciliopathies**. *Nat. Rev. Mol. Cell Biol. 18*, 533–547. DOI: 10.1038/nrm.2017.60.

Reith, A.D., Bamborough, P., Jandu, K., Andreotti, D., Mensah, L., et al. (2012). **GSK2578215A; A potent and highly selective 2-arylmethyloxy-5-substitutent- N-arylbenzamide LRRK2 kinase inhibitor**. *Bioorganic Med. Chem. Lett. 22*, 5625–5629. DOI: 10.1016/j.bmcl.2012.06.104.

Reyniers, L., Del Giudice, M.G., Civiero, L., Belluzzi, E., Lobbestael, E., et al. (2014). **Differential protein-protein interactions of LRRK1 and LRRK2 indicate roles in distinct cellular signaling pathways.** *J. Neurochem. 131*, 239–250. DOI: 10.1111/jnc.12798.

Reynolds, A., Doggett, E.A., Riddle, S.M., Lebakken, C.S., and Jeremy Nichols, R. (2014). **LRRK2 kinase activity and biology are not uniformly predicted by its autophosphorylation and cellular phosphorylation site status**. *Front. Mol. Neurosci. 7* DOI: 10.3389/fnmol.2014.00054.

Rideout, H.J., Chartier-Harlin, M.C., Fell, M.J., Hirst, W.D., Huntwork-Rodriguez, S., et al. (2020). **The Current State-of-the Art of LRRK2-Based Biomarker Assay Development in Parkinson's Disease**. *Front. Neurosci. 14* DOI: 10.3389/fnins.2020.00865.

Rink, J., Ghigo, E., Kalaidzidis, Y., and Zerial, M. (2005). **Rab conversion as a mechanism of progression from early to late endosomes**. *Cell 122*, 735–749. DOI: 10.1016/j.cell.2005.06.043.

Rivero-Ríos, P., Romo-Lozano, M., Fasiczka, R., Naaldijk, Y., and Hilfiker, S. (2020a). **LRRK2-Related Parkinson's Disease Due to Altered Endolysosomal Biology With Variable Lewy Body Pathology: A Hypothesis**. *Front. Neurosci. 14* DOI: 10.3389/fnins.2020.00556.

Rivero-Ríos, P., Romo-Lozano, M., Fernández, B., Fdez, E., and Hilfiker, S. (2020b). **Distinct Roles for RAB10 and RAB29 in Pathogenic LRRK2-Mediated Endolysosomal Trafficking Alterations**. *Cells 9* DOI: 10.3390/cells9071719.

Rivero-Ríos, P., Romo-Lozano, M., Madero-Pérez, J., Thomas, A.P., Biosa, A., et al. (2019). **The G2019S variant of leucine-rich repeat kinase 2 (LRRK2) alters endolysosomal trafficking by impairing the function of the GTPase RAB8A**. *J. Biol. Chem. 294*, 4738–4758. DOI: 10.1074/jbc.RA118.005008.

Rojas, R., Van Vlijmen, T., Mardones, G.A., Prabhu, Y., Rojas, A.L., et al. (2008). **Regulation of retromer recruitment to endosomes by sequential action of Rab5 and Rab7**. *J. Cell Biol. 183*, 513–526. DOI: 10.1083/jcb.200804048.

Roosen, D.A., and Cookson, M.R. (2016). **LRRK2 at the interface of autophagosomes, endosomes and lysosomes**. *Mol. Neurodegener. 11*, 1–10. DOI: 10.1186/s13024-016-0140-1.

Ross, O.A., Soto-Ortolaza, A.I., Heckman, M.G., Aasly, J.O., Abahuni, N., et al. (2011). **Association of LRRK2 exonic variants with susceptibility to Parkinson's disease: A case-control study**. *Lancet Neurol. 10*, 898–908. DOI: 10.1016/S1474-4422(11)70175-2.

Ross, O.A., Wu, Y.R., Lee, M.C., Funayama, M., Chen, M.L., et al. (2008). **Analysis of Lrrk2 R1628P as a risk factor for Parkinson's disease**. *Ann. Neurol. 64*, 88–92. DOI: 10.1002/ana.21405.

Royle, S.J. (2011). **Mitotic Moonlighting Functions for Membrane Trafficking Proteins**. *Traffic 12*, 791–798. DOI: 10.1111/j.1600-0854.2011.01184.x.

Rozés-Salvador, V., González-Billault, C., and Conde, C. (2020). **The Recycling Endosome in Nerve Cell Development: One Rab to Rule Them All?**. *Front. Cell Dev. Biol. 8* DOI: 10.3389/fcell.2020.603794.

Rudenko, I.N., Kaganovich, A., Hauser, D.N., Beylina, A., Chia, R., et al. (2012). **The G2385R variant of leucine-rich repeat kinase 2 associated with Parkinson's disease is a partial loss-of-function mutation**. *Biochem. J. 446*, 99–111. DOI: 10.1042/BJ20120637.

Salašová, A., Yokota, C., Potěšil, D., Zdráhal, Z., Bryja, V., et al. (2017). **A proteomic analysis of LRRK2 binding partners reveals interactions with multiple signaling components of the WNT/PCP pathway**. *Mol. Neurodegener. 12*, 1–19. DOI: 10.1186/s13024-017-0193-9.

Saporito, M.S., Thomas, B.A., and Scott, R.W. (2000). **MPTP activates c-Jun NH2-terminal kinase (JNK) and its upstream regulatory kinase MKK4 in nigrostriatal neurons in vivo**. *J. Neurochem. 75*, 1200–1208. DOI: 10.1046/j.1471-4159.2000.0751200.x.

Sassone, J., Reale, C., Dati, G., Regoni, M., Pellecchia, M.T., et al. (2020). **The Role of VPS35 in the Pathobiology of Parkinson's Disease**. *Cell. Mol. Neurobiol. 41*, 199–227. DOI: 10.1007/s10571-020-00849-8.

Satake, W., Nakabayashi, Y., Mizuta, I., Hirota, Y., Ito, C., et al. (2009). **Genome-wide association study identifies common variants at four loci as genetic risk factors for Parkinson's disease**. *Nat. Genet. 41*, 1303–1307. DOI: 10.1038/ng.485.

Sato, T., Iwano, T., Kunii, M., Matsuda, S., Mizuguchi, R., et al. (2014). **Rab8a and Rab8b are essential for several apical transport pathways but insufficient for ciliogenesis.** *J. Cell Sci. 127*, 422–431. DOI: 10.1242/jcs.136903.

Sauerbier, A., Aris, A., Lim, E.W., Bhattacharya, K., and Chaudhuri, K.R. (2018). **Impact of ethnicity on the natural history of parkinson disease**. *Med. J. Aust. 208*, 410–414. DOI: 10.5694/mja17.01074.

Saunders-Pullman, R., Barrett, M.J., Stanley, K.M., Luciano, M.S., Shanker, V., et al. (2010). **LRRK2 G2019S mutations are associated with an increased cancer risk in Parkinson disease**. *Mov. Disord. 25*, 2536–2541. DOI: 10.1002/mds.23314.

Schapansky, J., Khasnavis, S., DeAndrade, M.P., Nardozzi, J.D., Falkson, S.R., et al. (2018). **Familial knockin mutation of LRRK2 causes lysosomal dysfunction and accumulation of endogenous insoluble α-synuclein in neurons**. *Neurobiol. Dis. 111*, 26–35. DOI: 10.1016/j.nbd.2017.12.005.

Schaub, J.R., and Stearns, T. (2013). **The Rilp-like proteins Rilpl1 and Rilpl2 regulate ciliary membrane content**. *Mol. Biol. Cell 24*, 453–464. DOI: 10.1091/mbc.e12-08-0598.

Schindler, C., Chen, Y., Pu, J., Guo, X., and Bonifacino, J.S. (2015). **EARP is a multisubunit tethering complex involved in endocytic recycling**. *Nat. Cell Biol. 17*, 639–650. DOI: 10.1038/ncb3129.

Schlossmacher, M.G., and Mollenhauer, B. (2010). **Biomarker research in Parkinsons disease: Objective measures needed for patient stratification in future cause-directed trials**. *Biomark. Med. 4*, 647–650. DOI: 10.2217/bmm.10.93.

Schmidt, T.I., Kleylein-Sohn, J., Westendorf, J., Le Clech, M., Lavoie, S.B., et al. (2009). **Control of Centriole Length by CPAP and CP110**. *Curr. Biol. 19*, 1005–1011. DOI: 10.1016/j.cub.2009.05.016.

Seaman, M.N.J. (2012). **The retromer complex-endosomal protein recycling and beyond**. *J. Cell Sci. 125*, 4693–4702. DOI: 10.1242/jcs.103440.

Seaman, M.N.J., Harbour, M.E., Tattersall, D., Read, E., and Bright, N. (2009). **Membrane recruitment of the cargo-selective retromer subcomplex is catalysed by the small GTPase Rab7 and inhibited by the Rab-GAP TBC1D5**. *J. Cell Sci. 122*, 2371–2382. DOI: 10.1242/jcs.048686.

Seaman, M.N.J., McCaffery, J.M., and Emr, S.D. (1998). **A membrane coat complex essential for endosome-to-Golgi retrograde transport in yeast**. *J. Cell Biol. 142*, 665–681. DOI: 10.1083/jcb.142.3.665.

Sellier, C., Campanari, M., Julie Corbier, C., Gaucherot, A., Kolb-Cheynel, I., et al. (2016). **Loss of C9ORF72 impairs autophagy and synergizes with polyQ Ataxin-2 to induce motor neuron dysfunction and cell death**. *EMBO J. 35*, 1276–1297. DOI: 10.15252/embj.201593350.

Sepulveda, B., Mesias, R., Li, X., Yue, Z., and Benson, D.L. (2013). **Short- and long-term effects of LRRK2 on axon and dendrite growth.** *PLoS One 8*, e61986. DOI: 10.1371/journal.pone.0061986.

Seto, S., Tsujimura, K., and Koide, Y. (2011). **Rab GTPases Regulating Phagosome Maturation Are Differentially Recruited to Mycobacterial Phagosomes**. *Traffic 12*, 407–420. DOI: 10.1111/j.1600-0854.2011.01165.x.

Sharma, M., Giridharan, S.S.P., Rahajeng, J., Naslavsky, N., and Caplan, S. (2009). **MICAL-L1 links EHD1 to tubular recycling endosomes and regulates receptor recycling**. *Mol. Biol. Cell 20*, 5181–5194. DOI: 10.1091/mbc.E09-06-0535.

Sharma, M., Ioannidis, J.P.A., Aasly, J.O., Annesi, G., Brice, A., et al. (2012). **A multi-centre clinico-genetic analysis of the VPS35 gene in Parkinson disease indicates reduced penetrance for disease-associated variants**. *J. Med. Genet. 49*, 721–726. DOI: 10.1136/jmedgenet-2012-101155.

Sheng, Z., Zhang, S., Bustos, D., Kleinheinz, T., Le Pichon, C.E., et al. (2012). **Ser1292 autophosphorylation is an indicator of LRRK2 kinase activity and contributes to the cellular effects of PD mutations.** *Sci. Transl. Med. 4* DOI: 10.1126/scitranslmed.3004485.

Shin, N., Jeong, H., Kwon, J., Heo, H.Y., Kwon, J.J., et al. (2008). **LRRK2 regulates synaptic vesicle endocytosis**. *Exp. Cell Res. 314*, 2055–2065. DOI: 10.1016/j.yexcr.2008.02.015.

Shinde, S.R., and Maddika, S. (2016). **PTEN modulates EGFR late endocytic trafficking and degradation by dephosphorylating Rab7**. *Nat. Commun. 7* DOI: 10.1038/ncomms10689.

Shu, X., Lev-Ram, V., Deerinck, T.J., Qi, Y., Ramko, E.B., et al. (2011). **A genetically encoded tag for correlated light and electron microscopy of intact cells, tissues, and organisms**. *PLoS Biol. 9* DOI: 10.1371/journal.pbio.1001041.

Shu, Y., Ming, J., Zhang, P., Wang, Q., Jiao, F., et al. (2016). **Parkinson-related LRRK2 mutation R1628P enables Cdk5 phosphorylation of LRRK2 and upregulates its kinase activity**. *PLoS One 11* DOI: 10.1371/journal.pone.0149739.

Shulman, J.M., De Jager, P.L., and Feany, M.B. (2011). **Parkinson's disease: Genetics and pathogenesis**. *Annu. Rev. Pathol. Mech. Dis. 6*, 193–222. DOI: 10.1146/annurev-pathol-011110-130242.

Simón-Sánchez, J., Schulte, C., Bras, J.M., Sharma, M., Gibbs, J.R., et al. (2009). **Genome-wide association study reveals genetic risk underlying Parkinson's disease**. *Nat. Genet. 41*, 1308–1312. DOI: 10.1038/ng.487.

Sipos, É., Komoly, S., and Ács, P. (2018). **Quantitative Comparison of Primary Cilia Marker Expression and Length in the Mouse Brain.** *J. Mol. Neurosci. 64*, 397–409. DOI: 10.1007/s12031-018-1036-z.

van der Sluijs, P., Hull, M., Huber, L.A., Mâle, P., Goud, B., et al. (1992). **Reversible phosphorylation-dephosphorylation determines the localization of rab4 during the cell cycle.** *EMBO J. 11*, 4379–4389.

Smith, W.W., Pei, Z., Jiang, H., Moore, D.J., Liang, Y., et al. (2005). **Leucine-rich repeat kinase 2 (LRRK2) interacts with parkin, and mutant LRRK2 induces neuronal degeneration**. *Proc. Natl. Acad. Sci. U. S. A. 102*, 18676–18681. DOI: 10.1073/pnas.0508052102.

Sobu, Y., Wawro, P.S., Dhekne, H.S., Yeshaw, W.M., and Pfeffer, S.R. (2021). **Pathogenic LRRK2 regulates ciliation probability upstream of tau tubulin kinase 2 via Rab10 and RILPL1 proteins**. *Proc. Natl. Acad. Sci. U. S. A. 118* DOI: 10.1073/pnas.2005894118.

Sönnichsen, B., De Renzis, S., Nielsen, E., Rietdorf, J., and Zerial, M. (2000). **Distinct membrane domains on endosomes in the recycling pathway visualized by multicolor imaging of Rab4, Rab5, and Rab11**. *J. Cell Biol. 149*, 901–913. DOI: 10.1083/jcb.149.4.901.

Srinivasan, R., Henley, B.M., Henderson, B.J., Indersmitten, T., Cohen, B.N., et al. (2016). **Smoking-relevant nicotine concentration attenuates the unfolded protein response in dopaminergic neurons**. *J. Neurosci. 36*, 65–79. DOI: 10.1523/JNEUROSCI.2126-15.2016.

Steger, M., Diez, F., Dhekne, H.S., Lis, P., Nirujogi, R.S., et al. (2017). **Systematic proteomic analysis of LRRK2-mediated Rab GTPase phosphorylation establishes a connection to ciliogenesis.** *Elife 6* DOI: 10.7554/eLife.31012.

Steger, M., Tonelli, F., Ito, G., Davies, P., Trost, M., et al. (2016). **Phosphoproteomics reveals that Parkinson's disease kinase LRRK2 regulates a subset of Rab GTPases**. *Elife 5* DOI: 10.7554/eLife.12813.

Stenmark, H. (2009). **Rab GTPases as coordinators of vesicle traffic**. *Nat. Rev. Mol. Cell Biol. 10*, 513–525. DOI: 10.1038/nrm2728.

Struhal, W., Presslauer, S., Spielberger, S., Zimprich, A., Auff, E., et al. (2014). **VPS35 Parkinson's disease phenotype resembles the sporadic disease**. *J. Neural Transm. 121*, 755–759. DOI: 10.1007/s00702-014-1179-1.

Sullenberger, C., Vasquez-Limeta, A., Kong, D., and Loncarek, J. (2020). **With Age Comes Maturity: Biochemical and Structural Transformation of a Human Centriole in the Making**. *Cells 9*, 1429. DOI: 10.3390/cells9061429.

Sun, Y., Bilan, P.J., Liu, Z., and Klip, A. (2010). **Rab8A and Rab13 are activated by insulin and regulate GLUT4 translocation in muscle cells**. *Proc. Natl. Acad. Sci. U. S. A. 107*, 19909–19914. DOI: 10.1073/pnas.1009523107.

Szatmári, Z. (2018). RAB Family. In: Encyclopedia of Signaling Molecules, Springer International Publishing, 4343–4349 DOI: 10.1007/978-3-319-67199-4_101912.

Takeda, Y., Kuroki, K., Chinen, T., and Kitagawa, D. (2020). **Centrosomal and non-centrosomal functions emerged through eliminating centrosomes**. *Cell Struct. Funct. 45*, 57–64. DOI: 10.1247/csf.20007.

Tan, E.K., Peng, R., Teo, Y.Y., Tan, L.C., Angeles, D., et al. (2010). **Multiple LRRK2 variants modulate risk of Parkinson disease: A Chinese multicenter study**. *Hum. Mutat. 31*, 561–568. DOI: 10.1002/humu.21225.

Tan, E.K., Tan, L.C., Lim, H.Q., Li, R., Tang, M., et al. (2008). **LRRK2 R1628P increases risk of Parkinson's disease: Replication evidence**. *Hum. Genet. 124*, 287–288. DOI: 10.1007/s00439-008-0544-2.

Taylor, J.P., Hulihan, M.M., Kachergus, J.M., Melrose, H.L., Lincoln, S.J., et al. (2007). **Leucine-rich repeat kinase 1: A paralog of LRRK2 and a candidate gene for Parkinson's disease**. *Neurogenetics 8*, 95–102. DOI: 10.1007/s10048-006-0075-8.

Taylor, M., and Alessi, D.R. (2020). **Advances in elucidating the function of leucine-rich repeat protein kinase-2 in normal cells and Parkinson's disease**. *Curr. Opin. Cell Biol. 63*, 102–113. DOI: 10.1016/j.ceb.2020.01.001.

Taymans, J.-M., Vancraenenbroeck, R., Ollikainen, P., Beilina, A., Lobbestael, E., et al. (2011). **LRRK2 Kinase Activity Is Dependent on LRRK2 GTP Binding Capacity but Independent of LRRK2 GTP Binding**. *PLoS One 6*, e23207. DOI: 10.1371/journal.pone.0023207.

Taymans, J.M., Mutez, E., Drouyer, M., Sibran, W., and Chartier-Harlin, M.C. (2017). **LRRK2 detection in human biofluids: Potential use as a Parkinson's disease biomarker?** *Biochem. Soc. Trans. 45*, 207–212. DOI: 10.1042/BST20160334.

Thadathil, N., Xiao, J., Hori, R., Alway, S.E., and Khan, M.M. (2020). **Brain Selective Estrogen Treatment Protects Dopaminergic Neurons and Preserves Behavioral Function in MPTP-induced Mouse Model of Parkinson's Disease**. *J. Neuroimmune Pharmacol.* 1–12. DOI: 10.1007/s11481-020-09972-1.

Thirstrup, K., Dächsel, J.C., Oppermann, F.S., Williamson, D.S., Smith, G.P., et al. (2017). **Selective LRRK2 kinase inhibition reduces phosphorylation of endogenous Rab10 and Rab12 in human peripheral mononuclear blood cells.** *Sci. Rep. 7*, 10300. DOI: 10.1038/s41598-017-10501-z.

del Toro, D., Alberch, J., Lazaro-Dieguez, F., Martin-Ibaflez, R., Xifro, X., et al. (2009). **Mutant huntingtin impairs post-golgi trafficking to lysosomes by delocalizing optineurin/rab8 complex from the golgi apparatus**. *Mol. Biol. Cell 20*, 1478–1492. DOI: 10.1091/mbc.E08-07-0726.

Touchot, N., Chardin, P., and Tavitian, A. (1987). **Four additional members of the ras gene superfamily isolated by an oligonucleotide strategy: molecular cloning of YPT-related cDNAs from a rat brain library.** *Proc. Natl. Acad. Sci. U. S. A. 84*, 8210–8214. DOI: 10.1073/pnas.84.23.8210.

Trifonova, O.P., Maslov, D.L., Balashova, E.E., Urazgildeeva, G.R., Abaimov, D.A., et al. (2020). **Parkinson's disease: Available clinical and promising omics tests for diagnostics, disease risk assessment, and pharmacotherapy personalization**. *Diagnostics 10* DOI: 10.3390/diagnostics10050339.

Tsika, E., Glauser, L., Moser, R., Fiser, A., Daniel, G., et al. (2014). **Parkinson's disease-linked mutations in VPS35 induce dopaminergic neurodegeneration**. *Hum. Mol. Genet. 23*, 4621–4638. DOI: 10.1093/hmg/ddu178.

Valente, E.M., Abou-Sleiman, P.M., Caputo, V., Muqit, M.M.K., Harvey, K., et al. (2004). **Hereditary early-onset Parkinson's disease caused by mutations in PINK1**. *Science (80-.). 304*, 1158–1160. DOI: 10.1126/science.1096284.

Valente, E.M., Bentivoglio, A.R., Dixon, P.H., Ferraris, A., Lalongo, T., et al. (2001). **Localization of a novel locus for autosomal recessive early-onset parkinsonism, PARK6, on human chromosome 1p35-p36**. *Am. J. Hum. Genet. 68*, 895–900. DOI: 10.1086/319522.

Vancraenenbroeck, R., De Raeymaecker, J., Lobbestael, E., Gao, F., De Maeyer, M., et al. (2014). **In silico, in vitro and cellular analysis with a kinome-wide inhibitor panel correlates cellular LRRK2 dephosphorylation to inhibitor activity on LRRK2**. *Front. Mol. Neurosci. 7* DOI: 10.3389/fnmol.2014.00051.

Vilariño-Güell, C., Wider, C., Ross, O.A., Dachsel, J.C., Kachergus, J.M., et al. (2011). **VPS35 mutations in parkinson disease**. *Am. J. Hum. Genet. 89*, 162–167. DOI: 10.1016/j.ajhg.2011.06.001.

Voleti, B., and Duman, R.S. (2012). **The roles of neurotrophic factor and Wnt signaling in depression**. *Clin. Pharmacol. Ther. 91*, 333–338. DOI: 10.1038/clpt.2011.296.

Wakabayashi, K., Tanji, K., Odagiri, S., Miki, Y., Mori, F., et al. (2013). **The Lewy body in Parkinson's disease and related neurodegenerative disorders.** *Mol. Neurobiol. 47*, 495–508. DOI: 10.1007/s12035-012-8280-y.

Wallings, R., Connor-Robson, N., and Wade-Martins, R. (2019). **LRRK2 interacts with the vacuolar-type H+-ATPase pump a1 subunit to regulate lysosomal function**. *Hum. Mol. Genet. 28*, 2696–2710. DOI: 10.1093/hmg/ddz088.

Wang, G., Jiang, Q., and Zhang, C. (2014a). **The role of mitotic kinases in coupling the centrosome cycle with the assembly of the mitotic spindle**. *J. Cell Sci. 127*, 4111–4122. DOI: 10.1242/jcs.151753.

Wang, J., and Deretic, D. (2014). **Molecular complexes that direct rhodopsin transport to primary cilia**. *Prog. Retin. Eye Res. 38*, 1–19. DOI: 10.1016/j.preteyeres.2013.08.004.

Wang, S., Liu, Z., Ye, T., Mabrouk, O.S., Maltbie, T., et al. (2017). **Elevated LRRK2 autophosphorylation in brain-derived and peripheral exosomes in LRRK2 mutation carriers**. *Acta Neuropathol. Commun. 5*, 86. DOI: 10.1186/s40478-017-0492-y.

Wang, S., Ma, Z., Xu, X., Wang, Z., Sun, L., et al. (2014b). **A role of Rab29 in the integrity of the trans-golgi network and retrograde trafficking of mannose-6-phosphate receptor**. *PLoS One 9*, 96242. DOI: 10.1371/journal.pone.0096242.

Ward, H.H., and Wandinger-Ness, A. (2018). Rab8. In: Encyclopedia of Signaling Molecules, Springer International Publishing, 4396–4408 DOI: 10.1007/978-3-319-67199-4_19.

Waschbüsch, D., Hübel, N., Ossendorf, E., Lobbestael, E., Baekelandt, V., et al. (2019). **Rab32 interacts with SNX6 and affects retromer-dependent Golgi trafficking**. *PLoS One 14* DOI: 10.1371/journal.pone.0208889.

Waschbüsch, D., Michels, H., Strassheim, S., Ossendorf, E., Kessler, D., et al. (2014). **LRRK2 transport is regulated by its novel interacting partner Rab32**. *PLoS One 9* DOI: 10.1371/journal.pone.0111632.

Waschbüsch, D., Purlyte, E., Pal, P., McGrath, E., Alessi, D.R., et al. (2020). **Structural Basis for Rab8a Recruitment of RILPL2 via LRRK2 Phosphorylation of Switch 2**. *Structure 28*, 406-417.e6. DOI: 10.1016/j.str.2020.01.005.

Watanabe, R., Buschauer, R., Böhning, J., Audagnotto, M., Lasker, K., et al. (2020). **The In Situ Structure of Parkinson's Disease-Linked LRRK2**. *Cell 182*, 1508-1518.e16. DOI: 10.1016/j.cell.2020.08.004.

Wauters, F., Cornelissen, T., Imberechts, D., Martin, S., Koentjoro, B., et al. (2020). **LRRK2 mutations impair depolarization-induced mitophagy through inhibition of mitochondrial accumulation of RAB10**. *Autophagy 16*, 203–222. DOI: 10.1080/15548627.2019.1603548.

Webber, P.J., Smith, A.D., Sen, S., Renfrow, M.B., Mobley, J.A., et al. (2011). **Autophosphorylation in the leucine-rich repeat kinase 2 (LRRK2) GTPase domain modifies kinase and GTP-binding activities**. *J. Mol. Biol. 412*, 94–110. DOI: 10.1016/j.jmb.2011.07.033.

Wei, J., Zhang, Y.Y., Luo, J., Wang, J.Q., Zhou, Y.X., et al. (2017). **The GARP Complex Is Involved in Intracellular Cholesterol Transport via Targeting NPC2 to Lysosomes**. *Cell Rep. 19*, 2823–2835. DOI: 10.1016/j.celrep.2017.06.012.

Wei, Z., Xu, X., Fang, Y., Khater, M., Naughton, S.X., et al. (2021). **Rab43 GTPase directs postsynaptic trafficking and neuron-specific sorting of G protein–coupled receptors**. *J. Biol. Chem. 296* DOI: 10.1016/j.jbc.2021.100517.

Weiss, B. (2008). **ROCO kinase activity is controlled by internal GTPase function**. *Sci. Signal. 1* DOI: 10.1126/scisignal.123pe27.

West, A.B., Moore, D.J., Biskup, S., Bugayenko, A., Smith, W.W., et al. (2005). **Parkinson's disease-associated mutations in leucine-rich repeat kinase 2 augment kinase activity**. *Proc. Natl. Acad. Sci. U. S. A. 102*, 16842–16847. DOI: 10.1073/pnas.0507360102.

West, A.B., Moore, D.J., Choi, C., Andrabi, S.A., Li, X., et al. (2007). **Parkinson's disease-associated mutations in LRRK2 link enhanced GTP-binding and kinase activities to neuronal toxicity** . *Hum. Mol. Genet. 16*, 223–232. DOI: 10.1093/hmg/ddl471.

Westlake, C.J., Baye, L.M., Nachury, M. V, Wright, K.J., Ervin, K.E., et al. (2011). **Primary cilia membrane assembly is initiated by Rab11 and transport protein particle II (TRAPPII) complex-dependent trafficking of Rabin8 to the centrosome.** *Proc. Natl. Acad. Sci. U. S. A. 108*, 2759–2764. DOI: 10.1073/pnas.1018823108.

Wheway, G., Nazlamova, L., and Hancock, J.T. (2018). **Signaling through the primary cilium**. *Front. Cell Dev. Biol. 6*, 8. DOI: 10.3389/fcell.2018.00008.

Williams, E.T., Chen, X., and Moore, D.J. (2017). **VPS35, the retromer complex and Parkinson's disease**. *J. Parkinsons. Dis. 7*, 219–233. DOI: 10.3233/JPD-161020.

Wilson, G.R., Sim, J.C.H., McLean, C., Giannandrea, M., Galea, C.A., et al. (2014). **Mutations in RAB39B cause X-linked intellectual disability and early-onset parkinson disease with α-synuclein pathology**. *Am. J. Hum. Genet. 95*, 729–735. DOI: 10.1016/j.ajhg.2014.10.015.

Winner, B., Melrose, H.L., Zhao, C., Hinkle, K.M., Yue, M., et al. (2011). **Adult neurogenesis and neurite outgrowth are impaired in LRRK2 G2019S mice**. *Neurobiol. Dis. 41*, 706–716. DOI: 10.1016/j.nbd.2010.12.008.

Wirdefeldt, K., Adami, H.O., Cole, P., Trichopoulos, D., and Mandel, J. (2011). **Epidemiology and etiology of Parkinson's disease: A review of the evidence**. *Eur. J. Epidemiol. 26* DOI: 10.1007/s10654-011-9581-6.

Woodruff, J.B., Wueseke, O., and Hyman, A.A. (2014). **Pericentriolar material structure and dynamics**. *Philos. Trans. R. Soc. B Biol. Sci. 369* DOI: 10.1098/rstb.2013.0459.

Wu, C.T., Chen, H.Y., and Tang, T.K. (2018). **Myosin-Va is required for preciliary vesicle transportation to the mother centriole during ciliogenesis**. *Nat. Cell Biol. 20*, 175–185. DOI: 10.1038/s41556-017-0018-7.

Xiong, Y., Coombes, C.E., Kilaru, A., Li, X., Gitler, A.D., et al. (2010). **GTPase activity plays a key role in the pathobiology of LRRK2**. *PLoS Genet. 6* DOI: 10.1371/journal.pgen.1000902.

Xiong, Y., Yuan, C., Chen, R., Dawson, T.M., and Dawson, V.L. (2012). **ArfGAP1 is a GTPase activating protein for LRRK2: Reciprocal regulation of ArfGAP1 by LRRK2**. *J. Neurosci. 32*, 3877–3886. DOI: 10.1523/JNEUROSCI.4566-11.2012.

Yoon, J.H., Mo, J.S., Kim, M.Y., Ann, E.J., Ahn, J.S., et al. (2017). **LRRK2 functions as a scaffolding kinase of ASK1-mediated neuronal cell death**. *Biochim. Biophys. Acta - Mol. Cell Res. 1864*, 2356–2368. DOI: 10.1016/j.bbamcr.2017.09.001.

Yoshimura, K., Kawate, T., and Takeda, S. (2011). **Signaling through the primary cilium affects glial cell survival under a stressed environment.** *Glia 59*, 333–344. DOI: 10.1002/glia.21105.

Yoshimura, S.I., Egerer, J., Fuchs, E., Haas, A.K., and Barr, F.A. (2007). **Functional dissection of Rab GTPases involved in primary cilium formation**. *J. Cell Biol. 178*, 363–369. DOI: 10.1083/jcb.200703047.

Yoshimura, S.I., Gerondopoulos, A., Linford, A., Rigden, D.J., and Barr, F.A. (2010). **Family-wide characterization of the DENN domain Rab GDP-GTP exchange factors**. *J. Cell Biol. 191*, 367–381. DOI: 10.1083/jcb.201008051.

Yue, M., Hinkle, K.M., Davies, P., Trushina, E., Fiesel, F.C., et al. (2015). **Progressive dopaminergic alterations and mitochondrial abnormalities in LRRK2 G2019S knock-in mice.** *Neurobiol. Dis. 78*, 172–195. DOI: 10.1016/j.nbd.2015.02.031.

Yun, H.J., Park, J., Ho, D.H., Kim, H., Kim, C.H., et al. (2013). **LRRK2 phosphorylates Snapin and inhibits interaction of Snapin with SNAP-25**. *Exp. Mol. Med. 45* DOI: 10.1038/emm.2013.68.

Zabetian, C.P., Hutter, C.M., Yearout, D., Lopez, A.N., Factor, S.A., et al. (2006). **LRRK2 G2019S in families with Parkinson disease who originated from Europe and the Middle East: Evidence of two distinct founding events beginning two millennia ago**. *Am. J. Hum. Genet. 79*, 752–758. DOI: 10.1086/508025.

Zabetian, C.P., Samii, A., Mosley, A.D., Roberts, J.W., Leis, B.C., et al. (2005). **A clinic-based study of the LRRK2 gene in Parkinson disease yields new mutations**. *Neurology 65*, 741–744. DOI: 10.1212/01.WNL.0000172630.22804.73.

Zesiewicz, T.A., Sullivan, K.L., and Hauser, R.A. (2006). **Nonmotor symptoms of Parkinson's disease**. *Expert Rev. Neurother. 6*, 1811–1822. DOI: 10.1586/14737175.6.12.1811.

Zhang, J., Deng, X., Choi, H.G., Alessi, D.R., and Gray, N.S. (2012). **Characterization of TAE684 as a potent LRRK2 kinase inhibitor**. *Bioorganic Med. Chem. Lett. 22*, 1864–1869. DOI: 10.1016/j.bmcl.2012.01.084.

Zhang, L., Yang, X., Yang, S., and Zhang, J. (2011). **The Wnt/β-catenin signaling pathway in the adult neurogenesis**. *Eur. J. Neurosci. 33*, 1–8. DOI: 10.1111/j.1460-9568.2010.7483.x.

Zhang, W., Wang, T., Pei, Z., Miller, D.S., Wu, X., et al. (2005). **Aggregated α-synuclein activates microglia: a process leading to disease progression in Parkinson's disease**. *FASEB J. 19*, 533–542. DOI: 10.1096/fj.04-2751com.

Zhang, Z., Burgunder, J.M., An, X., Wu, Y., Chen, W., et al. (2009). **LRRK2 R1628P variant is a risk factor of Parkinson's disease among Han-Chinese from mainland China**. *Mov. Disord. 24*, 1902–1905. DOI: 10.1002/mds.22371.

Zhao, Y., Perera, G., Takahashi-Fujigasaki, J., Mash, D.C., Vonsattel, J.P.G., et al. (2018). **Reduced LRRK2 in association with retromer dysfunction in post-mortem brain tissue from LRRK2 mutation carriers**. *Brain 141*, 486–495. DOI: 10.1093/brain/awx344.

Zheng, Y., Liu, Y., Wu, Q., Hong, H., Zhou, H., et al. (2011). **Confirmation of LRRK2 S1647T variant as a risk factor for Parkinson's disease in Southern China**. *Eur. J. Neurol. 18*, 538–540. DOI: 10.1111/j.1468-1331.2010.03164.x.

Zhu, A.X., Zhao, Y., and Flier, J.S. (1994). **Molecular cloning of two small GTP-binding proteins from human skeletal muscle**. *Biochem. Biophys. Res. Commun. 205*, 1875–1882. DOI: 10.1006/bbrc.1994.2889.

Zimprich, A., Benet-Pagès, A., Struhal, W., Graf, E., Eck, S.H., et al. (2011). **A mutation in VPS35, encoding a subunit of the retromer complex, causes late-onset parkinson disease**. *Am. J. Hum. Genet. 89*, 168–175. DOI: 10.1016/j.ajhg.2011.06.008.

Zimprich, A., Biskup, S., Leitner, P., Lichtner, P., Farrer, M., et al. (2004). **Mutations in LRRK2 cause autosomal-dominant parkinsonism with pleomorphic pathology**. *Neuron 44*, 601–607. DOI: 10.1016/j.neuron.2004.11.005.

Zou, W., Yadav, S., DeVault, L., Nung Jan, Y., and Sherwood, D.R. (2015). **RAB-10-Dependent Membrane Transport Is Required for Dendrite Arborization**. *PLoS Genet. 11* DOI: 10.1371/journal.pgen.1005484.

List of publications

Research articles:

Blanca Ramírez, M, **Lara Ordóñez, AJ**, Fdez, E, Madero-Pérez, J, Gonnelli, A, Drouyer, M, Chartier-Harlin, MC, Taymans, JM, Bubacco, L, Greggio, E and Hilfiker, S. (2017) **GTP binding regulates cellular localization of Parkinson´s disease-associated LRRK2.** *Hum. Mol. Genet.* Jul 15. 26(14): 2747-2767. DOI: 10.1093/hmg/ddx161

Madero-Pérez, J, Fdez, E, Fernández, B, **Lara Ordóñez, AJ**, Blanca Ramírez, M, Gómez-Suaga, P, Waschbüsch, D, Lobbestael, E, Baekelandt, V, Nairn, AC, Ruiz-Martínez, J, Aiastui, A, López de Munaín, A, Lis, P, Comptdaer, T, Taymans, JM, Chartier-Harlin, MC, Beilina, A, Gonnelli, A, Cookson, M, Greggio, E and Hilfiker, S. (2018) **Parkinson disease-associated mutations in LRRK2 cause centrosomal defects via Rab8a phosphorylation.** *Mol. Neurodegener.* Jan 23. 13(1): 3. DOI: 10.1186/s13024-018-0235-y

Madero-Pérez, J, Fernández, B, **Lara Ordóñez, AJ**, Fdez, E, Lobbestael, E, Baekelandt, V and Hilfiker, S. (2018) **RAB7L1-mediated relocalization of LRRK2 to the Golgi complex causes centrosomal deficits via RAB8A**. *Front. Mol. Neurosci.* Nov 13. 11: 417. DOI: 10.3389/fnmol.2018.00417

Lara Ordóñez AJ, Fernández B, Fdez E, Romo-Lozano M, Madero-Pérez J, Lobbestael E, Baekelandt V, Aiastui A, López de Munaín A, Melrose HL, Civiero L and Hilfiker S. (2019) **RAB8, RAB10 and RILPL1 contribute to both LRRK2 kinase-mediated centrosomal cohesion and ciliogenesis deficits.** *Hum. Mol. Genet.* Nov 1; 28(21): 3552-3568. DOI: 10.1093/hmg/ddz201

Fernández B, **Lara Ordóñez AJ**, Fdez E, Mutez E, Comptdaer T, Leghay C, Kreisler A, Simonin C, Vandewynckel L, Defebvre L, Destée A, Bleuse S, Taymans JM, Chartier-Harlin MC and Hilfiker S. (2019) **Centrosomal cohesion deficits as cellular biomarker in lymphoblastoid cell lines from LRRK2 Parkinson's disease patients.** *Biochem. J.* Oct 15; 476(19): 2797-2813. DOI: 10.1042/BCJ20190315

Lara Ordóñez AJ, Fernández B, Fasiczka R, Naaldijk Y, Fdez E, Blanca Ramírez M, Phan S, Boassa D and Hilfiker S. **The LRRK2 signaling pathway causes centrosomal deficits via phosphorylated RAB10 and RILPL1 at centriolar subdistal appendages.** (under review)

Fernández B, Chittoor-Vinod, VG, Kluss, JH, Kelly, K, Nguyen, AP, Bukhari, SA, **Lara Ordóñez AJ**, Fdez E, Chartier-Harlin MC, Moore, DJ, Montine, TJ, Cookson, MR, Nichols, RJ, West, AB, and Hilfiker S. **Evaluation of current methods to detect LRRK2 kinase activity.** (under review)

Review articles:

Blanca Ramírez, M, **Lara Ordóñez, AJ**, Fdez, E and Hilfiker, S. (2017) **LRRK2: from kinase to GTPase to microtubules and back.** *Biochem. Soc. Trans.* Feb 8. 45(1): 141-146. DOI: 10.1042/BST20160333

Madero-Pérez, J, Fdez, E, Fernández, B, **Lara Ordóñez, AJ**, Blanca Ramírez, M, Romo Lozano, M, Rivero-Ríos, P and Hilfiker, S. (2017) **Cellular effects mediated by pathogenic LRRK2: homing in on Rab-mediated processes.** *Biochem. Soc. Trans.* Feb 8. 45(1): 147-154. DOI: 10.1042/BST20160392

Blanca Ramírez, M, Madero-Pérez, J, Rivero-Ríos, P, Martinez-Salvador, M, **Lara Ordóñez, AJ**, Fernández, B, Fdez, E and Hilfiker, S. (2017) **LRRK2 and Parkinson´s disease: from lack of structure to gain of function.** *Curr. Protein Pept. Sci.* Jul 1. 18(7): 677-686. DOI: 10.2174/1389203717666160311121748